CHEMICAL CONSTITUENTS AND BIOLOGICAL ACTIVITIES OF *ALPINIA MUTICA* ROXB. AND *LYSIPHYLLUM STRYCHNIFOLIUM* (CRAIB) A. SCHMITZ

MERANEE KIDRUANGPHOKIN

A Thesis Submitted to the Graduate School of Naresuan University
in Partial Fulfillment of the Requirements
for the Doctor of Philosophy in Chemistry- (Type 1.1)
2022

CHEMICAL CONSTITUENTS AND BIOLOGICAL ACTIVITIES OF *ALPINIA MUTICA* ROXB. AND *LYSIPHYLLUM STRYCHNIFOLIUM* (CRAIB) A. SCHMITZ

MERANEE KIDRUANGPHOKIN

A Thesis Submitted to the Graduate School of Naresuan University
in Partial Fulfillment of the Requirements
for the Doctor of Philosophy in Chemistry- (Type 1.1)
2022

Thesis entitled "Chemical constituents and biological activities of *Alpinia mutica* Roxb. and *Lysiphyllum strychnifolium* (Craib) A. Schmitz"

By Meranee Kidruangphokin

has been approved by the Graduate School as partial fulfillment of the requirements for the Doctor of Philosophy in Chemistry- (Type 1.1) of Naresuan University

Oral Defense Committee

..... Chair
(Assistant Professor Worrapong Phupong, Ph.D.)

..... Advisor
(Assistant Professor Surat Boonphong, Ph.D.)

..... Co Advisor
(Assistant Professor Nungruthai Suphrom, Ph.D.)

..... Internal Examiner
(Associate Professor Boonjira Rutnakornpituk, Ph.D.)

..... Internal Examiner
(Assistant Professor Chaturong Suparpprom, Ph.D.)

Approved

.....
(Associate Professor Krongkarn Chootip, Ph.D.)
Dean of the Graduate School

Title CHEMICAL CONSTITUENTS AND BIOLOGICAL ACTIVITIES OF *ALPINIA MUTICA* ROXB. AND *LYSIPHYLLUM STRYCHNIFOLIUM* (CRAIB) A. SCHMITZ

Author Meranee Kidruangphokin

Advisor Assistant Professor Surat Boonphong, Ph.D.

Co-Advisor Assistant Professor Nungruthai Suphrom, Ph.D.

Academic Paper Ph.D. Dissertation in Chemistry- (Type 1.1), Naresuan University, 2022

Keywords Alpinia, Alpinia mutica, Lysiphyllum, Lysiphyllum strychnifolium, Bauhinia strchnifolia, α-Glucosidase, Antioxidant, Flavonoid, Chemical constituents, Volatile component, brewing

ABSTRACT

This study described the phytochemical studies, *α*-glucosidase inhibitory activity, and antioxidants of *Alpinia mutica* and *Lysiphyllum strychnifolium*, along with the optimal infusion conditions for *L. strychnifolium* leaves tea. The study is divided into three sections listed below.

First, the chemical constituents and *a*-glucosidase inhibitory activity of *A. mutica* were investigated. The dichloromethane crude extracts of pericarps and seeds were analyzed by GC-MS in this section. The main volatile constituent of the pericarp extract was diarylheptanoid, namely 1,7-diphenyl-4,6-heptadien-3-one (45.28%). The most abundant volatile components in the seed extract were 5,6-dehydrokawain (64.94%), pinocembrin (22.51%) and farnesol (9.18%). Moreover, seven known compounds, including farnesol (1), 5,6-dehydrokawain (2), pinocembrin (3), cardamomin (4), naringenin (5), pinocembrin chalcone (6), and alpinetin (7) were isolated from dichloromethane extract of *A. mutica* seed and evaluated for *α*-glucosidase inhibitory activity. The most potent isolated compound against *α*-glucosidase was naringenin (5) with an IC_{50} value of 8.77 ± 1.04 μM.

The chemical constituents, *a*-glucosidase inhibitory and antioxidant

activities of *L. strychnifolium* were subsequently investigated. In this section, thirteen compounds, including astilbin (8), isoastilbin (9), neoastilbin (10), epicatechin (11), (*E*)-resveratrol (12), (*E*)-resveratrol 4'-*O*-*β*-D-glucoside (13), quercetin 3-*O*-*β*-D-arabinoside (14), phloretin (15), phloretin 4'-*O*-*β*-D-glucoside (16), phloretin 4'-*O*-(6"-*O*-galloyl)-*β*-D-glucoside (17), pinitol (18), gallic acid (19) and gallic acid ethyl ester (20) were isolated from the crude ethanolic extract of *L. strychnifolium* roots, stems, leaves and flowers. Compound 17 exhibited strong *α*-glucosidase inhibitory activity with an IC_{50} value of 16.2 ± 1.4 μM. In addition, compound 17 exhibited the highest antioxidant activity with an IC_{50} value of 19.26 ± 0.95 μM. The results of these two sections demonstrated that compounds 5 and 17 may provide therapeutic alternatives for type 2 diabetes.

The final part of the research focused on determining the optimal infusion conditions for *L. strychnifolium* leaves tea. In this section, the effects of infusion conditions, including time, temperature and water volume, as well as multiple infusions, were investigated. *L. strychnifolium* leaves tea had the highest extraction yield (26.99 ± 0.33%) when brewed using hot water at 70 °C with a leaf powder and water ratio of 1:40 (g/mL) for 5 min, followed by two steps of brewing. Moreover, a sweetener, phloretin 4'-*O*-*β*-D-glucoside (16) and anti-hyperglycemia agent, pinitol (18), were identified as the major components of *L. strychnifolium* leaves tea. This section provides evidence for the folk belief that *L. strychnifolium* tea promotes health and wellness.

ACKNOWLEDGEMENTS

This project was made possible by the generous support of the PhD scholarship funding program from the Science Achievement Scholarship of Thailand (SAST) and the Department of Chemistry, Faculty of Science, Naresuan University who provided essential scientific instruments.

To say that this thesis was completed as a personal achievement would be misleading. The completion of this work was done as a collaborative effort with the incredible people who surround me in my Faculty. I would first and foremost like to thank my advisor, Dr. Surat Boonphong. I will never be able to put into words just how thankful I am for all the guidance and trust you have given me. The skills and knowledge I have gained under your leadership are invaluable and I will be forever grateful to have been one of your graduate students.

Thank you to Dr. Nungruthai Suphrom for serving on my advisory committee and for all your generosity and encouragement in all of my projects and endeavors.

I would like to extend gratitude to the staff here at the Department of Chemistry, Faculty of Science, Naresuan University and Science lab centre, Faculty of Science, Naresuan University for devices and instruments support.

Thank you Graduate students from the Department of Chemistry, Faculty of Science, Naresuan University, for making my work easier during these years and thanked for their useful advice.

To my friends, thank you for listening to me through all my rants and always making me laugh, you all helped keep me sane during this process.

Also, many thanks to Mr. Roy I. Morien of the Naresuan University Graduate School for his editing of the grammar, syntax and general English expression in this thesis.

Finally, I would like to thank my family, especially my parents who continuously supported and encouraged me in all my endeavors. I attribute all my success to your unwavering support. This thesis is dedicated to all of you.

Meranee Kidruangphokin

TABLE OF CONTENTS

Page

List of tables

Page

List of figure

Page

ABBREVIATIONS

Abs	=	absorbance
amu	=	atomic mass unit
°C	=	degree Celsius
CC	=	column chromatography
$CDCl_3$	=	deuterated Chloroform
CH_2Cl_2	=	dichloromethane
^{13}C-NMR	=	carbon-13 Nuclear Magnetic Resonance
cm	=	centimeter
CoA	=	coenzyme A
COSY	=	^{1}H-^{1}H correlation Spectroscopy
d	=	doublet
dd	=	doublet of doublet
DEPTQ	=	distorsionless enhancement by polarization transfer including the detection of quaternary nuclei
DEPT135	=	distortionless enhancement by polarization transfer 135
1D NMR	=	one-dimensional nuclear magnetic resonance
2D NMR	=	two-dimensional nuclear magnetic resonance
DMSO	=	dimethyl sulfoxide
DPPH	=	2,2-diphenyl-1-picrylhydrazyl
ESI	=	electrospray ionisation
EtOAc	=	ethyl acetate
EtOH	=	ethanol
eV	=	electron volt
FTIR-ATR	=	fourier transform infrared - attenuated total reflectance
g	=	gram
GC-MS	=	gas chromatography–mass spectrometry
^{1}H-NMR	=	proton nuclear magnetic resonance
HMQC	=	heteronuclear multiple-quantum correlation
HMBC	=	heteronuclear multiple bond correlation
HPLC	=	high performance liquid chromatography

ABBREVIATIONS (CONT.)

HRESIMS	=	high resolution electrospray ionisation mass spectroscopy
Hz	=	hertz
IC_{50}	=	half-maximal inhibitory concentration
i.d.	=	inside diameter
IR	=	infrared spectroscopy
J	=	coupling Constant
L	=	liter
m	=	meter
mg	=	milligram
mg/mL	=	milligram per milliliter
mg/kg	=	milligram per kilogram
min	=	minute
mL	=	milliliter
mm	=	millimeter
mM	=	milli molar
M	=	molar
MeOH	=	methanol
MS	=	mass spectroscopy
μg/mL	=	microgram per milliliter
μL	=	microliter
μM	=	micro molar
Na_2CO_3	=	Disodium carbonate
nd	=	not detected
nm	=	nanometer
NMR	=	nuclear magnetic resonance
p-NPG	=	*p*-nitrophenyl-α-D-glucopyranoside
ppm	=	parts per million
q	=	quartet
QTOF	=	quadrupole time of flight

ABBREVIATIONS (CONT.)

Ref.	=	reference
RIs	=	retention indices
RP-HPLC	=	reversed phase-high performance liquid chromatography
RT	=	retention time
s	=	singlet
SD	=	standard deviation
t	=	triplet
U/mL	=	unit per milliliter
UV-Vis	=	ultraviolet–visible spectroscopy
%w/w	=	percent weight to weight
δ	=	chemical shift

CHAPTER I

INTRODUCTION

1.1 Background & Significance of the study

Plant extracts provide unlimited opportunities to treat diseases because they have a huge number of bioactive compounds [1]. The use of herbal medicines in Asian countries demonstrates a long history of human interaction with plants. Medicinal plants used in traditional medicine contain a wide variety of bioactive compounds that can be used to treat chronic diseases [2]. According to research, these biomolecules are alternatives to chemical-based drugs since they are safer, more effective, and have less adverse effects [3].

Alpinia mutica and *Lysiphyllum strychnifolium* are the plants used as herbs and ornaments. *A. mutica*, called Kha nam in Thai, is a perennial rhizomatous herbaceous plant. It is commonly found in Borneo, Java, India, Myanmar, peninsular Malaysia, Singapore, Sulawesi, Thailand, and Vietnam, where it can grow in humid forests on swampy soils close to streams [4]. The rhizomes of this plant are traditionally used to treat stomach problems and flatulence [5]. The phytochemical constituents of the whole *A. mutica* fruit are diverse, including styrylpyrones, flavanones, and chalcones [6]. In addition, chemical studies of the rhizome and leaves have led to the isolation of flavanones, chalcones, styrylpyrones, and diarylheptanoids [5, 7]. The majority of phytochemical studies of *A. mutica* have concentrated on the chemical constituents of the rhizomes, leaves, and whole fruit. The chemical constituents of the two separate parts (pericarp and seed) of *A. mutica* have not been well investigated.

L. strychnifolium, commonly known as Khayan, Khruea khayan or Ya nang daeng in Thai, is an endemic vine plant of Thailand. The stems and roots of this plant have been traditionally used for the treatment of various diseases such as fever, allergy, and cancer [8]. *L. strychnifolium* has been increasingly recognized and considerable research has been carried out, especially in Thailand. Previous studies have demonstrated the presence of compounds and biological activities in *L.*

strychnifolium [8-10]. The crude extracts of stem and leaves have demonstrated anti-microbial, anti-inflammatory, anti-hyperuricemic, antiviral and antioxidant activities [11-15]. The stem and leaves of *L. strychnifolium* contain a wide range of secondary metabolites, including flavonol, flavanone, chromone, dihydrochalcone, phenolic acid, and cyclitol [8, 10, 16]. However, there is limited information on *L. strychnifolium*, especially the phytochemicals in its roots and flowers. Furthermore, the leaves of *L. strychnifolium* are usually used as herbal tea and tonic for detoxification [12].

Diabetes mellitus is a major endocrine health problem that is rapidly spreading throughout the world. According to the WHO, the number of diabetic patients worldwide is expected to reach 300 million by 2025. Diabetes mellitus, commonly referred to as diabetes, is a serious chronic condition characterized by elevated blood glucose levels resulting from an inability of the body to produce or utilize insulin effectively. There are two types of diabetes: type 1 (insulin-dependent) and type 2 (non-insulin-dependent) [17]. Type 2 diabetes, the more prevalent form, has been the main driver of the global increase in diabetes prevalence[18]. Patients with diabetes have a high risk of developing atherosclerosis, which can result in a variety of vascular problems, including acute and long-term complications [19]. Chronic hyperglycemia and reactive oxygen species (ROS) are the important risk factors for the development of atherosclerosis [20]. Therefore, reducing hyperglycemia and oxidative stress is necessary for preventing or treating diabetic complications. α-Glucosidase inhibitors are widely used as monotherapy and in combination with other anti-diabetic agents to control hyperglycemia [21]. α-Glucosidase is a hydrolytic enzyme released from the intestine that breaks down polysaccharides into monosaccharides and enhances glucose absorption, thereby increasing blood glucose levels. The inhibition of α-glucosidase may delay sugar digestion and reduce glucose absorption [22]. However, long-term use of α-glucosidase inhibitors such as acarbose, miglitol and voglibose can cause abdominal distention, flatulence, and possibly diarrhea [23]. Thus, the active compound from a natural source that exhibits α-glucosidase inhibiting and antioxidant properties should be a more potent anti-diabetic agent.

From our preliminary research on α-glucosidase inhibitory activity revealed that the crude extracts of *A. mutica* seed and *L. strychnifolium* root, stem, leaves, and flower exhibited a high level of α-glucosidase inhibition. Extracts of root, stem, leaves and flower of *L. strychnifolium* exhibited a promising level of the antioxidant. This study is a continuation of ongoing research on the α-glucosidase inhibitor and antioxidant agent found in *A. mutica* and *L. strychnifolium*. The chemical constituents of *A. mutica* seed and *L. strychnifolium* root, stem, leaves, and flower were isolated and their α-glucosidase inhibitory and antioxidant activities were assessed. These bioactive constituents will be beneficial for further development of anti-diabetic agents from *A. mutica* and *L. strychnifolium*. In addition to their traditional use in folk medicine, the leaves of *L. strychnifolium* are commonly utilized in herbal tea. In this study, the optimal infusion conditions for producing *L. strychnifolium* leaf tea with the highest concentration of tea extract was investigated. The obtained infusion conditions facilitate the development of a simple, household- or small-scale brewing method for the production of high-quality *L. strychnifolium* leaf tea.

This thesis consists of three parts. In Part I, the chemical compositions of the pericarp and seed of *A. mutica* were examined, along with the isolation of phytochemical from the seed, and the chemical relationship of flavonoids from *A. mutica*, and the α-glucosidase inhibitory activity of isolated compounds. In Part II, the chemical constituents of root, stem, leaves, and flower of *L. strychnifolium* were isolated, and their α-glucosidase inhibitory and antioxidant activities were evaluated. In Part III, the optimal infusion conditions for tea made from *L. strychnifolium* leaves were investigated.

1.2 Research objectives

The overall intention of the study is to study an α-glucosidase inhibitor and antioxidant from *A. mutica* and *L. strychnifolium*, as well as a suitable infusion condition for *L. strychnifolium* leaves. The following objectives were outlined within this framework.

Part I: The investigation of chemical constituents from pericarp and seed of *A. mutica* and the α-glucosidase inhibitory activity of isolated compounds from the seed of *A. mutica*

1. To investigate the volatile constituents of *A. mutica* pericarp and seed using GC–MS
2. To isolate and identify the chemical constituents of *A. mutica* seed
3. To determine the α-glucosidase inhibitory activity of isolated compounds from the seeds of *A. mutica*

Part II: The investigation of chemical constituents, α-glucosidase inhibitory and antioxidant activities of *L. strychnifolium*

1. To isolate and identify the chemical constituents from the root, stem, leaves and flower of *L. strychnifolium*
2. To investigate the α-glucosidase inhibitory and antioxidant properties of isolated compounds

Part III: The investigation of the optimal conditions for brewing tea from *L. strychnifolium* leaves

1. To determine the optimal conditions for brewing tea from *L. strychnifolium* leaves
2. To investigate the chemical constituents of tea made from *L. strychnifolium* leaves

CHAPTER II

THEORETICAL AND RELATED LITERATURES

This chapter presents a literature review on the botanical description, medicinal uses, and chemistry of *A. mutica* and *L. strychnifolium*. In addition, the principle of the α-glucosidase and antioxidant activities are discussed and the information about the herbal tea are summarized. This chapter is divided into five sections, which are as follow:

2.1 Reviews of the literature on *A. mutica*

2.2 Reviews of the literature on *L. strychnifolium*

2.3 Diabetes and α-glucosidase

2.4 An overview of antioxidant

2.5 Herbal tea

2.1 Reviews of the literature on *A. mutica*

2.1.1 Botanical description

Name: *Alpinia mutica* Roxb. (Figure 1)

Family: Zingiberaceae

Stem: 1–2 m tall

Rhizome: rhizome rather slender

Leaf: Leaves narrowly lanceolate, up to 45 cm × 5 cm, long acuminate, glabrous, petiole about 2 cm long, ligule ovoid, 7–8 mm long, blunt, [4]

Flower: panicle few-many-flowered, up to 15 cm long, branches several, short, cincinni 3–5-flowered, bracts absent, bracteoles very small, oblong, 6 mm long, white, caducous; calyx tubular, 15–20 mm long, split halfway during flowering, white, corolla tube shorter, lobes oblong, 2.5–3 cm long, white, labellum broadly ovate, somewhat 3-lobed, basal part strongly concave, apex straight, bright yellow to orange with numerous red dots and veins, a dark red swelling at the base at each side, staminodes absent, stamen as long as corolla lobes, filament white, tinged pink, anther without crest, [4]

Fruit: capsule ovoid, up to 2 cm in diameter, sparsely short hairy, orange-red, seeds numerous, [4]

Distribution: The species is native to Borneo, Java, India, Myanmar, Peninsular Malaysia, Singapore, Sulawesi, Thailand, and Vietnam, where it lives in the humid forests on swampy soils close to water streams [4].

Traditional uses: *A. mutica* is valued for its foliage and inflorescences as an ornamental and landscape plant in the tropical and humid subtropical climate regions, where it blooms for the most of the year [4]. The rhizomes of this plant have been used traditionally to treat a stomach problems and flatulence [5, 24], and the fruits' pericarps and seeds have been used to treat diarrhea and reduce swelling [24, 25].

Figure 1 The appearance of *A. mutica* plant

2.1.2 Essential oil compositions

Essential oils are complex mixtures of many different compounds. The oil extracted from the *A. mutica* was analyzed using the GC–MS technique. Monoterpenes and sesquiterpenes are the most abundant volatile components of *A. mutica*. The main constituents of rhizome oil were camphor, 1,8-cineol, borneol, *β*-pinene and camphene [26, 27]. The majority of the leaves composed of sesquiterpenes, including *β*-sesquiphellandrene and *β*-bisabolene [7]. Moreover, the essential oil components of *A. mutica* fruit oils collected from three distinct locations varied significantly. The essential oils of fruit from Johor, Malaysia, and Vietnam contain a high amount of sesquiterpenes (75.9% and 52.7%, respectively). These oils contained 47.8% and 22.6% of farnesol and *β*-cayophyllene, respectively, as their major constituents [28, 29]. However, the essential oil of *A. mutica* fruit from Kuala Lumpur, Malaysia was found to be rich in monoterpenes, particularly camphor (21.0%) and camphene (16.6%) [25]. These differences could be attributed to the investigated species' origin, cultivation, vegetative stage and the growing season. Among the essential oils from *A. mutica*, the fruit oil possesses the antimicrobial activity against *Microsporum canis*, *Trichophyton mentagrophytes* and *Trichophyton rubrum* [25]. The major volatile constituents of *A. mutica* are shown in Figure 2.

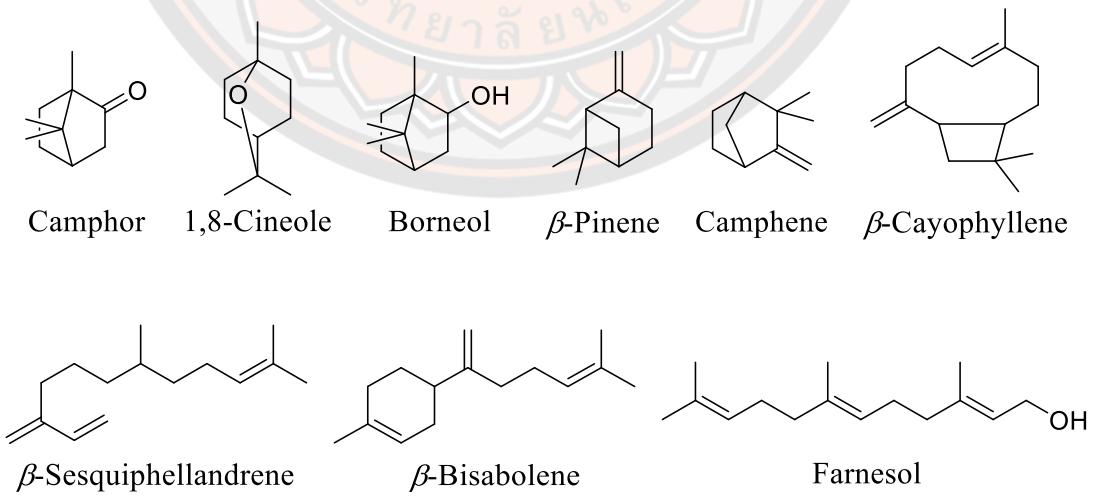

Figure 2 The chemical structure of major volatile constituents from *A. mutica*

2.1.3 Chemical constituents isolated from *A. mutica*

The chemical constituents of various *A. mutica* parts have been reported. Previous studies demonstrated that *A. mutica* contains styrylpyrones, chalcones, flavanones, diarylheptanoids, and triterpenes (Table 1, Figures 3 and 4). 5,6-Dehydrokawain, flavokawin B, pinocembrin chalcone, pinocembrin, alpinein, 1 ,7-diphenyl-5-hydroxy-6-hepten-3-one and *β*-sitosterol were isolated from the rhizomes and their cytotoxicity against human carcinoma cell lines were investigated [5, 24, 30]. Styrylpyrone, its dimer; 5,6-dehydrokawain and aniba dimer A have been isolated from *A. mutica* leaves [7]. Six compounds from the fruit, including flavokawin B, pinocembrin, alpinetin, 5,6-dehydrokawain, cardamomin, and 2',3',4',6'-tetrahydroxychalcone exhibited PAF receptor binding inhibitory and human platelet aggregation inhibitory properties [31, 32]. The chemical constituents and their biological activities of *A. mutica* are summarized in Table 1.

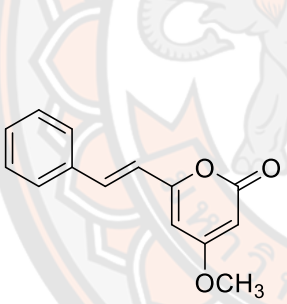

5,6-Dehydrokawain

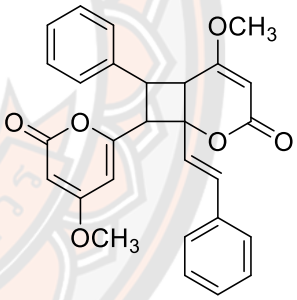

Aniba dimer A

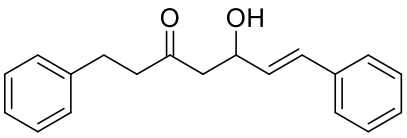

1,7-Diphenyl-5-hydroxy-6-hepten-3-one

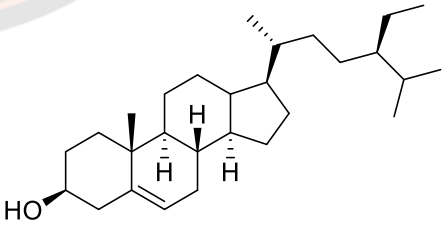

β-Sitosterol

Figure 3 Chemical structures of 5,6-dehydrokawain, aniba dimer A, 1,7-diphenyl-5-hydroxy-6-hepten-3-one and *β*-sitosterol from *A. mutica*

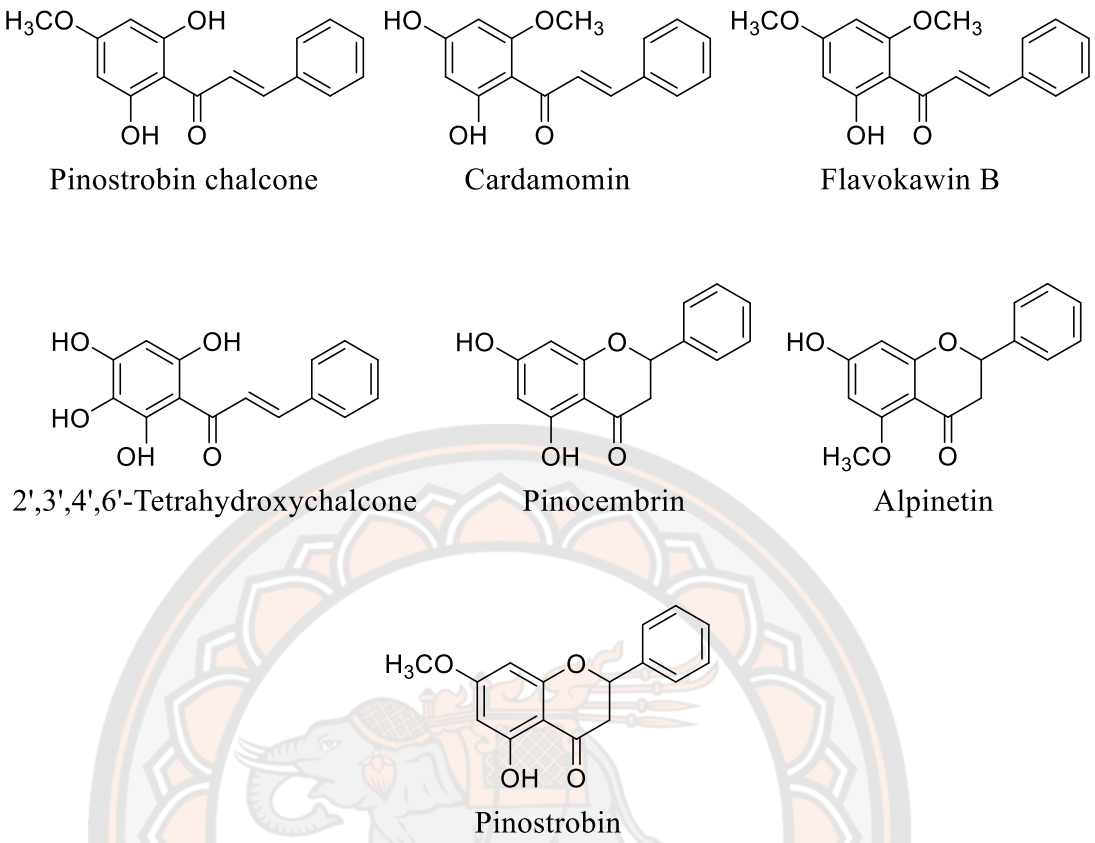

Figure 4 Chemical structures of pinostrobin chalcone, cardamomin, flavokawin B, 2′,3′,4′,6′-tetrahydroxychalcone, pinocembrin, alpinetin and pinostrobin from *A. mutica*

Table 1 Summary of chemical constituents from *A. mutica* and their bioactivities

Parts	Compounds	Class	Bioactivities	Ref.
Rhizome	5,6-Dehydrokawain Pinocembrin Alpinetin Pinostrobin Pinostrobin chalcone Flavokawin B 1,7-Diphenyl-5-hydroxy-6-hepten-3-one β-sitosterol	Styrylpyrone Flavanone Diarylheptanoid	• Pinostrobin chalcone showed cytotoxicity against epidermoid carcinoma (KB), hormone-dependent breast carcinoma (MCF7), and cervical carcinoma (CaSki) cell lines. • Flavokawin B demonstrated anticancer activity against KB, colon carcinoma (HCT116), and human T4 lymphoblastoid cancer (CEMss) cell lines.	[24], [33], [30]
Leaf	5,6-Dehydrokawain Anibadimer A	Styrylpyrone		[7]
Fruit	5,6-Dehydrokawain Pinocembrin Alpinetin Cardamomin Flavokawin 2',3',4',6'-Tetrahydroxychalcone	Styrylpyrone Flavanone Chalcone	• Alpinetin and 5,6-dehydrokawain showed inhibitory effects PAF receptor binding with IC_{50} values of 41.6 and 59.3 μm, respectively • 5,6-Dehydrokawain and 2',3',4',6'-tetrahydroxy chalcone showed platelet aggregation inhibition with IC_{50} value of 78 and 175 μM, respectively.	[6], [31]

A literature review on the chemical constituents of *A. mutica* revealed that the phytochemicals of the *A. mutica* plant included diarylheptanoid, styrypyrone and flavonoids, with 5,6-dehydrokawain being the major compound of this plant. The essential oil of this plant contained monoterpene hydrocarbons, oxygenated monoterpenes, sesquiterpene hydrocarbons, and oxygenated sesquiterpene. In addition, the pure compound from *A. mutica* exhibited cytotoxicity against cancer cell lines, inhibition of PAF receptor binding, and inhibition of platelet aggregation.

2.2 Reviews of the literature on *L. strychnifolium*

2.2.1 Botanical description

L. strychnifolium is a vine tree (Figure 5). The flowers bloom between the months of May and August. The propagation of this plant was accomplished by seed. The botanical descriptions of *L. strychnifolium* are listed below [34].

Name: *Lysiphyllum strychnifolium* (Craib) A. Schmitz

Family: Leguminosae-Cercidoideae

Synonyms: *Bauhinia strychnifolia* Craib

Stem: The length of its climbing stem with tendrils is 5 meters long.

Leaf: Leaves simple, entire, ovate-oblong, glabrous, 4–15 × 2–8 cm; secondary nerves 3–5, loobed; apex acuminate; base rounded to cordate; petioles 2–3.5 cm long.

Inflorescence: Inflorescences terminal, elongate racemose, reddish, dense-flowered. Bracts persistent and subulate. Calyx 5, pubescent, cup-shaped, pale pink to reddish, 0.5–1 cm long with short teeth. Petals 5, obovate, pubescent, red to dark red, with short claw. Stamens 3; filaments red, longer than the petals; staminodes 7, unequal. Ovary short stipitate, pubescent, about 0.7 cm long; style about 0.7 cm; stigma inconspicuous.

Pod: Pods dehiscent, lanceolate, 15–16 cm long. Seeds 8–9, oblong, about 1.7 cm long.

Distribution: *L. strychnifolium* is an endemic plant in the northern part of Thailand. It is widely distributed in Chiang Mai, Lampang, Sukhothai, Kamphaeng Phet, and Nakhon Sawan.

Traditional uses: The stem and root of *L. strychnifoilum* have been used to treat allergies and various type of cancers, such as colon, breast, and stomach cancer [8]. The leaves have been used detoxify alcohol and pesticides [12]. Additionally, leaves or stems boiled in water have been used as a tonic [11].

Figure 5 The appearance of the *L. strychnifoilum* plant

2.2.2 Phytochemical studies

According to various reports, the chemical constituent of *L. strychnifolium* varied. Chemical analyses of the stem and leaves of *L. strychnifolium* stem and leaves suggested that the phytochemicals of this plant include flavonol, flavanone, chromone, dihydrochalcone, cyclitol, and phenolic compounds. Eleven compounds were isolated from the stem and leaves of *L. strychnifolium* using chromatographic techniques (Table 2, Figures 6 and 7) and their structures were identified as quercetin, astilbin, β-sitosterol, stigmasterol, phloretin 4'-*O*-β-glucoside, pinitol, quinic acid, gallic acid, yanangdaengin, 3,5,7,3',5'-pentahydroxyflavanonol-3-*O*-α-L-rhamnopyranoside and 3,5,7-trihydroxychromone-3-α-L-rhamnopyranoside. [8, 10, 16, 35, 36]. However, there is limited information on *L. strychnifolium* species, especially the phytochemicals in their roots and flowers.

Table 2 Summary of chemical constituents from *L. strychnifolium*

Parts	Compounds	Class	Ref no.
Stem	Quercetin	Flavonol	[8], [9],
	3,5,7,3',5'-Pentahydroxyflavanonol-3-*O*-α-L-rhamnopyranoside	Flavanone	[36]
	Astilbin	Flavanone	
	3,5,7-Trihydroxychromone-3-α-L-rhamnopyranoside	Chromone	
	β-Sitosterol	Triterpene	
	Stigmasterol	Triterpene	
Leaf	Pinitol	Cyclitol	[10],
	Quinic acid	Phenolic acid	[16],
	Gallic acid	Phenolic acid	[35]
	Phloretin 4'-*O*-β-D-glucoside	Dihydrochalcone	
	Yanangdaengin	Dihydrochalcone	

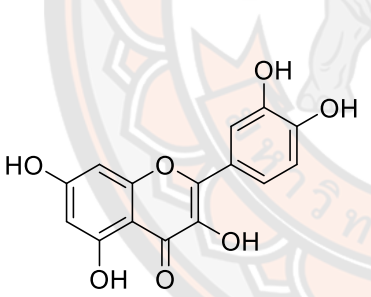

Quercetin

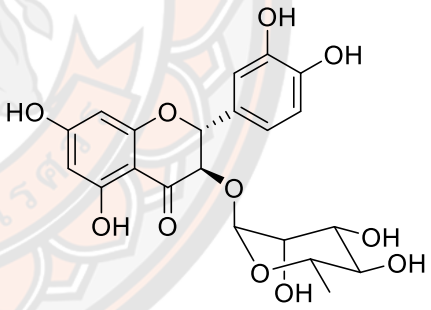

Astilbin

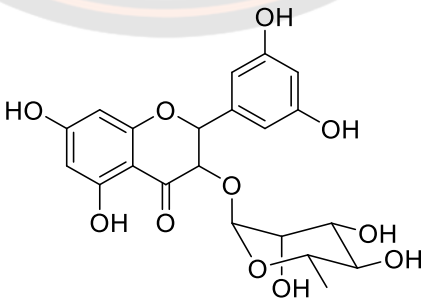

3,5,7,3',5'-Pentahydroxyflavanonol-3-*O*-*a*-L-rhamnopyranoside

Figure 6 Chemical structures of quercetin, astilbin and 3,5,7-trihydroxychromone-3-α-L-rhamnopyranoside from *L. strychnifolium*

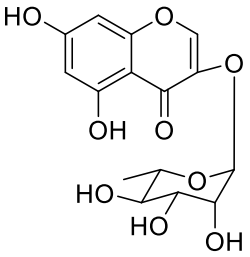

3,5,7-Trihydroxychromone-3-*a*-L-rhamnopyranoside

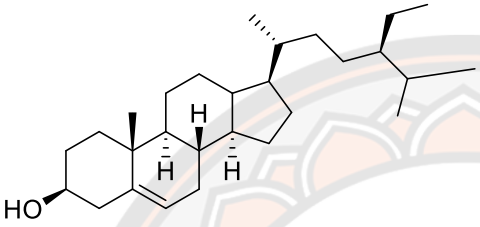

β-Sitosterol

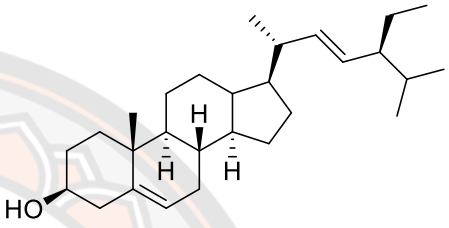

Stigmasterol

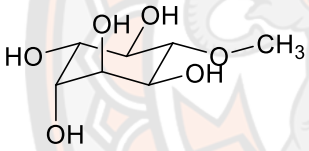

Pinitol

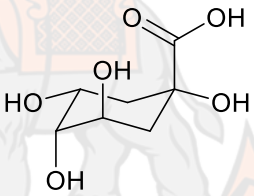

Quinic acid

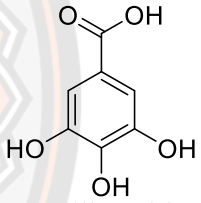

Gallic acid

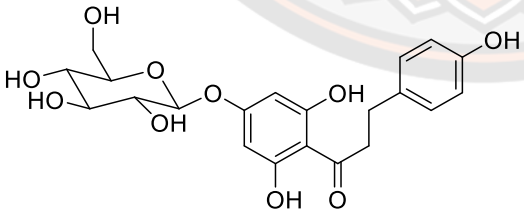

Phloretin 4'-*O*-*β*-D-glucoside

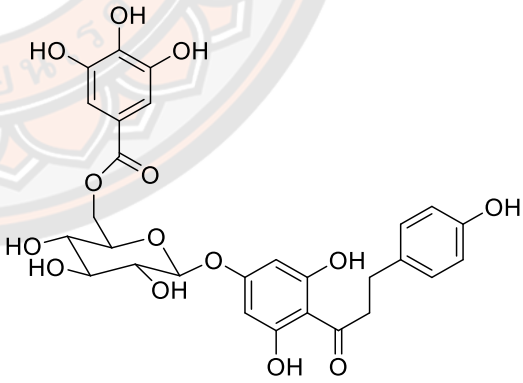

Yanangdaengin

Figure 7 Chemical structures of 3,5,6-trihydroxychromone-3-*α*-L-rhamnopyranoside, *β*-sitosterol, stigmasterol, pinitol, quinic acid, gallic acid, phloretin 4′-*O*-*β*-D-glucoside and yanangdaengin from *L. strycnifolium*

2.2.3 Biological activities of crude *L. strychnifolium* extract

Many research articles have reported the biological activities of the stem and leaves of *L. strychnifolium*. The details are summarized in Table 3.

Table 3 Summary of reported bioactivities from *L. strychnifolium*

Parts	Extracts	Bioactivities	Ref. no.
Stem	95% ethanol	Anti-HIV-1 integrase	[37]
		Antioxidant	[12]
		Antivirus against avian influenza virus A, strain H5N1	[38]
		Antidote activity against organophosphate pesticide	[15]
	50% ethanol	Antioxidant	[12]
	Aqueous	Anti-HIV-1 integrase	[9]
	Hexane	Cytotoxicity against human lung (A549), breast (MDA-MB-231), cervical (KB3-1) and colon (SW480) cancer cell lines	[39]
Leaf	95% ethanol	Antimalaria against *Plasmodium berghei* ANKA	[14]
		Antioxidant	[12]
		Antimicrobial against *Streptococcus mutans* and *Candida albican*	[40]
		Antivirus against avian influenza virus A, strain H5N1	[38]
		Antidote activity against organophosphate pesticide	[15]
	50% ethanol	Antibacterial activity	[41]
	Aqueous	Anti-inflammation	[13]
		Anti-hyperuricemia activity	

2.3 Diabetes and α-glucosidase

2.3.1 Diabetes

Diabetes is a group of metabolic disorders characterized by high blood sugar levels over a prolonged period of time [42]. Diabetes is caused by either insufficient insulin production by the pancreas or an insufficient insulin response by body cells [43]. There are two main types of diabetes: type 1 and type 2 diabetes. Type 1 diabetes is one of the most common metabolic disorders occurring in childhood [44]. The pathogenesis of type 1 diabetes involves T–cell mediated autoimmune destruction of insulin-producing pancreatic β–cells. Consequently, there is inadequate insulin secretion in the body, leading to the start of the disease [45]. In contrast, type 2 diabetes is the most common type of diabetes, accounting for 90%–95% of all cases [46]. Type 2 diabetes is caused by insulin resistance and impaired insulin secretion [47]. Chronic hyperglycemia in type 2 diabetes can be expressed in two indexes, postprandial and fasting blood glucose levels. Recent studies have found that postprandial high blood glucose levels are an important factor in the initiation and progression of type 2 diabetes [48].

In diabetic patients, high blood sugar levels can cause severe damage to various organs. Diabetes is associated with accelerated atherosclerosis, which leads to widely distributed vascular lesions including acute and long-term complications [49]. Acute diabetes complications include hyperosmolar hyperglycemic state, diabetic ketoacidosis, and death [50]. Serious long-term complications include stroke, cardiovascular disease, foot ulcers, eye and brain damage, chronic kidney disease and nerve damage [51]. Chronic hyperglycemia is one of the important risk factors for the atherosclerosis development. Chronic hyperglycemia increased oxidative stress, resulting in an increase in the formation of oxidized–LDL and a promotion of foam cell formation. The formation and accumulation of foam cells in the subendothelial space of vascular tissue is one of the early key steps in the progression of atherosclerosis. Atherosclerosis is the typical uppermost mediators of diabetes resulting in cardiovascular complications [49].

2.3.2 α-Glucosidase and α-Glucosidase inhibitors

The uptake of glucose in the intestine, in which α-glucosidase plays a key role due to the hydrolysis of starch and oligosaccharide is the important factor that contributes to postprandial hyperglycemia [52]. It is believed that inhibiting this enzyme can effectively control the postprandial rise in blood glucose levels. Hence, α-glucosidase inhibition is an important strategy for treating postprandial hyperglycemia [53].

α-Glucosidase (EC 3.2.1.20) is a digestive enzyme found in the brush border of the small intestine that converts starch and disaccharides to glucose by acting on $\alpha(1\rightarrow4)$ bonds [54]. The properties and substrate specificity of α-glucosidase are shown in Tables 4 and 5, respectively.

Table 4 Properties of purified α-glucosidase [55]

Properties	Type of α-glucosidase		
	Type I	Type II	Type III
Molecular weight	40 kDa	41 kDa	49 kDa
Isoelectric point	6.00	6.15	6.50
pH optimum	5.0	5.0	5.0
pH stability[a]	3.5–7.0	3.5–8.0	3.5–8.0
Temperature optimum (°C)	55	55	50
Heat stability (°C)[b]	Up to 45	Up to 45–55	Up to 45–50

[a] The enzyme was preincubated at 30 °C for 19 hour with buffers of various pHs, and the residual activity was determined at pH 5.0. [b] The enzyme was preincubated at various temperatures for 15 min with 25 μmol of acetate buffer, pH 5.0 and the residual activity was assayed at 37 °C.

Table 5 Substrate specificity of α-glucosidase [55]

Substrate	Relative rate of hydrolysis (%) of α-glucosidase		
	Type I	Type II	Type III
Isomaltose	3.3	4.0	51.9 (2.20)*
Maltose	100.0 (0.88)*	100.0 (0.86)*	100.0 (2.70)*
Sucrose	0	0	0
Maltotriose	46.2 (0.42)*	45.7 (0.55)*	44.9 (1.44)*
Panose	2.3	3.6	46.2
Methyl α-glucoside	0	0	0
Phenyl α-glucoside	2.5	2.4	12.0
Phenyl α-maltoside	39.9	46.3	55.3
Soluble starch	8.7	10.1	6.1

* ( ): K_m value in mM

α-Glucosidase inhibitors became a new class of antidiabetic drug. α-Glucosidase inhibitors retards the digestion and absorption of carbohydrates by competitively inhibiting or blocking the activity of glucosidase. Consequently, the peak concentration of postprandial blood glucose decreases, and blood sugar levels become more stable.

α-Glucosidase inhibitors are a non-invasive treatment with mild, dose-dependent gastrointestinal side effects, including diarrhea, stomach pain, and flatulence [56]. Dietary habits are directly linked to a practical method for regulating type 2 diabetes that has been described in previous research. Temporarily delaying the intestinal absorption of carbohydrates and thereby suppressing the elevation of postprandial blood glucose levels is an approach to controlling type 2 diabetes [23]. Only three α-glucosidase inhibitors are currently used in clinical practice, acarbose, miglitol, and voglibose (Figure 8). As a result, efforts to discover other inhibitors with greater effectiveness are intensifying.

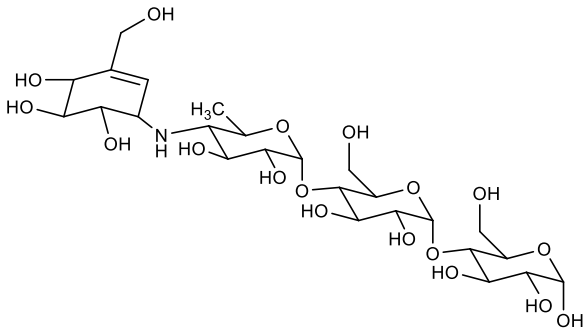

Acarbose

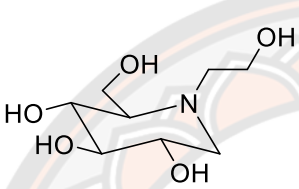

Miglitol

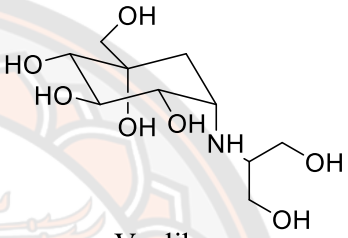

Voglibose

Figure 8 Chemical structures of α-glucosidase inhibitors

2.3.3 α-Glucosidase inhibition assay

The quantitative colorimetric method is one of the most widely used and practical methods for determining the inhibitory effect of various compounds on the α-glucosidase enzyme. This assay measures the inhibitory effects of *p*-nitrophenyl α-D-glucopyranoside, which is converted to *p*-nitrophenol (yellow product) by α-glucosidase. The change in absorbance was measured at 405 nm according to the following reaction (Figure 9) and the %inhibition was calculated using the following equation [57].

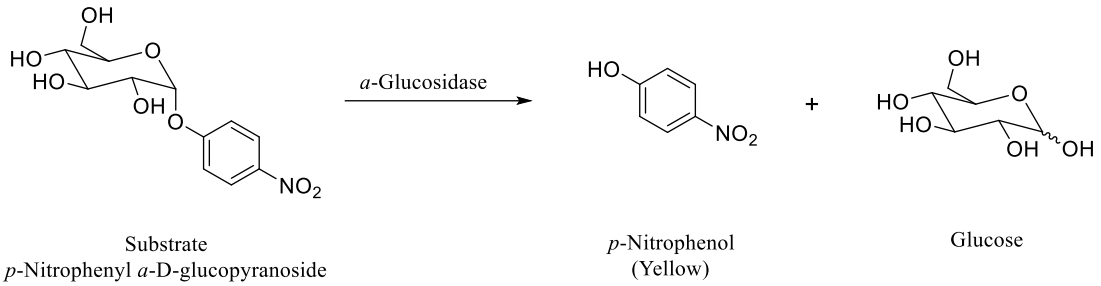

Figure 9 Hydrolysis reaction of α-glucosidase enzyme [57]

$$Inhibitory\ activity\ (\%) = 100 - \left[\left(\frac{Abs_{sample}}{Abs_{control}}\right) \times 100\right]$$

where Abs_{sample} = Absorbance of the sample solution at 405 nm

$Abs_{control}$ = Absorbance of the blank solution at 405 nm

2.4 An overview of antioxidant

Oxidative stress is an imbalance between free radicals and antioxidants. Free radicals such as reactive oxygen species (ROS) are oxygen-containing molecules with an unpair electrons. The unpair electron allows them to easily react with other molecules. Free radicals can cause large chain chemical reactions because they react so easily with other molecules. These reactions are called oxidation which can be beneficial or harmful [58]. From the previous publications, ROS play an important role in the development of diabetes complications. Therefore, the discovery of the active compound with α-glucosidase inhibitor and antioxidant properties derived from natural sources should result in a more effective anti-diabetic agent.

2.4.1 Definition of antioxidant

Antioxidants have been defined in several ways over the years; Halliwell and Gutteridge defined an antioxidant as “any substance that, when present at low concentrations compared with that of an oxidizable substrate, significantly delays or inhibits oxidation of that substrate” [59]. Lately, Halliwell described antioxidants as “any substance that delays, prevents or removes oxidative damage to a target molecule” [59]. In addition, an antioxidant molecule should be able to generate a new

stable radical after scavenging a free radical [60]. The stable radical will be less reactive with biological structures, such as proteins, DNA and lipids.

2.4.2 Mechanisms of action of antioxidant

The classical mechanism of reaction from an antioxidant can be shown by equation:

$$AH + R\cdot \longrightarrow A\cdot + RH$$

Where AH is the antioxidant, and R is the free radical. This equation describes the ability of antioxidants to inhibit many of the damaging processes caused by free radicals on biological structures, as well as their ability to generate a new stable free radical (A·) that is less reactive than the original (R·) [61].

The stability of the secondary free radicals A· generated after the reaction with the reactive intermediates is also an important consideration. It has been reported that some secondary free radicals have been shown to cause damage to DNA, proteins, and other biological targets [62]. As well, as shown by equations, secondary free radicals can react with oxygen to produce peroxyl and superoxide free radicals.

$$A\cdot + O_2 \longrightarrow AOO\cdot$$

$$A\cdot + O_2 \longrightarrow A_{OX} + O_2^{\cdot -}$$

2.4.3 Classification of antioxidants

Antioxidants can be classified into two types based on their sources: natural antioxidants and synthetic antioxidants [62]. Over the past several decades, some interests in synthetic antioxidants have dramatically increased. However, the potentially health and wellness of this natural antioxidant family remain the most popular and diverse.

2.4.3.1 Endogenous antioxidants

Endogenous antioxidants, which include antioxidant enzymes and their cofactors, are the first line of defense against oxidative stress. Superoxide dismutase (SOD), glutathione peroxidases, and catalase are the most important antioxidant enzymes. SOD converts the superoxide anion radical into hydrogen peroxide. The antioxidant effects of SOD are exerted by successive oxidative and reductive cycles of the transition metal ions at its active site [63, 64].

2.4.3.2 Exogenous antioxidants

Exogenous antioxidants are molecules that are derived from food, particularly fruit and vegetables. The consumption of these molecules is frequently associated with health and wellbeing because they function synergistically with endogenous antioxidants to maintain the physiological redox equilibrium [65]. The chemical structures of some exogenous antioxidants such as vitamin A, C, and E, phenolic compound, and stilbene are shown in Figure 10.

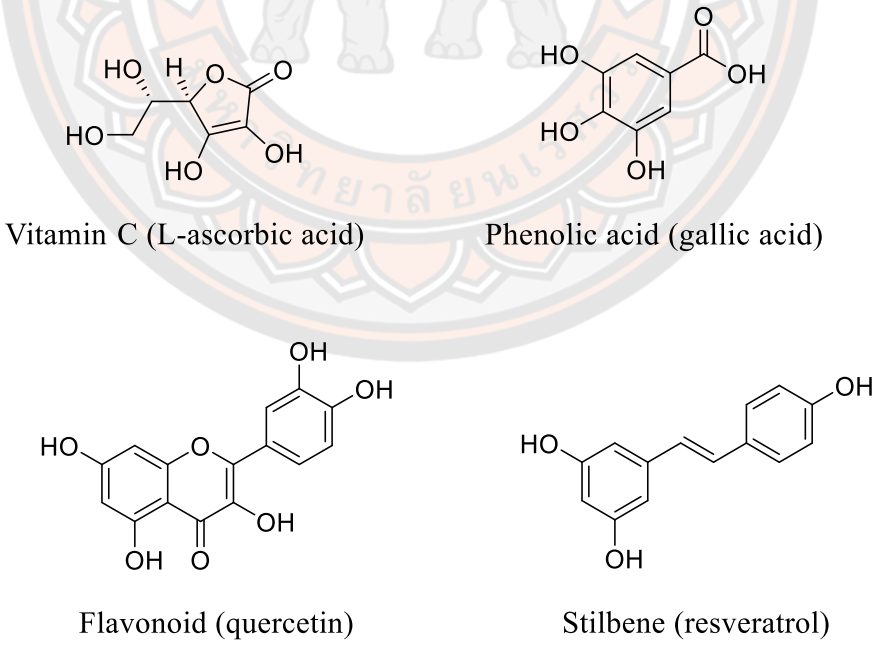

Figure 10 Chemical structures of some exogenous antioxidants

2.4.4 Antioxidant assay

Many antioxidant assays have been developed to assess antioxidant activity. To investigate the antioxidant activity of chemicals, it is essential to select an appropriate assay based on the chemical of interest. There are two types of assays that are commonly used for antioxidant research. The thiobarbituric acid assay (TBA), malonaldehyde/high-performance liquid chromatography (MA/HPLC) assay, malonaldehyde/gas chromatography (MA/GC) assay, beta-carotene bleaching assay, and conjugated diene assay are examples of lipid peroxidation-related assays. Other assays involve electron or radical scavenging, such as the 2,2-diphenyl-1-picrylhydrazyl (DPPH) assay, 2,2'-azinobis(3-ethylbenzothiazoline-6-sulfonic acid) (ABTS) assay, ferric reducing/antioxidant power (FRAP) assay, ferrous oxidation-xylenol orange (FOX) assay, ferric thiocyanate (FTC) assay, and aldehyde/carboxylic acid (ACA) assay [66]. In the present work, DPPH assay was used to determine the antioxidant activity.

2.4.5 DPPH radical scavenging assay

The DPPH assay is used to predict antioxidant activity. The scavenging of DPPH radicals is implied to determine free radical scavenging ability. The method is widely used due to its relatively short analysis time. The DPPH free radical is highly stable, reacts with compounds that can donate hydrogen atoms, and has a maximum UV–Vis absorption at 515 nm (Figure 11). The method is based on the scavenging of DPPH radical by antioxidants and measures the their ability to reduce the DPPH radical [67].

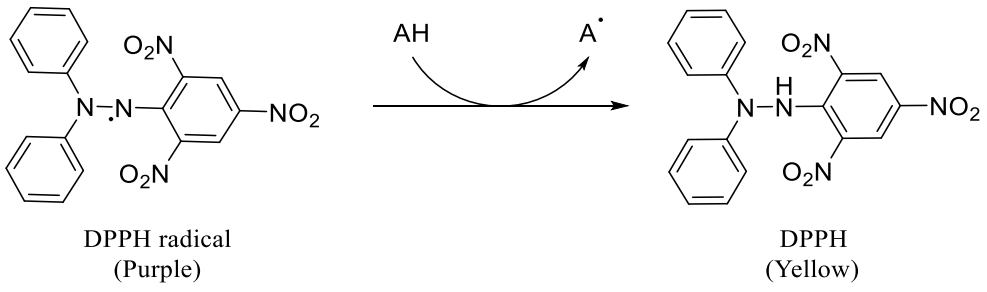

Figure 11 The reaction of DPPH radical with antioxidant (AH)

The ability to scavenge DPPH radicals is calculated by the equation.

$$\text{DPPH radical scavenging activity (\%)} = 100 - \left[\left(\frac{Abs_{sample}}{Abs_{control}}\right) \times 100\right]$$

where A_{sample} = Absorbance of the sample at 515 nm

$A_{control}$ = Absorbance of the solution without sample at 515 nm

A preliminary study indicated that *A. mutica* seed dichloromethane extract and the ethanolic extract of *L. strychnifolium* root, stem, leaves, and flower showed promising levels of α-glucosidase inhibition. Moreover, all extracts from *L. strychnifolium* exhibited good antioxidant property. Therefore, the propose of the present study is to isolate the α-glucosidase inhibitor from *A. mutica* seed and *L. strychnifolium* root, stem, leaves and flower as well as the antioxidant activity of isolated compound from *L. strychnifolium* root, stem, leaves, and flower will be investigated.

2.5 Herbal tea

Fresh or dried herbs have been used for the preparation of refreshing drinks and medicinal herbal infusions for the thousand years [68]. Herbal tea is typically consumed as a beverage brewed from the leaves, fruits, flowers, seeds, stems or roots of plant species instead of tea leaves (*Camellia sinensis*) [69]. Herbal tea has been used for thousands of years in many countries for health care and diseases prevention [69].

Herbal tea has become a popular beverage because it has several advantageous effects, including antioxidant, antimicrobial, anti-inflammatory, anti-aging, anticarcinogenic, cardioprotective, neuroprotective, and hepatoprotective activities, depending on the herbal that is used to make the tea. Herbal tea has multiple health benefits, including ability to reduce the risk of chronic diseases and improve human health [70].

2.5.1 Process for herbal tea preparation

According to the European Medicines Agency (2010), herbal teas consist of one or more herbal substances that are intended for oral liquid consumption and are prepared by infusion, decoction, or maceration. Typically, infusion is appropriate for leaves, flowers and delicate plant parts, whereas decoction and maceration are appropriate for roots, rhizomes, and barks. [71].

1. Infusion process involved pouring boiling water into the herbal substance and allowing it to steep for a defined period of time, normally 5 to 15 minutes.

2. Decoction is an herbal tea preparation created by pouring cold water over the plant material, heating it to a boil, and allowing it to simmer for a defined period of time, usually for 15 to 30 minutes, depending upon the type and size of the plant material. Decoction is generally not applicable to herbal substances containing volatile active constituents.

3. Maceration refers to liquid preparations made by soaking the herbal substance in water at room temperature for a defined period of time, usually for 30 minutes.

2.5.2 Factors affecting tea infusion

To ensure the safety and efficacy of herbal tea, it is crucial to pay attention to every step of the preparation process. However, there is no review related to the process of herbal tea infusion. According to a review of the brewing parameters affecting tea (*Camellia sinensis*), the extraction of catechins correlates with many parameters, including infusion time and temperature, particle size, number of extractions, storage time, and light exposure [72]. In order to determine the optimal infusion for *L. strychnifolium* leaf tea, some parameters including infusion time, temperature, and number of extractions, were considered in this research.

2.5.2.1 Time of infusion

There are observable effects of tea infusion time on the extraction of bioactive compounds and antioxidant capacity [73]. Langley-Evans et al. (2000) studied the effect of time (15 s to 15 min) on the antioxidant activity of green tea as

determine by the FRAP method [74]. The result indicated that the antioxidant capacity of green tea beverage increases with brewing time, reaching a maximum at 5 min. Although there was a slightly increase in antioxidant capacity after 15 min of brewing, the sensory properties of the beverage prevented its consumption [74]. In addition, the oxidation and epimerization of catechins led to a decrease in antioxidant activity over extremely long infusion times [75, 76].

2.5.2.2 Temperature of infusion

In the previous report, the infusion temperature increased the antioxidant activity and the solubility of catechins [77]. Saklar et al. (2015) investigated the effect of time (1, 2, 3, 5, 10, 20, 30 and 45 min) and temperature (75, 85 and 95 °C) on the extraction and epimerization of catechins in green tea [78]. The optimal conditions for the extraction of epigallocatechin gallate were determined to be brewing at 85 °C for 3 min. In addition, they found that increasing brewing time and temperature led to a 50% increase in the amount of non-epi isomers [78].

2.5.2.3 Number of extractions

Tea brewing can also be performed with re-infusion of used tea leaves because the many different bioactive compounds remain in the tea material. [79]. Komes et al. [76] found that a second and third infusion at 80 °C for 3 min extracted up to 25% of antioxidant activity. Additionally, Sharpe et al. (2016) studied the effect of six successive extractions on the antioxidant capacity of green tea. They discovered that after the first brew, teas do not release significant amounts of active antioxidants [79].

From above mentioned, it can be concluded that herbal tea has greatly increased in popularity in recent years, due in large part to a growing consumer interest in wellness. In Thailand, *L. strychnifolium* leaf tea is popular among people who believe that brewed tea helps to protect against gastroesophageal reflux disease. Unfortunately, there are some issues, such as a lack of information about *L. strychnifolium* leaf tea production and scientific evidence, especially the active constituents from the *L. strychnifolium* leaf tea. Therefore, the propose of this study

was to determine the effect of time, temperature, water volume, and the multiple infusions on the quantity of leaf tea extract. Moreover, the chemical constituents of *L. strychnifolium* leaf tea were also identified.

CHAPTER III

METHODOLOGY

The present work is divided into three parts. The first two parts describe the chemical constituents and biological activities of *A. mutica* and *L. strychnifolium*, respectively. In the final part, the optimal conditions for infusing *L. strychnifolium* leaf tea are investigated. The methodology is divided into the following five sections:

3.1 General experimental procedures

3.2 Chemicals

3.3 Part I: Methodology for the investigation of chemical constituents from pericarp and seed of *A. mutica* and the α-glucosidase inhibitory activity of isolated compounds from the seed of *A. mutica*

3.4 Part II: Methodology for the investigation of chemical constituents, α-glucosidase inhibitory and antioxidant activities of *L. strychnifolium*

3.5 Part III: Methodology for determining the optimal conditions for brewing tea from *L. strychnifolium* leaves

3.1 General experimental procedures

The 400 MHz ^{1}H NMR and 100 MHz ^{13}C NMR spectra were obtained from Bruker Avance 400 spectrometer (Bruker, Massachusetts, USA). The HRESIMS were obtained using an Agilent 1260 infinity high-performance liquid chromatograph via an ESI interface to a 6540 ultrahigh definition accurate mass Q−TOF (Agilent Technologies, California, USA). IR spectra were obtained using the Perkin Elmer Spectrum GX spectrometer in FTIR−ATR mode (PerkinElmer, Massachusetts, USA). UV spectra were taken by Analytik Jena Specord 200 Plus spectrometer (Analytik Jena, Jena, Germany). Semipreparative HPLC was performed on an Agilent 1260 Infinity equipped with a UV−Vis detector (Agilent Technologies, California, USA). The analysis for volatile components was performed by GC-MS, a Hewlett Packard (Agilent Technologies, Palo Alto, California, USA) model 6870N gas chromatograph equipped with a mass selective detector (MS). The temperature in the part III

experiment was controlled by an EKT Hei−Con Heidolph electronic temperature controller (Heidolph Instruments, Schwabach, Germany).

3.2 Chemicals

The column chromatography was carried out with silica gel (60−200 μM) from SiliCycle (Quebec City, Quebec Canada), sephadex LH-20 from Cytiva (Marlborough, Massachusetts, USA), dowex 1×8-200 ion-exchange resin from Sigma-Aldrich (Burlington, Massachusetts, USA) and dianion HP−20. The semi-preparative HPLC column was purchased from Grace, Hichrom (Berkshire, UK). The AR grade solvents of dichloromethane, acetone, methanol, 95% ethanol, acetic acid and hydrochloric acid as well as HPLC grade of acetonitrile and methanol were purchased from RCI Labscan (Bangkok, Thailand). Dichloromethane and hexane (AR grade) were purchased from Macron Fine Chemicals, Avantor (Radnor, Pennsylvania, USA). α-Glucosidase (lyophilized powder) from *Saccharomyces cerevisiae*, *p*-nitrophenyl α-D-glucoside, and 2,2-Di(4-tert-octylphenyl)-1-picrylhydrazyl were purchased from Sigma Aldrich (Burlington, Massachusetts, USA). Sodium phosphate dibasic, sodium carbonate anhydrous and sodium acetate trihydrate were purchased from Loba chemie PVT.LTD. (Mumbai, India). Sodium di hydrogen phosphate was purchased from Kemaus (New South Wales, Australia). The absolute ethanol was purchased from Merck (Darmstadt, Germany).

3.3 Part I: Methodology for the investigation of chemical constituents from pericarp and seed of *A. mutica* and the α-glucosidase inhibitory activity of isolated compounds from the seed of *A. mutica*

3.3.1 Plant material

The fruits of *A. mutica* were collected in May 2018, in Phitsanulok Province, Thailand. The plant material was identified by Assist. Prof. Dr. Pranee Nangngam, Faculty of Science, Naresuan University. A voucher specimen (004360) was deposited at the Department of Biology, Faculty of Science, Naresuan University, Phitsanulok, Thailand.

3.3.2 Preparation of *A. mutica* pericarp and seed extracts

The fresh mature fruits of *A. mutica* were washed and air-dried for seven days at room temperature. The pericarps and seeds were separated. The dried pericarps (43 g) were extracted in dichloromethane (2 × 300 mL, 7 days for each extraction) at room temperature. The solution was subsequently filtered to separate solid residue from the organic solution. The solution was evaporated under vacuum to yield dichloromethane crude extract (3.1 g, AMPD). The solid residue from the dichloromethane extraction was taken to the second extraction with 95% ethanol (2 × 300 mL, 7 days for each extraction) and followed the same procedure to produce the ethanolic crude extract (0.68 g, AMPE).

The dried seeds (44 g) were macerated in *n*-hexane (2 × 300 mL, 7 days for each time) by following the extraction process of the pericarp to afford hexane crude extract (1.0 g, AMSH). The solid residue from the first maceration was extracted with dichloromethane (2 × 400 mL, 7 days for each time). The solution was then filtered to separate the second residue and evaporated to yield dichloromethane crude extract (2.4 g, AMSD). After that, the third solid residue was macerated in 95% ethanol (2 × 300 mL, 7 days for each time) for a total 14 days. The solution was filtered and evaporated to obtain an ethanol crude extract (1.4 g, AMSE). The extraction process of *A. mutica* pericarp and seed is shown in Figure 12.

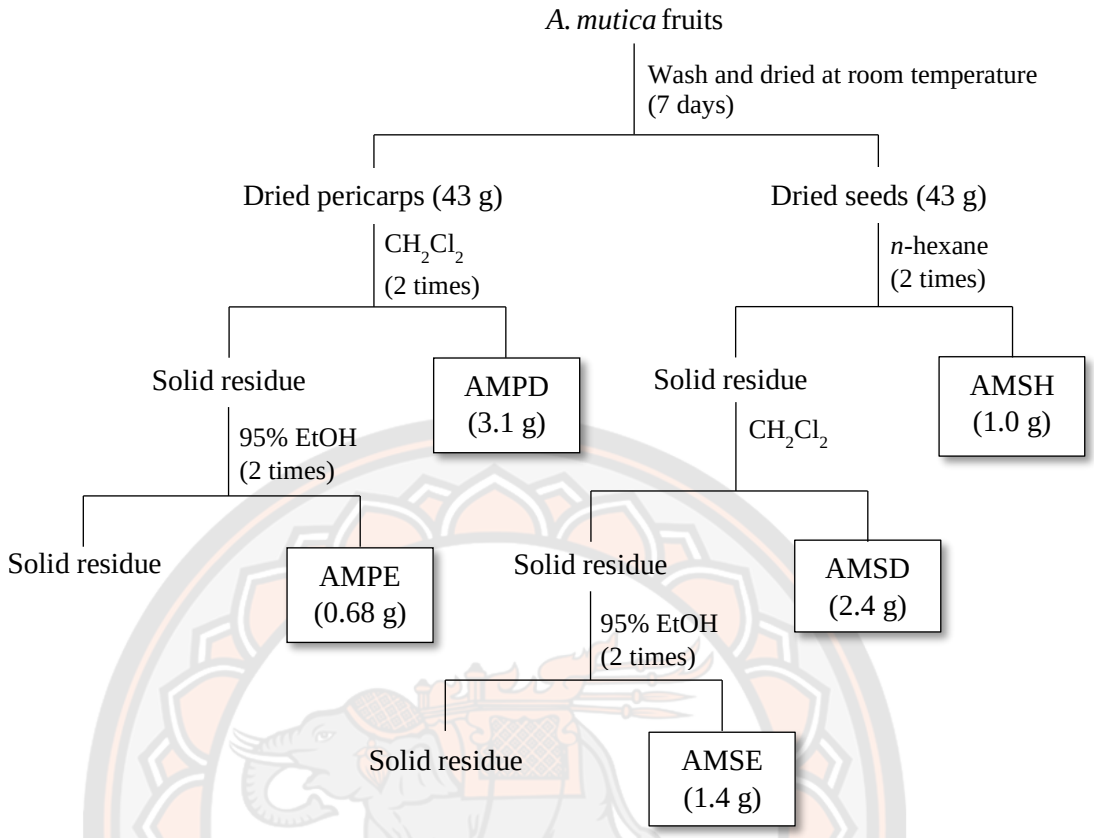

Figure 12 Extraction process of *A. mutica* pericarp and seed

3.3.3 GC-MS analysis of dichloromethane crude extracts from pericarp and seed of *A. mutica*

The AMPD and AMSD extracts were dissolved in dichloromethane at the concentration of 50 mg/mL and filtered. The two filtered sample solutions were then injected into a GC-MS. The condition parameters were as described by Suphrom et al. [80]. For the GC separation, a fused silica capillary HP−5 (5% phenyl methyl siloxane) column (30 m × 0.25 mm i.d., 0.25 μm film thickness) was employed. The carrier gas was high purity helium with a constant flow rate of 1.0 mL/min. The injection temperature was set to 250 °C, and the measurements were performed in split mode with a split ratio of 10:1 (volume per volume) in 1 μL. The temperature program for the GC oven was started at 70 °C and held for 3 min, then increased at 5 °C/min to 280 °C and held for 10 min. The temperature setting for the transfer line was 280 °C. Electron impact ionization mode at 70 eV was utilized for measurements.

The mass was scanned from 50 to 550 amu. The volatile components were identified by comparing the mass spectra to a standard library: Wiley 7n, and the National Institute of Standards and Technology (NIST) Chemistry WebBook. Retention indices (RIs) were determined by analyzing a solution containing the homologous series of *n*-alkanes (C_8−C_{20}) under the same chromatographic conditions and then calculating them as described by Van den Dool and Kratz [81]. The relative intensity of each volatile compound was calculated as the ratio of the area of the specific molecule to the sum of the areas of all identified peaks (peak area normalization method) in the chromatogram [82].

3.3.4 Isolation and purification of chemical constituents from *A. mutica* seed

CH_2Cl_2 crude extract (AMSD, 2.4 g) was subjected to a silica gel column and eluted with a gradient of sequential elution with the mixtures of *n*-hexane–CH_2Cl_2–EtOAc and CH_2Cl_2–MeOH in a gradient system to give five fractions (A-E). Fraction A (256 mg) was chromatographed on silica gel and eluted in the gradient system with *n*-hexane–CH_2Cl_2–EtOAc to give a compound **1** (43 mg). Fraction B (826 mg) was re-chromatographed with silica gel column using a gradient system of *n*-hexane–CH_2Cl_2–EtOAc as the eluent to obtain compounds **2** (618 mg) and **3** (66 mg). Fraction C was subjected to silica gel column chromatography and eluted with *n*-hexane–CH_2Cl_2–acetone in the gradient system to yield compound **4** (35 mg). Fraction D (153 mg) was isolated by silica gel column chromatography and eluted with *n*-hexane–CH_2Cl_2–acetone (gradient system) to give sub-fractions D1–D3. Sub-fraction D2 (27 mg) was separated using semi-preparative HPLC (eluted with ACN:H_2O, 80:20 v/v) to yield sub-fractions D2-1 and D2-2. Compound **5** (12 mg) was obtained from sub-fraction D2-1. Sub-fraction D2-2 (12 mg) was repeatedly purified on silica gel column with *n*-hexane–CH_2Cl_2–acetone in gradient system to give compound **6** (2 mg). Compound **7** (78 mg) was obtained as a crystal from fraction E (295 mg). The isolation flowchart of AMSD extract is shown in Figure 13.

3.3.5 Assay for α-glucosidase inhibitory activity

The assay was conducted with minor modifications to the methods described by Dong et al. [57] and Matsui et al. [83] with slight. Samples were dissolved in DMSO and diluted with 0.1 M phosphate buffer (pH 6.8). Briefly, 60 μL of sample solution and 50 μL of 0.1 M phosphate buffer (pH 6.8) containing α-glucosidase solution (0.2 U/ml) were incubated in 96 well plates at 37 °C for 10 min. followed by the addition of 50 μL of 2.5 mM *p*-NPG solution in 0.1 M phosphate buffer (pH 6.8). The enzymatic reaction was allowed to proceed at 37 °C for 20 min before being stopped by adding 40 μL of 0.2 M Na_2CO_3 solution. The mixture was then measured using a microplate reader at 405 nm. A standard α-glucosidase inhibitor acarbose was used as a positive control. A solution containing only 5% DMSO in 0.1 M phosphate buffer (pH 6.8) was used as a control including. The percentage of α-glucosidase inhibition was calculated using the following equation (1):

$$Inhibitory\ activity\ (\%) = 100 - \left[\left(\frac{Abs_{sample}}{Abs_{control}}\right) \times 100\right] \qquad (1)$$

where Abs_{sample} = Absorbance of the sample solution at 405 nm

$Abs_{control}$ = Absorbance of the blank solution at 405 nm

3.3.6 Statistical analysis

All of the experiments of α-glucosidase assay were carried out in triplicate and represented by mean ± standard deviation (SD). Statistical comparisons were analyzed using one-way analysis of variance (ANOVA), followed by Duncan's test. Differences were considered significant when $p < 0.05$.

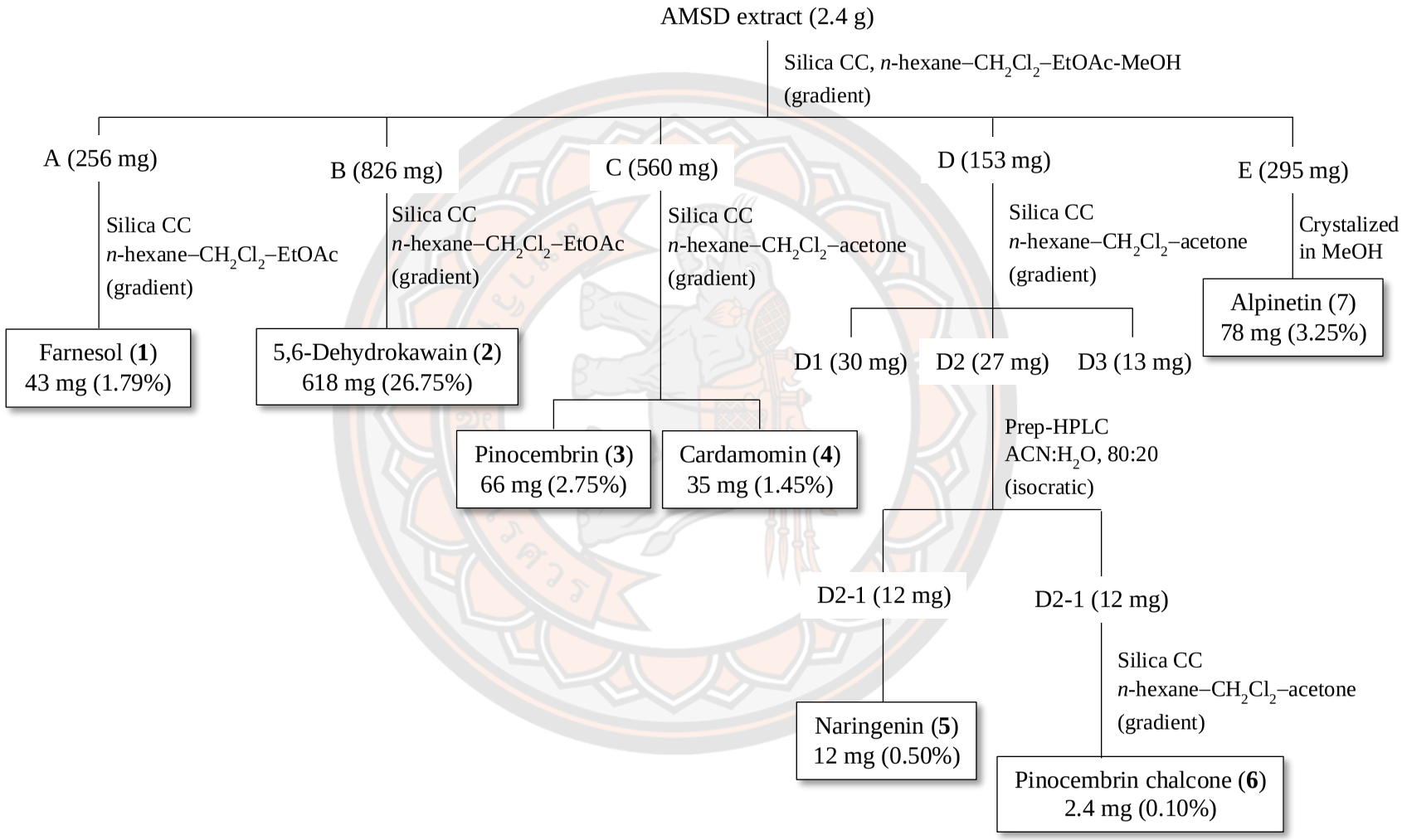

Figure 13 Isolation flowchart of AMSD extract

3.4 Part II: Methodology for the investigation of chemical constituents, α-glucosidase inhibitory and antioxidant activities of *L. strychnifolium*

3.4.1 Plant material

The roots, stems, leaves and flowers of *L. strychnifolium* were collected in November 2019, February 2020, April 2020 and June 2020, respectively, from the Department of Chemistry, Faculty of Science, Naresuan University, Phitsanulok, Thailand. The plant material was identified by Assist. Prof. Dr. Pranee Nangngam, Faculty of Science, Naresuan University. A voucher specimen (specimen number 004064) was deposited at the Department of Biology, Faculty of Science, Naresuan University, Phitsanulok, Thailand.

3.4.2 Extraction and isolation of chemical constituents from the root of *L. strychnifolium*

The fresh roots (50 g) were cut into small pieces and extracted with 95% EtOH (2 × 300 mL, 15 days for each time) at room temperature. The combined solvent was evaporated under reduced pressure to yield the ethanolic extract (LSR, 8.4 g), which was then evaluated for its α-glucosidase inhibiting and antioxidant properties. The root extract (7.9 g) was chromatographed on a silica gel column and eluted with a gradient of CH_2Cl_2 and MeOH to produce three fractions (A1−A3) based on the TLC profile. Fraction A2 (2.3 g) was washed with acetone and MeOH to yield compound **8** (1.6 g). Fraction A3 (5 g) was chromatographed on silica gel using a gradient system eluting with CH_2Cl_2 and MeOH in a to give sub-fractions A3-1 and A3-2. Sub-fraction A3-1 (4.1 g) was washed with acetone and MeOH to yield **8** (3.8 g). Sub-fraction A3-2 (580 mg) was repeatedly purified on a silica gel column with CH_2Cl_2 and MeOH in a gradient system to give compounds **9** (57 mg) and **18** (12 mg). The isolation flow chart of LSR is shown in Figure 14.

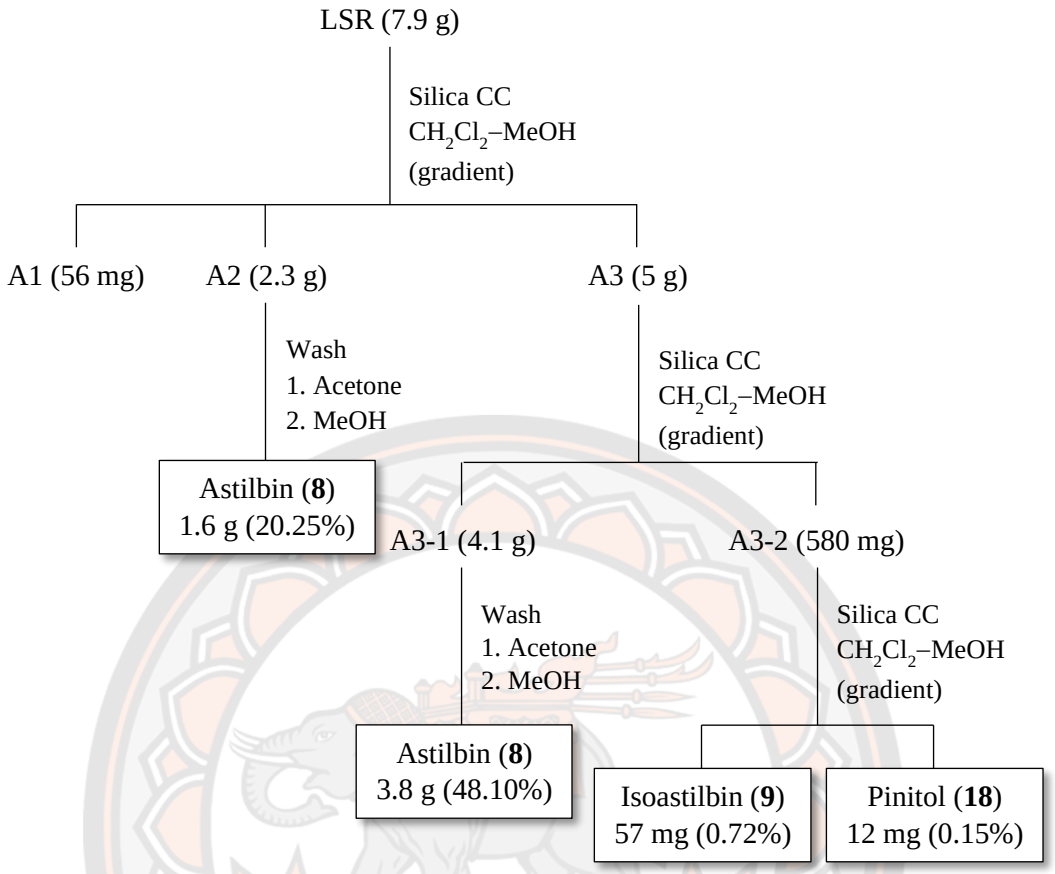

Figure 14 Isolation flowchart of LSR extract

3.4.3 Extraction and isolation of chemical constituents from the stem of *L. strychnifolium*

The fresh stems (200 g) were chopped into small pieces and macerated with 95% EtOH (2 × 1.5 L, 15 days for each time) at room temperature. The combined ethanolic extracts were concentrated using a rotary evaporator to produce 12.7 g of reddish-brown stem ethanolic extract (LSS), which was then evaluated for its α-glucosidase inhibitory and antioxidant activities. The stem ethanolic extract (10.9 g) was separated on a sephadex LH-20 column eluted with MeOH to afford five major fractions (B1–B5). During the process, compound **18** (705 mg) precipitated from fraction B1 (3.9 g) as a white solid. Fraction B2 (1.6 g) was chromatographed on a sephadex LH-20 and eluted with MeOH to give sub-fractions B2-1 to B2-3. Sub-fraction B2-2 (1.2 g) was fractionated using silica gel column chromatography, eluting with a gradient of CH_2Cl_2 and MeOH formed sequentially to yield three sub-

fractions (B2-2a – B2-2c). Sub-fraction B2-2c (543 mg) was further purified on a silica gel column and eluted with a gradient of CH_2Cl_2 and MeOH to yield compound **18** (271 mg). Fraction B3 (1.3 g) was eluted with MeOH from a sephadex LH-20 column, yielding sub-fractions B3-1 and B3-2. Sub-fraction B3-1 (733 mg) was fractionated on a silica gel with the mobile phase of the two mixtures, CH_2Cl_2 and MeOH, with increasing polarity to give four sub-fractions (B3-1a–B3-1d). Fraction B3-1c (476 mg) was repeatedly separated on a silica gel column eluted with a gradient of CH_2Cl_2 and MeOH to yield five sub-fractions (B3-1c1 – B3-1c5). Compounds **10** (36 mg) and **11** (32 mg) were isolated by semipreparative HPLC from sub-fraction B3-1c2 (170 mg). The eluent was monitored at 254 and 290 nm using a semi-preparative column (Grace platinum EPS C18 100A 5u column) with an injection volume of 50 μL. The solvent system consisted of 65% water and 35% MeOH in an isocratic system with a flow rate of 2.5 mL/min. Sub-fraction B3-1c5 (102 mg) was isolated using a silica gel column eluted with a gradient of CH_2Cl_2 and MeOH to give compound **9** (16 mg). Fraction B4 (533 mg) was fractionated using a silica column chromatography with a gradient mobile phase system of CH_2Cl_2–MeOH to give compound **13** (76 mg). The purification of fraction B5 (354 mg) was performed using a silica gel column with CH_2Cl_2–MeOH in a gradient system, giving compound **12** (17.4 mg). The isolation flow chart of LSS is shown in Figures 15–17.

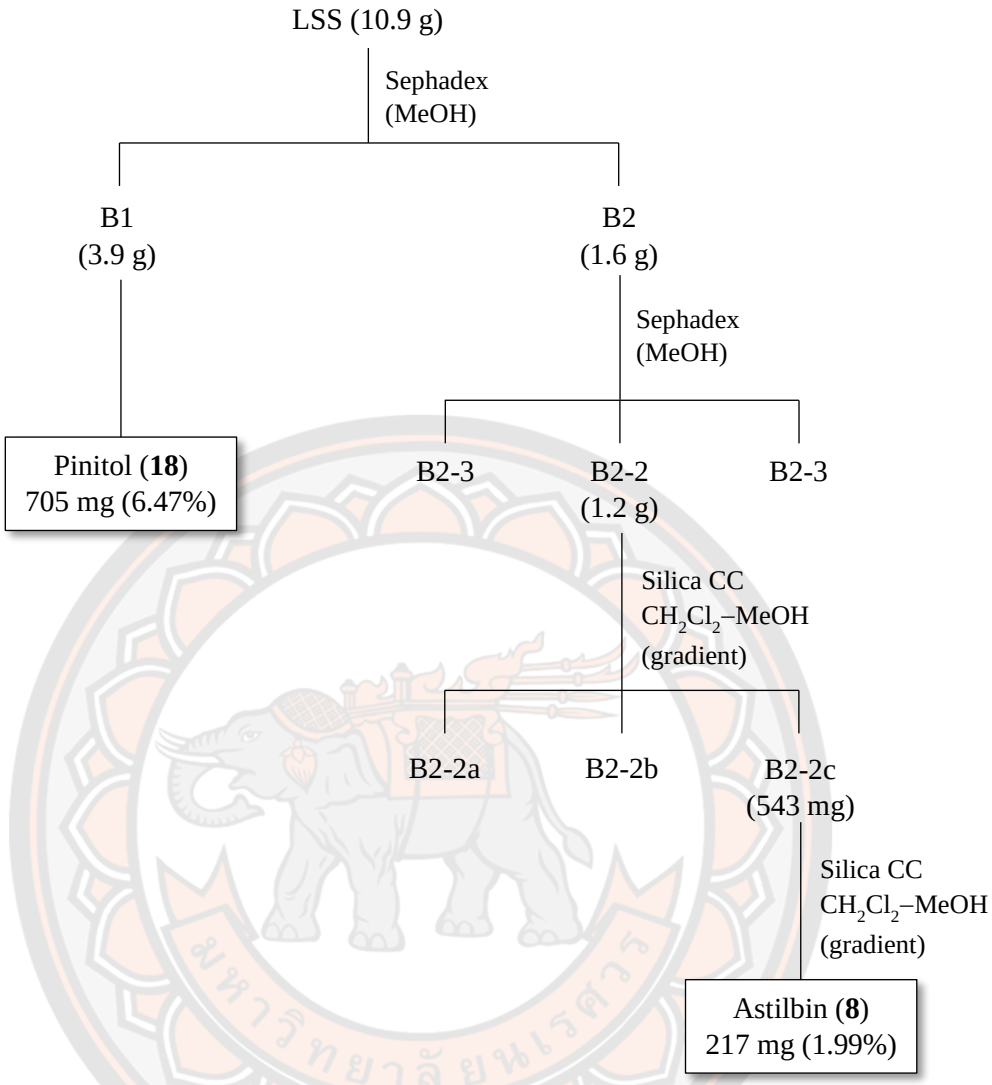

Figure 15 Isolation flowchart of LSS extract (fractions B1 and B2)

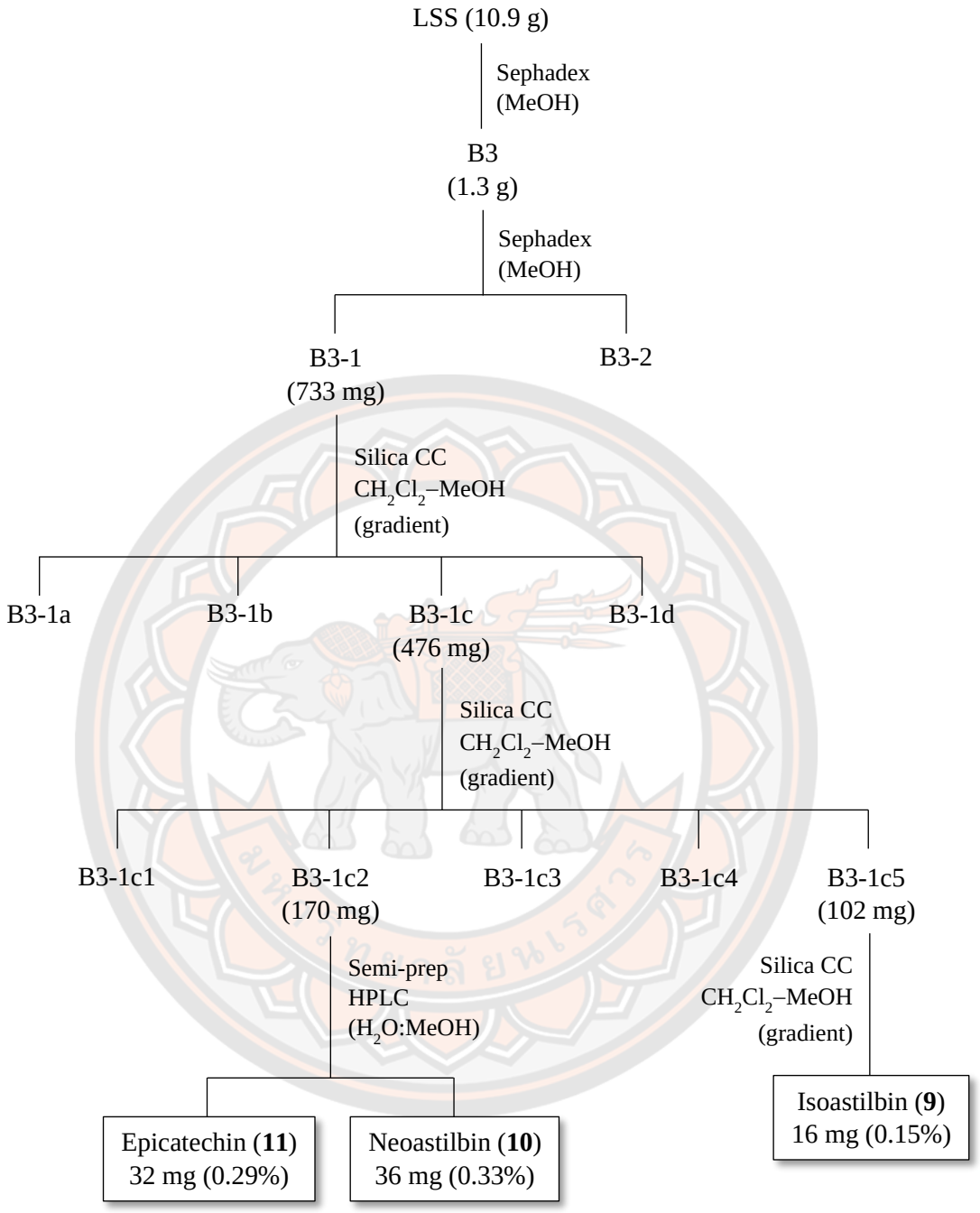

Figure 16 Isolation flowchart of LSS extract (fraction B3)

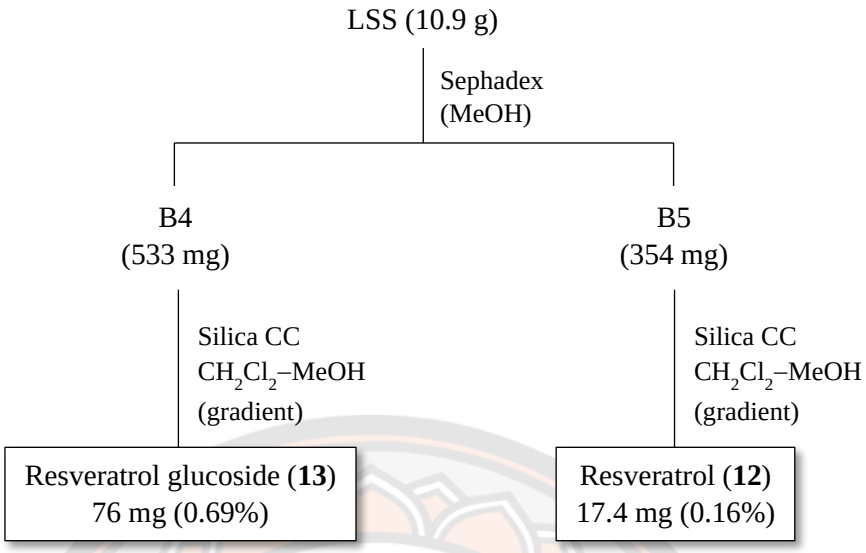

Figure 17 Isolation flowchart of LSS extract (fractions B4 and B5)

3.4.4 Extraction and isolation of chemical constituents from the leaves of *L. strychnifolium*

The dried leaves (135 g) were extracted with 95% EtOH (2 × 2 L, 15 days for each time) at room temperature. The extracts were evaporated under vacuum to yield a dark green crude extract (LSL, 5.9 g). After testing the α-glucosidase inhibitory and antioxidant activities, the leaves extract (2.35 g) was fractionated using sephadex LH-20 column chromatography and eluted with MeOH to obtain five fractions (C1–C5). Compound **18** (520.3 mg) was precipitated from fraction C1 (697.2 mg). Fraction C2 (437 mg) was purified by silica column chromatography with a gradient mobile phase system of MeOH–CH_2Cl_2 to give compound **16** (368 mg). Fraction C4 (89 mg) was purified by silica gel column chromatography with a gradient system to yield compound **15** (56 mg). Fraction C5 (408.2 mg) was separated using a silica gel column with a gradient solvent system of MeOH–CH_2Cl_2, resulting in compounds **14** (16.4 mg) and **17** (253 mg). The isolation flow chart of LSL is shown in Figure 18.

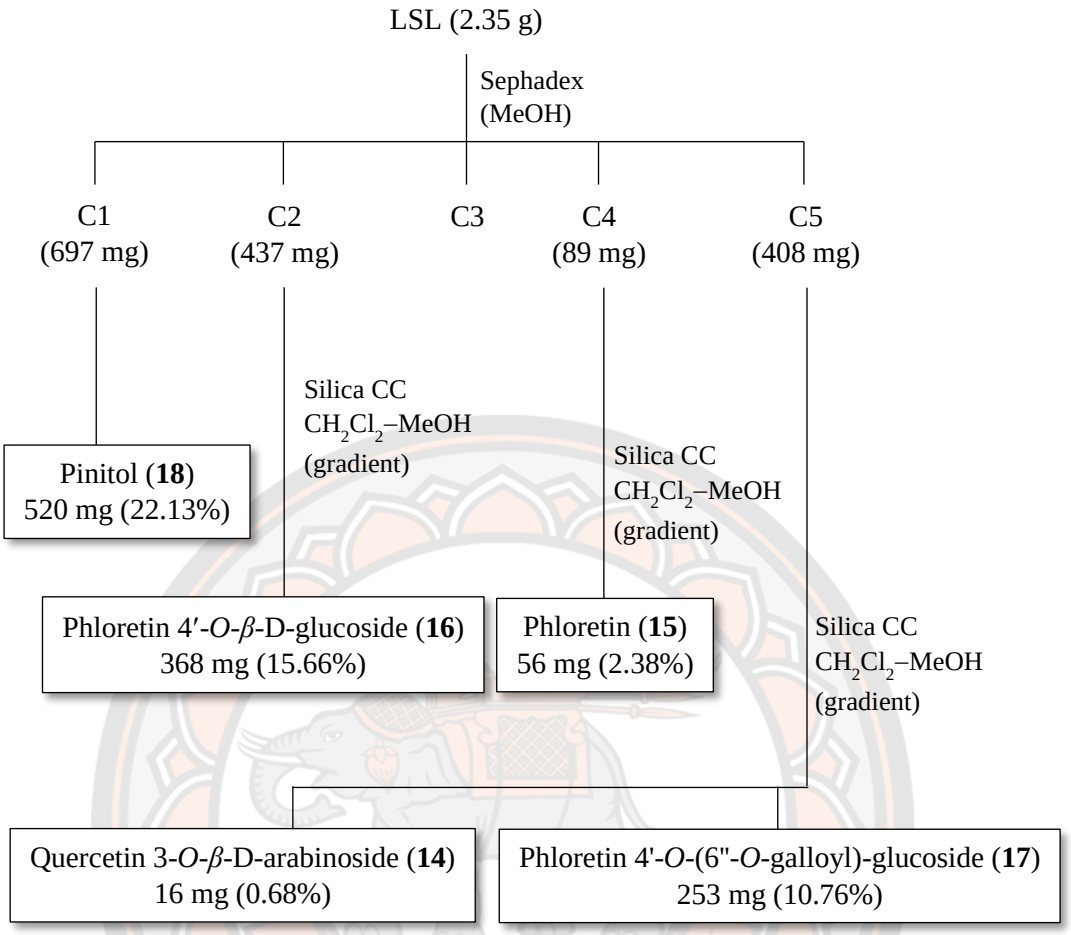

Figure 18 Isolation flowchart of LSL extract

3.4.5 Extraction and isolation of chemical constituents from the flower of *L. strychnifolium*

The fresh flowers (44 g) were extracted with 95% EtOH (2 × 1 L, 15 days, for each time) at room temperature. The extracts were evaporated under a vacuum to obtain flower ethanolic extract (LSF, 9.3 g). After evaluating the biological activities of the extract, the extract (3 g) was fractionated using sephadex LH-20 column chromatography and eluted with MeOH to give three fractions (D1–D3). Compound **18** (841.6 mg) was precipitated from fraction D1 (2.37 g) during the process. Fraction D2 (223.6 mg) was purified on a sephadex LH-20 column using MeOH as the mobile phase to obtain compound **19** (67 mg). Fraction D3 (205.9 mg) was purified by a silica column to afford compounds **16** (43 mg) and **20** (85 mg). The isolation flow chart of LSF is shown in Figure 19.

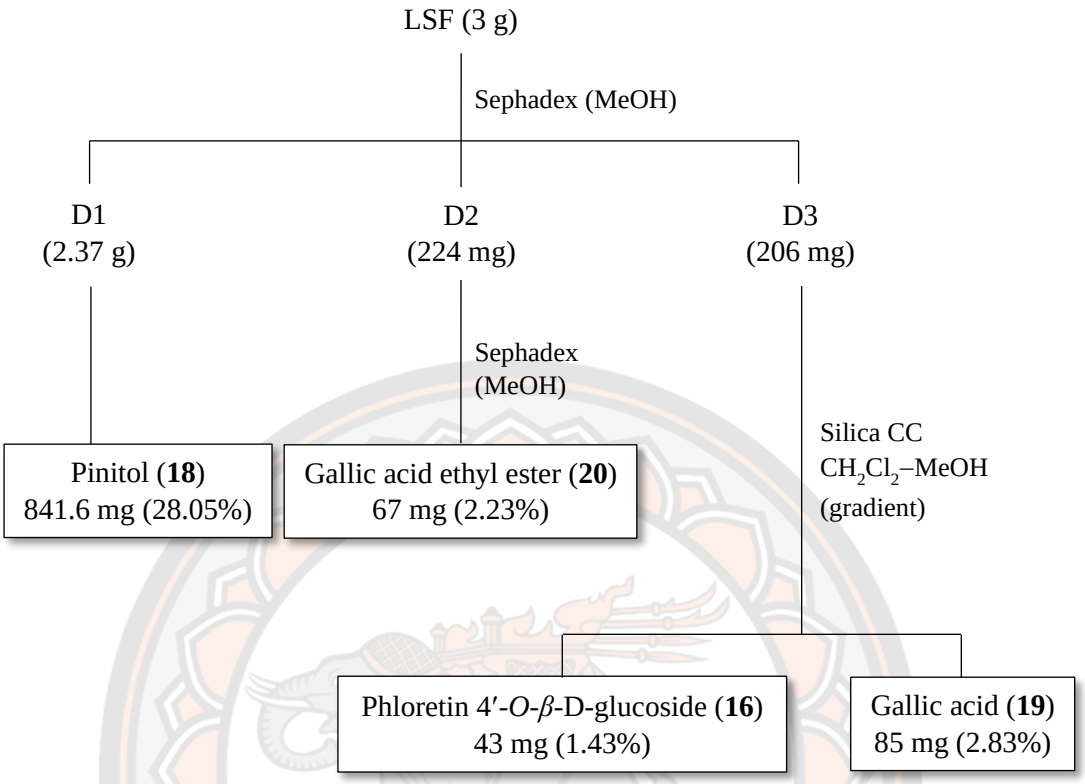

Figure 19 Isolation flowchart of LSF extract

3.4.6 α-Glucosidase inhibitory assay

The α-glucosidase inhibitory activity of crude extracts and isolated compounds was determined using α-glucosidase assay as described in 3.3.5.

3.4.7 DPPH radical scavenging assay

The free radical scavenging activity of extracts was determined using the DPPH method described by Piangpraichom et al. [84]. The experiment was carried out in a 96-well microplate with a total volume of 200 μL. The 100 μL of samples were placed to a well-microplate. The reaction was started by adding of 500 μM DPPH (in absolute EtOH) to each well. An equal volume of absolute EtOH was used as a control. The mixture was left for 30 min at room temperature and in the dark. The decrease in absorbance (Abs) of the resulting solution was then measured at 515 nm

using a microplate reader. L-ascorbic acid and trolox were used as positive controls. DPPH radical scavenging activity (%) was calculated using equation (2):

$$DPPH\ radical\ scavenging\ activity\ (\%)\ =\ 100 - \left[\left(\frac{Abs_{sample}}{Abs_{control}}\right) \times 100\right] \quad (2)$$

where A_{sample} = Absorbance of the sample at 515 nm

$A_{control}$ = Absorbance of the solution without sample at 515 nm

3.4.8 Statistical analysis

All of the experiments of α-glucosidase assay were carried out in triplicate and represented by mean ± standard deviation (SD). Statistical comparisons were analyzed using one-way analysis of variance (ANOVA), followed by Duncan's test. Differences were considered significant when $p < 0.05$.

3.5 Part III: Methodology for determining the optimal conditions for brewing tea from *L. strychnifolium* leaves

3.5.1 Plant material

Fresh leaves of *L. strychnifolium* were collected from from the Department of Chemistry, Faculty of Science, Naresuan University, Phitsanulok, Thailand in March and April 2019. The plant material was identified by Assist. Prof. Dr. Pranee Nangngam, Faculty of Science, Naresuan University. A voucher specimen (specimen number 004064) was deposited at the Department of Biology, Faculty of Science, Naresuan University, Phitsanulok, Thailand.

3.5.2 Preparation of tea infusions from *L. strychnifolium* leaves

The fresh leaves were washed and dried in a hot air oven at 50°C for 24 hr. The dried leaves were ground into a powder and kept in a desiccator at room temperature prior to being brewed with water. In experiments to determine the effects of time and temperature on the infusion procedure, the ratio of leaf powder to water was fixed at 1:60 (g/mL). The optimal time and temperature were used to investigate the effect of water volume. The infusion process was performed with a hot plate stirrer at

750 rpm. The slurry solution was filtered through Whatman filter paper No. 5 (7 cm) using a Buchner funnel and a vacuum supply into a 250 mL filter flask. The aqueous solution was evaporated until dry, and the remaining residue was weighed. To study the effect of the multiple infusion, 5 g of leaf powder was infused with varying amounts of water in a single or multiple steps. The temperature in the experiment was controlled by the electronic temperature controller.

3.5.3 Isolation and purification of chemical constituents from *L. strychnifolium* leaf tea

The leaf powder of *L. strychnifolium* (25 g) was brewed under the optimal conditions determined in a previous experiment to obtain the crude extract (6.37 g, 25.48%). The crude extract was isolated by dianion HP-20 column chromatography and eluted using a gradient system of 1:0 to 0:1 (v/v) water–MeOH ratio. A total of 80 fractions (A1–A80, 50 mL for each) were obtained. The water fractions (A1–A15) were combined and evaporated to yield 2.90 g of residue. The residue was then suspended in MeOH to afford soluble and insoluble portions. The soluble portion was evaporated to produce 1.8 g of residue, which was then isolated using anion-exchange column chromatography. In order to perform anion exchange column chromatography, 40 g of Dowex 1×8-200 anion exchange resin was prepared in deionized water and packed into a glass column. First, 1 M of sodium hydroxide (100 mL) was passed through the column, followed by 2 M of sodium acetate (250 mL). Crude MeOH extract was dissolved in deionized water and loaded into the column. The column was eluted with 100 mL of deionized water followed by 150 mL of 25% acetic acid. The 15 fractions (B1–B15, 15 mL of each) were collected and the solvent was removed by evaporation. Fraction B4 was identified as a pure compound **18** (1.25 g). Fraction B14 (307.3 mg) was washed with methanol to afford 166.5 mg of **2**. Fractions A51–A65 (2.07 g) were pooled and subjected to a Sephadex LH-20 column eluted with MeOH to give 40 subfractions (C1–C40, 25 mL for each). Compound **3** (1.28 g) was derived from subfractions C21–C26. The isolation of the LSW extract is shown in Figure 20.

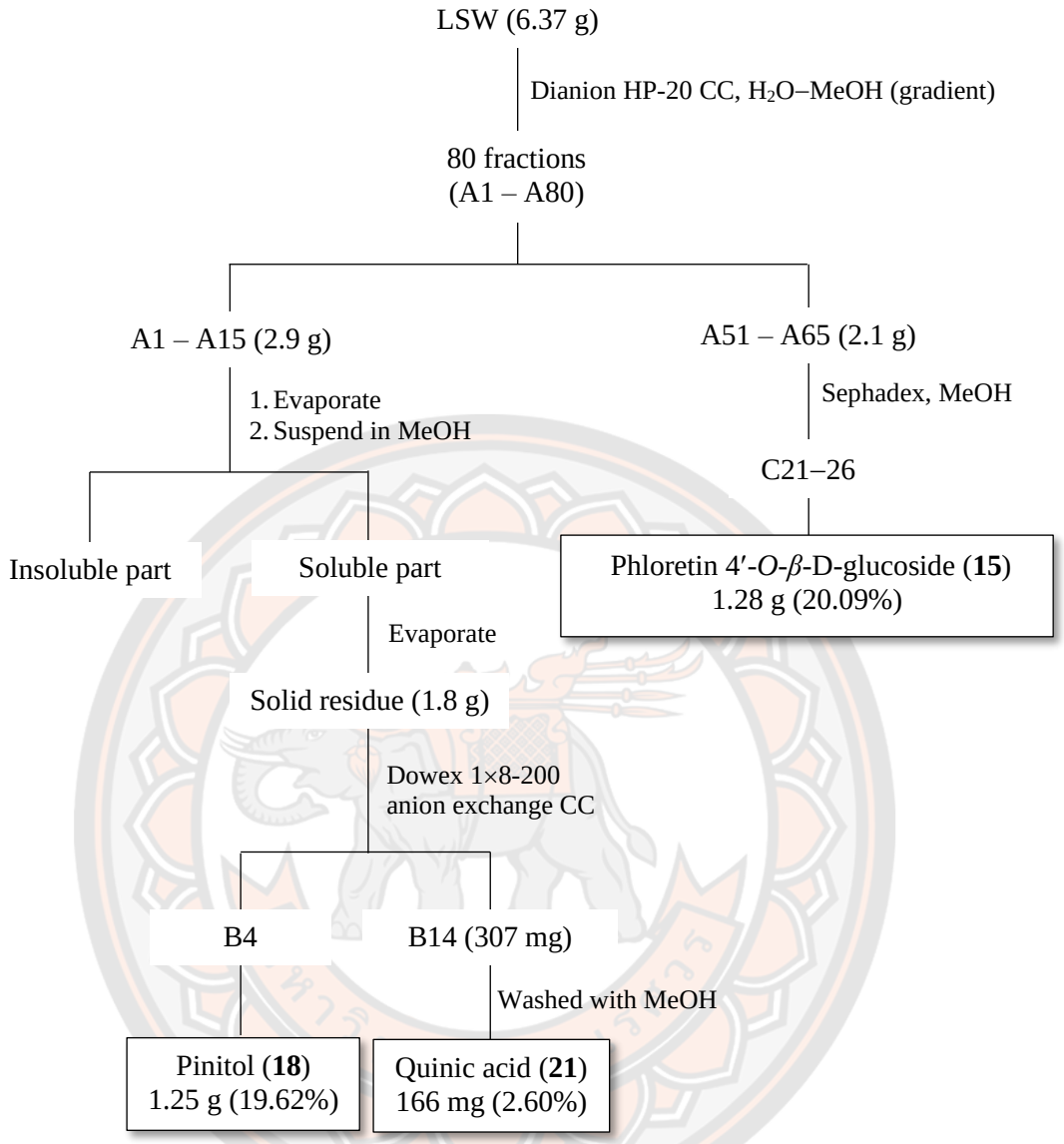

Figure 20 Isolation flowchart of LSW extract

CHAPTER IV
RESULTS AND DISCUSSION

According to the present work is divided into three sections, as described in Chapter 3, the results and discussion for each section are described below.

4.1 Part I: The investigation of chemical constituents from pericarp and seed of *A. mutica* and the α-glucosidase inhibitory activity of isolated compounds from the seed of *A. mutica*

4.1.1 Extraction yields and crude extract from pericarp and seed of *A. mutica*

The dried pericarps of *A. mutica* were sequentially extracted with dichloromethane and 95% ethanol to obtain AMPH and AMPE crude extracts. In addition, the dried seeds were extracted with *n*-hexane, dichloromethane and 95% ethanol, respectively, to afford AMSH, AMSD and AMSE crude extracts. The weight and extraction yield of the crude extracts from the pericarps and seeds are presented in Table 6. The dichloromethane crude extract of pericarp (AMPD) and seed (AMSD) demonstrated greater weight and yield than the other extracts.

Table 6 Weight and extraction yield of crude extracts from pericarp and seed of *A. mutica*

Part of *A. mutica* used	Extraction solvents	Crude extracts[a]	Weight (g)	% Yield[b]
Pericarp	CH_2Cl_2	AMPD	3.1013	7.21
	95% EtOH	AMPE	0.6848	1.59
Seed	*n*-hexane	AMSH	0.9990	2.27
	CH_2Cl_2	AMSD	2.4283	5.52
	95% EtOH	AMSE	1.3710	3.12

[a]AM: *A. mutica*, P: Pericarp, S: Seed, D: dichloromethane, E: 95% Ethanol, H: Hexane; [b]% Yield was reported in terms of weight by dried weight of raw material.

Moreover, ^{1}H NMR spectroscopy was used to preliminary identify and compare the secondary metabolite groups in the pericarp and seed of *A. mutica*. Overall, the ^{1}H NMR profiles of pericarp extract (Figures 21(a) and 21(b)) revealed

similar signals for four regions of proton signals. The signals of the aromatic proton (δ 6–8 ppm), double bond proton (δ 6–5.5 ppm), methoxy proton (δ 3.5–4 ppm), and aliphatic proton (δ 0–2 ppm) were presented in the dichloromethane (AMPD) and ethanol (AMPE) extracts of the pericarp (AMPD and AMPE). Similar spectra were observed for the ^{1}H NMR spectra of the seed extracts ((Figures 21(c), 21(d) and 21(e)). The hexane (AMSH), dichloromethane (AMSD) and ethanol (AMSE) extracts of the seed displayed the signal of the aromatic proton (δ 7–8 ppm), double bond proton (δ 5.5–6.5 ppm), methoxy proton (δ 3.5–4 ppm), and aliphatic proton (δ 1-2 ppm). However, the clear spectra with the highest yield were observed from the dichloromethane extract of the pericarp and seed. To fill the gap in the chemical composition of *A. mutica* pericarp and seed, the GC–MS analysis of dichloromethane extract of the pericarp (AMPD) and seed (AMSD) was performed in this study.

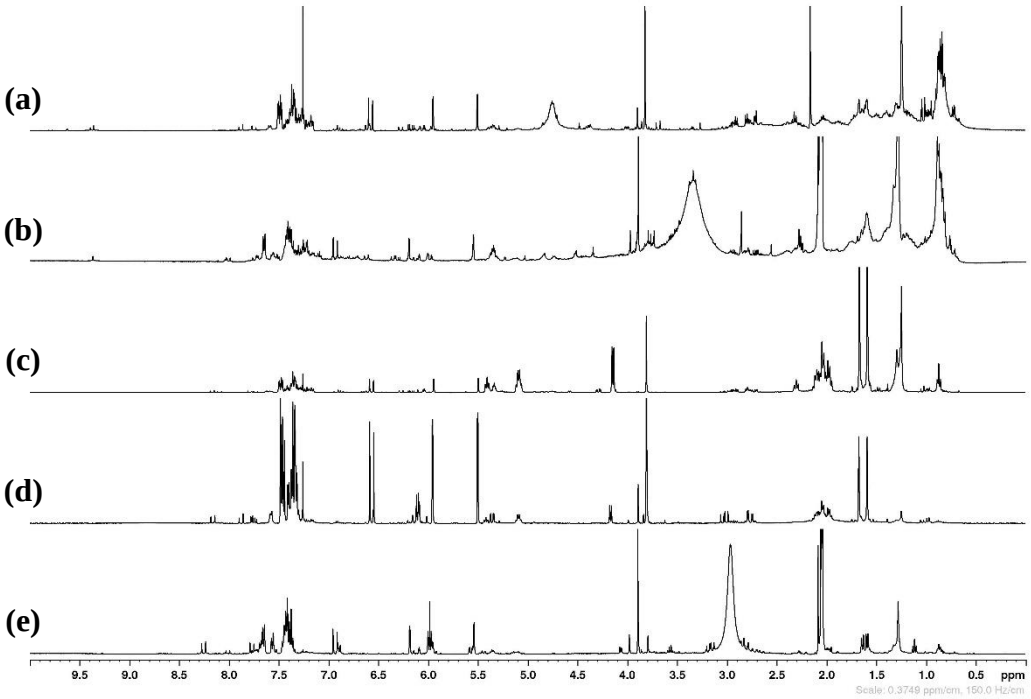

Figure 21 ^{1}H NMR (400 MHz) spectra of *A. mutica* extracts from different solvents; (a) AMPD in $CDCl_3$, (b) AMPE in acetone-d_6, (c) AMSH in $CDCl_3$, (d) AMSD in $CDCl_3$, (e) AMSE in acetone-d_6

4.1.2 GC–MS analysis of dichloromethane crude extracts from pericarp and seed of *A. mutica*

The volatile components of dichloromethane extracts from the pericarp and seed were analyzed by GC–MS. Slightly different profiles of the volatile compositions in the AMPD and AMSD extracts were observed (Figure 22). Ten compounds and eleven compounds were identified in the pericarp and seed extracts, respectively. The relative amount (%) of the compositions was calculated by peak-area normalization. As listed in Table 5, the relative amounts of total identified compounds in the pericarp and seed were calculated as 94.96% and 99.24%, respectively. In *A. mutica* pericarps, the majority of the volatile compounds (RT 39.50 min) was diarylheptanoid, namely 1,7-diphenyl-4,6-heptadien-3-one, which was about 45.28% of the detected compounds. As well, the various groups of compounds, including stryrylpyrone, fatty acids, and phenyl derivatives, were also distributed as the minor components. These minor compounds included 5,6-dehydrokawain, palmitic acid, linoleic acid, phenyl butanone, and cinnamaldehyde.

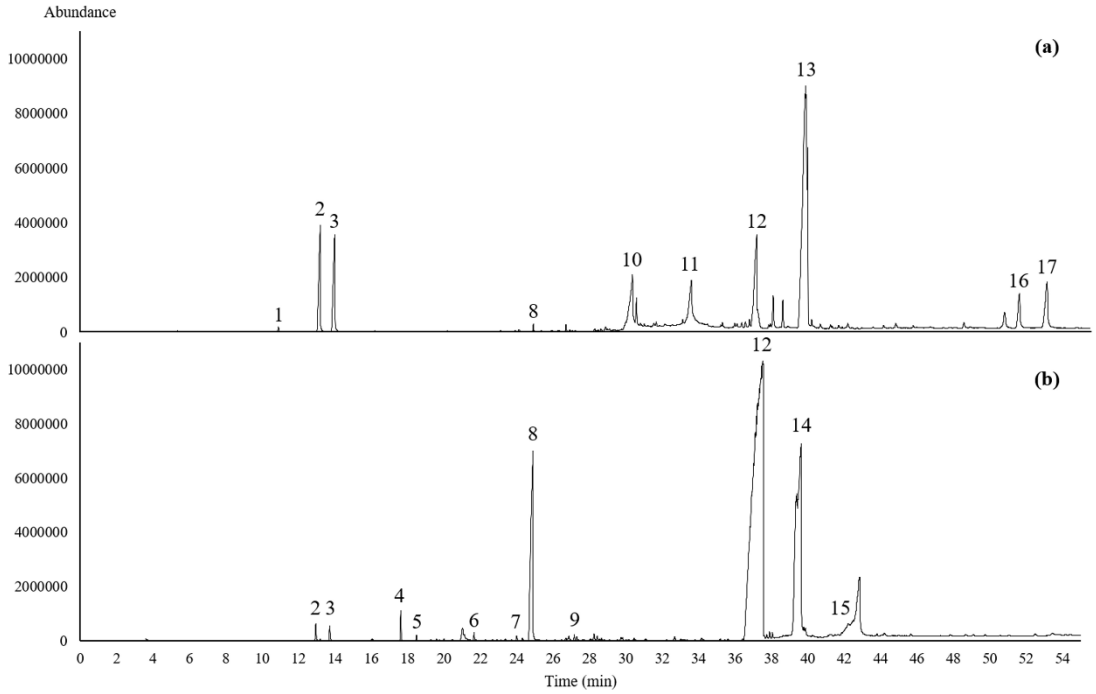

Figure 22 Total ion chromatograms of (a) AMPD and (b) AMSD crude extracts

As shown in Figures 22(b) and Table 7, the chemical components of the seed extract were styrylpyrone, flavonoids, and sesquiterpenes, with 5,6-dehydrokawain (64.94%), pinocembrin (22.51%) and farnesol (9.18%) as major components. Two flavonoids (RT 39.63 min and 42.48 min) were only presented in the seed extract, whereas sesquiterpenes, phenyl derivatives and styrylpyrones compounds were present in both the pericarp and seed extracts. Notably, the relative contents of these three classes of compounds in the pericarp and seed extracts were dramatically different. The chemical structures of volatile components from pericarp and seed extract are shown in Figures 23 and 24.

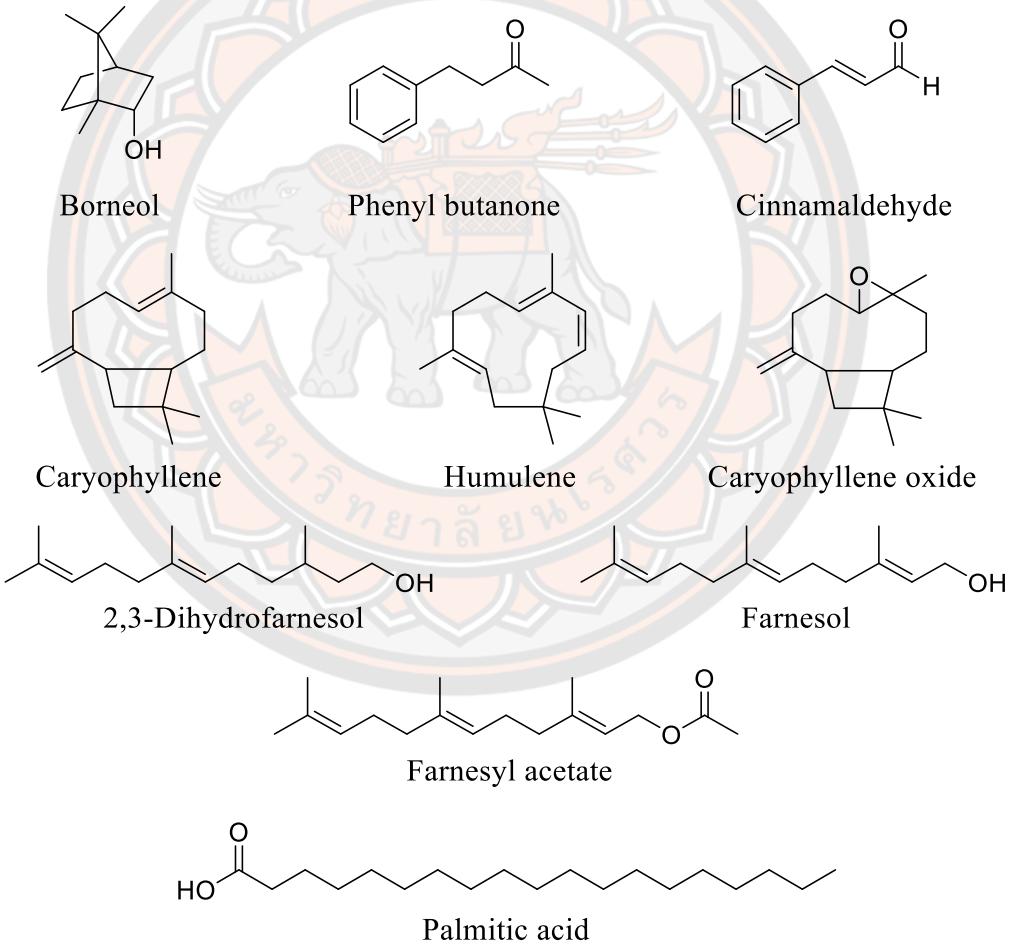

Figure 23 Chemical structures of volatile components consist of terpenes and fatty acids from the dichloromethane extracts of pericarp and seed from *A. mutica*

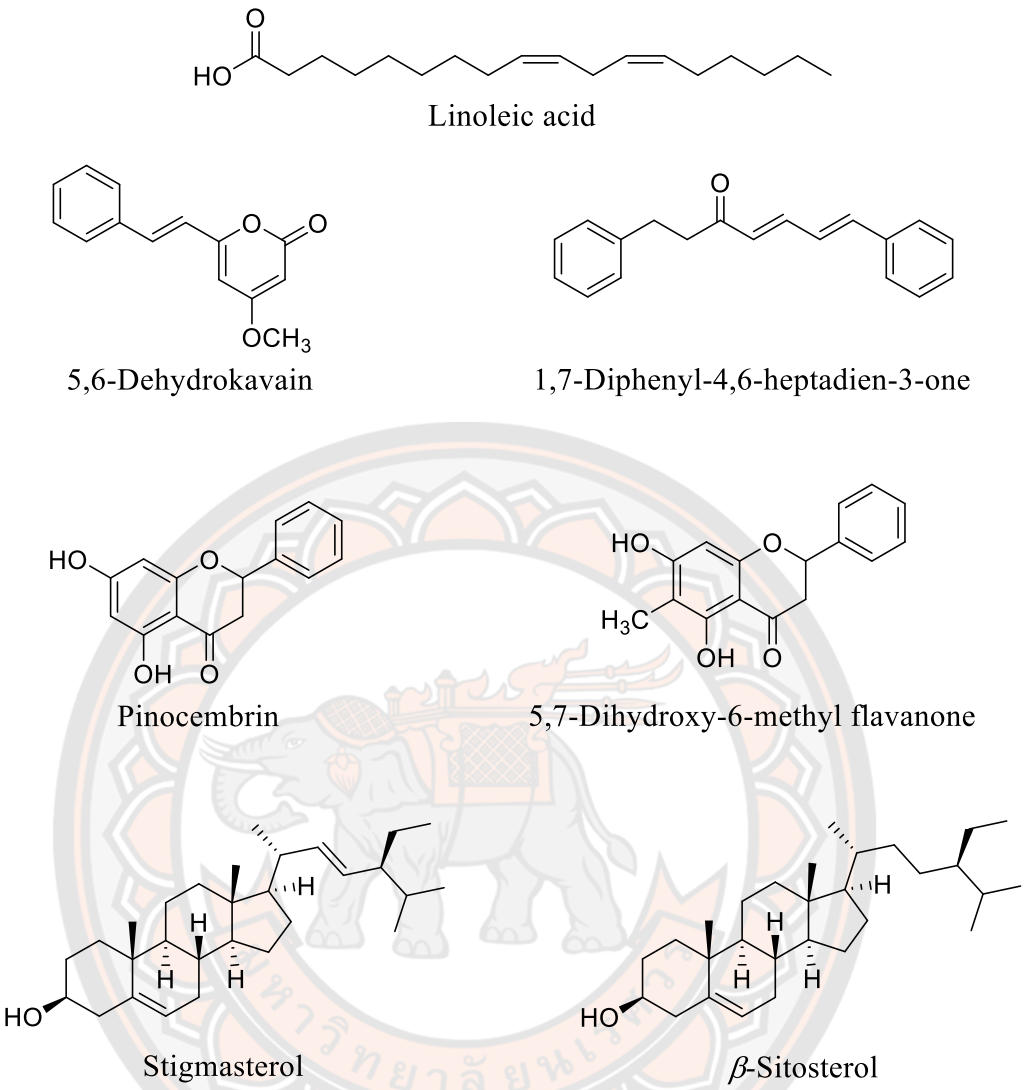

Figure 24 Chemical structures of volatile components consist of fatty acid, stryrylpyrone, diarylheptanoid, flavonoids and steroids from the dichloromethane extracts of pericarp and seed from *A. mutica*

Table 7 Volatile compositions of the dichloromethane extracts of pericarp and seed from *A. mutica*

Peak	RT[1]	RI_{exp}[2]	RI_{lit}[3]	Identified compounds	Molecular formula	Classification	Relative amount (%)[4]	
							AMPD	AMSD
1	10.79	1164	1168 [85]	Borneol	$C_{10}H_{18}O$	Monoterpene	0.21	nd
2	12.95	1240	1243 [86]	Phenyl butanone	$C_{10}H_{12}O$	Phenyl derivative	7.77	0.37
3	13.72	1268	1258 [87]	Cinnamaldehyde	C_9H_8O	Phenyl derivative	7.64	0.32
4	17.62	1415	1419 [88]	Caryophyllene	$C_{15}H_{24}$	Sesquiterpene	nd	0.54
5	18.48	1449	1454 [87]	Humulene	$C_{15}H_{24}$	Sesquiterpene	nd	0.10
6	21.65	1579	1583 [85]	Caryophyllene oxide	$C_{15}H_{24}O$	Sesquiterpene	nd	0.13
7	24.00	1683	1684 [89]	2,3-Dihydrofarnesol	$C_{15}H_{28}O$	Sesquiterpene	nd	0.10
8	24.87	1722	1740 [85]	Farnesol	$C_{15}H_{26}O$	Sesquiterpene	0.28	9.18
9	27.16	1830	1812 [90]	Farnesyl acetate	$C_{17}H_{28}O_2$	Sesquiterpene	nd	0.10
10	30.08	1976	1970 [91]	Palmitic acid	$C_{16}H_{32}O_2$	Fatty acid	7.87	nd
11	33.28	2149	2159 [91]	Linoleic acid	$C_{18}H_{32}O_2$	Fatty acid	6.77	nd
12	36.84	2456	2352 [92]	5,6-Dehydrokavain	$C_{14}H_{12}O_3$	Stryrylpyrone	10.37	64.94
13	39.50	2542	-	1,7-Diphenyl-4,6-heptadien-3-one	$C_{19}H_{18}O$	Diarylheptanoid	45.28	nd
14	39.63	2545	2513	Pinocembrin	$C_{15}H_{12}O_4$	Flavonoid	nd	22.51
15	42.48	2704	-	5,7-Dihydroxy-6-methyl flavanone	$C_{16}H_{13}O_4$	Flavonoid	nd	0.95

nd: Not detected, [1]RT: Retention time (min); [2]RI_{exp}: Experiment retention index obtained from the relative calculation of to C_8-C_{20} *n*-alkane series;

[3]RI_{lit}: Retention index found in reported literature; [4]Relative amount was obtained by peak normalization

Table 7 (cont.)

Peak	RT[1]	RI_{exp}[2]	RI_{lit}[3]	Identified compounds	Molecular formula	Classification	Relative amount (%)[4]	
							AMPD	AMSD
16	51.14	-	-	Stigmasterol	$C_{29}H_{48}O$	Triterpene	3.40	nd
17	52.65	-	-	*β*-Sitosterol	$C_{29}H_{50}O$	Triterpene	5.37	nd
				Total monoterpenes			0.21	-
				Total sesquiterpenes			0.28	10.15
				Total triterpenes			8.77	-
				Total diarylheptanoid			45.28	-
				Total stryrylpyrone			10.37	64.94
				Total flavonoids			-	23.46
				Total fatty acids			14.64	-
				Total aromatic ketone			7.77	0.37
				Total aromatic aldehyde			7.64	0.32

nd: Not detected, [1]RT: Retention time (min); [2]RI_{exp}: Experiment retention index obtained from the relative calculation of to C_8-C_{20} *n*-alkane series;

[3]RI_{lit}: Retention index found in reported literature; [4]Relative amount was obtained by peak normalization

Styrylpyrones, flavanones, chalcones, and diarylheptanoid have previously been isolated from various parts of *A. mutica* [5-7, 24]. Styrylpyrone is commonly found in the rhizome, leaves and fruit while flavanones and chalcones were reported in the rhizome and the whole fruit. Interestingly, diarylheptanoid was only found in the rhizome. However, no scientific studies on the chemical composition of the pericarp and seeds of the *A. mutica* have been published. In our study, GC–MS analysis revealed that both pericarp and seed contain some identical chemical components. In the pericarp, 1,7-diphenyl-4,6-heptadien-3-one was the most abundant component, followed by stryrylpyrone, fatty acids, and phenyl derivatives. In contrast, the seed was predominantly composed of stryrylpyrone, flavonoids, and sesquiterpene. The identification of the two main groups of compounds including styrylpyrones and flavanones, in the seed was consistent with a previous study [6] that isolated these compounds from the methanolic extract of the whole fruit of *A. mutica*. A diarylheptanoid (1,7-diphenyl-5-hydroxy-6-hepten-3-one) was isolated from the chloroform extract of *A. mutica* rhizome [5]. It should be noted that diarylheptanoid (1,7-diphenyl-4,6-heptadien-3-one) was identified in the pericarp for the first time in our study.

In addition, farnesol identified in the dichloromethane crude extracts of the pericarp and seed in our study was similar to the previous report by Sirat et al. [29]. Sirat et al. extracted the young and mature fruit of *A. mutica* using hydrodistillation, and the obtained oils were characterized using GC–MS. Their finding demonstrated that farnesol was a major individual constituent of both young and mature fruit oils [29]. The chemical components of the essential oils obtained by hydrodistillation from *A. mutica* fruit have been previously reported. Sesquiterpenes, including β-caryophyllene and α-cadinol, were reported as the major components in the essential oil of *A.mutica* fruit collected from Vietnam [28]. As well, other types of sesquiterpene including farnesol and α-farnesene were detected in Malaysia fruit oil [29]. The study of Ibrahim et al. revealed that camphor, camphene, β-pinene, 1,8-cineole, and α-pinene were the predominant monoterpenes in the fruit oil of *A. mutica* collected from the another region of Malaysia [25]. This implied that the location of plants collected influences the chemical compositions of the plants. The method of

extraction is one of the several factors the influence the extraction of the compounds of interest. A conventional extraction method, maceration with dichloromethane, was used to prepare both extracts for our study. The chemical compositions of *A. mutica* maceration crude extracts obtained in our study differed from hydrodistillation extracts previously cited in other publications. Comparing our results to those of previous studies indicated that the abundance of monoterpenes and sesquiterpenes in our extracts were lower than those reported in previous research. Styrylpyrone, diarylheptanoid, flavonoids, fatty acids, and triterpene, were only found in our pericarps and seeds extracts. Several factors, including source locations, cultivation method, vegetative stage, solvent polarity, and extraction method of *A. mutica* fruits, may account for these differences.

Our results and previous publications [25, 29] on the chemical composition of the fruit from *A. mutica* revealed that the pericarps and seeds of *A. mutica* contain various secondary metabolites. The metabolites are also related to the reported pharmacological activities and the usage of *A. mutica* fruits. It is noteworthy that our research is the first study to identify diarylheptanoid in the *A. mutica* pericarp. According to the GC–MS analysis, it can conclude that the *A. mutica* pericarp had diarylheptanoid as a major component, as well as the seed composed of styrylpyrones, flavonoid and sesquiterpene. The GC–MS analysis also reached the purpose of our study, which was to identify chemical constituents of *A. mutica* pericarp and seed. Moreover, the dichloromethane extracts of the pericarp and seed were evaluated for their α-glucosidase inhibiting and antioxidant properties. The AMSD extract exhibited the highest α-glucosidase inhibitory activity with an IC_{50} value of 8.9×10^{-2} ± 2.73 μg/mL (the IC_{50} value of positive control (acarbose) was 340.27 ± 0.47 μg/mL). The antioxidant activity of AMSD extract was not observed. In addition, the AMPD extract exhibited neither α-glucosidase inhibitory nor antioxidant activities. In ther following section, further study on the isolation and identification of α-glucosidase inhibitor from the seed dichloromethane extract is presented.

4.1.3 Structure elucidation of isolated compounds from the dichloromethane extract of the seed from *A. mutica*

The AMSD extract was purified by silica column chromatography to obtain seven pure compounds (Figure 25). The isolated compounds were identified by spectroscopic analysis and they were identified as farnesol (**1**), 5,6-dehydrokawain (**2**), pinocembrin (**3**), cardamomin (**4**), naringenin (**5**) pinocembrin chalcone (**6**) and alpinetin (**7**). Among these seven compounds, naringenin and pinocembrin chalcone were isolated for the first time from *A. mutica* in our study. The elucidation of the structure of isolated compounds was described as follows.

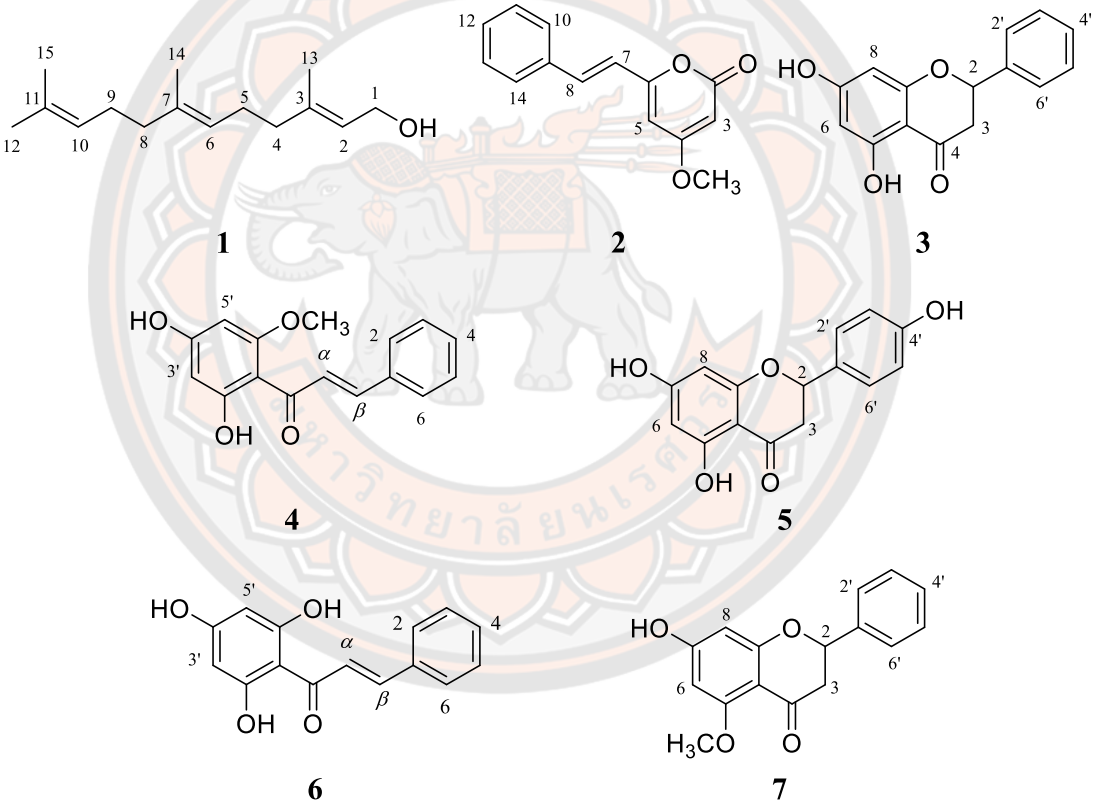

Figure 25 Chemical structures of isolated compounds from the dichloromethane extract of the seed from *A. mutica*

Compound **1** was isolated as a pale-yellow liquid. HRESIMS gave the molecular ion $[M-H_2O+H]^+$ peak at *m/z* 205.1947, corresponding to $C_{15}H_{26}O$ (calcd 222.1984). The IR spectrum displayed absorption bands at 3348 (O–H stretching), 2918 (C–H stretching) and 1637 (C=C stretching) cm^{-1}. The ^{1}H-NMR spectrum of **1** showed signals at δ 1.59 (6H, s, H-14, H-15) and 1.67 ppm (6H, s, H-12, H-13) for methyl groups. The methylene signal of H-4, H-5, H-8 and H-9 was shown in multiplet at δ 2.04 ppm (8H). The doublet signal at δ 4.14 ppm (2H, *J* = 7.0 Hz) is for the methylene group adjacent to oxygen. The quartet signal at δ 5.09 ppm (2H, *J* = 6.9 Hz) and the triplet at 5.40 ppm (1H, *J* = 7.0 Hz) which is assigned to three olefinic protons. The ^{13}C NMR and DEPT135 spectra showed four methyl carbons (δ 25.8, 17.8, 16.4, 16.1), five methylene carbons (δ 59.5, 39.8, 39.7, 26.8, 26.4), three methine carbons (δ 124.4, 123.9, 123.4) and three quaternary carbons (δ 139.8, 135.5, 131.4) with 15 of these carbons being defined as sesquiterpene. The assignments were confirmed by HMQC and HMBC experiments. On the basis of these assignments and by comparing them with the previous literature [93] the structure of this sesquiterpene was established as farnesol. Complete ^{1}H and ^{13}C NMR chemical shift assignments and the correlations of all the hydrogen bearing carbons, determined from the HMBC spectrum, are shown in Table 8**.**

Compound **2** was isolated as a white amorphous solid. HRESIMS gave the molecular ion $[M+H]^+$ peak at *m/z* 229.0883, corresponding to $C_{14}H_{12}O_3$ (calcd 228.0786). The UV absorption maxima were observed at 254 and 340 in methanol. The IR spectrum displayed absorption bands at 3076 (O–H stretching), 1718 (C=O stretching) and 1634 (C=C stretching) cm^{-1}. For the ^{1}H NMR spectrum, the methoxy group was seen at δ 3.78 ppm (3H, *s*, -OCH_3). Five aromatic protons at δ 7.29 – 7.48 ppm with a multiplet pattern (5H) also observed. The two vinylic *trans*-proton signals at δ 6.55 (1H, d, *J* = 16.0 Hz) and 7.46 (1H, d, *J* = 16.0 Hz) ppm were presented, and there were two doublets at δ 5.46 (1H, *J* = 2.2 Hz) and 5.92 ppm (1H, *J* = 2.1 Hz) attributable to M shape coupling. The ^{1}H NMR spectrum indicated that the chemical structure of **2** consists of one aromatic ring which was substituted and also showed *trans*-double bond and one methoxy group in the molecule. The ^{13}C and DEPT135 NMR spectra showed twelve carbon signals, including one methyl group of methoxy

group (δ 56.0), seven methine groups (δ 135.8, 129.5, 128.9, 127.5, 118.7, 101.4, 89.0) and four quaternary (δ 171.1, 164.0, 158.6, 135.3) carbon atoms. In addition, the chemical structure of **2** was assigned and confirmed by HMQC and HMBC spectra. The HMBC spectrum implied that the methoxy group was placed on C-4. The chemical structure of compound **2** was investigated by 1D and 2D NMR techniques and with a comparison with previously reported findings [5]. The chemical structure was determined to be 5,6-dehydrokawain. Complete ^{1}H and ^{13}CNMR chemical shift assignments and the correlations of all the hydrogen bearing carbons, determined from the HMBC spectrum, are shown in Table 9.

Compound **3** was isolated as a pale yellow amorphous solid. HRESIMS gave the molecular ion $[M+H]^+$ peak at *m/z* 257.0809, corresponding to $C_{15}H_{12}O_4$ (calcd 256.0736). The UV absorption maxima were observed at 210 and 289 in methanol. The IR spectrum displayed absorption bands at 3033 (O–H stretching), 1599 (C=O stretching) and 1155 (C–O stretching) cm^{-1}. The ^{1}H NMR spectra data displayed the ABX system of H-2 and H-3 at δ 5.55 ppm (1H, dd, *J* = 3.1, 12.8 Hz, H-2), 3.16 (1H, dd, *J* = 12.8, 17.1 Hz) and 2.80 (1H, dd, *J* = 3.1, 17.1 Hz) ppm and the monosubstituted benzene ring at δ 7.40 – 7.56 ppm. The *meta*-coupling of H-6 and H-8 was shown in doublet signals at δ 6.01 (1H, *J* = 2.2 Hz) and 5.98 (1H, *J* = 2.2 Hz). In addition, ^{1}H NMR spectral data displayed a singlet signal of chelated hydroxyl group at δ 12.16 ppm and a broad singlet at δ 9.78 ppm, whose signal suggested the locations of hydroxyl at C-5 and C-7, respectively. The ^{13}C and DEPTQ NMR spectra showed 15 carbon signals, including one methylene carbon (δ 43.6), six methine carbons (δ 129.4, 129.4, 127.3, 96.9, 95.9, 79.9) and six quaternary carbons (δ 196.8, 167.4, 165.2, 164.1, 103.2), which were assigned and confirmed by using HMQC and HMBC techniques. This assignment is supported by a comparison with that previously reported [5]. All the data was in agreement with the structure of pinocembrin. Complete ^{1}H and ^{13}C NMR chemical shift assignments and the correlations of all the hydrogen bearing carbons, determined from the HMBC spectrum, are shown in Table 10.

Compound **5** was isolated as a white amorphous solid. HRESIMS gave the molecular ion $[M+H]^+$ peak at *m/z* 273.0760, corresponding to $C_{15}H_{12}O_5$ (calcd

272.0685). The UV absorption maxima were observed at 213 and 288 in methanol. The IR spectrum displayed absorption bands at 3033 (O–H stretching), 1599 (C=O stretching) and 1155 (C–O stretching) cm^{-1}.

Compound **7** was isolated as a colorless crystalline needle. HRESIMS gave the molecular ion $[M+H]^+$ peak at *m/z* 271.0974, corresponding to $C_{16}H_{14}O_4$ (calcd 270.0892). The UV absorption maxima were observed at 202 and 282 in methanol. The IR spectrum displayed absorption bands at 3177 (O–H stretching), 1658 (C=O stretching) and 1574 (C–C stretching) cm^{-1}.

The ^1H and ^{13}C NMR spectra of **5** and **7** showed similar signals and patterns to **3**. For **5**, the only difference in ^1H NMR spectra between **5** and **3** was the two doublet signals of H-2′, 6′ (7.39 ppm, 2H, J = 8.5 Hz) and H-3′, 5′ (6.90 ppm, 2H, J = 8.6 Hz) at and of the B ring in **5**. These doublet signals indicated that this aromatic ring was substituted in 1 and 4 positions. For **7**, the singlet signal of the methoxy group (δ 3.74 ppm) was observed. In addition, the disappearance of the chelating proton of 5-OH and the HMBC spectrum suggested that the methoxy group was replaced at the C-5 position. Based on the spectroscopic data, as well as a comparison with the literature, **5** and **7** were characterized as naringenin and alpinetin, respectively [94, 95]. Complete ^1H and ^{13}C NMR chemical shift assignments and the correlations of all the hydrogen bearing carbons, determined from the HMBC spectrum, are shown in Tables 12 and 14 for compounds **5** and **7**, respectively.

Compound **4** was isolated as a yellow crystal. HRESIMS gave the molecular ion $[M+H]^+$ peak at *m/z* 271.0982, corresponding to $C_{16}H_{14}O_4$ (calcd 270.0892). The UV absorption maxima were observed at 210 and 342 in methanol. The IR spectrum displayed absorption bands at 3098 (O–H stretching) and 1624 (C=O stretching) cm^{-1}. The ^1H NMR spectrum showed a singlet signal of the methoxy group at δ 3.97 ppm (3H) and *meta*-coupling related to two doublets of H-5′ (δ 6.08, 1H, J = 2.3 Hz) and H-3′ (δ 6.01, 1H, J = 2.2 Hz). Another two sets of doublets were found to be *trans*- olefinic proton of H-β and H-α at δ 8.01 (1H, J = 15.6 Hz) and 7.75 (1H, J = 15.5 Hz) ppm. The multiplet signal appeared between δ 7.43 – 7.72 ppm (5H) due to a monosubstituted ring B of chalcone. Moreover, the ^1H NMR spectra of **4** showed a singlet signal of the chelated hydroxyl group at δ 14.17 ppm. This signal

implied the location of hydroxyl at the C-2' position. The ^{13}C and DEPT135 NMR spectra showed 16 carbon signals, including one methyl carbon (δ56.4), nine methine carbons (δ 129.4, 129.4, 127.3, 96.9, 95.9, 79.9) and six quaternary carbons (δ 196.8, 167.4, 165.2, 164.1, 103.2). The signal of the methoxy and carbonyl groups appeared at δ 56.4 and 193.1 ppm, respectively. The HMBC spectrum indicated that the methoxy group was placed in the C-6' position. This assignment is supported by a comparison with that previously reported [95]. All the data was in agreement with the structure of cardamomin. Complete ^{1}H and ^{13}C NMR chemical shift assignments and the correlations of all the hydrogen bearing carbons, determined from the HMBC spectrum, are shown in Table 11.

Compound **6** was isolated as an orange amorphous solid. HRESIMS gave the molecular ion $[M+H]^+$ peak at *m/z* 257.0809, corresponding to $C_{15}H_{12}O_4$ (calcd 256.0736). The ^{1}H NMR spectra of **6** and **4** showed structural similarity except for the disappearance of a methoxy signal at δ 3.97 ppm. Therefore, **6** was identified as pinocembrin chalcone. Complete ^{1}H and ^{13}C NMR chemical shift assignments are shown in Table 13.

Table 8 The ^{1}H and ^{12}C NMR assignments and HMBC correlations of compound **1** in $CDCl_3$ and farnesol in MeOD

Position	Compound **1**			Farnesol [93]	
	δ_H, (mult, *J* in Hz)	δ_C	HMBC correlations	δ_H, (mult, *J* in Hz)	δ_C
1	4.14 (d, 7.0)	59.5	C-2, C-3	4.08 (d, 6.5)	59.3
2	5.40 (t, 7.0)	123.4	C-13, C-4, C-1	5.36 (t, 6.5)	123.4
3	-	139.8	-	-	139.6
4	2.04 (m)	39.7	-	2.04 (m)	39.6
5		26.8	-	2.13 (m)	26.3
6	5.09 (q, 6.9)	123.9	C-14, C-5, C-4	5.13 (t, 6.5)	123.8
7	-	135.5	-	-	135.4
8	2.04 (m)	39.8	-	1.98 (m)	39.7
9		26.4	-	2.09 (m)	26.7
10	5.09 (q, 6.9)	124.4	C-15, C-12, C-9	5.09 (t, 6.0)	124.3
11	-	131.4	-	-	131.3
12	1.67 (s)	25.8	C-15, C-10, C-11	1.67 (s)	25.7
13	1.67 (s)	16.4	C-4, C-1, C-2, C-3	1.67 (s)	16.3
14	1.59 (s)	16.1	C-8, C-6	1.60 (s)	16.0
15	1.59 (s)	17.8	C-12, C-11	1.60 (s)	17.7

Table 9 The ^{1}H and ^{13}C NMR assignments and HMBC correlations of compound **2** in $CDCl_3$ and 5,6-dehydrokawain in benzene-d_6

Position	Compound **2**			5,6-dehydrokawain [5]	
	δ_H, (mult, *J* in Hz)	δ_C	HMBC correlations	δ_H, (mult, *J* in Hz)	δ_C
2	-	164.0	-	-	164.0
3	5.46 (d, 2.2)	89.0	C-5, C-3	5.40 (d, 2.5)	88.8
4	-	171.1	-	-	171.1
5	5.92 (d, 2.1)	101.4	C-4, C-3, C-7, C-6	5.85 (d, 2.5)	101.3
6	-	158.6	-	-	158.6
7	6.55 (d, 16.0)	118.7	C-5, C-9, C-6	6.40 (d, 16.0)	118.6
8	7.46 (d, 16.0)	135.8	C-6, C-7, C-10, 14	7.40 (d, 16.0)	135.8
9	7.29 – 7.48 (m)	135.3	-	7.30 (m)	135.2
10, 14		127.5	-	7.29 – 7.48 (m)	127.4
11, 13		128.9	-		128.9
12		129.5	-		129.4
$-OCH_3$	3.78 (s)	56.0	C-4	3.75 (s)	55.9

Table 10 The ^{1}H and ^{13}C NMR assignments and HMBC correlations of compound **3** in acetone-d_6 and pinocembrin in $CDCl_3$

Position	Compound **3**			Pinocembrin [5]	
	δ_H, (mult, *J* in Hz)	δ_C	HMBC correlations	δ_H, (mult, *J* in Hz)	δ_C
2	5.55 (dd, 3.1, 12.8)	79.9	C-3, C-2', 6', C-1', C-9, C-4	5.49 (dd, 3.0, 13.0)	79.2
3ax	3.16 (dd, 12.8, 17.1)	43.6	C-2, C-1', C-4	3.15 (dd, 13.0, 17.0)	43.4
3eq	2.80 (dd, 3.1, 17.1)		C-10, C-1', C-4	2.83 (dd, 3.0, 17.0)	
4	-	196.8	-	-	195.6
5	-	165.2	-	-	164.3
6	5.98 (d, 2.2)	96.9	C-10, C-8, C-4, C-5, C-7	6.02 (s)	96.8
7	-	167.4		-	167.3
8	6.01 (d, 2.2)	95.9	C-10, C-6, C-4, C-9, C-7	6.02 (s)	95.5
9	-	164.1	-	-	163.1
10	-	103.2	-	-	103.0
1'	-	140.0	-	-	138.4
2', 6'	7.56 (m)	127.3	C-2, C-2', 6', C-4'	7.40 (m)	126.2
3', 5'	7.44 (m)	129.4	C-1', C-3', 5'		128.9
4'	7.40 (m)	129.4	C-2', 6'		128.9
-OH-5	12.16 (s)	-	C-6, C-10, C-5, C-7, C-4	12.05 (s)	-
-OH-7	9.78 (broad s)	-	-	-	-

Table 11 The ^{1}H and ^{13}C NMR assignments and HMBC correlations of compound **4** in acetone-d_6 and cardamomin in MeOD

Position	Compound **4**			Cardamomin [95]	
	δ_H, (mult, *J* in Hz)	δ_C	HMBC correlations	δ_H, (mult, *J* in Hz)	δ_C
α	8.01 (d, 15.6)	128.5	C-2, 6, C-1, C-β, C=O	7.59 (d, 15.6)	128.9
β	7.75 (d, 15.1)	142.6	C-2, 6, C-1, C=O	7.84 (d, 15.6)	142.9
1	-	136.4	-	-	137.0
2, 6	7.72 (m)	129.2	C-4, C-β	7.43 (m)	129.3
3, 5	7.43 (m)	129.8	C-2, 6, C-1	7.43 (m)	130.1
4	7.43 (m)	131.0		7.43 (m)	131.2
1'	-	106.3	-	-	106.6
2'	-	164.3	-	-	164.8
3'	6.01 (d, 2.2)	96.9	C-5', C-1', C-4', C-2'	5.85 (d, 2.8)	97.1
4'	-	166.1	C-3', C-1', C-6', C-4'	-	167.0
5'	6.08 (d, 2.3)	92.2	-	5.93 (d, 2.8)	92.6
6'	-	169.0	-	-	168.8
-OH-2'	14.17	-	C-3', C-1', C-4', C-2', C=O	-	
-OH-4'	9.76 (broad s)	-	-	-	
C=O	-	193.1	-	-	193.9
$-OCH_3$	3.97 (s)	56.4	C-5', C-2'	3.84 (s)	56.3

Table 12 The ^{1}H and ^{13}C NMR assignments of compound **5** in acetone-d_6 and naringenin in MeOD

Position	Compound **5**		Naringenin [94]	
	δ_H, (mult, *J* in Hz)	δ_C	δ_H, (mult, *J* in Hz)	δ_C
2	5.45 (dd, 3.0, 12.9)	79.8	5.27 (dd, 12, 3.0)	80.2
3ax	3.18 (dd, 12.8, 17.1)	43.4	3.06 (dd, 18.0, 12.0)	43.8
3eq	2.72 (dd, 3.0, 17.1)		2.64 (dd, 18.0, 3.0)	
4	-	197.2	-	197.5
5	-	165.0	-	165.2
6	5.96 (d, 1.2)	95.7	5.88 (s)	96.8
7	-	167.1		168.0
8	5.96 (d, 1.2)	96.6	5.88 (s)	96.0
9	-	164.4	-	164.9
10	-	103.2	-	103.1
1'	-	130.7	-	131.8
2', 6'	7.39 (d, 8.5)	129.0	7.28 (m)	128.9
3', 5'	6.90 (d, 8.6)	116.2	6.81 (m)	116.1
4'	-	15.6	-	158.7
-OH-5	12.18	-	-	-

Table 13 The ^{1}H and ^{13}C NMR assignments of compound **6** (pinocembrin chalcone) in acetone-d_6

Position	Compound **6**	
	δ_H, (mult, J in Hz)	δ_C
α	8.26 (d 15.6)	130.9
β	7.78 (d, 15.6)	142.6
1	-	136.6
2, 6	7.69 (dd, 2.0, 1.5, 7.6)	129.1
3, 5	7.44 (m)	129.8
4	7.44 (m)	130.9
1'	-	
2', 6'	-	
3', 5'	6.01 (d, 2.2)	96.1
4'	-	
C=O	-	193.3

Table 14 The ^{1}H and ^{13}C NMR assignments and HMBC correlations of compound **7** in DMSO-d_6 and alpinetin in MeOD

Position	Compound **7**			Alpinetin [95]	
	δ_H, (mult, *J* in Hz)	δ_C	HMBC correlations	δ_H, (mult, *J* in Hz)	δ_C
2	5.48 (dd, 3.0, 12.4)	78.0	C-2', 6', C-1', C-9, C-4	5.33 (dd, 2.8, 10.1)	80.2
3ax	2.98 (dd, 12.4, 16.4)	44.9	C-2, C-1', C-4	2.90 (dd, 12.8, 16.4)	46.4
3eq	2.62 (dd, 3.1, 16.4)		C-10, C-1', C-4	2.63 (dd, 3.7, 16.4)	
4	-	187.5	-	-	191.8
5	-	162.3	-	-	166.6
6	6.07 (d, 2.2)	95.4	C-8, C-5, C-7	6.01 (d, 1.8)	97.2
7	-	164.4		-	167.2
8	6.00 (d, 2.2)	93.4	C-10, C-6, C-9	5.96 (d, 2.8)	94.3
9	-	164.1	-	-	164.3
10	-	104.6	-	-	105.7
1'	-	139.2	-	-	140.6
2', 6'	7.49 (m)	126.5	C-2, C-3', 5', C-4'	7.32 (m)	127.3
3', 5'	7.41 (m)	128.5	C-1', C-2', 6'		129.7
4'	7.38 (m)	128.4	C-2', 6', C-3', 5'		129.5
-OCH_3	3.74 (s)	55.6	C-5, C-6	3.74 (s)	56.2

The isolation of the chemical constituents from *A. mutica* seed led to the isolation of seven compounds, namely farnesol (**1**), 5,6-dehydrokawain (**2**), pinocembrin (**3**), cardamomin (**4**), naringenin (**5**) pinocembrin chalcone (**6**) and alpinetin (**7**). In the previous literature by Jantan et al. [6], flavokawin B, pinocembrin, alpinetin, 5,6-dehydrokawain, cardamomin and 2′,3′,4′,6′-tetrahydroxchalcone were reported from the whole fruit (pericarp and seed) of *A. mutica*. A comparison of the chemical constituents of the *A. mutica* fruit with those previously isolated [6] revealed marked differences. Unlike Jantan et al., farnesol (**1**), naringenin (**5**) and pinocembrin chalcone (**6**) were isolated in our study. However, we were not able to isolate flavokawin B and 2′,3′,4′,6′-tetrahydroxchalcone. The presence of **6** in the seed supports the postulation that it is a biogenetic precursor of the flavanone and chalcone compounds from *A. mutica*. The cyclization of **6** leads to **3**. Indeed, methylation of **6** to the 4-OH leads to **4**. Compound **7** could be a methylation of **3** or a cyclization product of **4**. It is noted that the methylation of flavanone (**7**) and chalcone (**4**) from the seed occurred in the first unit of malonyl-CoA.

From the results of the present study and previous publications, numerous chalcones and flavanones have been isolated and identified from the rhizome, fruit and seed of *A. mutica*. The co-existence of flavokawin B in the fruit and its structurally related chalcone within the same tissue of *A. mutica* suggests that **4** may be the precursor of flavokawin B [31]. Similarly to the rhizome, flavokawin B might form via methylation of pinostrobin chalcone. In addition, the structure relationship suggests that the hydroxylation at the C-6 position of **6** resulted in 2',3',4',6'-tetrahydroxy chalcone, a compound isolated from the fruit of *A. mutica* [31]. Moreover, the methylation on C-7 position of **3** or cyclization of pinostrobin chalcone led to the formation of pinostrobin in the rhizome [24, 27]. The isolation of **6** from the seed in the present study was the key point to understanding the biosynthetic pathway of chalcones and flavanones from *A. mutica*. Although, during the present investigation, it was not possible to isolate or even detect any traces of the other flavonoid compounds that we postulated to support this biosynthetic scheme (Figure 26), the presence of those other flavonoid compounds in some other tissues of *A. mutica*, such as rhizome and fruit, has been reported in previous publications [6, 24, 27].

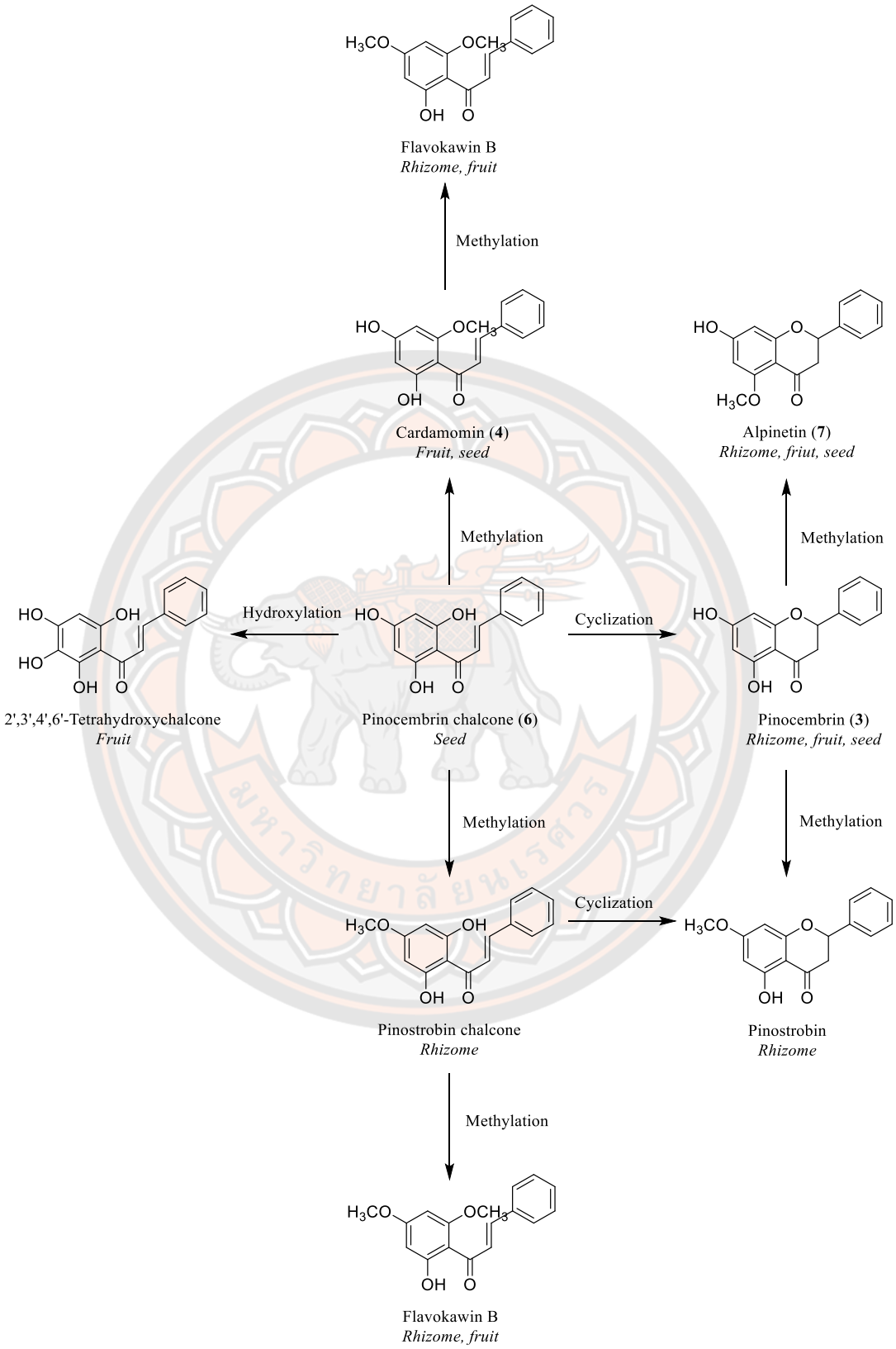

Figure 26 Biosynthetic pathway suggested for flavanones and chalcones from *A. mutica*

4.1.4 α-Glucosidase inhibitory activity of isolated compounds from the seed of *A. mutica*

The isolated compounds were tested for their ability to α-glucosidase. At 100 μg/mL, compounds **3**, **4**, and **5** exhibited inhibitory activity of 91.26, 25.58, and 94.74%, respectively (Table 15). Among the seven isolated compounds, compounds **3** and **5** with IC_{50} values 62.77 ± 2.18 and 8.77 ± 1.04 μM, respectively, exhibited the highest inhibitory activity. In addition, compounds **3** and **5** exhibited greater α-glucosidase inhibition than acarbose (IC_{50} = 527.03 ± 0.76 μM). These results correspond to previous studies on the α-glucosidase inhibition by compounds **3** and **5**. Potipiranun et al. demonstrated that compound **3** inhibited α-glucosidase activity against rat intestinal maltase and sucrase with IC_{50} values of 0.35 and 0.39 mM, respectively [96]. Compound **5** exhibited potent α-glucosidase inhibitory activity, consistent with the studies of Priscilla et al. (IC_{50} = 6.51 μM) [97]. The results from the assay suggested that the methylation of chalcone and flavanone molecules affected their inhibitory activity. Furthermore, the presence of a hydroxy group in ring B of flavanone resulted in a high level of inhibition, consistent with the finding of Proença et al., who investigated the *in vitro* and *in silico* inhibitory activity of 44 flavonoids against α-glucosidase [98]. From present study, it can conclude that the hydroxyl group on an aromatic ring can increase the α-glucosidase inhibitory activity.

Table 15 Inhibition effects of isolated compounds on the α-glucosidase. The percentage inhibition of isolated compounds was measured at the final concentration of 100 μg/mL except for acarbose (positive control) which was tested at 500 μg/mL. The determinations were done in triplicate and the data are expressed as means ± SD.

Compounds	Inhibitory activity (%)	IC_{50} (μM)
Farnesol (**1**)	Not detected	Not determined
5,6-Dehydrokawain (**2**)	Not detected	Not determined
Pinocembrin (**3**)	91.26 ± 2.15^{c}	62.77 ± 2.18^{b}
Cardamomin (**4**)	25.58 ± 2.98^{a}	Not determined
Naringenin (**5**)	94.74 ± 2.24^{c}	8.77 ± 1.04^{a}
Pinocembrin chalcone (**6**)*	Not determined	Not determined
Alpinetin (**7**)	Not detected	Not determined
Acarbose	39.99 ± 1.05^{b}	527.03 ± 0.14^{c}

* compound **6** is not determined because it is presented in a small amount, $^{a\text{-}c}$ Values not sharing the same letters are significantly different from another within a column ($p < 0.05$)

4.2 Part II: The investigation of chemical constituents, α-glucosidase inhibitory and antioxidant activities of *L. strychnifolium*

4.2.1 Extraction yields and crude extracts from the root, stem, leaves, and flower of *L. strychnifolium*

The roots, stems, leaves and flowers of *L. strychnifolium* were extracted with 95% ethanol to yield ethanolic root (LSR), stem (LSS), leaves (LSL), and flower (LSF) extracts. The percent yields obtained from the extract of roots, stems, leaves, and flowers extracts were as follows: LSF, LSR, LSS and LSL (Table 16).

Table 16 Weight and extraction yields of crude extracts from roots, stems, leaves and flowers of *L. strychnifolium*

Part of *L. strychnifolium* used	Crude extracts[a]	Weight (g)	% Yield[b]
Root	LSR	8.43	16.86
Stem	LSS	12.7	6.35
Leaves	LSL	5.92	4.38
Flower	LSF	9.30	21.14

[a]LS: *L. strychnifolium*, R: Root, S: Stem, L: Leaves, F: Flower; [b]% Yield was reported in terms of %weight by weight of raw material.

As shown in Figure 31, all ethanolic crude extracts of *L. strychnifolium* were consequently detected by ^{1}H NMR spectroscopy. Similar ^{1}H NMR profiles were observed in the extracts of the root (Figure 27(a)) and stem (Figure 27(b)). The aromatic protons displayed at δ 5.5–7 ppm. The characteristic region of hydroxy methylene proton at δ 3–4 ppm suggested the presence of the signals from sugar molecules. The methyl proton signal was shown at δ 1–1.5 ppm. Overall ^{1}H NMR profiling of leaves (Figure 27(c)) and flower (Figure 27(d)) extracts revealed similar proton signals, including aromatic region (δ 7–6 ppm), hydroxyl methylene proton (δ 3–4 ppm), and aliphatic proton (δ 1–3 ppm). The ^{1}H NMR profiles of all crude extracts suggest that the chemical composition of the root is nearly identical to that of the stem, whereas the chemical composition of the leaves is comparable to that of the flower.

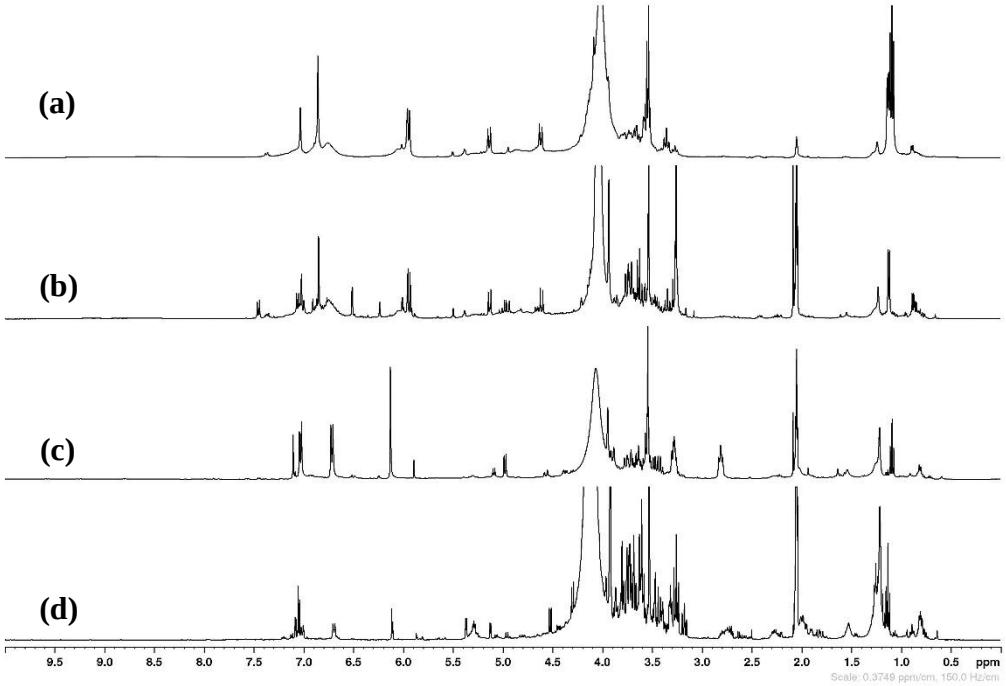

Figure 27 ^{1}H NMR (400 MHz) spectra of *L. strychnifolium* extracts from different parts; (a) LSR in acetone-d_6, (b) LSS in acetone-d_6, (c) LSL in acetone-d_6, (d) LSF acetone-d_6

4.2.2 α-Glucosidase and antioxidant activities of crude extracts from roots, stems, leaves and flowers of *L. strychnifolium*

The α-glucosidase inhibitory and antioxidant activities of *L. strychnifolium* ethanolic crude extracts were investigated using an *in-vitro* α-glucosidase inhibitory and DPPH radical scavenging assay. The α-glucosidase inhibitory activity is compared to an anti-diabetic drug, acarbose. As observed, the ethanolic extracts of *L. strychnifolium*; LSR, LSS, LSL and LSF extracts were found to have a significant inhibitory effect against α-glucosidase activity (Table 17). All crude extracts displayed potent inhibitory activity, with IC_{50} values ranging from 0.68 ± 0.04 to 10.52 ± 0.49 μg/mL, which were significantly higher than the positive control. The IC_{50} value for the positive control, acarbose was 340.27 ± 0.47 μg/mL or 0.5270 ± 0.7608 mM, which was in agreement with the results of Proença et al. (IC_{50}

= 0.607 mM) [98]. Moreover, the root extract exhibited the highest α-glucosidase inhibition.

The stem extract of *L. strychnifolium* ethanolic crude extracts had the highest antioxidant activity, with an IC_{50} value of 12.63 ± 0.04 μg/mL, followed by root, leaf and flower extracts (Table 17). Although, the antioxidant activity of all the ethanolic crude extracts was lower than that of L-ascorbic acid and trolox, there are no significant differences between stem extract and positive controls in terms of antioxidant activity.

According to these results, it would be interesting to isolate the α-glucosidase inhibitors and antioxidants from *L. strychnifolum* root, stem, leaf and flower extracts. Thus, the isolation of α-glucosidase inhibitors and antioxidants from LSR, LSS, LSL and LSF extracts was performed.

Table 17 The α-glucosidase inhibition and antioxidant by *L. strychnifolium* root, stem, leaf, and flower crude extracts. The results represent the mean ± SD of triplicate experiments.

Crude extracts*	IC_{50} (μg/mL)	
	α-Glucosidase inhibition	Antioxidant
LSR	0.68 ± 0.04^{a}	19.78 ± 2.41^{b}
LSS	2.89 ± 0.38^{b}	12.63 ± 0.04^{a}
LSL	3.44 ± 0.53^{b}	21.95 ± 2.95^{b}
LSF	10.52 ± 0.49^{c}	30.30 ± 2.20^{c}
Acarbose	340.27 ± 0.47^{d}	Not determined
L-ascorbic acid	Not determined	10.17 ± 0.32^{a}
Trolox	Not determined	10.90 ± 0.83^{a}

*LS: *L. strychnifolium*, R: Root, S: Stem, L: Leaves, F: Flower; [a-d]Values not sharing the same letters are significantly different from another within a column ($p < 0.05$)

4.2.3 Structure elucidation of the isolated compounds from root, stem, leaves and flower of *L. strychnifolium*

The ethanolic extracts of the roots, stems, leaves, and flowers of *L. strychnifolium* were isolated by chromatography techniques. The 13 compounds (Figures 28–30) were characterized, including three dihydroflavonols, three dihydrochalcones, two stilbenes, flavan-3-ol, flavonol, cyclitol, phenolic acid, and phenolic ethyl ester. As well, the isolated compounds were identified as astilbin (**8**), isoastilbin (**9**), neoastilbin (**10**), epicatechin (**11**), (*E*)-resveratrol (**12**), (*E*)-resveratrol 4'-*O*-*β*-D-glucoside (**13**), quercetin 3-*O*-*β*-D-arabinoside (**14**), phloretin (**15**), phloretin 4'-*O*-*β*-D-glucoside (**16**), phloretin 4'-*O*-(6''-*O*-galloyl)-*β*-D-glucoside (**17**), pinitol (**18**), gallic acid (**19**), and gallic acid ethyl ester (**20**). In Figure 32, the chemical structures of these compounds are depicted. For structure elucidation, various spectroscopic techniques (1D and 2D NMR, HRESIMS, IR, and UV) were applied. This section describes the structural elucidation of compounds **8**–**20**.

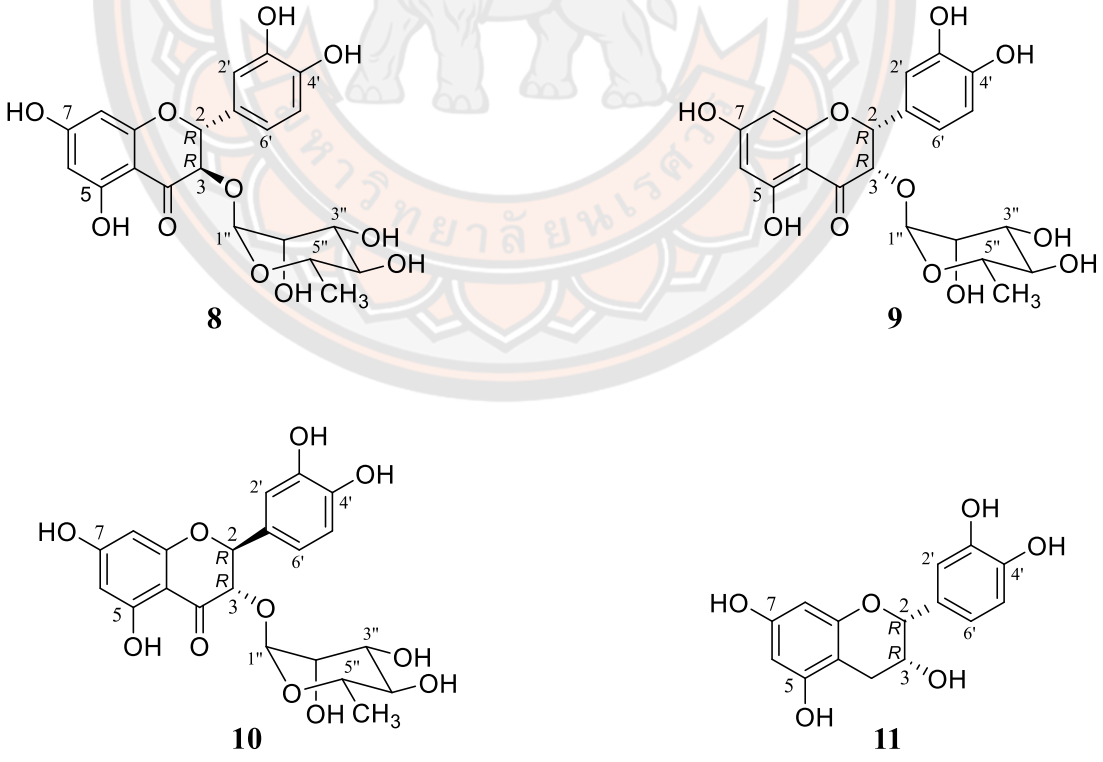

Figure 28 Chemical structures of astilbin (**8**), isoastilbin (**9**), neoastilbin (**10**), epicatechin (**11**) isolated from the root of *L. strychnifolium*

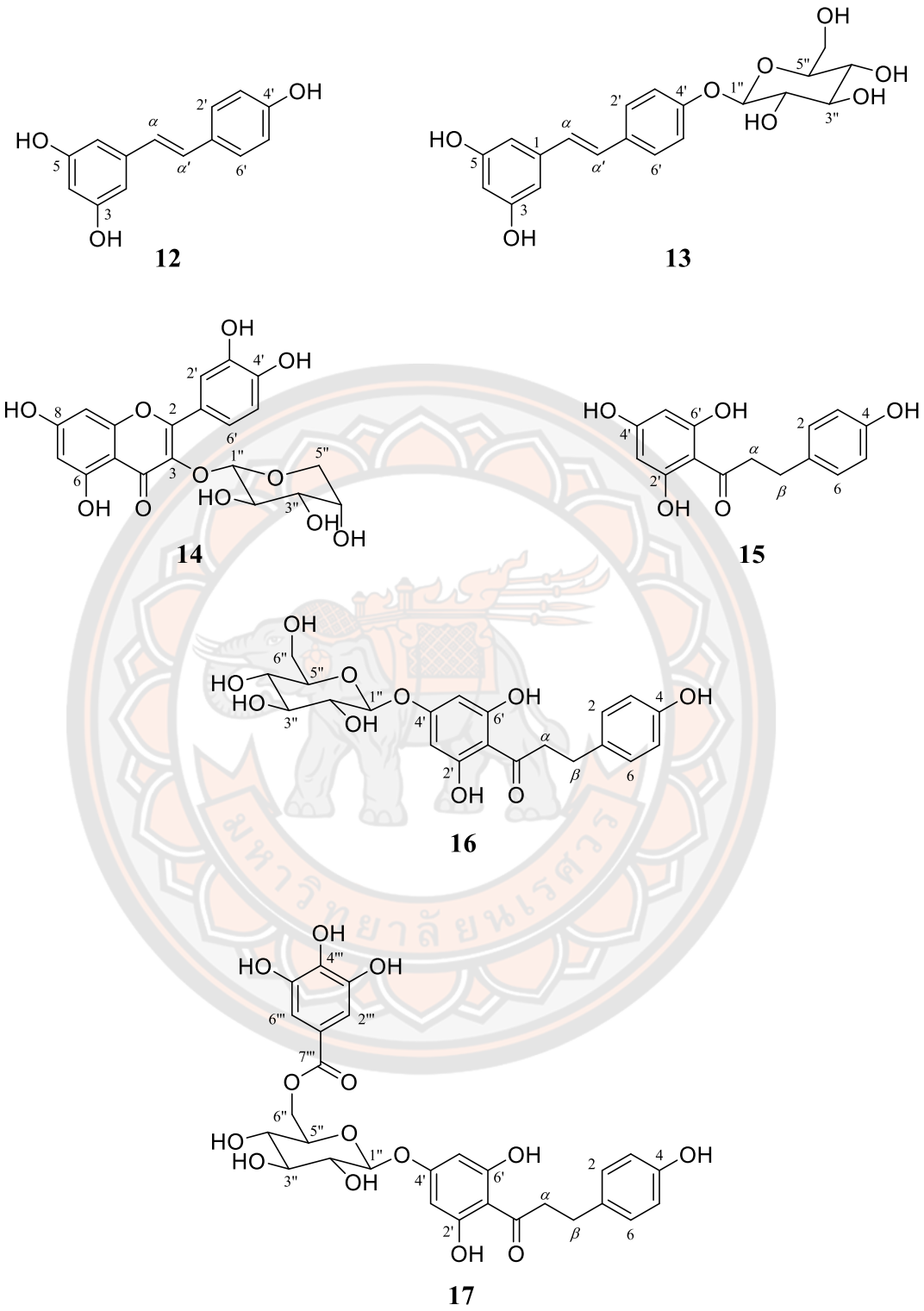

Figure 29 Chemical structures of (*E*)-resveratrol (**12**), (*E*)-resveratrol 4'-*O*-*β*-D-glucoside (**13**), quercetin 3-*O*-*β*-D-arabinoside (**14**), phloretin (**15**), phloretin 4'-*O*-*β*-D-glucoside (**16**), phloretin 4'-*O*-(6"-*O*-galloyl)-*β*-D-glucoside (**17**) isolated from the stem, leaves and flower of *L. strychnifolium*

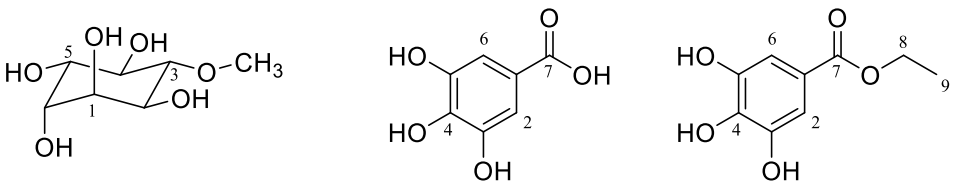

18 **19** **20**

Figure 30 Chemical structures of pinitol, gallic acid and gallic acid ethyl ester isolated from root, stem, leaves and flower of *L. strychnifolium*

Compound **8** was isolated as a white amorphous solid. HRESIMS gave the molecular ion $[M–H]^-$ peak at *m/z* 449.1088 corresponding to $C_{21}H_{22}O_{11}$ (calc. 450.1162). The UV absorption maxima were observed at 210 and 291 in methanol. The IR spectrum displayed absorption bands at 3382 (O–H stretching), 1634 (C=O stretching) and 1148 (C–O stretching) cm^{-1}. The ^1H NMR spectra data of **8** (Table 18) displayed the ABX system of flavonoid ring A at δ 7.09 (1H, d, J = 1.8 Hz), 6.90 (1H, d, J = 8.1 Hz), and 6.86 (1H, dd, J = 1.7, 1.8 Hz). The proton signals at δ 5.99 and 5.95 (each 1H, d, J = 2.1 Hz) corresponded to the *meta*-coupling of flavonoid ring B. Two additional doublets at δ 5.18 and 4.69 (each 1H, J = 10.6 Hz) confirmed the dihydroflavonol skeleton and were attributed to H-2 and H-3. The coupling constant at 10.6 Hz of H-2 and H-3 corresponds to the *trans*-conformation of these protons, which means that there are two possible configurations, either the *trans*-form (2*R*,3*R*) or the *trans*-form (2*S*,3*S*). The configuration was determined to be 2*R*, and 3*R* by comparison of the pattern and coupling constant of the literature [99]. An anomeric proton appeared as a singlet signal at δ 4.10 (1H). The remaining sugar protons appeared as separate peaks in the region of 3.33 – 4.42. The up-field doublet integrating for three protons, resonated at δ 1.15 (3H, d, J = 6.2 Hz) was attributed to H-6" of the rhamnose moiety. The ^{13}C NMR spectrum of **8** (Table 18) displayed resonances for all 21 carbons. DEPT135 spectra showed one methyl carbon, 12 methine carbons, and eight quaternary carbons. The carbonyl signal appeared at δ 195.9. The connectivity of protons from the rhamnose moiety could be determined by the correlations observed in the COSY spectrum. The attachment of the rhamnose to the dihydroflavonol was determined by the correlation observed in the HMBC

spectrum, and the correlation between anomeric proton at δ 4.10 and C-3 at δ 77.3 was observed. These assignments are supported by the comparison with those previously reported [99]. All data were in agreement with the structure of astilbin.

Compound **9** was isolated as a white amorphous solid. HRESIMS gave the molecular ion $[M-H]^-$ peak at *m/z* 449.1080 corresponding to $C_{21}H_{22}O_{11}$ (calc. 450.1162). The UV absorption maxima were observed at 210 and 291 in methanol. The IR spectrum displayed absorption bands at 3382 (O–H stretching), 1634 (C=O stretching) and 1148 (C–O stretching) cm^{-1}.

Compound **10** was isolated as a white amorphous solid. HRESIMS gave the molecular ion $[M-H]^-$ peak at *m/z* 449.1091 corresponding to $C_{21}H_{22}O_{11}$ (calc. 450.1162). The UV absorption maxima were at 215 and 302 in methanol. The IR spectrum displayed absorption bands at 3242 (O–H stretching), 1634 (C=O stretching) and 1148 (C–O stretching) cm^{-1}.

The ^1H NMR spectral data of **8**, **9** and **10** showed proton signals of dihydroflavonol rhamnoside structure. For **9**, the coupling constant of C-2 and C-3 was 2.5 Hz for each of which these *J* coupling corresponds to the *cis*- conformation of these protons, which means that there are two possible configurations, either the *cis*-form (2*R*,3*S*) or the *cis*-form (2*S*,3*R*). The configuration was determined to be 2*R*,3*S* by comparison of the pattern and coupling constant in the literature [99]. All data agreed with the structure of isoastilbin. The ^1H, ^{13}C NMR data and HMBC correlation of compound **9** are shown in Table 19.

Compound **10** and **8** showed similar *J* coupling constant of H-2 and H-2. The coupling constant of C-2 and C-3 for **10** was determined to be 11.2 Hz. Moreover, the signals of rhamnose with chemical shifts of **10** and **8**, specifically H-5″ and H-6″, are exhibited differently. These two protons of **10** were shown in more up-field than those of **9**. According to the published data [99], **10** was determined to be neoastilbin with 2*S*, and 3*S* configurations. The ^1H, ^{13}C NMR data and HMBC correlation of compound **10** are shown in Table 20.

Compound **11** was isolated as a white-yellowish amorphous solid. HRESIMS gave the molecular ion $[M-H]^-$ peak at *m/z* 289.0719 corresponding to $C_{15}H_{14}O_6$ (calc. 290.0790). The UV absorption maxima were observed at 210 and 292

in methanol. The IR spectrum displayed absorption bands at 3452 (O–H stretching), 1606 (C=O stretching) and 1140 (C–O stretching) cm^{-1}. The ^{1}H NMR spectra data of **11** (Table 21) displayed the ABX system of flavonoid ring A at δ 7.05 (1H, d, J = 1.9 Hz), 6.84 (1H, d, J = 8.1 Hz) and 6.78 (1H, dd, J = 2.0, 2.0 Hz). The proton signals at δ 6.02 and 5.92 (each 1H, d, J = 2.3 Hz) corresponded to the *meta*-coupling of flavonoid ring B. The presence of a multiplet signal at δ 4.20 (1H) and two doublets of doublet signals at δ 2.86 (1H, J = 4.6, 4.6 Hz) and 2.74 (1H, J = 3.3, 3.3 Hz) together with the appearance of the oxygen-attached tertiary carbon at δ 78.5 and 66.0 in the DEPT135 spectrum indicated that **11** should be a flavan with oxygenation at C-3. The ^{13}C NMR and DEPT135 spectra (Table 21) showed the methylene carbon at δ 28.1, seven methine carbons (δ 66.0, 78.5, 94.8, 95.2, 114.3, 114.5, 118.4) and seven quaternary carbons (δ 156.7, 156.6, 156.2, 144.3, 144.3, 131.4, 98.9). The ^{1}H and ^{13}C NMR assignments of **11** were performed with the aid of HMQC and HMBC experiments. The absolute configuration at C-2 and C-3 of **11** has been demonstrated to be 2*R* and 3*R*, respectively, by comparing the optical rotation to those reported in the literature [99]. Compound **11** was identified as (-)-epicatechin by the spectroscopic analysis and comparison with previously reported data [99].

Compound **12** was isolated as a light brown solid. HRESIMS gave the molecular ion $[M–H]^-$ peak at *m/z* 227.0706, corresponding to $C_{14}H_{12}O_3$ (calc. 228.0786). The UV absorption maxima were observed at 217 and 306 in methanol. The IR spectrum displayed absorption bands at 3175 (O–H stretching) and 1583 (C=C stretching) cm^{-1}. The ^{1}H-NMR spectral data (Table 22) displayed the doublet signals at δ 7.41 and 6.83 (each 2H, J = 8.6 Hz) suggested the presence of 1,4 disubstituted benzene ring, whereas the doublet signal at δ 6.54 (2H, d, J = 2.1 Hz) and triplet signal at δ 6.27 (1H, J = 2.1, 2.0 Hz) indicated the presence of 1,3,5-trisubstituted benzene ring. Moreover, low field resonances at δ 6.88 (1H, d, J = 16.4 Hz) and 7.01 (1H, d, J = 16.3 Hz) were assigned as protons of the *trans*-double bond. The ^{13}C NMR and DEPT spectral data (Table 22) revealed the presence of 14 carbon signals, including nine methines and five quaternary carbon atoms. The connection of two benzene rings, 1,3,5-trisubstituted and 1,4 disubstituted benzenes was confirmed by

HMBC correlations. Thus, **12** was identified as resveratrol and the spectroscopic data as well as comparison with the literature [100].

Compound **13** was isolated as a light brown powder. HRESIMS gave the molecular ion $[M+H]^+$ peak at *m/z* 391.1396 corresponding to $C_{20}H_{22}O_8$ (calc. 390.1315). The UV absorption maxima were observed at 210 and 290 in methanol. The IR spectrum displayed absorption bands at 3199 (O–H stretching) and 1508 (C=C stretching) and 1080 (C–H bending) cm^{-1}. The ^1H- and ^{13}C-NMR spectra of **13** show similar signals and patterns to compound **12** (Table 23). The only differences in ^1H-NMR between **13** and **12** were the presence of a glucose signal in **13**. The presence of an anomeric proton signal at δ 4.93 (1H, d, J = 7.3 Hz) suggested that **13** should be a monoglucoside of resveratrol aglycone. The HMBC correlation between the C-4' (δ 158.6) of resveratrol unit and the H-1" protons of glucose unit confirmed the substitution of glucose on C-4' of the resveratrol molecule. Based on the above spectral evidence and a comparison of its NMR data with the report data [101], **13** was identified as (*E*)-resveratrol 4'-*O*-β-D-glucoside.

Compound **14** was isolated as a yellow solid. HRESIMS gave the molecular ion $[M–H]^-$ peak at *m/z* 433.0762, corresponding to $C_{20}H_{18}O_{11}$ (calcd 434.0849). The UV absorption maxima were observed at 210 and 258 in methanol. The IR spectrum displayed absorption bands at 3469 (O–H stretching), 1738 (C=O stretching) and 1352 (C–O stretching) cm^{-1}. The ^1H and ^{13}C NMR spectra of **14** (Table 24) showed the typical pattern of flavonol glycoside. The aglycone unit was identified as quercetin from the ABX system of ring A at δ 7.66 (1H, dd, J = 8.5, 2.2 Hz), 7.50 (1H, d, J = 2.2 Hz) and 6.84 (1H, d, J = 8.5 Hz) together with two doublet signals at δ 6.40 and 6.20 (each 1H, J = 2.0 Hz) for ring B. The presence of an anomeric proton at δ 5.28 (1H, d, J = 5.2 Hz) and a sugar region at δ 3.20 – 3.40 was observed. The J coupling and pattern of these sugar signals corresponded to the arabinose structure. The configuration of the arabinose was determined by the coupling constant of the anomeric proton, where **14** was 5.2 Hz, showing a β-configuration. The ^{13}C NMR and DEPTQ signals for **14** were in good agreement with those of quercetin arabinoside, which contained nine methine carbons, ten quaternary carbons and one methylene carbon. The cross peak between H-5″ and C-1″ in the

HMBC spectrum confirmed the structure of arabinopyranoside. Furthermore, the observed HMBC correlation between the anomeric proton and C-3 indicated that arabinose was connected to the C-3 position of quercetin. The NMR data for **14** were consistent with quercetin 3-*O*-*β*-D-arabinoside [102].

Compound **15** was isolated as a white solid. HRESIMS gave the molecular ion $[M-H]^-$ peak at *m/z* 273.0766, corresponding to $C_{15}H_{14}O_5$ (calcd 274.0841). The UV absorption maxima were observed at 223 and 286 in methanol. The IR spectrum displayed absorption bands at 3207 (O–H stretching) and 1602 (C=O stretching) cm^{-1}. The ^1H NMR spectral data (Table 25) displayed the presence of a 1,4-disubstituted benzene ring at δ 7.08 and 6.75 (each 2H, d, J = 8.5 Hz). The *meta*-coupled aromatic protons at δ 5.94 (2H, s) were assigned as H-3' and H-5'. Additionally, the proton signals at δ 3.33 (2H, t, J = 8.0, 7.6 Hz) and 2.87 (2H, t, J = 8.1, 7.5 Hz) were deduced as methylene protons at C-α and C-β, respectively. The ^{13}C NMR spectral data (Table 25) exhibited 15 carbon signals, including two methylene carbons (δ 30.7, 46.7), three methine carbons (δ 95.8, 115.9, 130.1), and six quaternary carbons (δ 105.1, 133.4, 156.2, 165.2, 165.3). The structure of **15** was confirmed by HMBC correlations. Therefore, **15** was identified as phloretin, which was previously isolated from crabapple leaves [103].

Compound **16** was isolated as a white amorphous solid. HRESIMS gave the molecular ion $[M-H]^-$ peak at *m/z* 435.1281, corresponding to $C_{21}H_{24}O_{10}$ (calc. 436.1369). The UV absorption maxima were observed at 223 and 286 in methanol. The IR spectrum displayed absorption bands at 3200 (O–H stretching) and 1628 (C=O stretching) cm^{-1}. The ^1H and ^{13}C NMR spectra of **16** (Table 26) show similar signals and patterns to compound **15**. The only differences in ^1H-NMR between **16** and **15** were the presence of glucose signals (δ 3.5 – 5.0, 7H) in **16**. Furthermore, the presence of an anomeric proton signal at δ 5.01 with J coupling of 7.6 Hz suggested that the glucose was determined to be β-form. The ^{13}C NMR and DEPT135 spectra (Table 26) displayed 15 carbon signals of the phloretin aglycone, together with six carbon signals, indicating a glucose unit within the molecule. The HMBC correlation between the C-4' of phloretin unit and the H-1" methylene protons of the glucose unit confirmed the substitution of glucose on the C-4' of the phloretin molecule. According

to the above spectral evidence and a comparison of its NMR data with the report data [10], **16** was identified as phloretin 4'-*O*-*β*-D-glucoside or trilobatin.

Compound **17** was isolated as a white amorphous solid. HRESIMS gave the molecular ion $[M–H]^-$ peak at *m/z* 587.1394, corresponding to $C_{28}H_{27}O_{14}$ (calc. 587.1401). The UV absorption maxima were observed at 219 and 279 in methanol. The IR spectrum displayed absorption bands at 3415 (O–H stretching), 1693 (C=O stretching) and 1194 (C–O stretching) cm^{-1}. The ^1H and ^{13}C NMR spectra of **17** (Table 27) showed similar signals and patterns to compound **16**. The only differences in ^1H NMR between **17** and **16** were the presence of a singlet proton at δ 7.15 (2H). The presence of a singlet signal of two protons and seven carbon signals, including six methine aromatic carbons (δ 109.3, 121.0, 138.1, and 145.3) and carbonyl carbon of ester (δ 166.1), were indicated for a galloyl group. The connecting position of the galloyl group was determined as methylene of the glucose unit based on the characteristic low field shift of H-6" (δ 4.41, 1H, dd, J = 4.9, 4.8 Hz) and 4.61 (δ 4.61, 1H, dd, J = 2.0, 1.9 Hz) compared to those of compound **16**. Moreover, the HMBC correlation between H-6" and C-7"' was observed. According to the above spectral evidence and a comparison of its NMR data with the report data [10], **17** was identified as phloretin 4'-*O*-(6"-*O*-galloyl)-*β*-D-glucoside or yanangdaengin.

Compound **18** was isolated as a white solid. HRESIMS gave the molecular ion $[M+H]^+$ peak at *m/z* 195.0867, corresponding to $C_7H_{14}O_6$ (calc. 194.0790). The UV absorption maxima were observed at 190 in water. The IR spectrum displayed absorption bands at 3297 (O–H stretching), 2906 (C–H stretching), and 1124 (C–O stretching) cm^{-1}. The ^1H NMR spectral data of **18** (Table 28) exhibited six signals of nine protons at δ 3 – 4, which is the range of oxygenated proton C-H proton located near oxygen. The signals of two triplets of H-3 at δ 3.21 (1H, J = 9.6 Hz) and H-4 at 3.52 (1H, J = 9.6 Hz) showed a large J coupling constant, which means this proton coupling with the neighboring protons at a 180° angle. The two doublet of doublet signals of H-5 (δ 3.62, 1H, J = 9.9, 2.7 Hz) and H-2 (δ 3.68, 1H, J = 10.0, 2.7 Hz) suggested that these protons are located between two neighboring protons with different dihedral angle, large and small dihedral angles. Moreover, the singlet signal of the methoxy group was displayed at δ 3.46. The ^{13}C

and DEPT135 NMR spectral data (Table 28) displayed six methine carbon atoms and one methyl carbon atom for the methoxy group. The COSY NMR spectral data implied that these protons are linked to each other as cyclic molecules. The position of the methoxy group was determined by the HMBC spectrum and the correlation between the proton of the methoxy group and C-3 was observed. The structure of **18** was identified by NMR spectroscopic techniques and by comparing the data with that previously reported [104]. This evidence completed the assignment of **18** as pinitol.

Compound **19** was isolated as a white solid. HRESIMS gave the molecular ion $[M-H]^-$ peak at *m/z* 169.0136, corresponding to $C_7H_6O_5$ (calc. 170.0215).

Compound **20** was isolated as a white solid. HRESIMS gave the molecular ion $[M-H]^-$ peak at *m/z* 197.0445, corresponding to $C_9H_{10}O_5$ (calc. 198.0528). The UV absorption maxima were observed at 218 in methanol. The IR spectrum displayed absorption bands at 3281 (O–H stretching), 1704 (C=O stretching) and 1194 (C–O stretching) cm^{-1}.

The ^1H NMR spectrum of **19** showed only one singlet signal of an aromatic proton at δ 7.14 ppm. The ^{13}C NMR spectral data displayed two methine carbons and four quaternary carbons in the aromatic carbon region. Moreover, the signal carbonyl carbon of carboxylic acid was observed at δ 167.6 ppm. Similar to **19**, the ^1H NMR spectral data of **20** presented a singlet signal at δ 7.11 (2H, *s*). Additionally, the quartet (δ 4.24, 2H, J = 2.4, 2, 2.4 Hz) and triplet (δ 1.31, 3H, J = 6.8, 7.2 Hz) signals were observed. The ^{13}C NMR spectrum showed seven carbon signals of nine carbon atoms, including one methyl, one, methylene, two methines, and five quaternary carbon atoms. All of the data from spectroscopic techniques of **19** and **20** were in agreement with the structures of gallic acid and gallic acid ethyl ester, respectively. The complete chemical shift assignments for ^1H and ^{13}C NMR of compounds **19** and **20** are shown in Table 29.

Table 18 The ^{1}H and ^{13}C NMR assignments and HMBC correlations of compound **8** in acetone-d_6 and astilbin DMSO-d_6

Position	Compound **8**			Astilbin [99]	
	δ_H, (mult, *J* in Hz)	δ_C	HMBC correlations	δ_H, (mult, *J* in Hz)	δ_C
2	5.18 (d, 10.6)	83.3	C-3, C-4, C-2', C-6'	5.24 (d, 11.2)	82.6
3	4.69 (d, 10.6)	77.3	C-2, C-1'', C-4, C-1'	4.65 (d, 11.2)	77.2
4	-	195.9	-	-	194.6
5	-	165.2	-	-	164.1
6	5.95 (d, 2.1)	97.1	C-8, C-10, C-9, C-5, C-7,	5.88 (d, 2.4)	96.0
7	-	167.7	-	-	167.2
8	5.99 (d, 2.1)	95.8	C-10, C-6, C-9, C-5, C-7	5.90 (d, 2.4)	94.9
9	-	164.9	-	-	162.7
10	-	102.3	-	-	101.1
1'	-	128.9	-	-	127.8
2'	7.09 (d, 1.8)	116.0	C-2, C-5', C-6', C-4',	6.88 (s)	114.9
3'	-	145.9	-	-	145.2
4'	-	146.8	-	-	146.0
5'	6.90 (d, 8.1)	115.3	C-2, C-1', C-3'	6.73 (s)	114.1
6'	6.86 (dd, 8.1, 1.8)	120.4	C-2', C-4'	6.73 (s)	119.1
1''	4.10 (s)	101.0	C-3, C-3'', C-5'', C-2''	4.03 (s)	100.8

Table 18 (cont.)

Position	Compound **8**			Astilbin [99]	
	δ_H, (mult, *J* in Hz)	δ_C	HMBC correlations	δ_H, (mult, *J* in Hz)	δ_C
2"	3.95 (m)	71.3	C-4"	3.37 (m)	70.4
3"	3.68 (m)	72.1	-	3.38 (m)	70.8
4"	3.33 (dd, 11.3, 8.0)	73.4	C-2"	3.12 (d, 5.4)	72.4
5"	4.22 (m)	69.9	C-4"	3.90 (dd, 9.6, 3)	69.1
6"	1.15 (d, 6.2)	17.9	C-6", C-5", C-4"	1.04 (d, 6.0)	16.4
5-OH	11.92	-	-	11.80	-
7-OH	9.88	-	-	10.88	-
3'-OH	8.19	-	-	9.54	-
4'-OH	8.21	-	-	9.97	-

Table 19 The ^{1}H and ^{13}C NMR assignments and HMBC correlations of compound **9** in DMSO-d_6 and isoastilbin in DMSO-d_6

Position	Compound **9**			Isoastilbin [99]	
	δ_H, (mult, *J* in Hz)	δ_C	HMBC correlations	δ_H, (mult, *J* in Hz)	δ_C
2	5.53 (d, 2.5)	79.9	C-3, C-4, C-2', C-6', C-1', C-9	5.55 (d, 2.4)	80.7
3	4.19 (d, 2.5)	73.3	C-1", C-4, C-1'	4.21 (d 2.4)	74.1
4	-	193.4	-	-	192.9
5	-	164.0	-	-	164.8
6	5.90 (d, 2.0)	96.2	C-8, C-10, C-7	5.92 (d, 1.8)	96.0
7	-	167.2	-	-	167.4
8	5.93 (d, 2.0)	95.2	C-10, C-6, C-9, C-7	5.95 (d, 2.4)	94.8
9	-	162.5	-	-	163.1
10	-	100.3	-	-	100.4
1'	-	126.4	-	-	127.3
2'	6.82 (d, 1.2)	114.0	C-2, C-3', C-6', C-4',	6.84 (s)	114.9
3'	-	145.0	-	-	145.0
4'	-	143.1	-	-	145.3
5'	6.70 (m)	115.1	C-2, C-1', C-3', C-2', C-4'	6.72 (m)	113.8
6'	6.70 (m)	117.6	C-2, C-1', C-3', C-2', C-4'	6.72 (m)	118.0

Table 19 (cont.)

Position	Compound **9**			Isoastilbin [99]	
	δ_H, (mult, *J* in Hz)	δ_C	HMBC correlations	δ_H, (mult, *J* in Hz)	δ_C
1"	4.74 (d, 1.03)	98.8	C-3, C-3", C-2"	4.47 (s)	98.8
2"	3.44 (m)	70.2	C-4"	3.46 (s)	70.6
3"	3.16 (m)	70.3	C-4"	3.19 (m)	70.6
4"	3.02 (m)	71.2	C-2", C-3", C-6"	3.05 (m)	71.9
5"	2.43 (m)	69.0	C-4", C-6"	2.45 (m)	69.0
6"	0.82 (d, 6.2)	17.6	C-5", C-4"	0.84 (d, 6.0)	16.4
OH-5	11.75 (s)	-	C-6, C-10, C-7	11.76 (s)	-

Table 20 The ^{1}H and ^{13}C NMR assignments and HMBC correlations of compound **10** in acetone-d_6 and neoastilbin in DMSO-d_6

Position	Compound **10**			Neoastilbin [99]	
	δ_H, (mult, *J* in Hz)	δ_C	HMBC correlations	δ_H, (mult, *J* in Hz)	δ_C
2	5.08 (d, 11.2)	83.0	C-3, C-4, C-9, C-1', C-2', C-6'	5.10 (d, 11.2)	94.9
3	4.70 (d, 11.2)	75.6	C-2, C-4, C-1', C-1"	4.75 (d, 11.2)	82.3
4	-	197.4	-	-	196.2
5	-	164.8	-	-	167.4
6	5.94 (d, 2.1)	95.8	C-4, C-7, C-8, C-9	5.85 (d, 2.4)	100.6
7	-	167.8	-	-	167.5
8	5.98 (d, 2.1)	97.0	C-4, C-5, C-6, C-7	5.90 (d, 2.4)	96.1
9	-	163.7	-	-	164.1
10	-	99.3	-	-	101.4
1'	-	129.5	-	-	145.2
2'	7.07 (s)	115.2	C-4', C-6'	6.90 (s)	119.6
3'	-	145.8	-	-	146.0
4'	-	146.6	-	-	162.9
5'	6.86 (d, 0.9)	115.6	C-1', C-2', C-3', C-4', C-5'	6.70 (s)	114.9
6'	6.86 (d, 0.9)	120.5	C-1', C-2', C-3', C-4'	6.70 (s)	128.6

Table 20 (cont.)

Position	Compound **10**			Neoastilbin [99]	
	δ_H, (mult, *J* in Hz)	δ_C	HMBC correlations	δ_H, (mult, *J* in Hz)	δ_C
1"	5.19 (d, 1.0)	101.9	C-3, C-2", C-3", C-5"	4.93 (d, 0.8)	114.1
2"	3.99 (dd, 3.2, 1.5)	71.3	C-1", C-3", C-4"	3.15 (dd, 9.6, 3.0)	70.5
3"	3.38 (dd, 9.4, 3.4)	71.7	C-2", C-4", C-5"	3.15 (dd, 9.6, 3.0)	72.0
4"	3.23 (t, 9.4, 9.4)	73.0	C-2", C-3", C-5", C-6"	3.03 (m)	75.5
5"	2.34 (m)	69.4	C-1", C-3", C-4", C-6"	2.26 (m)	68.9
6"	0.89 (d, 6.2)	17.8	C-4", C-5"	0.79 (d, 6.0)	16.5

Table 21 The ^{1}H and ^{13}C NMR assignments and HMBC correlations of compound **11** in acetone-d_6 and epicatechin in DMSO-d_6

Position	Compound **11**			Epicatechin [99]	
	δ_H, (mult, *J* in Hz)	δ_C	HMBC correlations	δ_H, (mult, *J* in Hz)	δ_C
2	4.88 (s)	78.5	C-4, C-2', C-6', C-1', C-9	4.70 (s)	78.5
3	4.20 (m)	66.0	-	4.00 (m)	66.1
4	2.74 (dd, 16.6, 3.3)	28.1	C-4, C-3, C-2, C-10, C-5	2.46 (dd, 3.6, 5.4)	27.9
	2.86 (dd, 16.5, 4.6)			2.67 (dd, 4.8, 4.8)	
5	-	156.2	-	-	156.0
6	5.92 (d, 2.3)	94.8	C-8, C-10, C-5	5.71 (d, 2.4)	95.0
7	-	156.6	-	-	156.3
8	6.02 (d, 2.3)	95.2	C-6, C-10, C-7	5.89 (2.4)	94.5
9	-	156.7	-	-	156.6
10	-	98.9	-	-	98.7
1'	-	131.4	-	-	130.9
2'	7.05 (d, 1.9)	114.3	C-2, C-6', C-1', C-4',	6.89 (s)	113.9
3'	-	144.3	-	-	144.4
4'	-	144.4	-	-	144.6
5'	6.78 (d, 8.1)	114.6	C-1', C-3'	6.65 (t, 8.0)	114.5
6'	6.84 (dd, 8.2, 2.0)	118.5	C-2', C-2, C-4'	6.65 (t, 8.0)	118.0

Table 22 The ^{1}H and ^{13}C NMR assignments and HMBC correlations of compound **12** in acetone-d_6 and (*E*)-resveratrol in MeOD

Position	Compound **12**			(*E*)-Resveratrol [100]	
	δ_H, (mult, *J* in Hz)	δ_C	HMBC correlations	δ_H, (mult, *J* in Hz)	δ_C
1	-	150.6	-	-	140.9
2	6.54 (d, 2.1)	105.3	C-3, C-4, C-5, C-6, C-α	6.56 (d, 2.0)	105.7
3	-	159.3	-	-	159.6
4	6.27 (t, 2.1, 2.0)	102.3	C-2, C-3, C-5, C-6	6.29 (t, 2,3)	102.7
5	-	159.3	-	-	159.6
6	6.54 (d, 2.1)	105.3	C-2, C-3, C-4, C-5, C-α	6.56 (d, 2.0)	105.7
α	6.88 (d, 16.4)	126.4	C-1, C-2, C-6, C-α', C-1'	6.90 (d, 16.5)	129.1
α'	7.01 (d, 16.3)	129.1	C-1, C-α, C-2', C-6'	7.04 (d, 16.0)	130.0
1'	-	129.7	-	-	126.9
2'	7.41 (d, 8.6)	128.7	C-α', C-4', C-6'	7.43 (d, 8.5)	128.7
3'	6.83 (d, 8.6)	115.5	C-1', C-4', C-5'	6.86 (d, 9.0)	116.4
4'	-	158.0	-	-	158.2
5'	6.83 (d, 8.6)	115.5	C-1', C-3', C-5'	6.68 (d, 9.0)	116.4
6'	7.41 (d, 8.6)	128.7	C-α', C-2', C-4'	7.44 (d, 8.5)	128.7
OH-5, 3	8.31 (s)	-	C-2, C-3, C-4, C-5, C-6	8.23 (s)	-
OH-4'	8.58 (s)	-	C-3', C-4', C-5'	8.49 (s)	-

Table 23 The ^{1}H and ^{13}C NMR assignments and HMBC correlations of compound **13** in acetone-d_6 and (*E*)-resveratrol 4'-*O*-*β*-D-glucoside in MeOD

Position	Compound **13**			(*E*)-Resveratrol 4'-*O*-*β*-D-glucoside [101]	
	δ_H, (mult, *J* in Hz)	δ_C	HMBC correlations	δ_H, (mult, *J* in Hz)	δ_C
1	-	141.0	-		139.6
2, 6	6.48 (d, 2.1)	105.9	C-4, C-α, C-3,5	6.49 (d, 2.2)	104.5
3, 5	-	159.6	-		158.3
4	6.19 (t, 2.1, 2.1)	102.9	C-3, 5, C-2, 6	6.23 – 6.18 (m)	101.5
1'	-	133.1	-		131.8
2', 6'	7.44 (d, 8.7)	128.6	C-α', C-3', 5', C-4'	7.48 (d, 8.7)	127.2
3', 5'	7.08 (d, 8.7)	117.8	C-1', C-4'	7.11 (d, 8.7)	116.5
4'	-	158.6	-		157.3
1"	4.93 (d, 7.3)	102.1	C-4", C-3", C-4'	4.94 (d, 7.2)	100.8
2"	3.45 (m)	74.8	C-6", C-4", C-2", C-3", C-5"	3.51 – 3.34 (m)	73.5
3"		77.9			76.6
4"		71.3			67.0
5"		78.1			76.8
6"	3.90 (dd, 12.0, 1.7)	62.4	C-4", C-3"	3.73 (dd, 12.1, 5.7)	61.1
	3.72 (dd, 12.1, 5.2)		C-4", C-3"	3.93 (dd, 12.1, 2.4)	

Table 22 (cont.)

Position	Compound **13**			(*E*)-Resveratrol 4'-*O*-*β*-D-glucoside [101]	
	δ_H, (mult, *J* in Hz)	δ_C	HMBC correlations	δ_H, (mult, *J* in Hz)	δ_C
α	6.87 (d, 16.3)	128.5	C-2,6, C-α', C-1', C-1	6.90 (d, 16.2)	127.1
α'	6.99 (d, 16.3)	128.8	C-2',6', C-α', C-1', C-1	7.02 (d, 16.3)	127.4

Table 24 The ^{1}H and ^{13}C NMR assignments and HMBC correlations of compound **14** in DMSO-d_6 and quercetin 3-*O*-β-D-arabinoside in MeOD

Position	Compound **14**			Quercetin 3-*O*-β-D-arabinoside [102]	
	δ_H, (mult, *J* in Hz)	δ_C	HMBC correlations	δ_H, (mult, *J* in Hz)	δ_C
2	-	156.3	-	-	156.1
3	-	133.8	-	-	133.5
4	-	177.6	-	-	177.3
5	-	161.3	-	-	161.1
6	6.20 (d, 2.0)	98.7	C-8, C-4, C-10, C-7, C-5	6.41 (d, 2.1)	98.5
7	-	164.3	-	-	164.3
8	6.40 (d, 2.0)	93.5	C-6, C-4, C-10, C-7, C-9	6.23 (d, 2.1)	93.4
9	-	156.3	-	-	155.9
10	-	104.0	-	-	103.5
1'	-	121.0	-	-	120.3
2'	7.50 (d, 2.2)	115.7	C-6', C-2, C-4', C-3'	7.51 (d, 2.0)	115.3
3'	-	148.7	-	-	145.3
4'	-	145.1	-	-	148.7
5'	6.84 (d, 8.5)	115.4	C-2, C-4', C-3', C-1'	6.85 (d, 8.3)	115.7
6'	7.66 (dd, 8.5, 2.2)	122.1	C-2', C-2, C-3'	7.25 (dd, 8.3, 2.0)	123.0

Table 24 (cont.)

Position	Compound **14**			Quercetin 3-*O*-*β*-D-arabinoside [102]	
	δ_H, (mult, *J* in Hz)	δ_C	HMBC correlations	δ_H, (mult, *J* in Hz)	δ_C
1''	5.28 (d, 5.2)	101.4	C-5'', C-3'', C-3	5.27 (d, 5.1)	100.9
2''	3.75 (t, 6.3, 5.8)	70.7	C-4'', C-3'', C-1''	3.23 – 3.62 (m)	70.5
3''	3.51 (m)	71.6	C-2'', C-1''	3.23 – 3.62 (m)	71.4
4''	3.65 (m)	66.1	C-3''	3.23 – 3.62 (m)	65.5
5''	3.60 (dd, 5.2, 5.3)	64.3	C-1'', C-3''	3.23 – 3.62 (m)	63.6
	3.21 (dd, 2.1, 2.0)		C-1'', C-3'', C-4''		
OH-5	12.6 (s)	-	C-6, C-7, C-5, C-10	-	-

Table 25 The ^{1}H and ^{13}C NMR assignments and HMBC correlations of compound **15** in acetone-d_6 and phloretin in MeOD

Position	Compound **15**			Phloretin [103]	
	δ_H, (mult, *J* in Hz)	δ_C	HMBC correlations	δ_H, (mult, *J* in Hz)	δ_C
α	3.33 (t, 7.6, 8.0)	46.7	C-β, C-1, C=O	3.20 (t, 7.6)	45.9
β	2.88 (t, 8.1, 7.5)	30.7	C-α, C-2,6, C-1, C=O	2.86 (t, 7.6)	30.1
1	-	133.4	-	-	132.6
2, 6	7.08 (d, 8.5)	130.1	C-3,5, C-4, C-β	7.00 (d, 8.5)	128.9
3, 5	6.75 (d, 8.5)	115.9	C-1, C-4, C-2,6	6.65 (d, 8.5)	143.9
4	-	156.2	-	-	155.0
1'	-	105.1	-	-	103.9
2', 6'	-	165.3	-	-	164.7
3', 5'	5.94 (s)	95.8	C=O, C-2', 6', C-1', C-4'	5.80 (s)	94.3
4'	-	165.2	-	-	164.4
C=O	-	205.5	-	-	205.0

Table 26 The ^{1}H and ^{13}C NMR assignments and HMBC correlations of compound **16** in acetone-d_6 and phloretin 4'-*O*-β-D-glucoside in MeOD

Position	Compound **16**			Phloretin 4'-*O*-β-D-glucoside [10]	
	δ_H, (mult, *J* in Hz)	δ_C	HMBC correlations	δ_H, (mult, *J* in Hz)	δ_C
α	3.33 (t, 7.2, 8.2)	46.1	C-β, C-1, C=O	3.30 (m)	47.6
β	2.86 (t, 7.8, 7.7)	29.6	C-α, C-2,6, C-1, C=O	2.86 (m)	31.2
1	-	132.5	-	-	133.8
2, 6	7.07 (d, 8.3)	129.3	C-β, C-3,5, C-4	7.04 (d, 8.5)	130.3
3, 5	6.74 (d, 8.4)	115.2	C-1, C-4	6.69 (d, 8.5)	116.1
4	-	155.2	-	-	156.5
1'	-	105.6	-	-	106.8
2', 6'	-	164.1	-	-	165.4
3', 5'	6.13 (s)	95.5	C-1', C-4', C=O, C-2',6'	6.09 (s)	96.4
4'	-	163.7	-	-	165.0

Table 26 (cont.)

Position	Compound **16**			Phloretin 4'-*O*-*β*-D-glucoside [10]	
	δ_H, (mult, *J* in Hz)	δ_C	HMBC correlations	δ_H, (mult, *J* in Hz)	δ_C
1"	5.01 (d, 7.6)	99.9	C-4', C-3"	4.93 (d, 7.4)	101.1
2"	3.62-3.45 (m)	73.5	C-4", C-5", C-2", C-6", C-4", C-3'', C-1''	3.43 (m)	74.6
3"		76.9		3.39 (m)	77.9
4"		70.3		3.45 (m)	71.1
5"		76.9		3.45 (m)	78.3
6"	3.94 (dd, 1.6, 1.4)	61.7	C-5", C-4"	3.90 (dd, 12.1, 2.1)	62.3
	3.74 (dd, 5.7, 5.7)		C-5", C-4"	3.71 (dd, 12.1, 5.5)	
C=O		205.7	-	-	207.0

Table 27 The ^{1}H and ^{13}C NMR assignments and HMBC correlations of compound **17** in acetone-d_6 and phloretin 4'-*O*-(6"-*O*-galloyl)-*β*-D-glucoside in MeOD

Position	Compound **17**			Phloretin 4'-*O*-(6"-*O*-galloyl)-*β*-D-glucoside [10]	
	δ_H, (mult, *J* in Hz)	δ_C	HMBC correlations	δ_H, (mult, *J* in Hz)	δ_C
α	3.35 (t, 7.4, 8.2)	46.3	C-β, C=O, C-1	3.30 (m)	31.2
β	2.87 (t, 8.1, 7.3)	29.3	C-α, C-6,2, C=O, C-1	2.85 (m)	47.5
1	-	132.5	-	-	133.9
2, 6	7.08 (d, 8.5)	129.4	C-β, C-3,5, C-4	7.04 (d, 8.6)	130.3
3, 5	6.74 (d, 8.6)	115.3	C-1, C-4	6.69 (d, 8.6)	116.1
4	-	155.6	-	-	156.4
1'	-	105.9	-	-	107.0
2', 6'	-	164.2	-	-	165.4
3', 5'	6.16 (s)	95.6	C-1', C-4', C-2', 6', C=O	6.08 (s)	96.4
4'	-	163.7	-	-	164.9
1"	5.12 (d, 7.8)	99.9	C-4'	4.98 (d, 7.5)	101.1
2"	3.55 (m)	73.6	C-3", C-1"	3.47 (m)	74.6
3"	3.65 (m)	76.9	C-4", C-2"	3.50 (m)	77.7
4"	3.65 (m)	70.1	C-2", C-3"	3.53 (m)	71.1
5"	3.89 (m)	74.5	-	3.74 (ddd, 9.3, 4.8, 2.2)	75.7

Table 27 (cont.)

Position	Compound **17**			Phloretin 4'-*O*-(6''-*O*-galloyl)-*β*-D-glucoside [10]	
	δ_H, (mult, *J* in Hz)	δ_C	HMBC correlations	δ_H, (mult, *J* in Hz)	δ_C
6"	4.61 (dd, 2.0, 1.9)	63.4	C-4", C-5", C-7'''	4.55 (dd, 12.1, 2.2)	64.3
	4.41 (dd, 4.9, 4.8)			4.46 (dd, 12.1, 4.8)	
1'''	-	121.0	-	-	121.2
2''', 6'''	7.15 (s)	109.3	C-1''', C-4''', C-3''', 5''', C-7'''	7.08 (s)	110.2
3''', 5'''	-	145.3	-	-	146.5
4'''	-	138.1	-	-	139.8
7'''	-	166.1	-	-	168.3
C=O	-	205.5	-	-	207.0

Table 28 The ^{1}H and ^{13}C NMR assignments and HMBC correlations of compound **18** in D_2O and pinitol in D_2O

Position	Compound **18**			Pinitol [104]	
	δ_H, (mult, *J* in Hz)	δ_C	HMBC correlations	δ_H, (mult, *J* in Hz)	δ_C
1	3.88 (m)	71.6	C-2, C-3, C-5	3.85 (m)	72.3
2	3.68 (dd, 10.0, 2.7)	69.8	C-3	3.66 (dd, 9.9, 2.6)	71.7
3	3.21 (t, 9.6)	82.7	C-1, C-5, -OCH_3	3.19 (dd, 9.9, 9.5)	83.0
4	3.52 (t, 9.6)	72.1	C-3, C-5	3.50 (dd, 9.5, 10.0)	70.7
5	3.62 (dd, 9.9, 2.7)	70.5	C-4	3.61 (dd, 10.0, 2.6)	71.9
6	3.87 (m)	71.4	C-2, C-5	3.85 (m)	70.0
-OCH_3	3.46 (s)	59.7	C-3	3.45 (s)	59.9

Table 29 The ^{1}H and ^{13}C NMR assignments and HMBC correlations of gallic acid (**19**) and gallic acid ethyl ester (**20**) in acetone-d_6

Position	Compound **19**		Compound **20**	
	δ_H, (mult, *J* in Hz)	δ_C	δ_H, (mult, *J* in Hz)	δ_C
1	-	121.6	-	122.0
2, 6	7.14 (s)	109.6	7.11 (s)	109.6
3, 5	-	145.6	-	146.0
4	-	138.2	-	138.7
7	-	167.6	-	166.0
8	-	-	4.24 (q, 2.4, 2.0, 2.4)	60.9
9	-	-	1.31 (t, 6.8, 7.2)	14.4

The thirteen compounds were isolated from *L. strychnifolium*. The results indicated that compounds **8**, **9** and **18** were isolated from the root, in the same manner that compounds **8**–**13** and **18** were isolated from the stem. Compounds **14**–**18** were isolated from the extract of the leaves. Moreover, compounds **16** and **18**–**20** were isolated from the flower extract. All isolated compounds are listed in Table 30.

Table 30 Chemical constituents isolated from *L. strychnifolium*

Parts	Compounds	Class
Root	Astilbin (**8**)	Flavanones
	Isoastilbin (**9**)	Flavanones
	Pinitol (**18**)	Cyclitol
Stem	Astilbin (**8**)	Flavanones
	Isoastilbin (**9**)	Flavanones
	Neoastilbin (**10**)	Flavanones
	Epicatechin (**11**)	Flavan 3-ol
	Resveratrol (**12**)	Stilbenes
	Resveratrol 4'-*O*-*β*-D-glucoside (**13**)	Stilbenes
	Pinitol (**18**)	Cyclitol
Leaves	Quercetin 3-*O*-*β*-D-arabinoside (**14**)	Flavonol
	Phloretin (**15**)	Dihydrochalcone
	Phloretin 4'-*O*-*β*-D-glucoside (**16**)	Dihydrochalcone
	Phloretin 4'-*O*-(6"-*O*-galloyl)-*β*-D-glucoside (**17**)	Dihydrochalcone
	Pinitol (**18**)	Cyclitol
Flower	Phloretin 4'-*O*-*β*-D-glucoside (**16**)	Dihydrochalcone
	Gallic acid (**19**)	Phenolic acid
	Gallic acid ethyl ester (**20**)	Phenolic acid
	Pinitol (**18**)	Cyclitol

As shown in Table 30, pinitol (**18**) was isolated from all stems, leaves, flower and root extracts. Additionally, the chemical constituents of the root and stem, as well as the chemical constituents of the leaves and flower, are related. in the stems, astilbin (**8**) and its stereoisomers (**9**, **10**) were detected. In addition, astilbin (**8**) and

isoastilbin (**9**) were also found in the roots. Epicatechin (**11**) and stilbenes (**12**, **13**) were isolated only from the stems. Likewise, quercetin 3-*O*-β-D-arabinoside (**14**) was only isolated from the leaves. Dihydrochalcones (**15**–**17**) were found in the leaves and flowers. Moreover, gallic acid (**19**) and its ethyl ester derivative (**20**) were found in flowers. It should be noted that the chemical constituents of *L. strychnifolium* roots and flowers were isolated and identified in our study for the first time, and the isolation of **9**–**15** from *L. strychnifolium* is also reported for the first time. Although **20**, the ethyl ester of gallic acid, was isolated from the flower in our study. The possible artifact resulting from the ethanol extraction process should be noted and cause concern.

All compounds isolated from the root, stem, leaves and flower of *L. strychnifolium* were evaluated for their α-glucosidase inhibiting and antioxidant properties. The results are displayed in the following section.

4.2.4 The α-glucosidase inhibitory and antioxidant activities of isolated compounds from the root, stem, leaves and flower of *L. strychnifolium*

The α-glucosidase inhibitory effect and antioxidant activity of isolated compounds from *L. strychnifolium* were investigated using an *in vitro* α-glucosidase inhibitory and DPPH radical scavenging assay. Their IC_{50} values were calculated using nonlinear regression. The results are described below.

4.2.4.1 α-Glucosidase inhibitory activity of isolated compounds from L. strychnifolium

The IC_{50} values of ten isolated compounds that inhibit α-glucosidase are shown in Table 31. However, the IC_{50} values of **14**, **16** and **19** were not determined because their interference colors in the assay limited the tests. The results indicate that **17**, **11**, and **12** exhibited extremely potent activity, while **15**, **20,** and **10** showed moderate activity. There were no significant differences between the inhibitory effects of these isolated compounds and the standard drug on α-glucosidase.

Table 31 The α-glucosidase inhibitory activity of isolated compounds from the root, stem, leaves and flower of *L. strychnifolium* extracts and the standard drug. The results represent the mean ± SD of triplicate experiments.

Compounds	IC_{50} (mM)
Astilbin (**8**)	10.1857 ± 0.4801^{c}
Isoastilbin (**9**)	2.8063 ± 1.5423^{b}
Neoastilbin (**10**)	0.2264 ± 0.0269^{a}
Epicatechin (**11**)	0.0172 ± 0.0005^{a}
(*E*)-Resveratrol (**12**)	0.0266 ± 0.0080^{a}
(*E*)-Resveratrol 4'-*O*-β-D-glucoside (**13**)	0.8930 ± 0.1144^{a}
Quercetin 3-*O*-β-D-arabinoside (**14**)	Not determined
Phloretin (**15**)	0.1378 ± 0.0334^{a}
Phloretin 4'-*O*-β-D-glucoside (**16**)	Not determined
Phloretin 4'-*O*-(6"-*O*-galloyl)-β-D-glucoside (**17**)	0.0162 ± 0.0014^{a}
Pinitol (**18**)	36.35 ± 1.4452^{d}
Gallic acid (**19**)	Not determined
Gallic acid ethyl ester (**20**)	0.1971 ± 0.0508^{a}
Acarbose	0.5270 ± 0.7608^{a}

[a-d] Value not sharing the same letters are significantly different from another within a column ($p < 0.05$)

The α-glucosidase inhibitory activity of isolated compounds enabled us to draw relevant conclusions about the relationships between structure and activity. There were significant differences in α-glucosidase inhibitory activity between groups of flavonol. In terms of flavanonol structure, neoastilbin (**10**) was remarkable among all other compounds. The IC_{50} value of **10** was 0.2264 ± 0.0269 mM, which was the most active flavanonol compound discovered for the first time in our study. As can be seen in Figure 31, the configuration at C-2 and C-3 positions distinguished compound **10** from its related compounds (**8** and **9**). According to the results, the *S*-configuration at the C-3 position (**9** and **10**) seems to be the more favorable configuration for the inhibition of the enzyme. Moreover, the enzyme

inhibitory effect of *S*-configuration (**10**) at C-2 and C-3 positions is better than that of *R*-configuration (**8**).

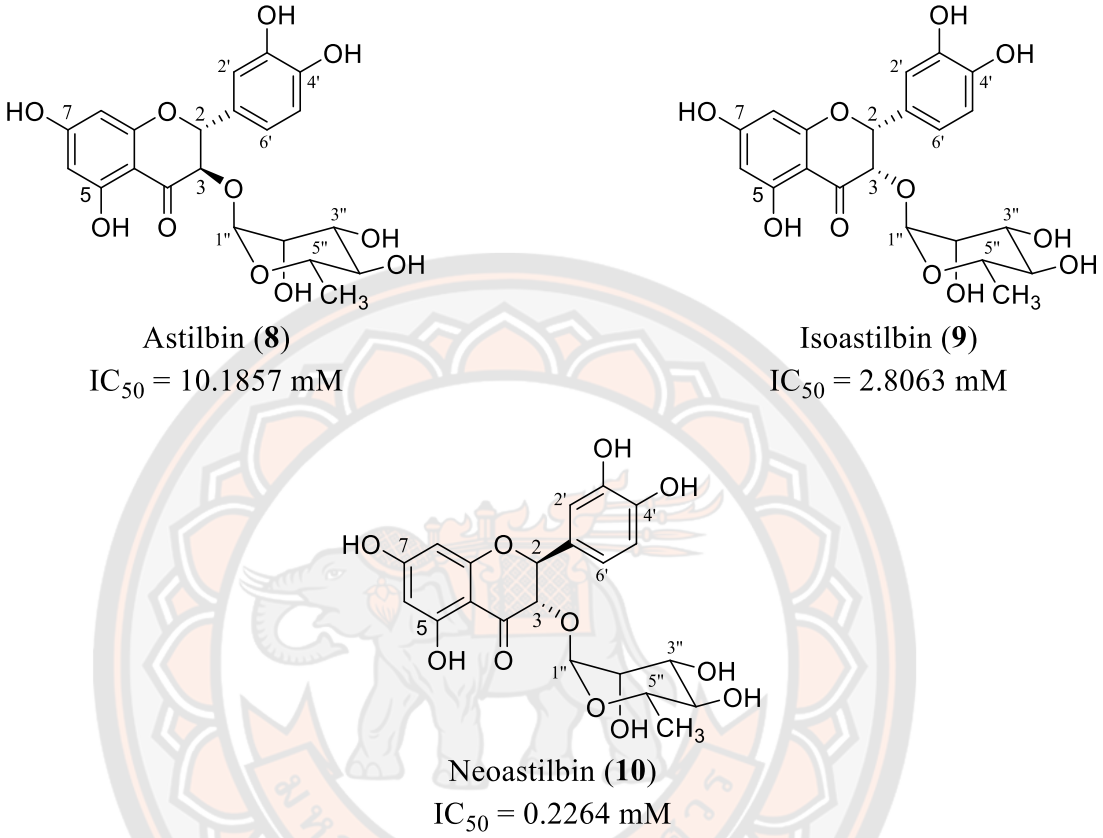

Figure 31 Chemical structures and α-glucosidase inhibitory activities of compounds **8**, **9** and **10**

Based on the α-glucosidase inhibitory activity of the dihydrochalcone structure (Figure 32), the dihydrochalcone galloyl glucoside (**17**) was one of the most active compounds tested in the present study, with an IC_{50} of 0.0162 ± 0.0014 mM followed by phloretin (**15**) with an IC_{50} of 0.1378 ± 0.0334 mM. The results showed that the phloretin structure has a favorable structure for the intended effects. This result is in agreement with a previous study [105] which suggested that phloretin is easily inserted into the active site of α-glucosidase. However, dihydrochalcone **16** showed lower enzyme inhibitory activity than 50% at the maximum tested concentration (1 mg/mL). From this observation, the activity decreased substantially with the replacement of the hydroxy group at the 4'-position

by glucose. In addition, comparing the activities of **15** and **16**, it is possible to infer that the presence of glucose weakens the activity of the dihydrochalcone. In turn, having the galloyl glucoside in the 4'-position enhanced the inhibitory activity of the dihydrochalcone. We can conclude from these results that the addition of a galloyl group in the dihydrochalcone glucoside increases its activity, as the gallic acid ethyl ester demonstrated a high level of inhibitory activity. It should be noted that the *α*-glucosidase inhibitory activity of **17** had never been described before. The *α*-glucosidase inhibitory activity of this compound is reported here for the first time.

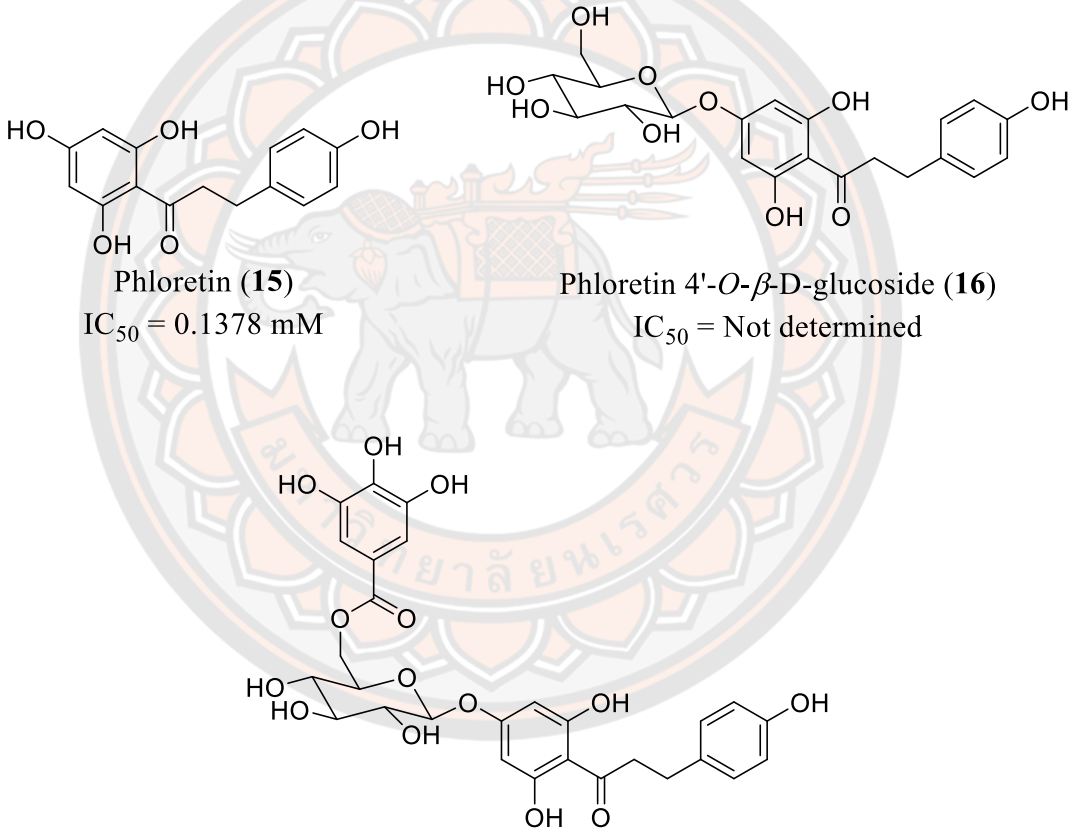

Figure 32 Chemical structures and *α*-glucosidase inhibitory activities of compounds 15, **16** and **17**

In addition, the α-glucosidase inhibitory activity of resveratrol and its derivatives (Figure 33) was investigated. The IC_{50} value for resveratrol (**12**) was 0.0266 ± 0.0080 mM, which was more potent than the positive control. The results are in agreement with the information reported by Zhang et al. [106]. They reported that resveratrol had an inhibitory effect against α-glucosidase activity. However, resveratrol 4′-*O*-β-D-glucoside (**13**) exhibited a lower inhibitory effect than resveratrol (**12**).

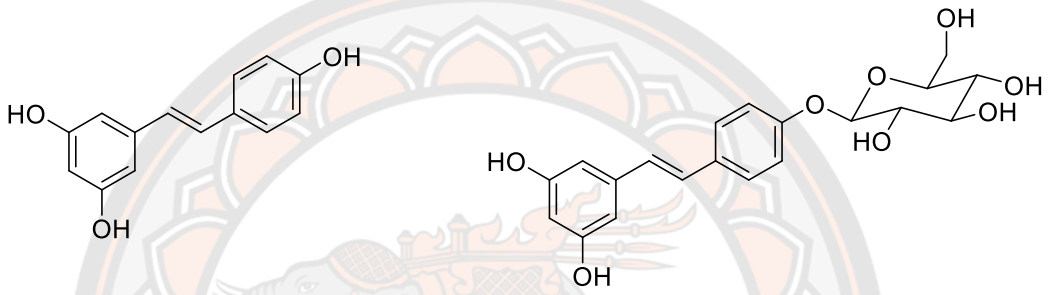

Figure 33 Chemical structures and α-glucosidase inhibitory activity of compounds **12** and **13**

These results allow us to hypothesize that the hydroxy group is favorable for the inhibitory activity of the compounds. Proença et al. [98] compared the inhibition of α-glucosidase by quercetin and quercetin-3-*O*-rutinoside (rutin). They suggested that quercetin had greater α-glucosidase inhibitory activity than rutin, which contains aglycoside in the molecule. Additionally, our results indicated that **15** and **12** are more potent than their glycoside, **16** and **13**, respectively. These findings demonstrated that the hydroxy groups in the aromatic ring might be responsible for the increased inhibitory effect.

4.2.4.2 Antioxidant of the isolated compounds from L. strychnifolium

Oxidative stress is a key mechanism promoting diabetes complications [107]. Consequently, a natural compound with α-glucosidase inhibitory effect and antioxidant properties can be a potential strategy to prevent hyperglycemia

and diabetes complications. In our study, the DPPH radical scavenging assay was used to determine the antioxidant activity of isolated compounds. The DPPH radical scavenging activity of isolated compounds is shown in Table 32. Compounds **10, 11, 17, 19,** and **20** showed greater antioxidant activity than positive controls, with compound **17** exhibited the highest DPPH scavenging activity. The IC_{50} value for **17** was 19.26 ± 0.95 μM, which is threefold more potent than L-Ascorbic acid (57.74 ± 1.81 μM) and twofold more potent than Trolox (43.89 ± 3.31 μM).

Table 32 The antioxidant activity of isolated compounds from the root, stem, leaves and flower from *L. strychnifolium* extracts and the standard drug. The results represent the mean ± SD of triplicate experiments.

Compounds	IC_{50} (μM)
Astilbin (**8**)	48.05 ± 4.08^{d}
Isoastilbin (**9**)	44.96 ± 2.59^{d}
Neoastilbin (**10**)	30.99 ± 2.44^{b}
Epicatechin (**11**)	36.50 ± 0.44^{c}
(*E*)-Resveratrol (**12**)	125.80 ± 1.78^{g}
(*E*)-Resveratrol 4'-*O*-*β*-D-glucoside (**13**)	277.07 ± 4.04^{i}
Quercetin 3-*O*-*β*-D-arabinoside (**14**)	74.86 ± 1.27^{f}
Phloretin (**15**)	265.33 ± 4.75^{h}
Phloretin 4'-*O*-*β*-D-glucoside (**16**)	842.03 ± 4.62^{j}
Phloretin 4'-*O*-(6"-*O*-galloyl)-*β*-D-glucoside (**17**)	19.26 ± 0.95^{a}
Pinitol (**18**)	Not determined
Gallic acid (**19**)	19.83 ± 3.52^{a}
Gallic acid ethyl ester (**20**)	24.37 ± 0.23^{a}
L-ascorbic acid	57.74 ± 1.81^{e}
Trolox	43.89 ± 3.31^{d}

[a-j] Value not sharing the same letters are significantly different from another within a column ($p < 0.05$)

From the information observed in Table 32, it is interesting to consider the correlation between antioxidant activity and the number and position of hydroxyl groups in the aromatic ring of isolated compounds. The significant activity differences between these compounds were probably due to the number of hydroxyls present in the aromatic ring [108]. The results showed that compound **17** had significant DPPH radical scavenging capacity with an IC_{50} value of 19.26 ± 0.95 μM because of its six hydroxyl groups. Interestingly, compound **17** is much more active than positive controls. However, other dihydrochalcones (**15**, **16**) with four and three hydroxyl groups showed lower antioxidant activity than **17** as shown in Figure 34.

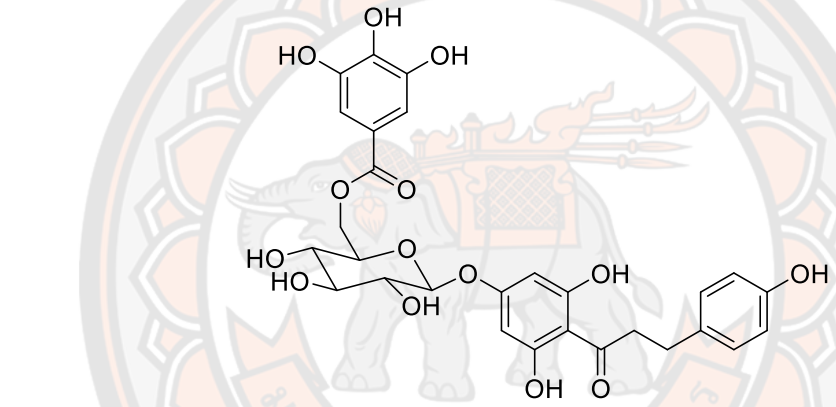

Phloretin 4'-*O*-(6"-*O*-galloyl)-*β*-D-glucoside (**17**)
IC_{50} = 19.26 μM

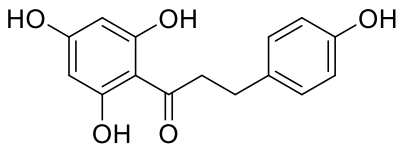

Phloretin (**15**)
IC_{50} = 265.33 μM

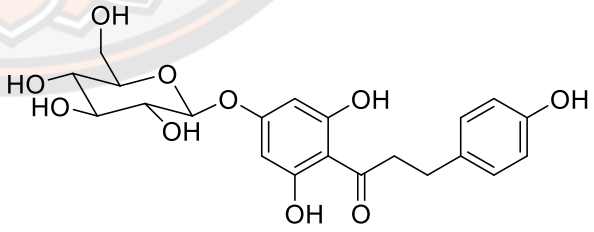

Phloretin 4'-*O*-*β*-D-glucoside (**16**)
IC_{50} = 842.03 μM

Figure 34 Chemical structures and antioxidant activity of compounds **13**–**15**

Similarly, the antioxidant capacity of compounds **12** and **19** with three and four hydroxyl groups, respectively, was greater than that of their derivatives **13** and **20** with two and three hydroxyl groups, respectively (Figure 35). In addition, it is noteworthy that **10** showed higher antioxidant activity than its stereoisomer (**8** and **9**), indicating that the configuration of their C-2 and C-3 positions affected their ability to scavenge free radical.

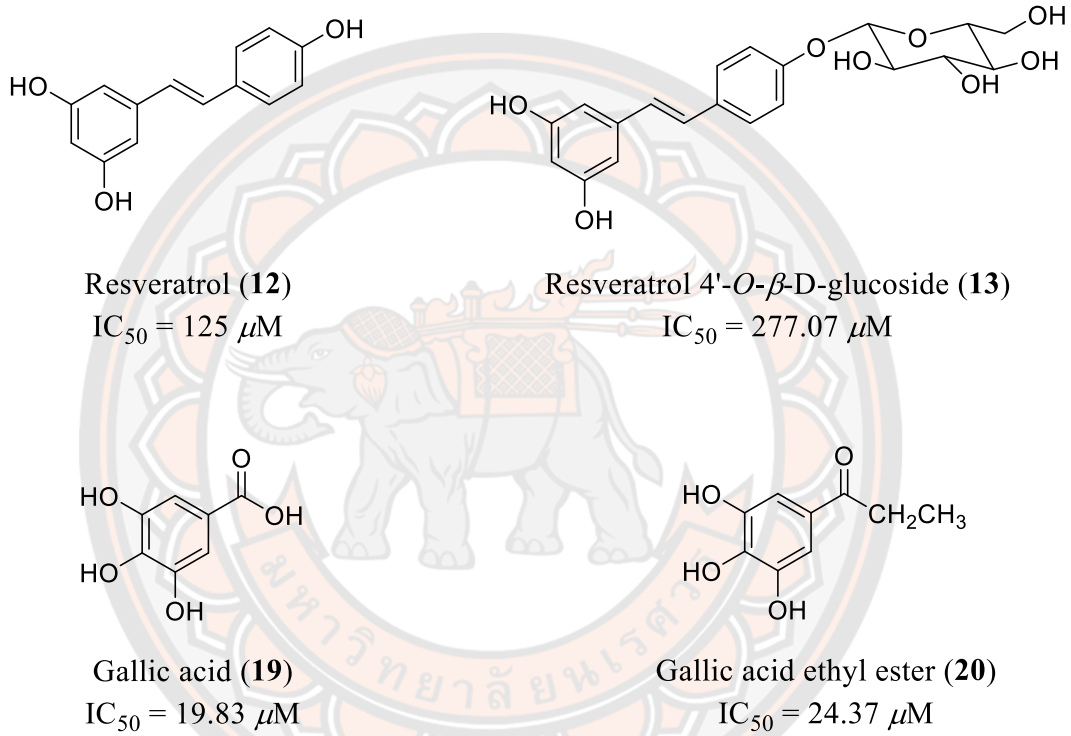

Figure 35 Chemical structures and antioxidant activities of compounds **12**, **13**, **19** and **20**

This part of the work examined the α-glucosidase inhibitory effect and antioxidant activity of the ethanolic extracts of roots, stems, leaves, and flowers of *L. strychnifolium* and their isolated compounds. The observation of α-glucosidase inhibitory and antioxidant properties of root, stem, leaf, and flower extracts showed the potential to inhibit α-glucosidase enzyme and antioxidant activity. In particular, the root, stem, and leaf extracts presented stronger activities than the positive control. These results indicated that *L. strychnifolium* extracts were as effective as acarbose,

L-ascorbic acid, and trolox. This is the first report on the α-glucosidase inhibitory effect of the root, stem, leaf, and flower of *L. strychnifolium*.

In addition, the results demonstrated the predominance of bioactive components in the extracts. The roots, stems, leaves, and flowers contained isoastilbin (**9**), epicatechin (**11**), phloretin 4'-*O*-(6"-*O*-galloyl)-β-D-glucoside (**17**), and gallic acid ethyl ester (**20**), respectively. Among thirteen isolated compounds, phloretin 4'-*O*-(6"-*O*-galloyl)-β-D-glucoside (**17**) exhibited the strongest α-glucosidase inhibitory and antioxidant activities. Additionally, pinitol (**18**) has been isolated from all the plant tissue. Although pinitol did not inhibit α-glucosidase or act as antioxidant in the present study, numerous in vitro and in vivo studies have shown that it has anti-diabetic properties [109-114].

The present study proved that *L. strychnifolium* extracts and phloretin 4'-*O*-(6"-*O*-galloyl)-β-D-glucoside (**17**) may offer therapeutic alternatives for type 2 diabetes. Furthermore, the intake of *L. strychnifolium* is linked with health and wellbeing, given the synergistic relationship between the α-glucosidase inhibitory and antioxidant activities of bioactive compounds. Moreover, our study supports the traditional use of *L. strychnifolium* roots, stems, and leaves as traditional medicine and herbal tea for detoxification or prevention of chronic diseases, and provides a useful basis information for the development of the *L. strychnifolium* plants for food and pharmaceutical products.

4.3 Part III: The investigation of the optimal conditions for brewing tea from *L. strychnifolium* leaves

For use in folk medicine, the leaves of *L. strychnifolium* are commonly processed to dried for use as a detoxifying herbal tea and tonic [12]. Previous literatures demonstrated that the brewing conditions such as water temperature, water volume, and brewing time, affected the content of the desired composition in tea infusion [79, 115]. Although there have been studies on the extraction of *L. strychnifolium* leaves using a variety of solvents [12], there are few comprehensive studies establishing a practical brewing method for producing a high-quality *L.*

strychnifolium leaf tea infusion. As well, the bioactive constituents of *L. strychnifolium* leaf tea have not been adequately described.

The results of Part II indicated that the leaves contain the most potent α-glucosidase inhibitor and antioxidant compound. From the tradition used of the *L. strychnifolium* leaves and the results from of Part II, it is interesting to determine the optimal infusion conditions for producing *L. strychnifolium* leaf tea with the highest content of *L. strychnifolium* leaves extracts. Moreover, the bioactive compounds in leaf tea were isolated and elucidated using spectroscopic data. The findings contribute to the development of a simple brewing method for producing high-quality *L. strychnifolium* leaf tea in a household or on a small scale.

4.3.1 Effect of infusion conditions on *L. strychnifolium* leaf tea extract

Several parameters that could affect the infusion of *L. strychnifolium* leaf tea were investigated, including time, temperature, and the volume of water, as well as the multiple infusion. The three replicates of each optimization experiment were carried out to obtain a mean value.

4.3.1.1 Effects of infusion time on the extraction yield of L. strychnifolium leaf tea

The infusion time is an important factor influencing the amount of tea extract. Therefore, the impact of infusion duration was investigated. 1 g of ground leaves was placed in 60 mL of water maintained at 30 °C for various infusion time-interval from 1 to 60 minutes. The tea extract content of the infusions reached its maximum level after 5 minutes of brewing, then remained stable with increasing infusion time (Figure 36).

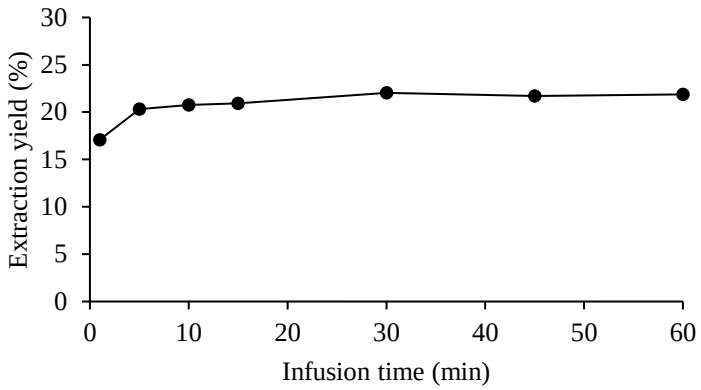

Figure 36 Effect of infusion time on the extraction yield (%w/w) of *L. strychnifolium* leaf tea, the brewing process was carried out by brewing 1 g of leaf powder at 30 °C with a water volume of 60 mL. The values are mean ± standard deviations for triplicate extraction.

The literature on the extraction of Turkish green tea reported that the total catechin content did not increase with increased brewing times [78]. Astill et al. [116] revealed that tea drinkers' infusion habits varied considerably within countries in Europe. Infusion times less than 5 min are commonly observed, and most consumers brew for less than 2 min. According to the previous literatures [78, 116] and our results, infusion of *L. strychnifolium* leaves for 5 min was found to be the optimal scenario for brewing the maximum tea extract from *L. strychnifolium* leaf tea.

4.3.1.2 Effect of infusion temperature on the extraction yield of L. strychnifolium leaf tea

Temperature of water is also a significant factor in brewing efficiency. In this experiment, 60 mL of water was infused for 5 min with 1 g of leaf powder. During the brewing process, a wide range of water temperatures from 30 to 100 °C was applied to evaluate the optimal infusion temperature. The result indicated that a prolonged 70 °C water temperature increased the amount of crude extract (Figure 37). The amount of crude extract slightly increased as the infusion temperature increased from 70 °C to 100 °C. It has been demonstrated that brewing temperature influences the diffusion of water into tea particles and the solubility of tea

components in the leaf matrix [117]. However, the majority of bioactive compounds from plant sources are very sensitive and easily decompose under high temperatures [118]. Overall, the results suggest that the optimal temperature for brewing *L. strychnifolium* leaves was 70°C.

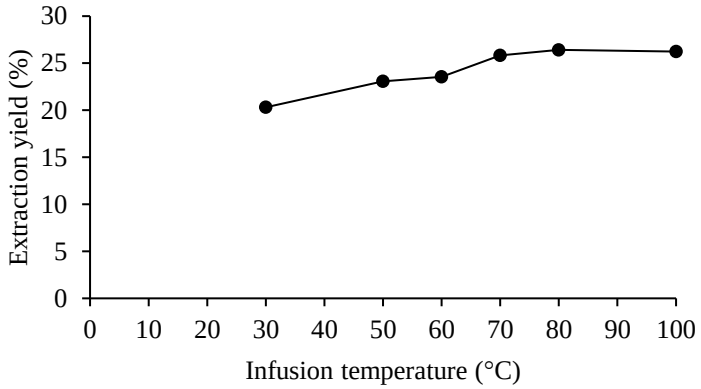

Figure 37 Effect of infusion temperature on the extraction yield (%w/w) of *L. strychnifolium* leaf tea, the brewing process was carried out by brewing 1 g of leaf powder with a water volume of 60 mL for 5 minutes. The values are mean ± standard deviations for triplicate extraction.

4.3.1.3 Effect of water volume for brewing the L. strychnifolium leaf tea on extraction yield

Water was used to infuse the *L. strychnifolium* leaf tea. To establish the optimal water volume, 1 g of leaf powder was mixed with different volumes of 70 °C water ranging from 20 to 140 mL and infused for 5 minutes. The yield of tea extract increased dramatically as the water volume was increased from 20 to 40 mL and reached a plateau when the water volume exceeded 40 mL (Figure 38). In the subsequent experiments, 40 mL of water was employed.

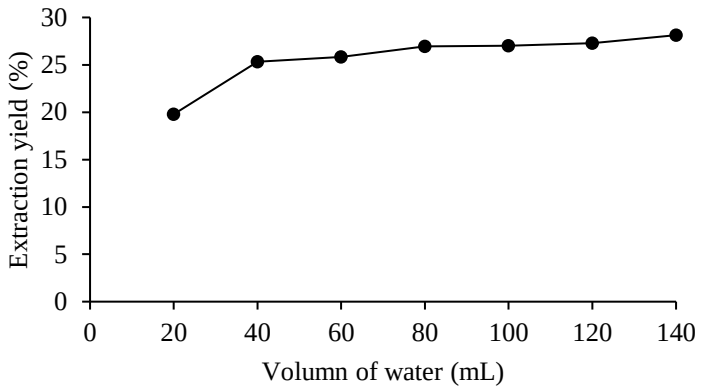

Figure 38 Effect of water volume for brewing the *L. strychnifolium* leaf tea on the extraction yield (%w/w), the brewing process was carried out by brewing the leaf powder with water at 70 °C for 5 minutes. The values are mean ± standard deviations for triplicate extraction.

The extraction yield of the compounds was affected by the solvent volume. Vuong et al. investigated the effect of the water volume on the catechins extraction from green tea. The authors found that increasing the water volume increased the catechins content [119]. However, the study of the effects of brewing conditions on the total soluble solid content of Roselle tea demonstrated that increasing the amount of water did not increase the extraction yield. When an excessive amount of solvent was used, the increasing rate of extraction yield gradually decreased [120]. This trend was observed in our study when the water volume for brewing *L. strychnifolium* leaves varied between 40 and 140 mL. The results indicated that the best extraction yield was achieved using a leaf powder-to-water ratio of 1:40 (g/mL) for 5 minutes at 70 °C. The effect of multi-step infusion was therefore examined under this optimal condition.

4.3.1.4 Effect of multi-step infusion on the extraction yield of L. strychnifolium leaf tea

The above optimal conditions were used to investigate the effect of multiple infusions on the extraction yield. To examine the effect of multiple infusions, three experiments were designed with a ratio of 5:200 (g/mL) of leaf powder to water. Each experiment was described in detail below.

Experiment 1; tea was prepared by brewing 5 g of leaf powder in 200 mL of water. The aqueous extract was filtered and evaporated to achieve the tea extract.

Experiment 2: the leaf powder (5 g) was infused with 200 mL of water. The liquid was filtered off. A second infusion was made by adding a further 200 mL of water to the remaining leaf powder from the first infusion and filtering off the aqueous extract. The first and second tea infusions were combined and the solvent was removed to obtain the tea extract.

Experiment 3: the leaf powder was brewed using a three-step brewing process. In the first step, 5 g of leaf powder was infused with 200 mL of water, then the tea infusion was filtered, and the leaf powder was taken. The same leaf powder from the first step was repeatedly infused in 200 mL of water. After that, the tea infusion was filtered, and the leaf powder was taken to the third infusion. In the third infusion, the leaf powder from the second infusion was brewed in 200 mL of water. The aqueous was filtered to get the tea infusion. Afterward, the three tea infusions from three-step brewing were evaporated and the tea extract was yielded.

The results showed that the highest yield, 31.15% was achieved when the leaf powder was infused three times, while twice extracted powder yielded 29.74%, and the lowest yield was observed in experiment 1, as shown in Figure 39. However, there was no difference in the yield from two-step and three-step brewing. Our results were in agreement with the results from the previous study. Yang et al. [121] dipped the tea bag in 150 mL of hot water for 30 seconds. They found that the steeping of bag tea two times produced a higher level of caffeine, catechins, and gallic acid than the steeping of a tea bag for a single time. Interestingly, all of these compounds were reduced gradually in later steeping. The results from our study and Yang et al. suggested that brewing the same leaf powder of *L. strychnifoilum* twice with 200 mL of water (the leaf powder to water ratio of 1:40, g/mL) each time gave the best results. Additionally, a two-step infusion process with the same water volume was the easiest way to make *L. strychnifolium* leaf tea.

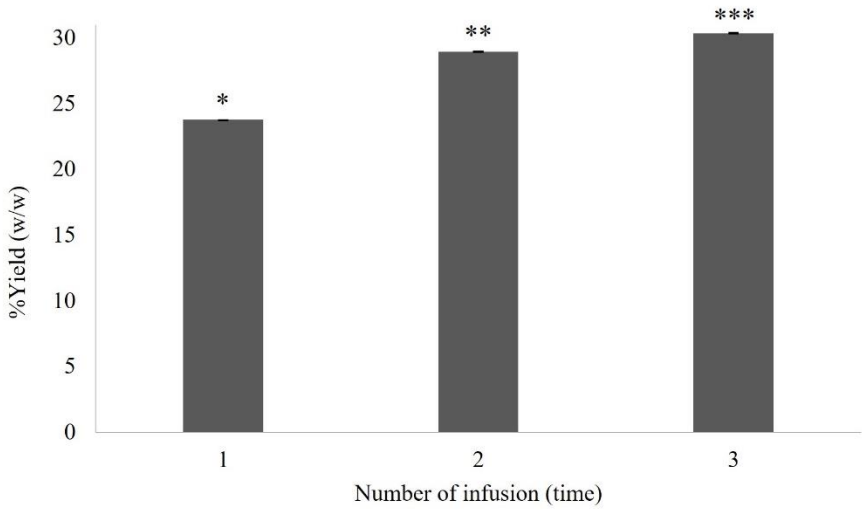

Figure 39 Effect of multi-step brewing on extraction yield (%w/w) of *L. strychnifolium* leaf tea; * The 5 g of leaf powder was brewed with 200 mL of water.; ** The 5 g of leaf powder was brewed with two-step brewing with 200 mL of water for each step.; *** The 5 g of leaf powder was brewed with three-step brewing with 200 mL of water for each step.

4.3.2 Chemical identification of compounds from *L. strycnifolium* leaf tea

The crude extract obtained under the optimal conditions was analyzed by ^{1}H-NMR and isolated by column chromatography. Pure compounds were identified using UV, IR 1D NMR, and 2D NMR. Pinitol (**18**), phloretin 4'-*O*-*β*-D-glucoside (**16**) and quinic acid (**21**) (Figure 40) were identified from the *L. strychnifolium* leaf tea. The structure of compounds **16** and **18** was already elucidated in topic 4.2.3. Compound **21** was obtained as a pale-yellow solid. The UV absorption maximum was observed at 190 in water. The IR spectrum displayed absorption bands of OH-stretching at 3508 and 3332 together with the band of C=O stretching at 1678 cm^{-1}. Furthermore, the structure elucidation of compound **21** is supported by spectroscopic data and comparison with that previous report of quinic acid by Ailiesei et al. [122]. The NMR data of compound **21** are shown in Table 33.

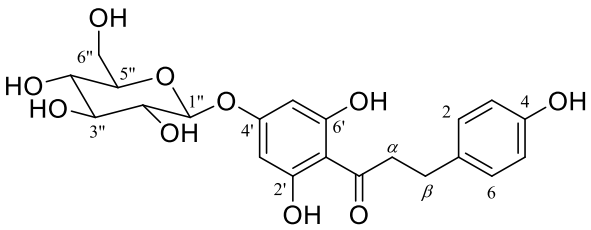

16

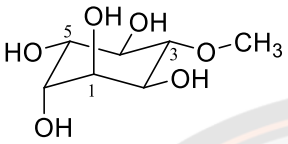

18

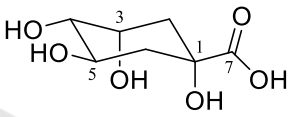

21

Figure 40 The isolated compounds from *L. strycnifolium* leaf tea

The isolation of *L.strychnifolium* leaf tea yielded pinitol, quinic acid, and phloretin 4'-*O*-*β*-D-glucoside. Additionally, the ^{1}H NMR spectrum of leaf tea was compared with the ^{1}H NMR spectra of isolated compounds from the tea (Figure. 41). Both the position and pattern of the leaf tea extract spectrum closely resembled the signals of isolated compounds. The results indicated that the *L. strychnifolium* leaf tea was composed of pinitol (**18**), quinic acid (**21**) and phloretin 4'-*O*-*β*-D-glucoside (**16**) which matched with the ^{1}H NMR spectrum. The results also infer that pinitol (**18**) and phloretin 4'-*O*-*β*-D-glucoside (**16**) are the major components in leaf tea.

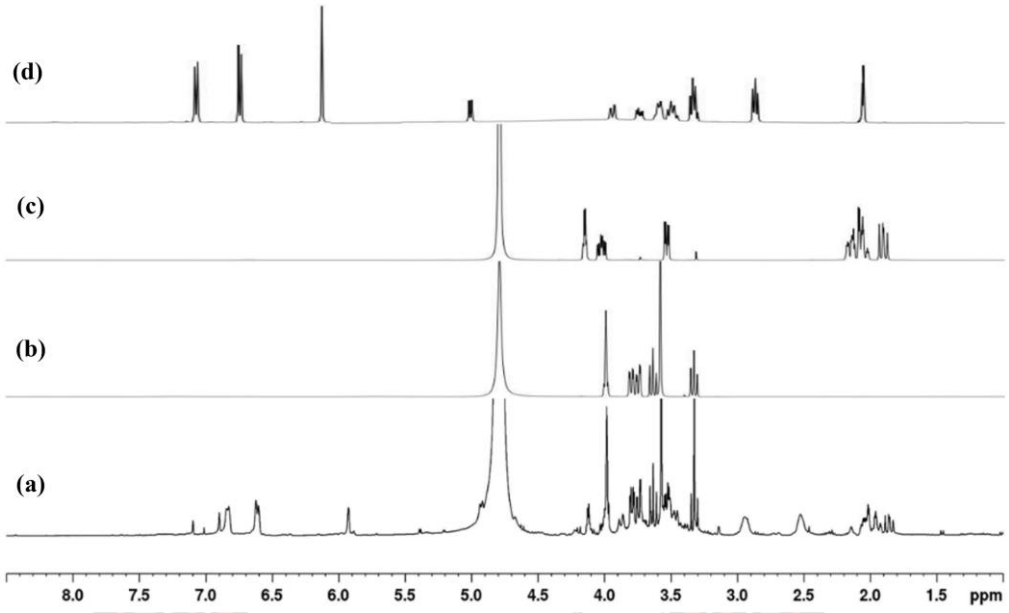

Figure 41 ^{1}H NMR (400 MHz) spectra of *L. strychnifolium* leaf tea and chemical components in the *L. strychnifolium* leaf tea (a) *L. strychnifolium* leaf tea in D_2O, (b) pinitol in D_2O, (c) quinic acid in D_2O, (d) phloretin 4'-*O*-*β*-D-glucoside in acetone-d_6

In Thailand, the leaves of *L. strychnifolium* are commonly used as an herbal tea for detoxification and pesticide elimination. Although the phytochemical constituents of *L. strychnifolium* leaves have been studied [10], the chemical constituents of aqueous leaves extract have not been reported. Importantly, none of the studies has investigated the bioactive ingredients in the aqueous leaves extract. Moreover, the herbal tea infusion procedure of *L. strychnifolium* leaves for a high yield of bioactive components was interesting. The results from our study suggested that the brewing of leaves powdered *L. strychnifolium* for 5 min at 70 °C with the leaf powder to water ratio of 1:40 (g/mL) was the optimal condition and showed the extraction yield of 25.32%. Additionally, brewing the leaf powder twice with 200 mL of water for each was the best way to make *L. strychnifolium* leaf tea with a high yield of tea extract.

The isolation of bioactive compounds from *L. strychnifolium* leaf tea, pinitol and phloretin 4'-*O*-*β*-D-glucoside were found to be high content with a yield of 19.62% and 20.09%, respectively. Pinitol is a cyclitol compound. The primary industrial sources for obtaining pinitol are carob pods and soybean leaves [123]. This

compound possesses multifunctional properties, including anti-diabetic [124], cancer chemopreventive [125], anti-inflammatory [126] and antitumoral [127] effects. Additionally, Kim et al. [113] also reported the hypoglycemic effect of pinitol in humans with type 2 diabetes. After 12 weeks of treatment with pinitol and current medications, fasting glucose, post-prandial glucose, and hemoglobin A1c levels decreased significantly.

Phloretin 4'-*O*-*β*-D-glucoside or trilobatin is a naturally occuring sweetener which is reported to be 100 times sweeter than sucrose [57]. Trilobatin is abundant in the leaves of crabapple species, including *Malus trilobata*, *Malus sieboldii*, and *Malus toringoides* [128, 129], but not in the domesticated apple. Moreover, the leaves of the wild grape and *Lithocarpus polystachyus* contain trilobatin [130, 131]. Trilobatin is a sweetener used in many foods and beverages, however, its usefulness is limited by its scarcity [132].

The optimal conditions and bioactive compounds of *L. strychnifolium* leaf tea were reported in our study. The pinitol had an anti-hyperglycemia effect and trilobatin served as a sweetener [57, 113]. Thus, the consumption of *L. strychnifolium* leaf tea can be a good choice for someone with type 2 diabetes. Moreover, *L. strychnifolium* leaves can become a new source of the sweetener, trilobatin.

Table 33 The ^{1}H and ^{13}C NMR assignments of compound **21** in acetone-d_6 and quinic acid in D_2O

Position	Compound **21**			Quinic acid [122]	
	δ_H, (mult, *J* in Hz)	δ_C		δ_H, (mult, *J* in Hz)	δ_C
1	-	75.8	-	-	78.5
2ax	2.09 (dd, 14.9, 3.4)	36.8	C-6, C-3, C-4, C-1	2.13 (dd, 14.8, 3.2)	39.6
2eq	2.03 (ddd, 15.0, 3.7, 3.8)			2.07 (ddd, 14.8, 3.4, 2.8)	
3	4.14 (q, 3.5)	69.9	C-2, C-5, C-4, C-1, C-7	4.18 (ddd, 3.2)	72.9
4	3.52 (dd, 9.4, 3.4)	74.7	C-6, C-5, C-3	3.57 (dd, 9.2, 3.2)	77.7
5	4.02 (ddd, 11.0, 9.4, 4.6)	66.2	C-6, C-4	4.05 (ddd, 10.8, 9.4, 4.4)	69.2
6ax	1.89 (dd, 13.5, 10.9)	40.2	C-2, C-5, C-4, C-1	1.94 (dd, 13.6, 10.8)	43.1
6eq	2.14 (ddd, 13.6, 4.5, 4,7)		C-2, C-5, C-4, C-1	2.18 (ddd, 13.2, 4.6, 2.4)	
7	-	177.8	-	-	180.6

CHAPTER V

CONCLUSION

5.1 Part I: The investigation of chemical constituents from pericarp and seed of *A. mutica* and the α-glucosidase inhibitory activity of isolated compounds from the seed of *A. mutica*

In this section, the pericarps and seeds of *A. mutica* were extracted. The sequential extraction of organic solvents started with *n*-hexane, followed by dichloromethane and 95% ethanol. The dichloromethane (AMPD) and 95% ethanol (AMPE) crude extracts of the pericarp and the hexane (AMSH), dichloromethane (AMSD) and 95% ethanol (AMSE) crude extracts of the seed were obtained. After that, all crude extracts were identified by ^{1}H NMR data. The results showed that AMPD and AMSD extracts exhibited the proton signal of the aromatic, double bond, methoxy group, and aliphatic protons. Moreover, the AMPD and AMSD extracts also showed a higher yield than other crude extracts. Therefore, the GC–MS analysis of dichloromethane crude extracts from the pericarp and seed was performed. The results from GC–MS analysis showed a difference in volatile compositions between the dichloromethane extract of the pericarp and seed. The predominant content of 1,7-diphenyl-4,6-heptadien-3-one was reported in the pericarp. Three bioactive compounds, 5,6-dehydrokawain, pinocembrin, and farnesol, were the main components detected in the seeds. Moreover, the dichloromethane extract of the seed showed good inhibitory activity of α-glucosidase, thus the α-glucosidase inhibitor in the seed was isolated and identified.

The isolation of the dichlorometane extract of the seed by column chromatographic techniques afforded seven known compounds. The spectroscopic data were used to elucidate the structures. Farnesol (**1**), 5,6-dehydrokawain (**2**), pinocembrin (**3**), cardamomin (**4**), naringenin (**5**), pinocembrin chalcone (**6**) and alpinetin (**7**) were identified. Interestingly, our study described the isolation and identification of naringenin and pinocembrin chalcone in *A. mutica* for the first time. In addition, the discovery of the important precursor, pinocembrin chalcone, in the

seed has led to a better understanding of biosynthesis and the possible formation pathway of the flavonoids in *A. mutica*. The inhibitory activty against α-glucosidase of compounds isolated from the seed was evaluated using a colorimetric method. Pinocecmbrin and naringenin were the most active with IC_{50} values of 62.77 ± 2.18 and 8.77 ± 1.04 μM, respectively. Moreover, these compounds had a greater inhibitory effect than the positive control, acarbose (IC_{50} = 527.03 ± 0.14 μM).

5.2 Part II: The investigation of chemical constituents, α-glucosidase inhibitory and antioxidant activities of *L. strychnifolium*

The roots, stems, leaves and flowers of *L. strychnifolium* were extracted with 95% ethanol to produce ethanolic extracts of the roots (LSL), stems (LSS), leaves (LSL), and flowers (LSF). All the extracts were individually isolated by column chromatographic techniques and the thirteen compounds were obtained. The thirteen compounds were dihydroflavonols, dihydrochalcones, stilbenes, flavan-3-ol, flavonol, cyclitol phenolic acid and phenolic ethyl ester. Astilbin (**8**), isoastilbin (**9**), neoastilbin (**10**), epicatechin (**11**), (*E*)-resveratrol (**12**), (*E*)-resveratrol 4'-*O*-β-D-glucoside (**13**), quercetin 3-*O*-β-D-arabinoside (**14**), phloretin (**15**), phloretin 4'-*O*-β-D-glucoside (**16**), phloretin 4'-*O*-(6"-*O*-galloyl)-β-D-glucoside (**17**), pinitol (**18**), gallic acid (**19**), and gallic acid ethyl ester (**20**) were identified. Furthermore, seven compounds including isoastilbin, neoastilbin, epicatechin, resveratrol, resveratrol 4′-*O*-β-D-glucoside, quercetin 3-*O*-β-arabinoside and phloretin were isolated from *L. strychnifolium* for the first time. This is the first study to describe the isolation and identification of compounds from the roots and flowers of *L. strychnifolium*.

The investigation of α-glucosidase inhibitors from the root, stem, leaves and flower of *L. strychnifolium* yielded phloretin 4'-*O*-(6"-*O*-galloyl)-β-D-glucoside (**17**) as the most potent α-glucosidase inhibitor (IC_{50} = 0.0162 ± 0.0014 mM), which was more potent than the positive control (acarbose, IC_{50} = 0.5270 ± 0.7608 mM). Although compounds **10**, **15** and **20** were slightly less active than compound **17**, these compounds were more active than the positive control. Additionally, the antioxidant activity of thirteen compounds was determined. Compound **17** had a greater antioxidant capacity (IC_{50} = 19.26 ± 0.95 μM) than the positive controls (L-ascorbic

acid, IC_{50} = 57.74 ± 1.81 μM and trolox, IC_{50} = 43.89 ± 3.31 μM. Compounds **10**, **11**, **19** and **20** exhibited greater antioxidant activity than positive controls, but exhibitrd slightly less antioxidant activity than compound **17**. Evaluation of the structure-activity relationship of isolated compounds from the root, stem, leaves, and flower of *L. strychnifolium* indicated that the position and number of hydroxyl groups influenced the α-glucosidase inhibitory and antioxidant activities.

5.3 Part III: The investigation of the optimal conditions for brewing tea from *L. strychnifolium* leaves

L. strychnifolium leaves have been used as an herbal tea for detoxification in Thailand. The effects of infusion conditions, including time, temperature and water volume, on the crude extract of *L. strychnifolium* leaf tea were investigated in this study. The optimal conditions were a brewing process using hot water at 70°C and a ratio of 1:40 (g/ml) leaf powder to water for 5 min. Moreover, the use of the above-mentioned optimal conditions, combined with the twice infusion with the same volume of water, resulted in a high yield of tea extract.

The bioactive components in the leaf tea of *L. strychnifolium* were identified. The powdered leaf was brewed twice under optimal conditions, and the obtained tea extract was isolated by column chromatography. Phloretin 4′-*O*-(6′′-*O*-galloyl)-*β*-D-glucoside (**16**), pinitol (**18**), and quinic acid (**21**) were identified from the tea extract. High contents of compounds **16** and **18** were found in the leaf tea of *L. strychnifolium*. From the literature, compound **16** was used as a sweetener, while compound **18** had an anti-hyperglycemia effect. Therefore, the infusion of dried *L. strycnifolium* leaves using our conditions is recommended for the production of *L. strycnifolium* leaves tea with a high concentration of beneficial ingredients.

In conclusion, our studies provide information regarding the chemical constituents of the seed of *A. mutica* as well as the root, stem, leaves and flower of *L. strychnifolium*. The inhibitory effect on α-glucosidase and antioxidant activity of these isolated compounds were evaluated. The results indicated that compounds **5** and **17** may be an alternative treatment for type 2 diabetes. Moreover, the optimal brewing conditions for *L. strychnifolium* leaves tea and the bioactive compounds in the tea

were investigated. Our findings support the traditional use of *L. strychnifolium* leaves as an herbal tea for health and well-being.

APPENDIX

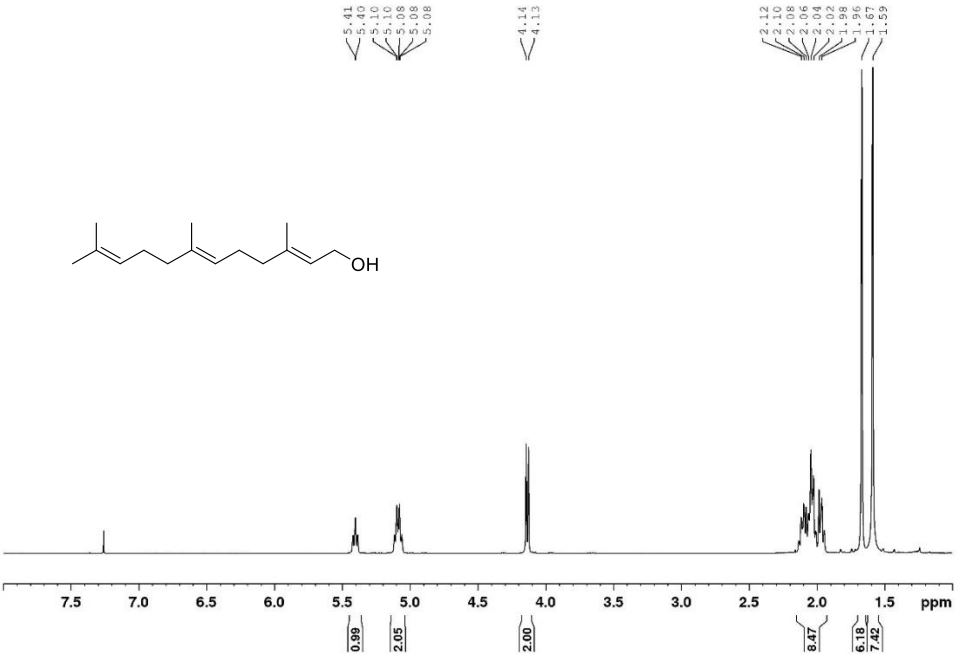

Figure A1 ^{1}H NMR spectrum ($CDCl_3$, 400 MHz) of farnesol (**1**)

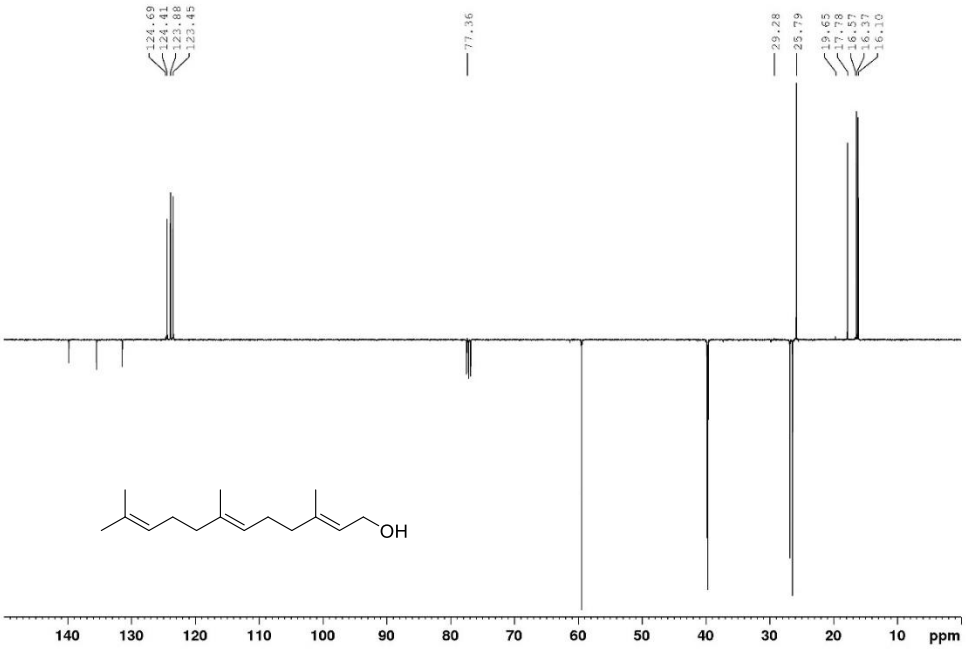

Figure A2 DEPTQ spectrum ($CDCl_3$, 400 MHz) of farnesol (**1**)

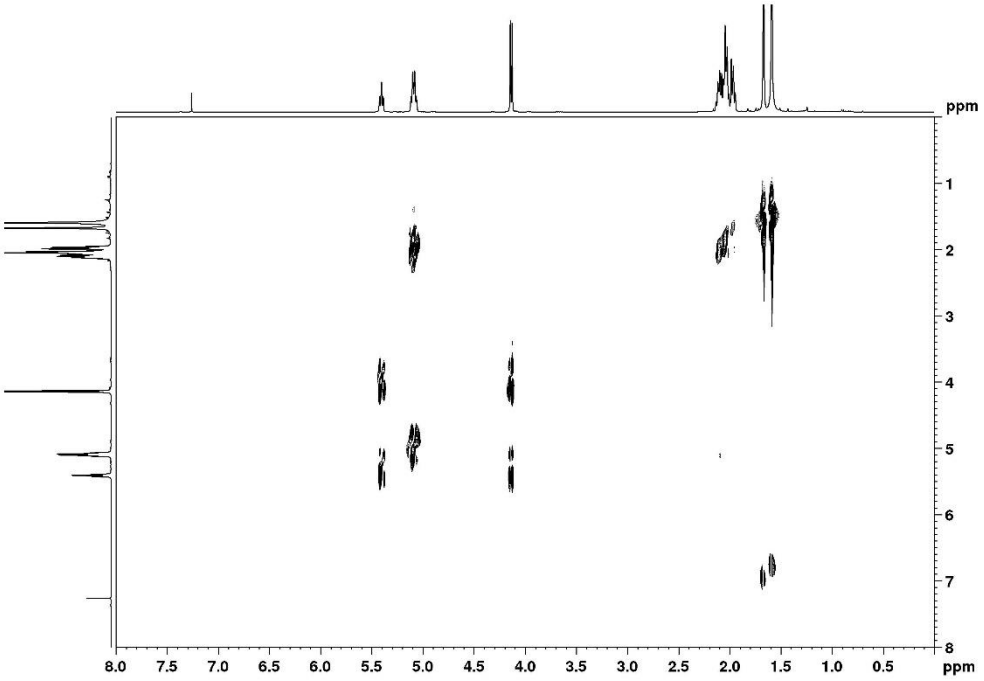

Figure A3 COSY spectrum of farnesol (**1**)

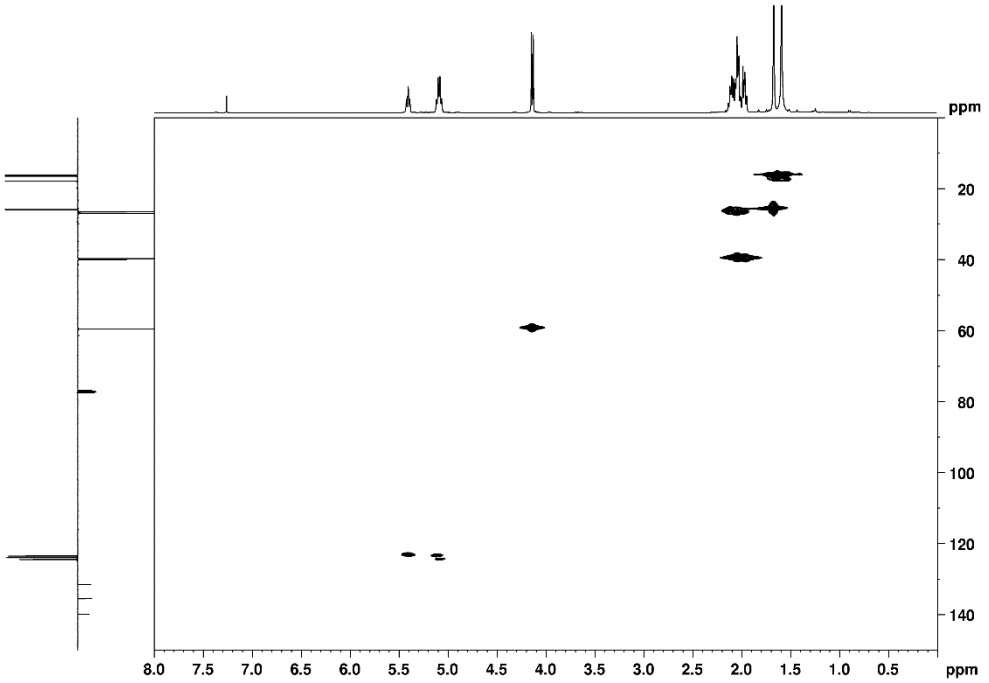

Figure A4 HMQC spectrum of farnesol (**1**)

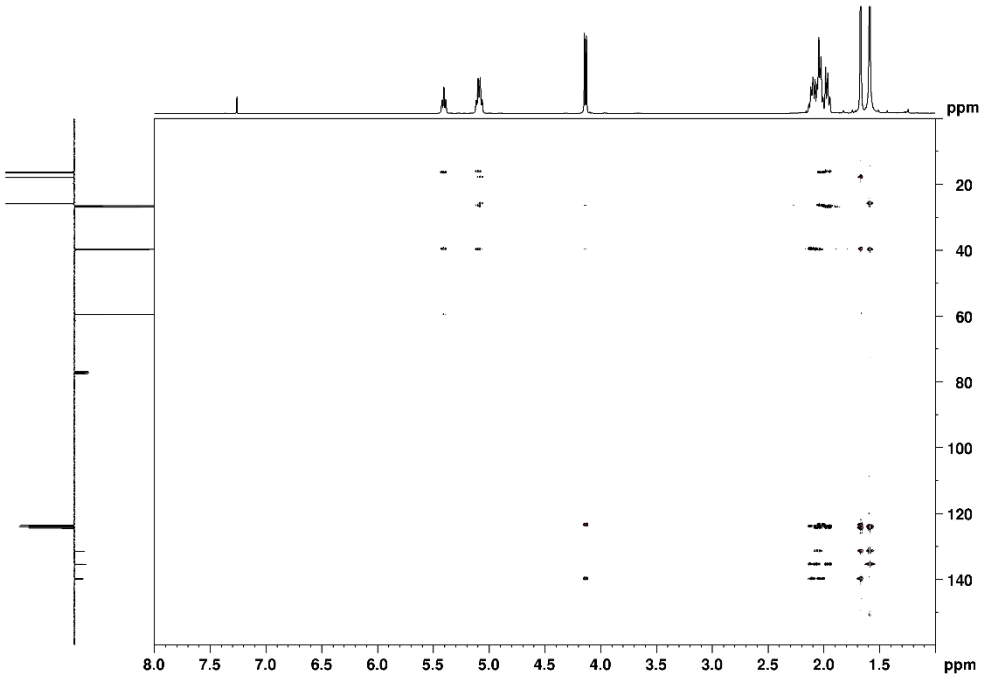

Figure A5 HMBC spectrum of farnesol (**1**)

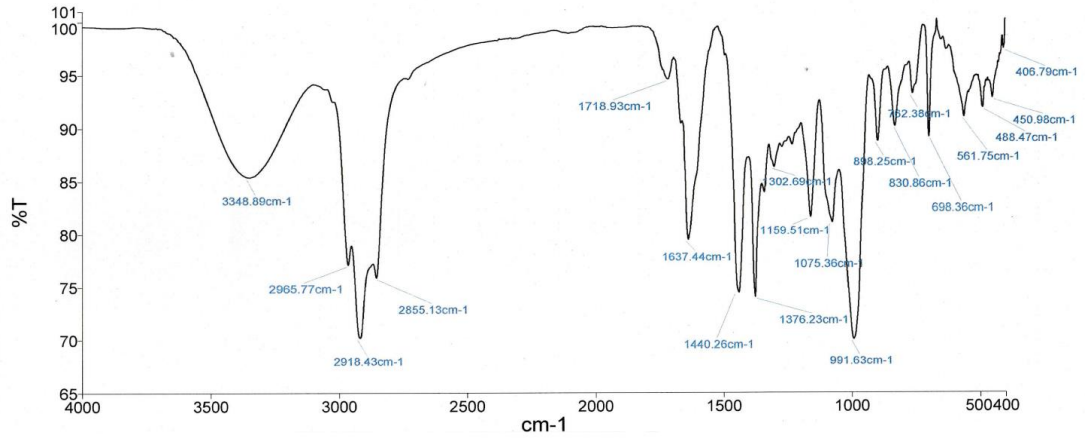

Figure A6 IR (ATR) spectrum of farnesol (**1**)

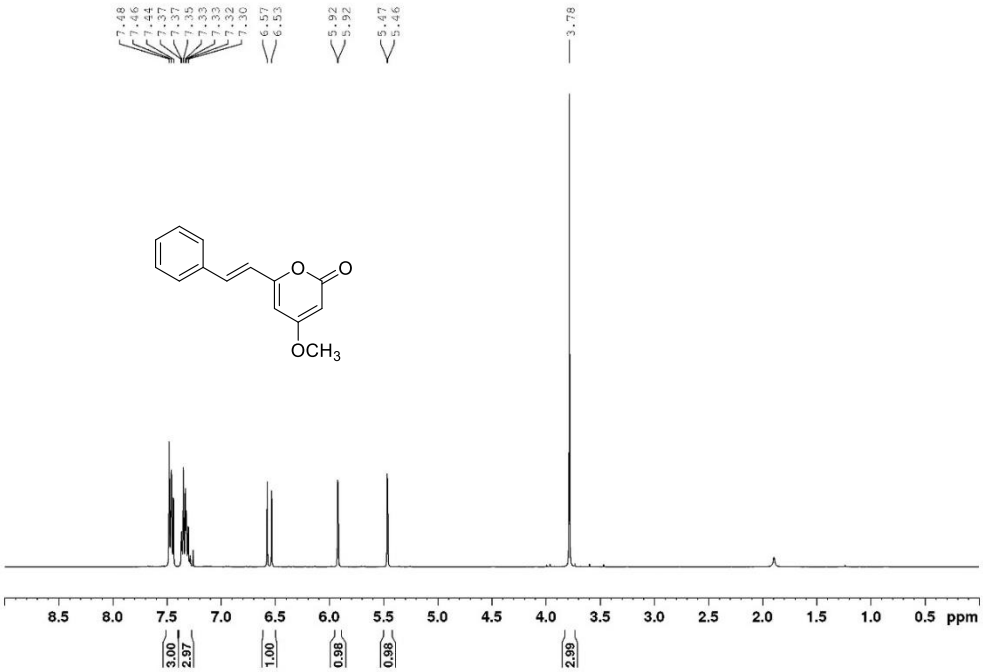

Figure A7 ^{1}H NMR spectrum ($CDCl_3$, 400 MHz) of 5,6-dehydrokawain (**2**)

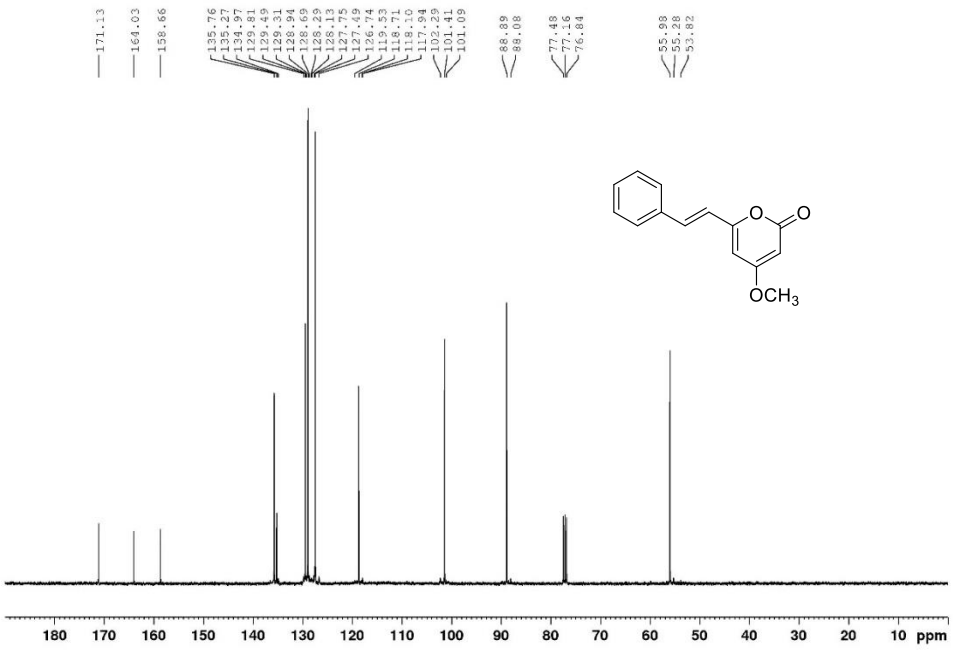

Figure A8 ^{13}C NMR spectrum ($CDCl_3$, 400 MHz) of 5,6-dehydrokawain (**2**)

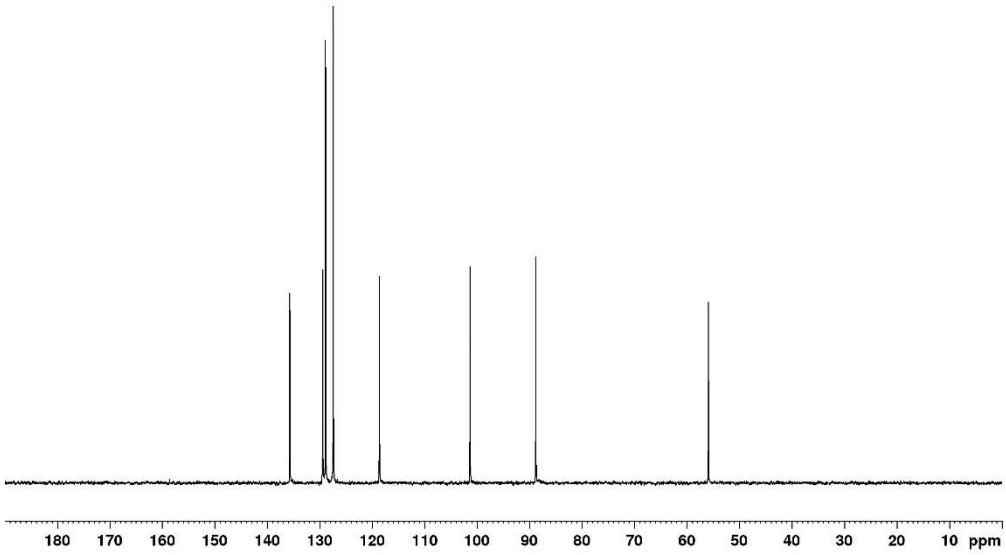

Figure A9 DEPT135 spectrum ($CDCl_3$, 400 MHz) of 5,6-dehydrokawain (**2**)

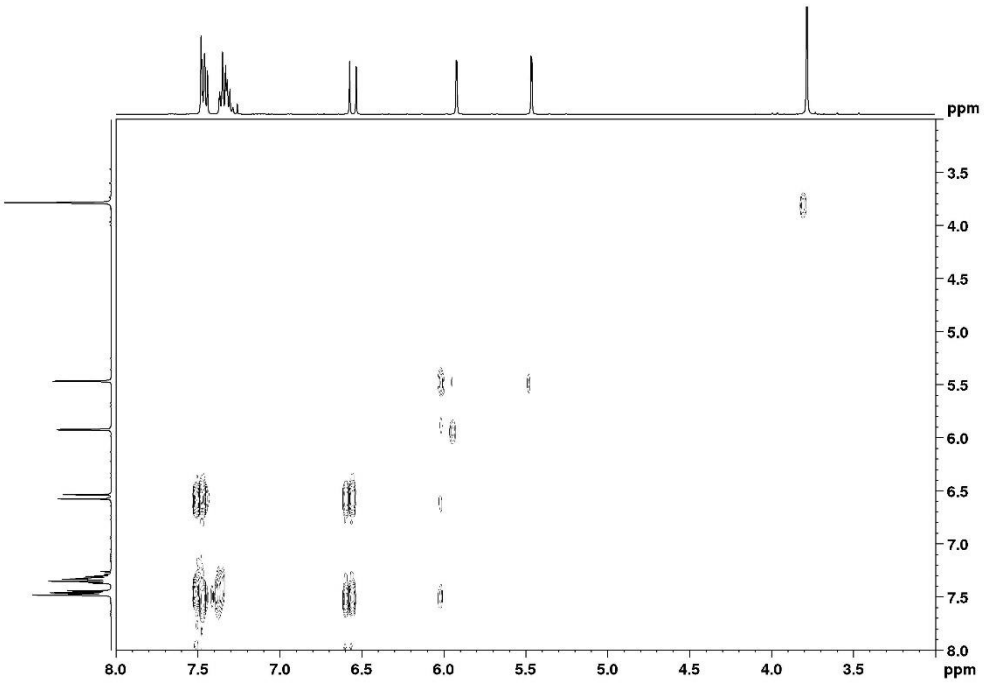

Figure A10 COSY spectrum ($CDCl_3$, 400 MHz) of 5,6-dehydrokawain (**2**)

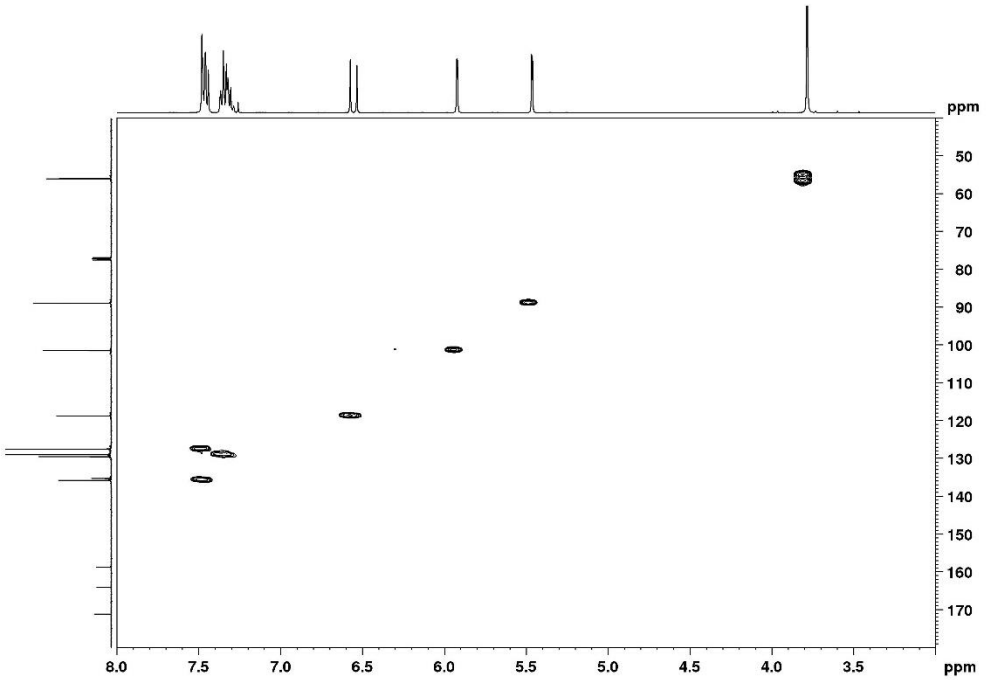

Figure A11 HMQC spectrum ($CDCl_3$, 400 MHz) of 5,6-dehydrokawain (**2**)

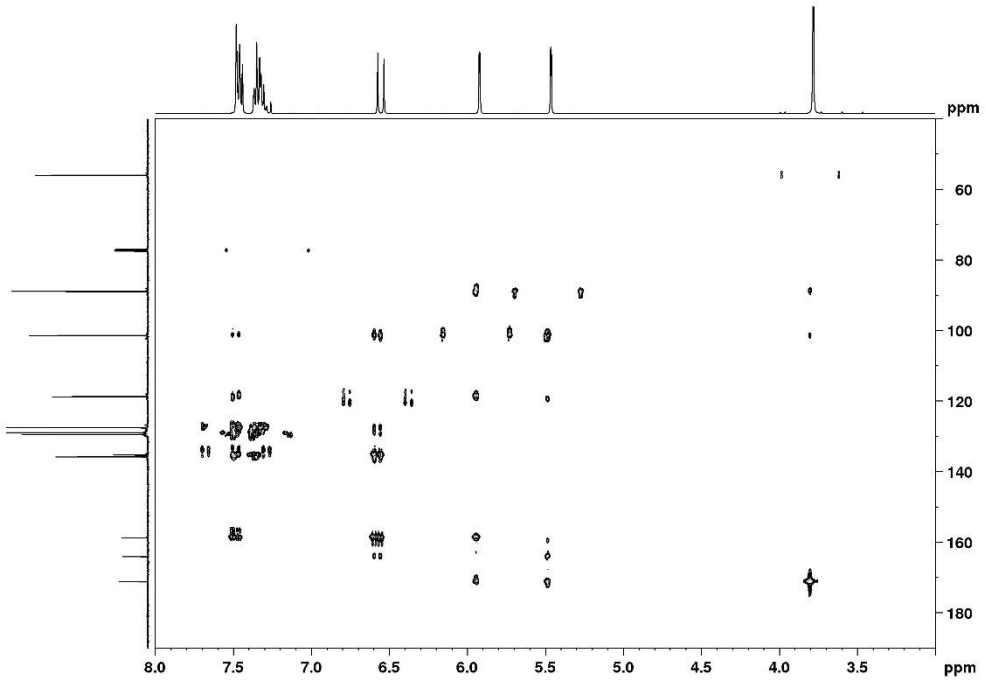

Figure A12 HMBC spectrum ($CDCl_3$, 400 MHz) of 5,6-dehydrokawain (**2**)

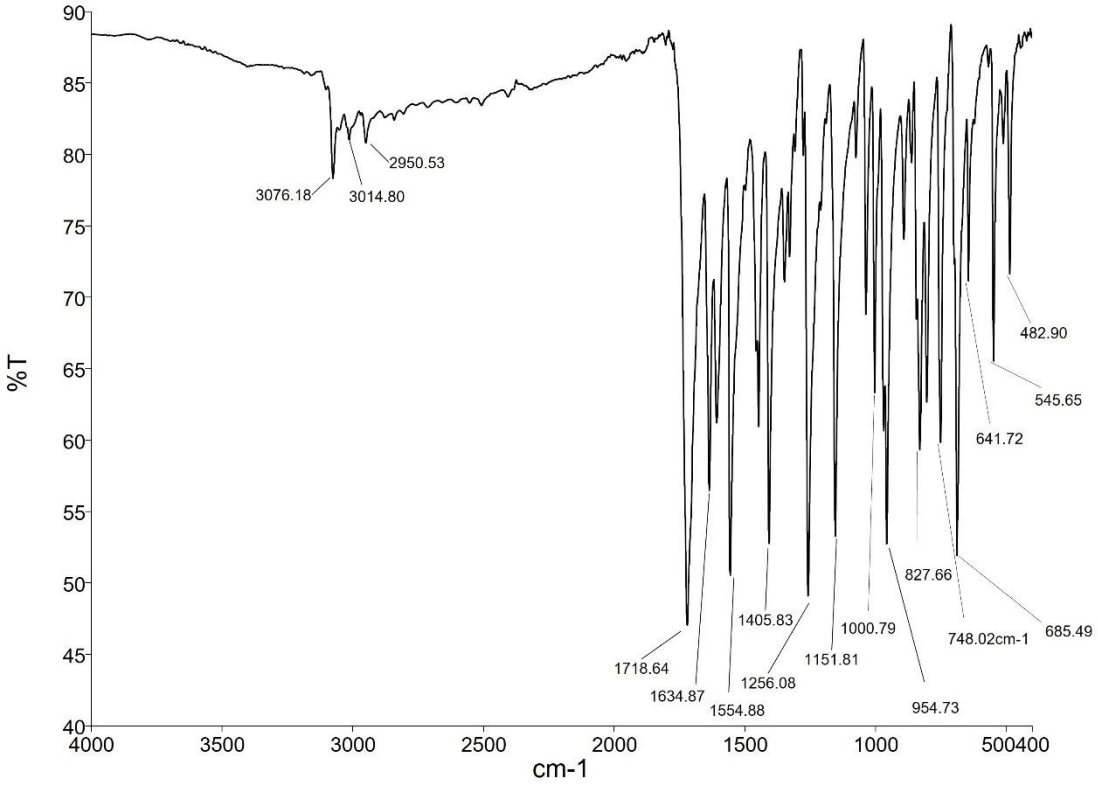

Figure A13 IR (ATR) spectrum of 5,6-dehydrokawain (**2**)

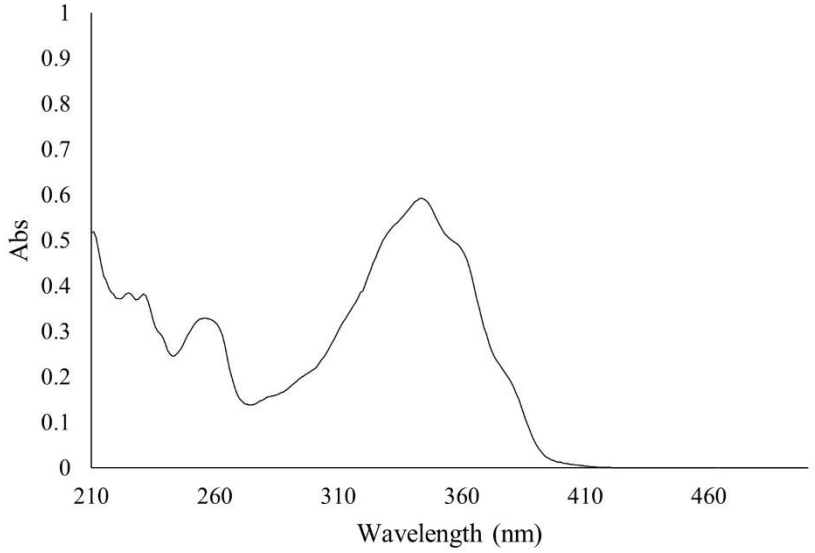

Figure A14 UV spectrum of 5,6-dehydrokawain (**2**) in MeOH

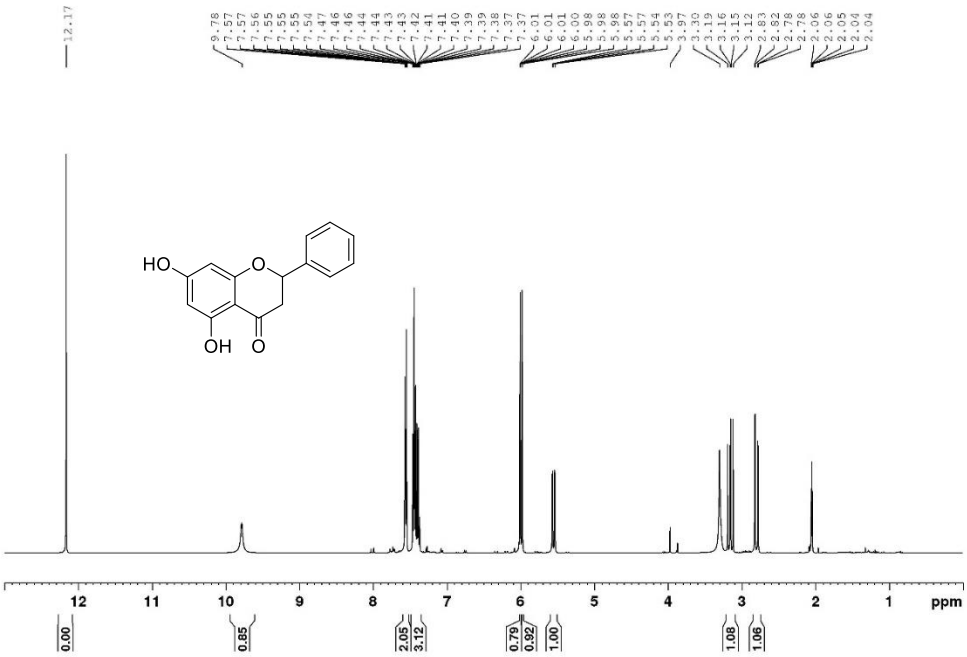

Figure A15 ^{1}H NMR spectrum (acetone-d_6, 400 MHz) of pinocembrin (**3**)

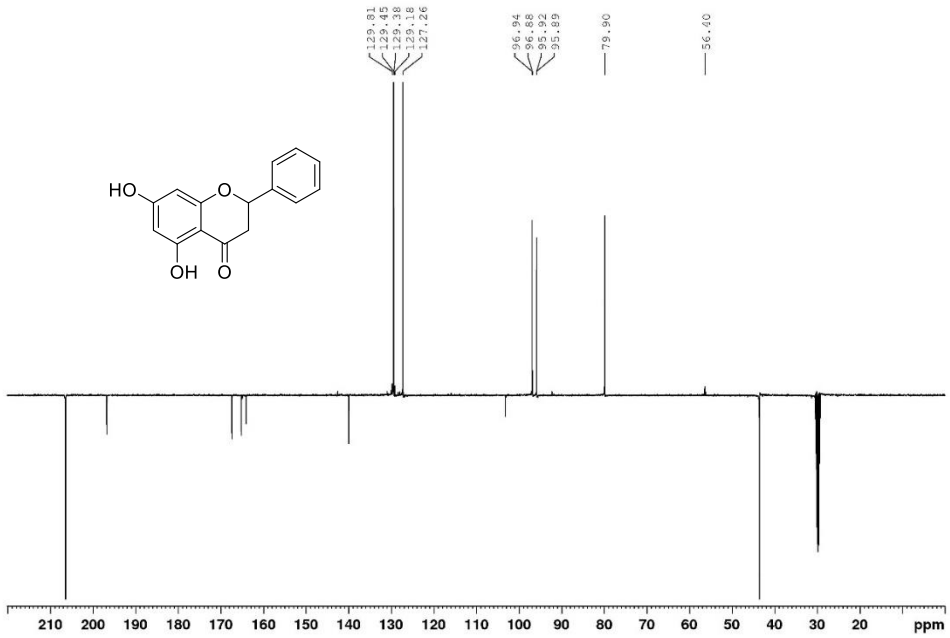

Figure A16 DEPTQ spectrum (acetone-d_6, 400 MHz) of pinocembrin (**3**)

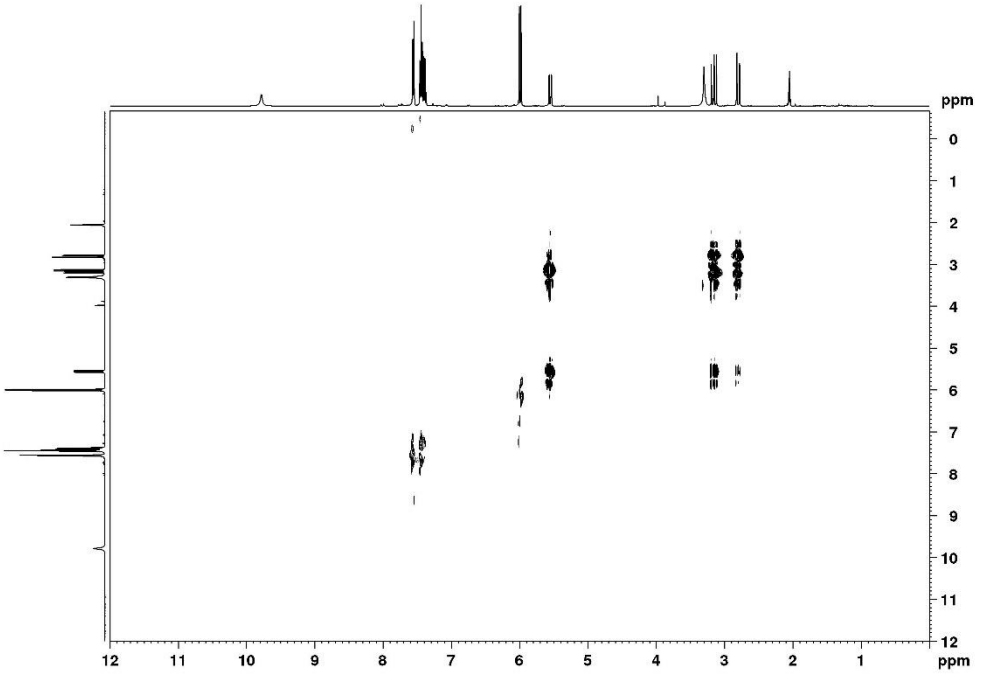

Figure A17 COSY spectrum (acetone-d_6, 400 MHz) of pinocembrin (**3**)

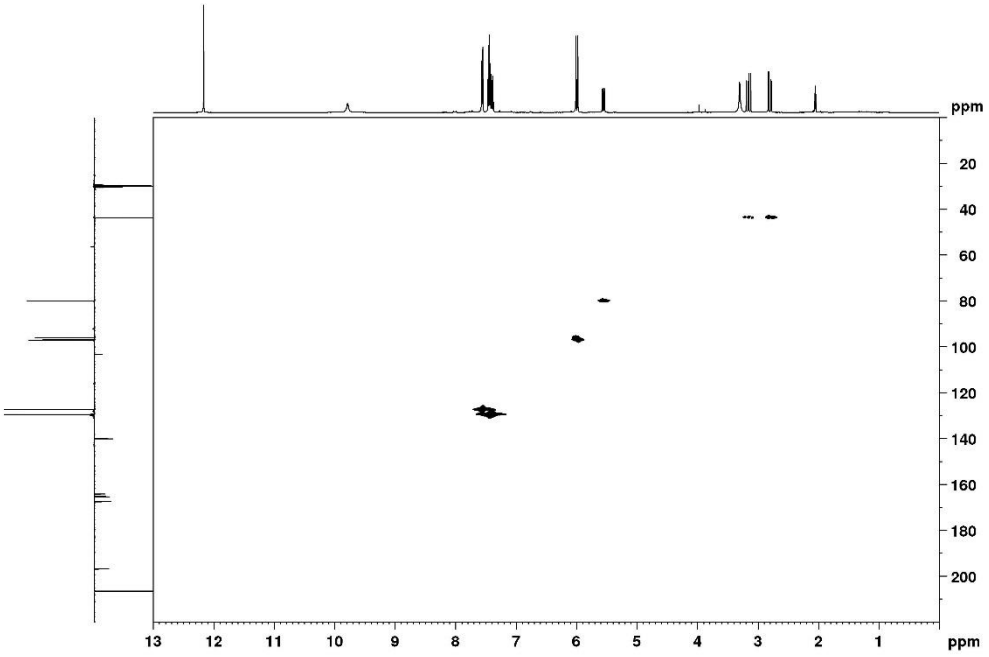

Figure A18 HMQC spectrum (acetone-d_6, 400 MHz) of pinocembrin (**3**)

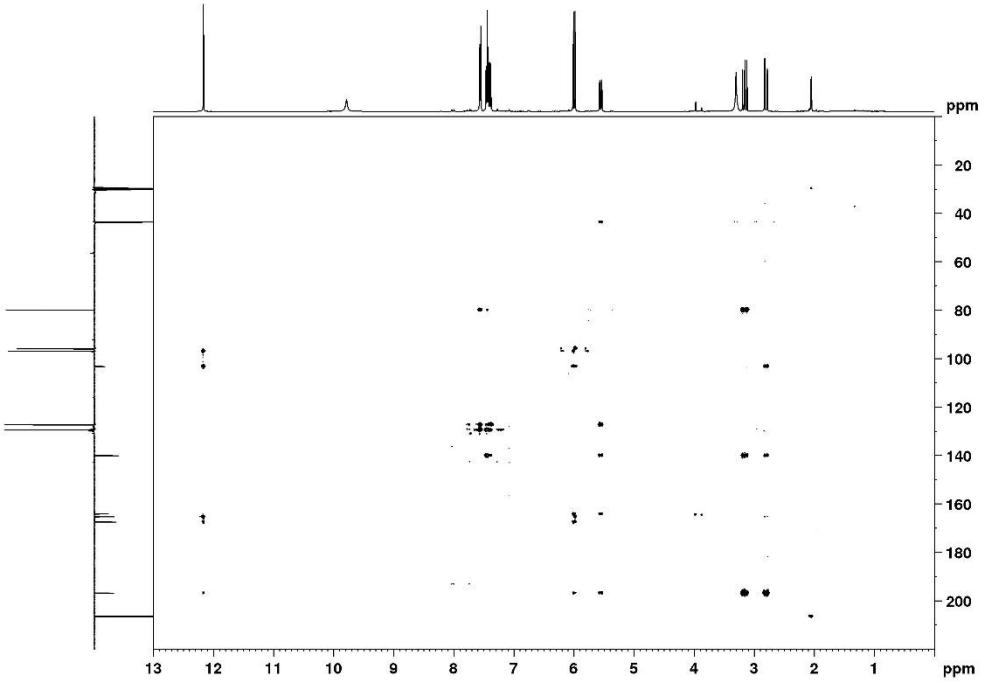

Figure A19 HMMBC spectrum (acetone-d_6, 400 MHz) of pinocembrin (**3**)

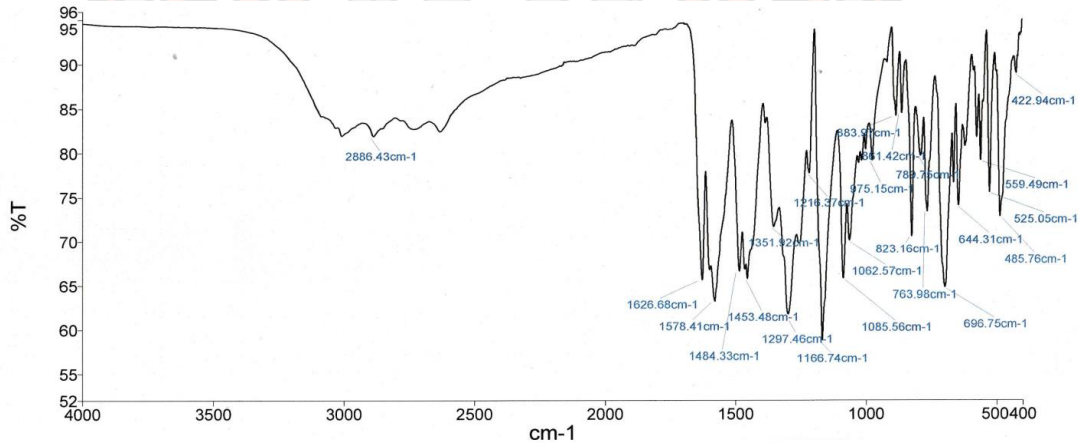

Figure A20 IR (ATR) spectrum of pinocembrin (**3**)

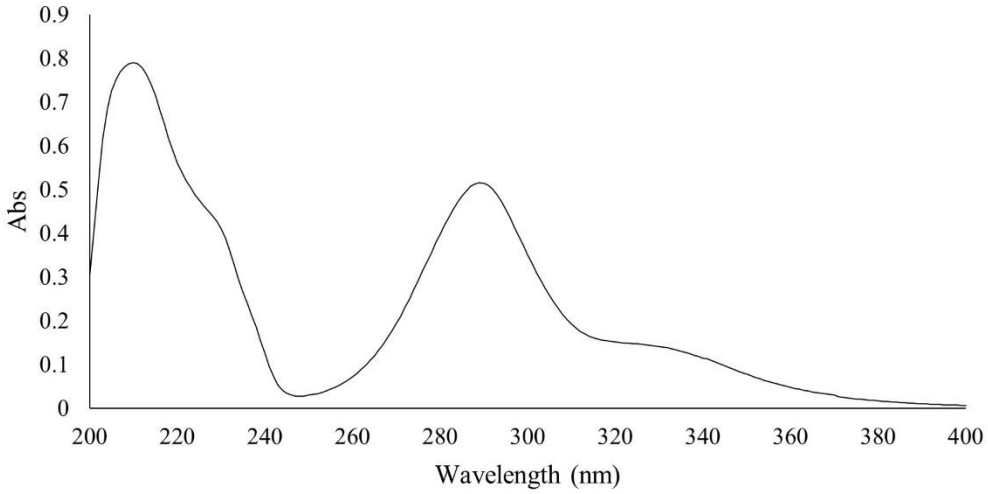

Figure A21 UV spectrum of pinocembrin (**3**) in MeOH

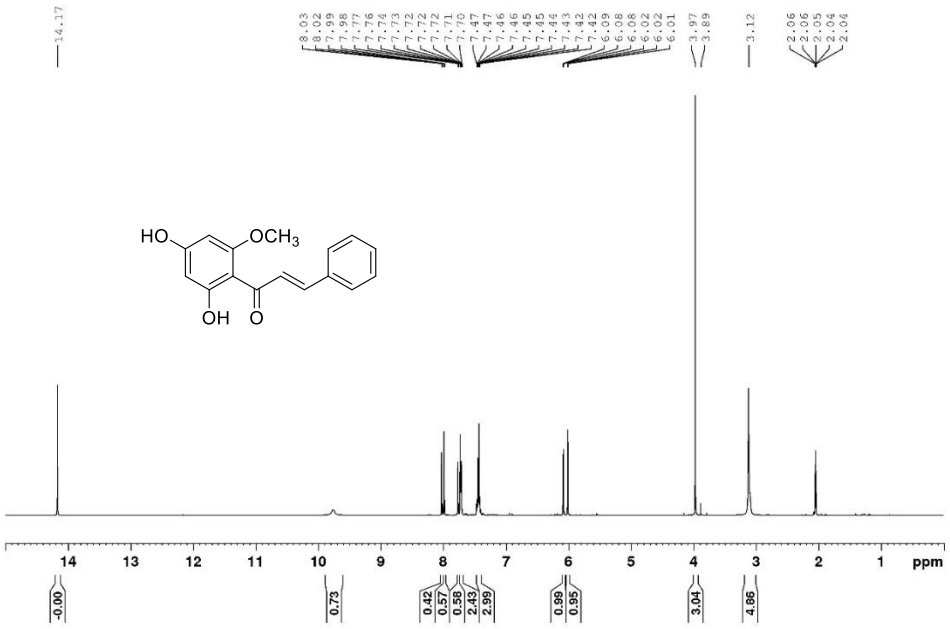

Figure A22 ^{1}H NMR spectrum (acetone-d_6, 400 MHz) of cardamomin (**4**)

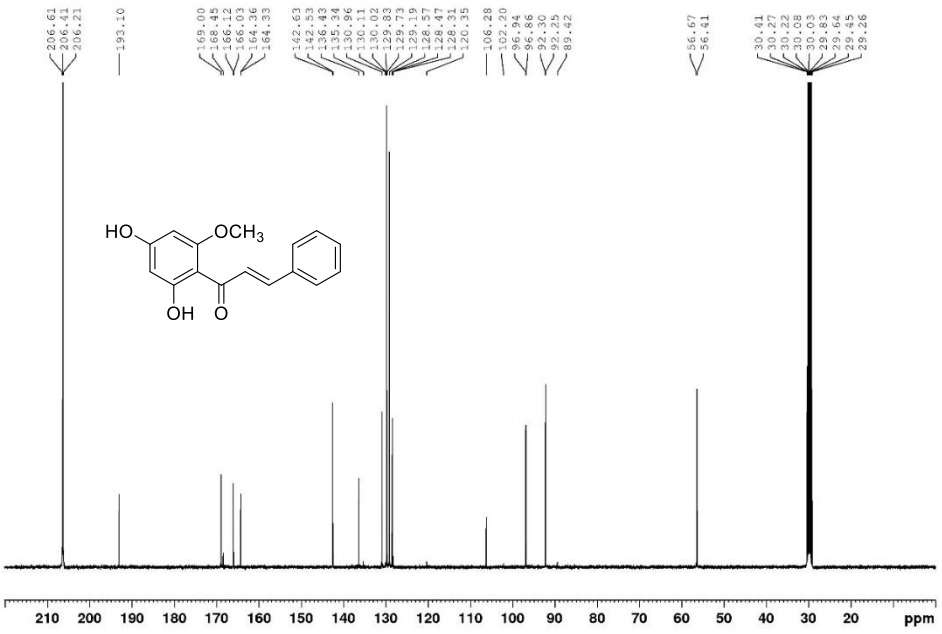

Figure A23 ^{13}C NMR spectrum (acetone-d_6, 400 MHz) of cardamomin (**4**)

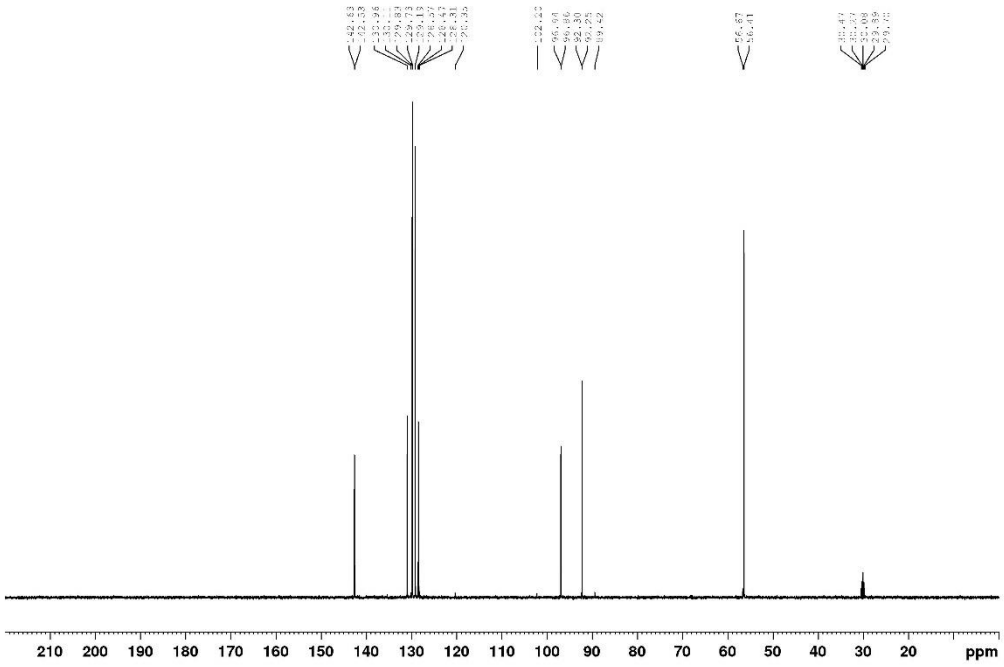

Figure A24 DEPT135 spectrum (acetone-d_6, 400 MHz) of cardamomin (**4**)

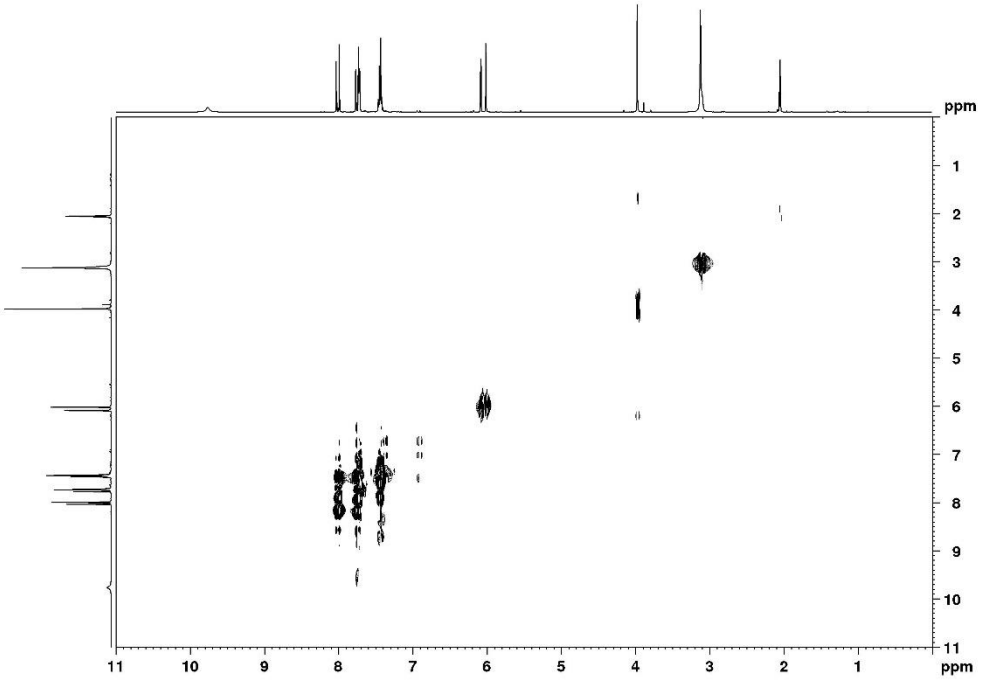

Figure A25 COSY spectrum (acetone-d_6, 400 MHz) of cardamomin (**4**)

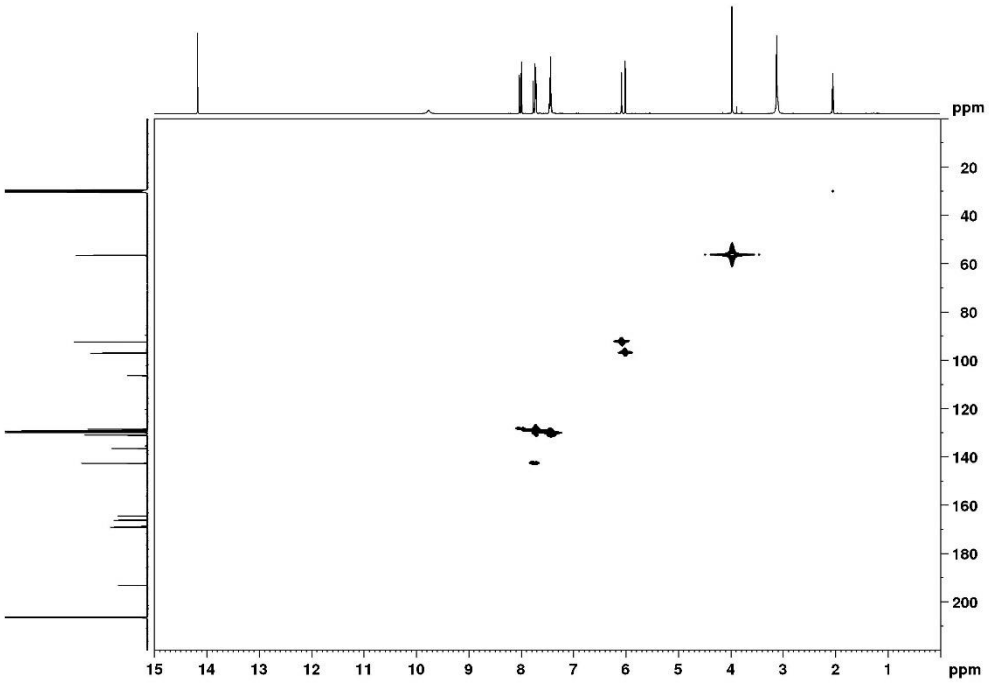

Figure A26 HMQC spectrum (acetone-d_6, 400 MHz) of cardamomin (**4**)

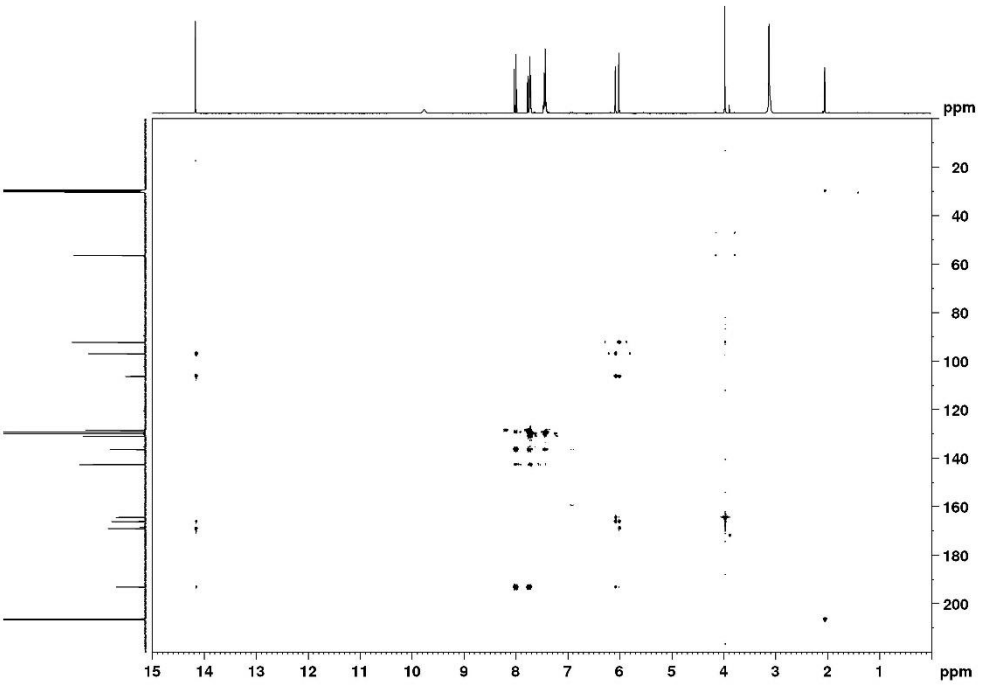

Figure A27 HMBC spectrum (acetone-d_6, 400 MHz) of cardamomin (**4**)

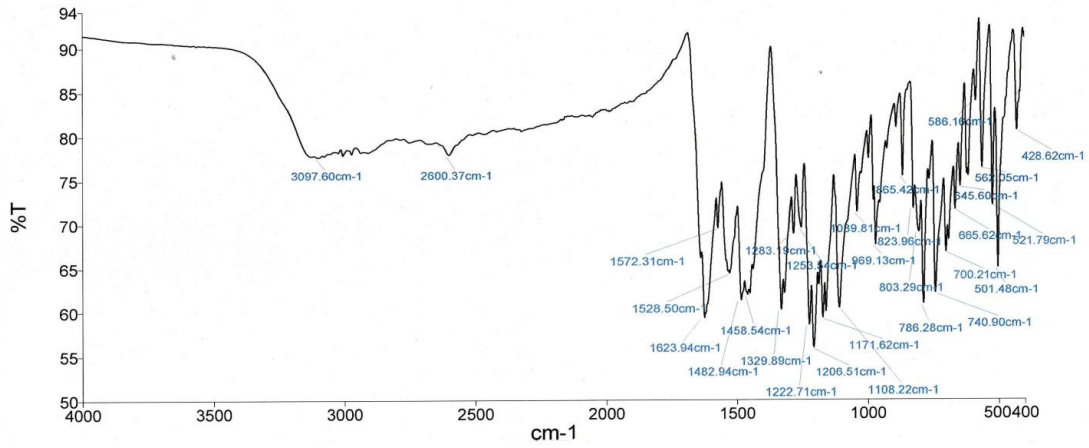

Figure A28 IR (ATR) spectrum of cardamomin (**4**)

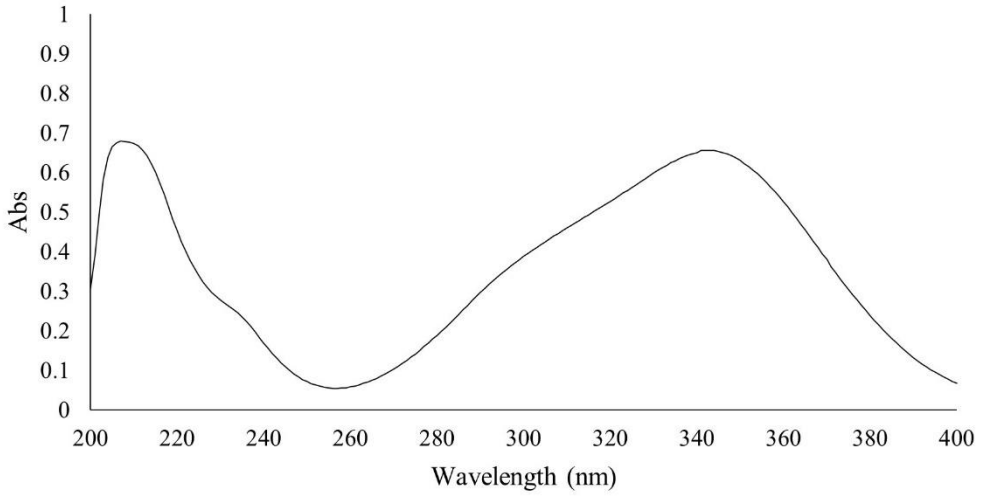

Figure A29 UV spectrum of cadamomin (**4**) in MeOH

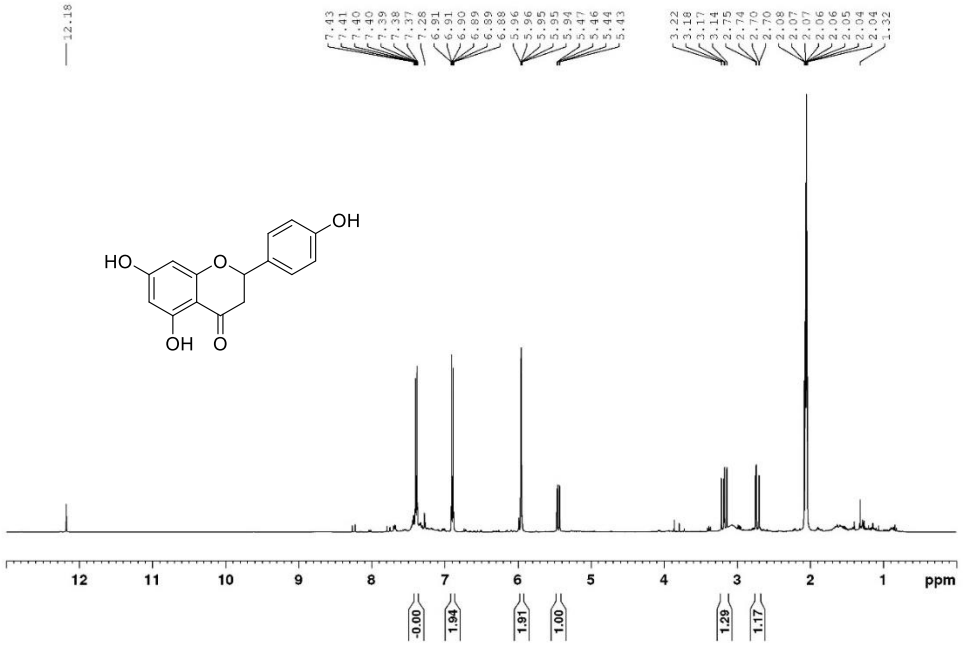

Figure A30 ^{1}H NMR spectrum (acetone-d_6, 400 MHz) of naringenin (**5**)

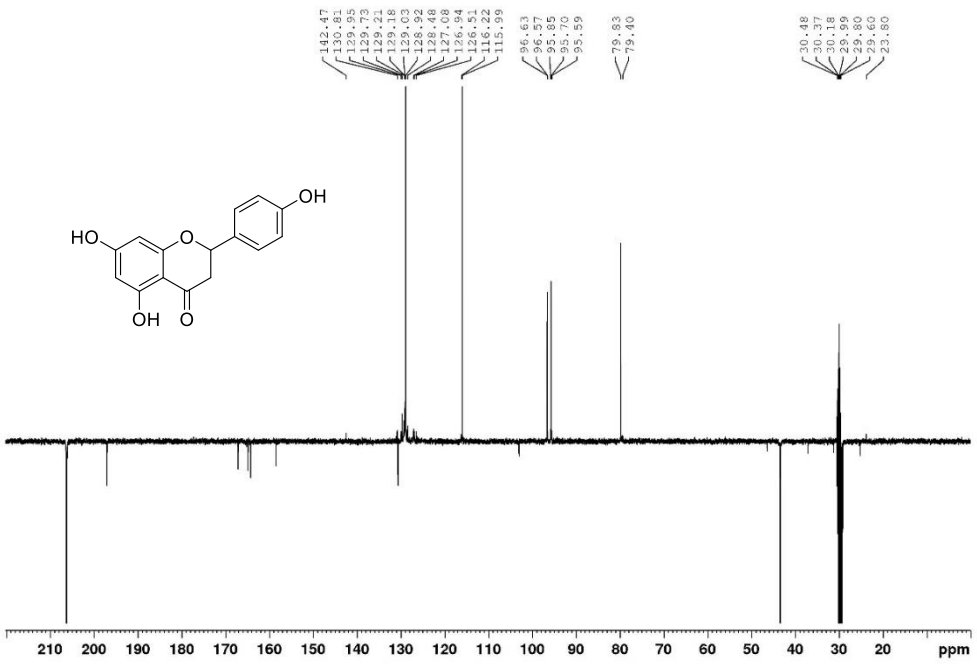

Figure A31 DEPTQ spectrum (acetone-d_6, 400 MHz) of naringenin (**5**)

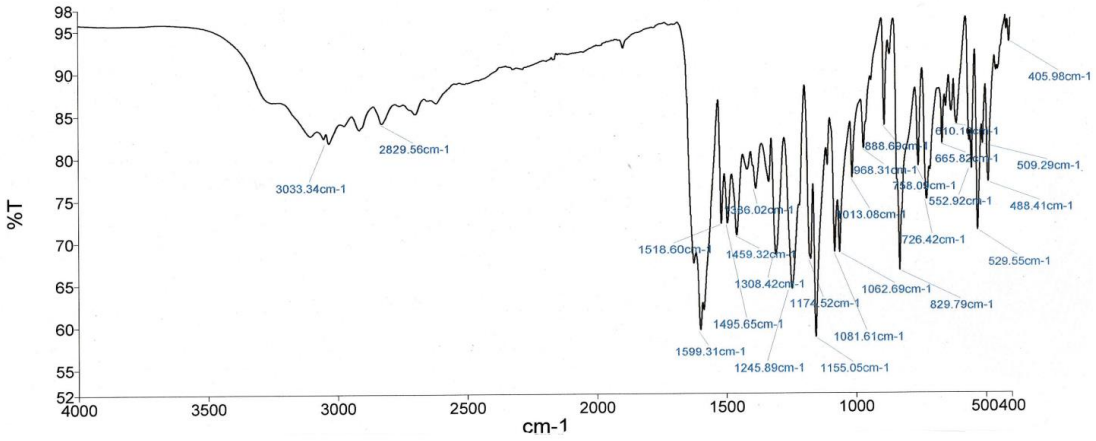

Figure A32 IR (ATR) spectrum of naringenin (**5**)

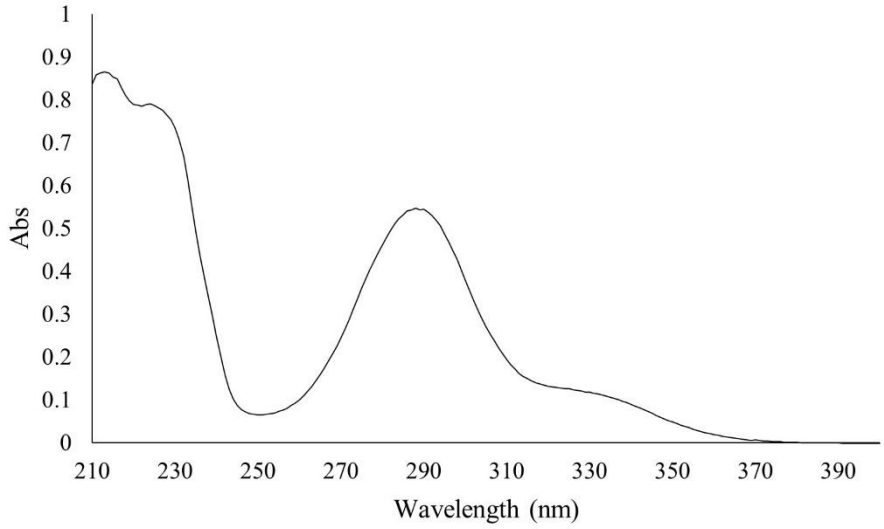

Figure A33 UV spectrum of naringenin (**5**) in MeOH

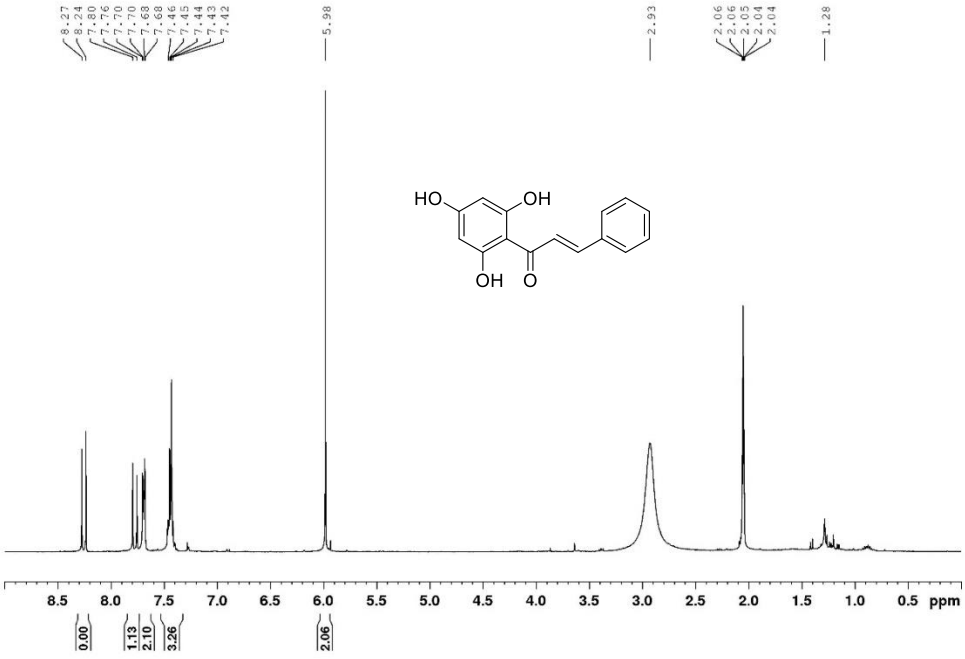

Figure A34 ^{1}H NMR spectrum (acetone-d_6, 400 MHz) of pinocembrin chalcone (**6**)

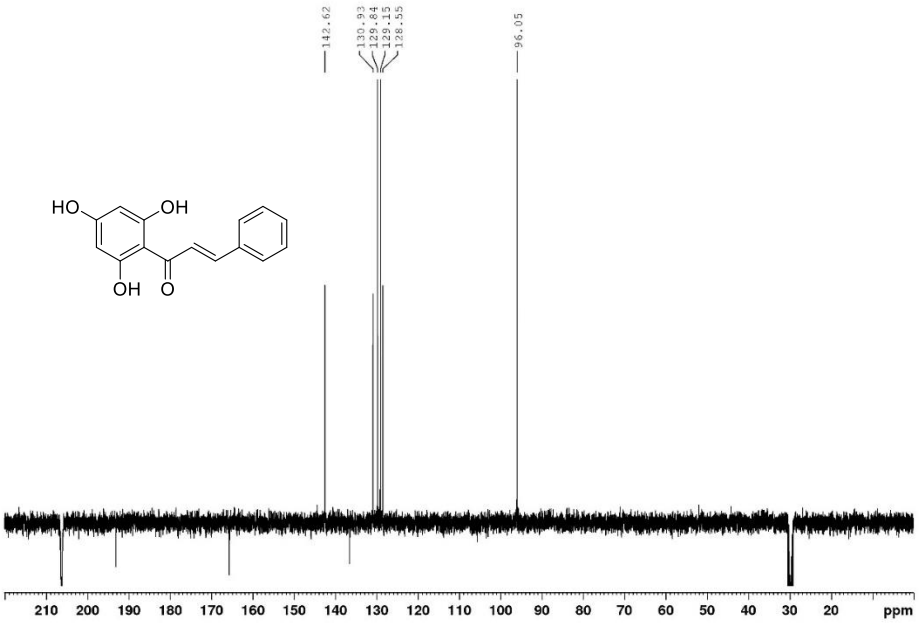

Figure A35 DEPTQ spectrum (acetone-d_6, 400 MHz) of pinocembrin chalcone (**6**)

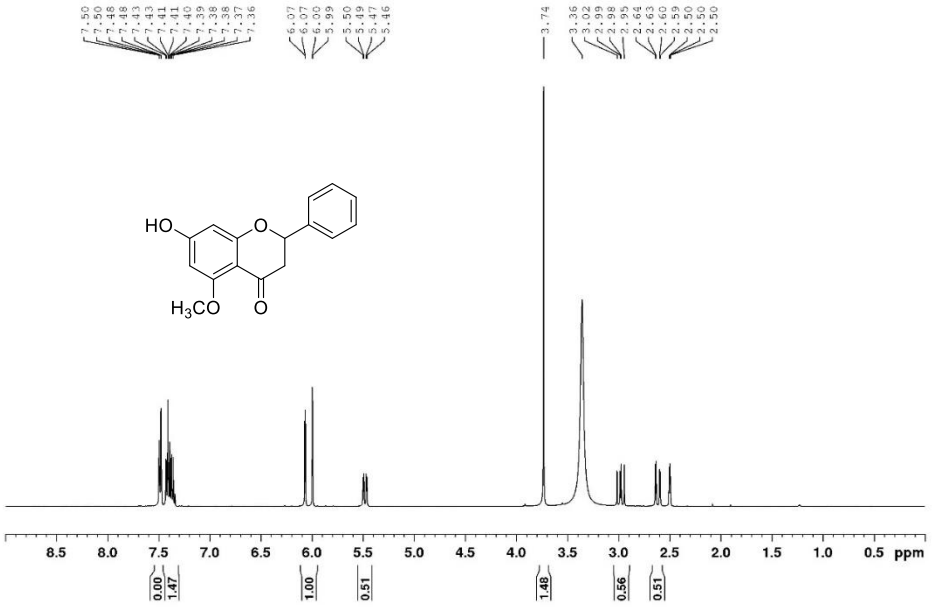

Figure A36 ^{1}H NMR spectrum (DMSO-d_6, 400 MHz) of alpinetin (**7**)

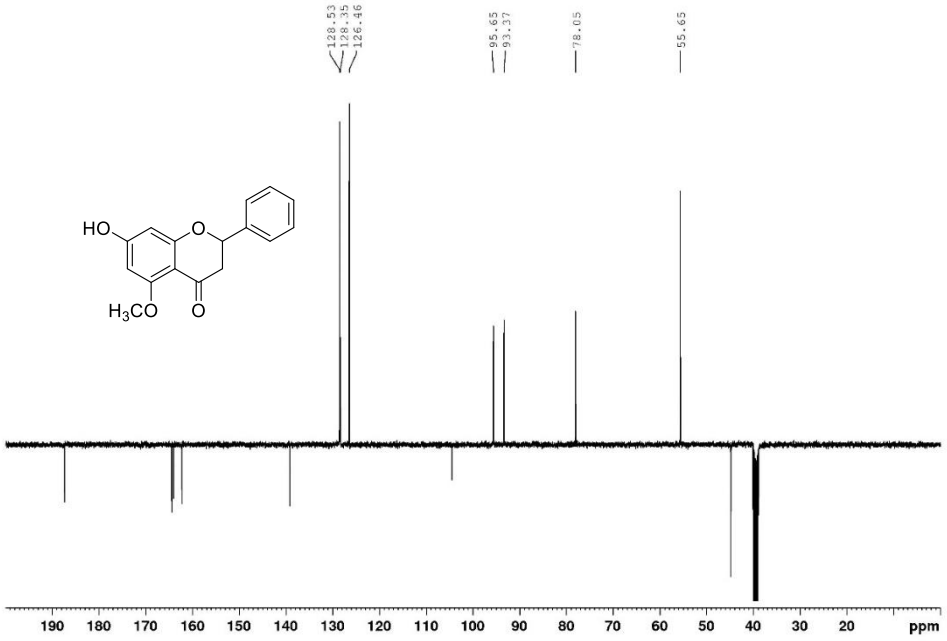

Figure A37 DEPTQ spectrum (DMSO-d_6, 400 MHz) of alpinetin (**7**)

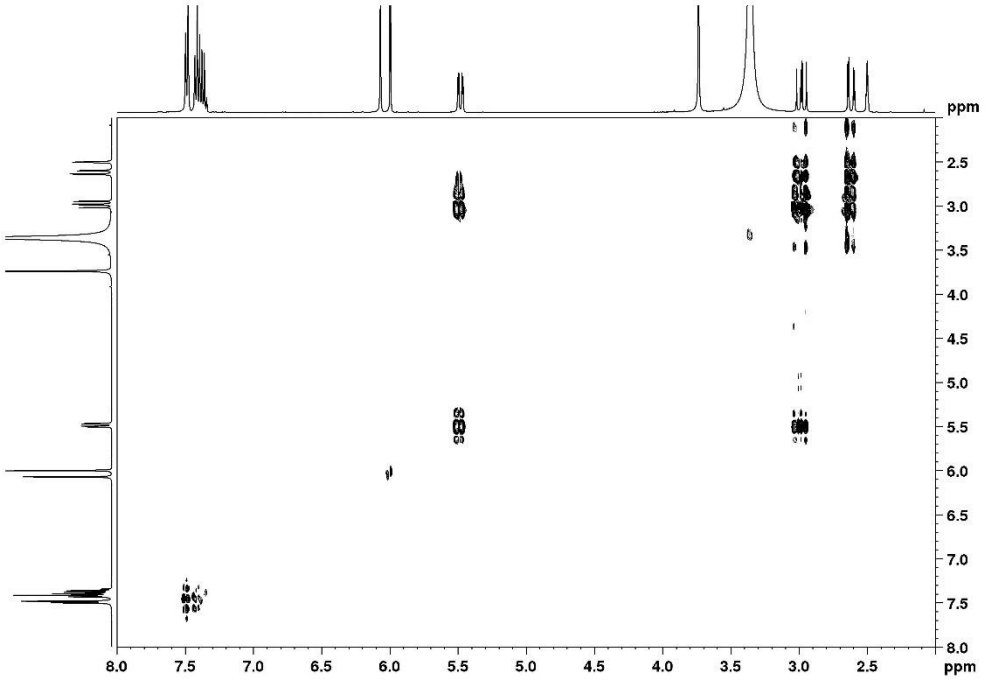

Figure A38 COSY spectrum (DMSO-d_6, 400 MHz) of alpinetin (**7**)

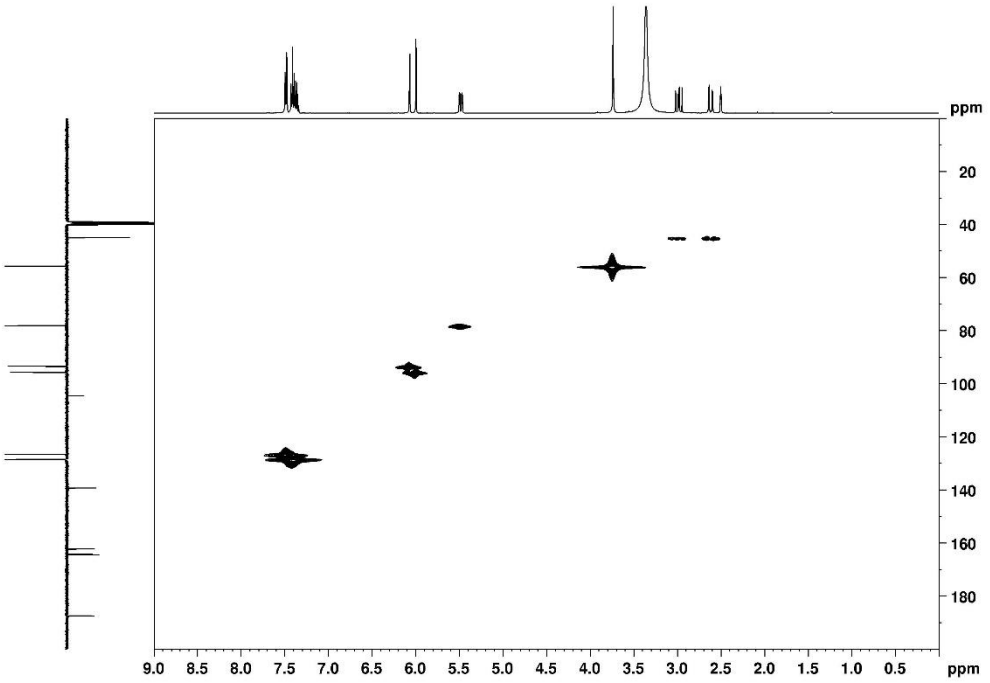

Figure A39 HMQC spectrum (DMSO-d_6, 400 MHz) of alpinetin (**7**)

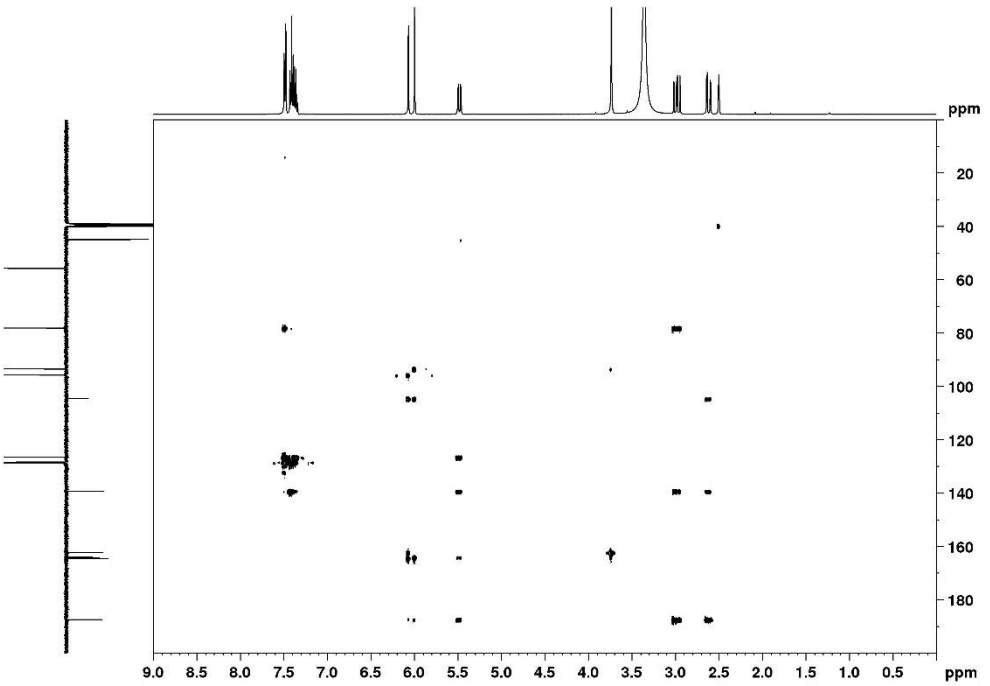

Figure A40 HMBC spectrum (DMSO-d_6, 400 MHz) of alpinetin (**7**)

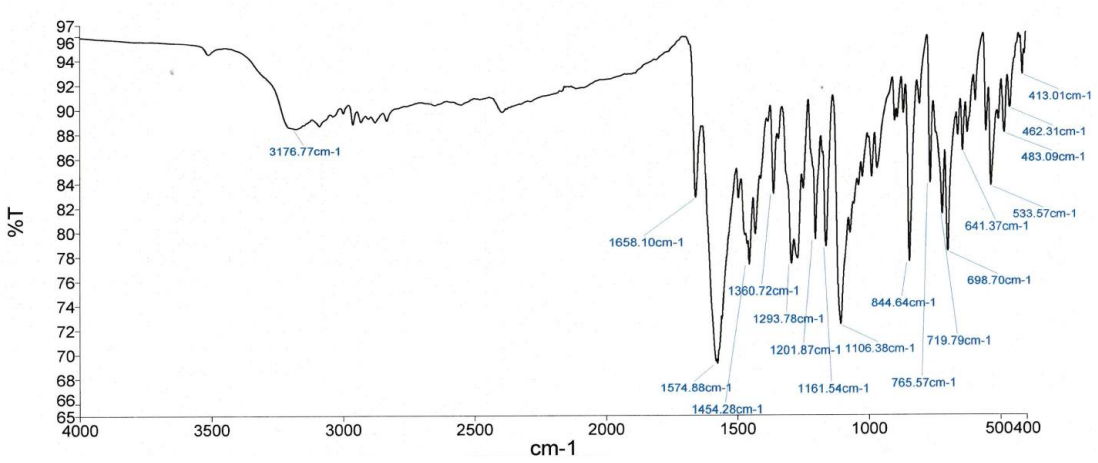

Figure A41 IR (ATR) spectrum of alpinetin (**7**)

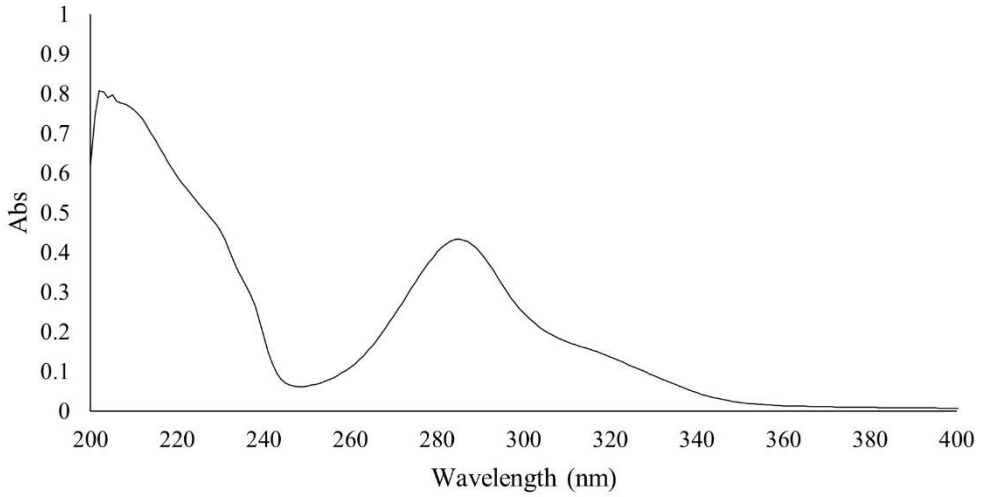

Figure A42 UV spectrum of alpinetin (**7**) in MeOH

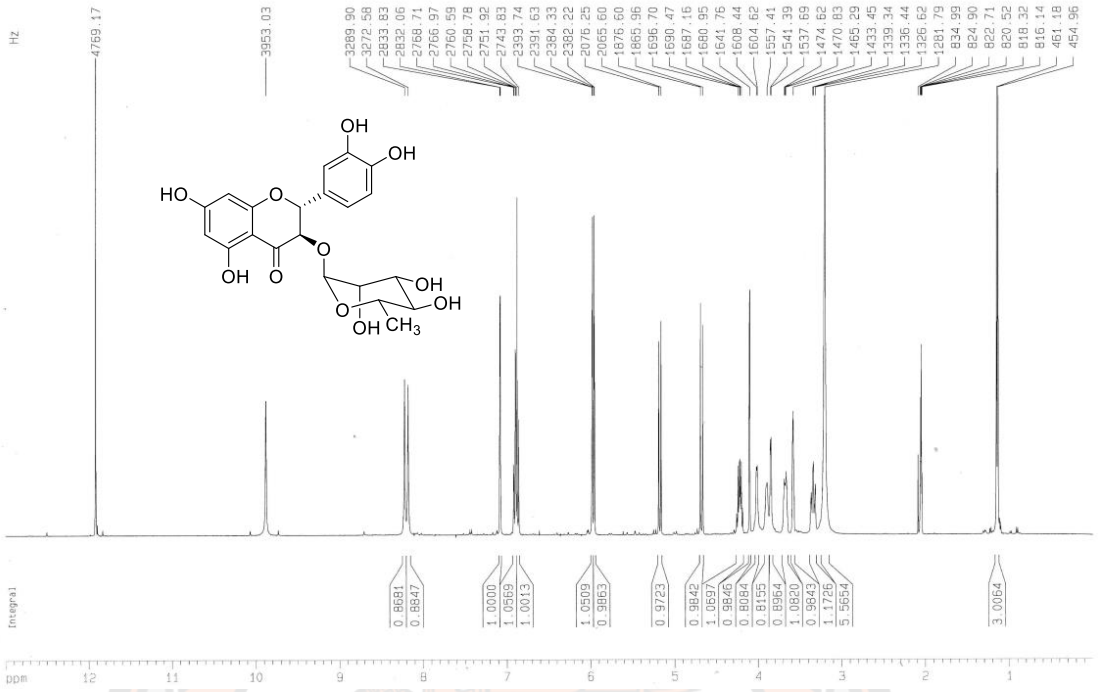

Figure A43 ^{1}H NMR spectrum (acetone-d_6, 400 MHz) of astilbin (**8**)

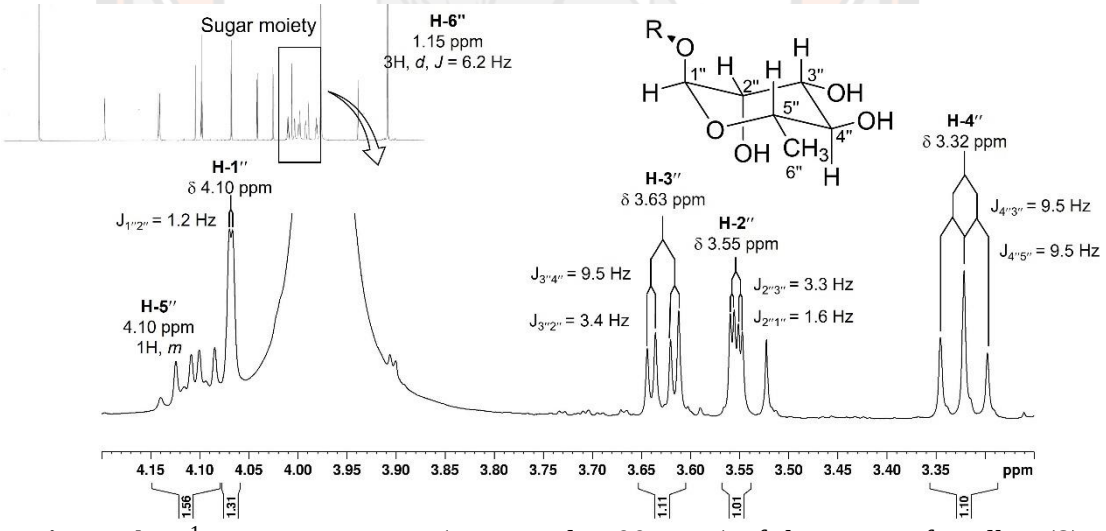

Figure A44 ^{1}H NMR spectrum (acetone-d_6, 400 MHz) of rhamnose of astilbin (**8**)

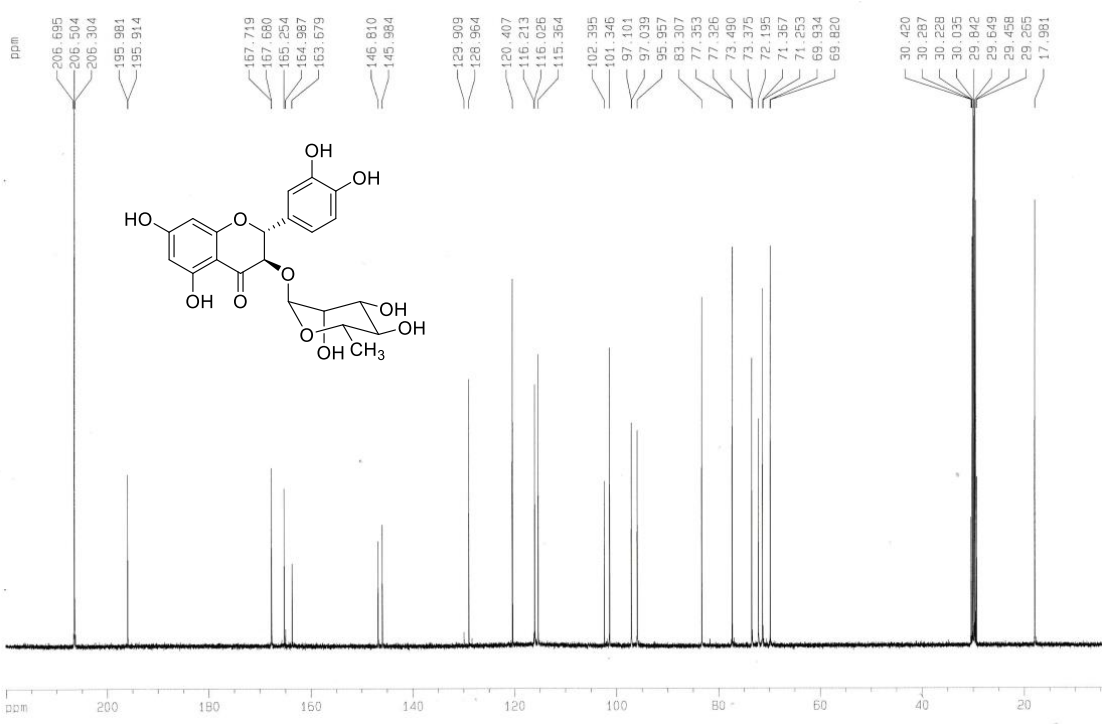

Figure A45 ^{13}C NMR spectrum (acetone-d_6, 100 MHz) of astilbin (**8**)

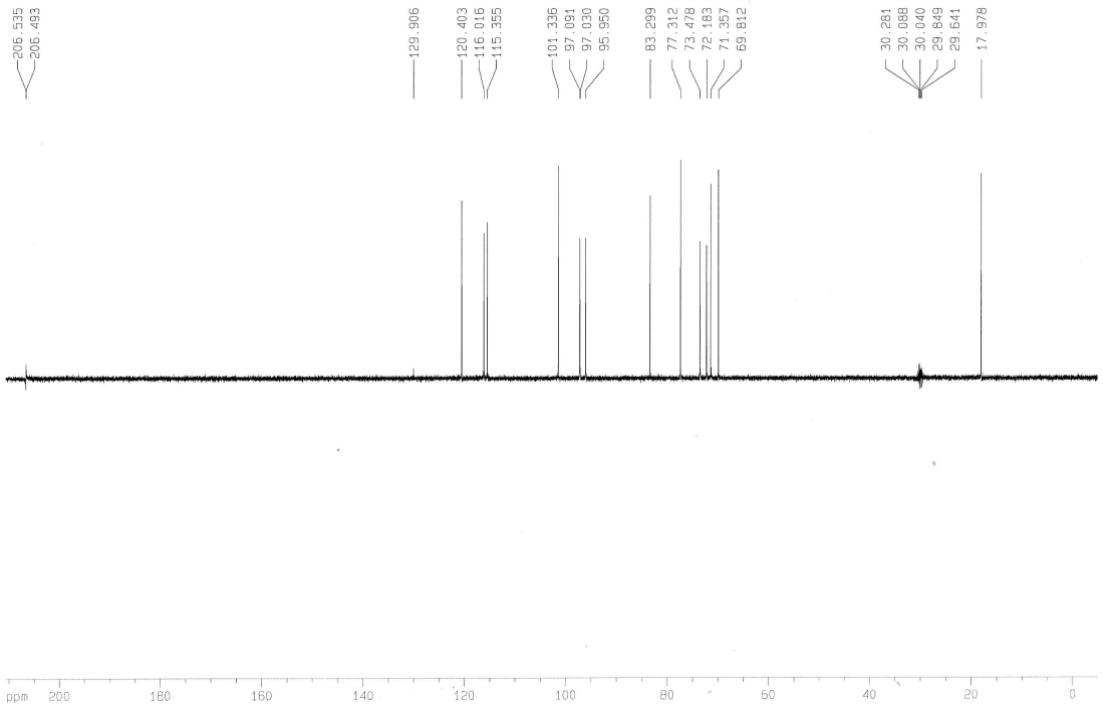

Figure A46 DEPT135 spectrum (acetone-d_6, 100 MHz) of astilbin (**8**)

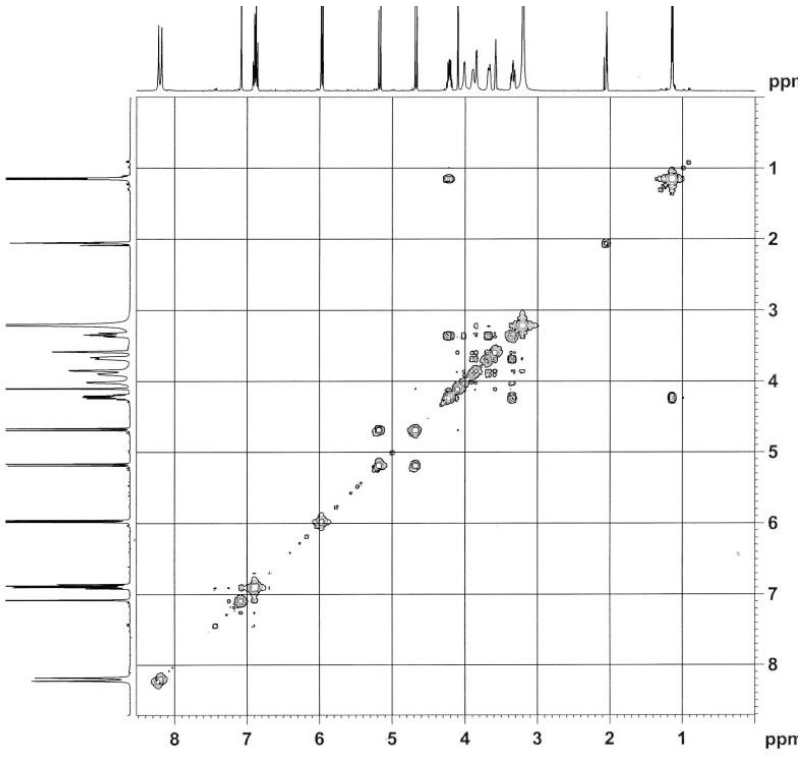

Figure A47 COSY spectrum (acetone-d_6, 400 MHz) of astilbin (**8**)

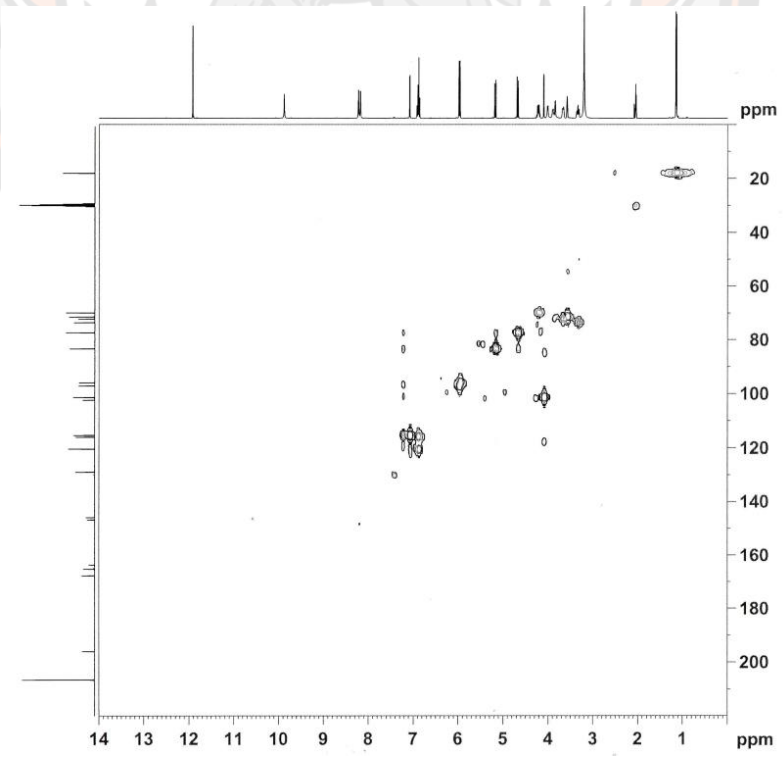

Figure A48 HMQC NMR spectrum (acetone-d_6) of astilbin (**8**)

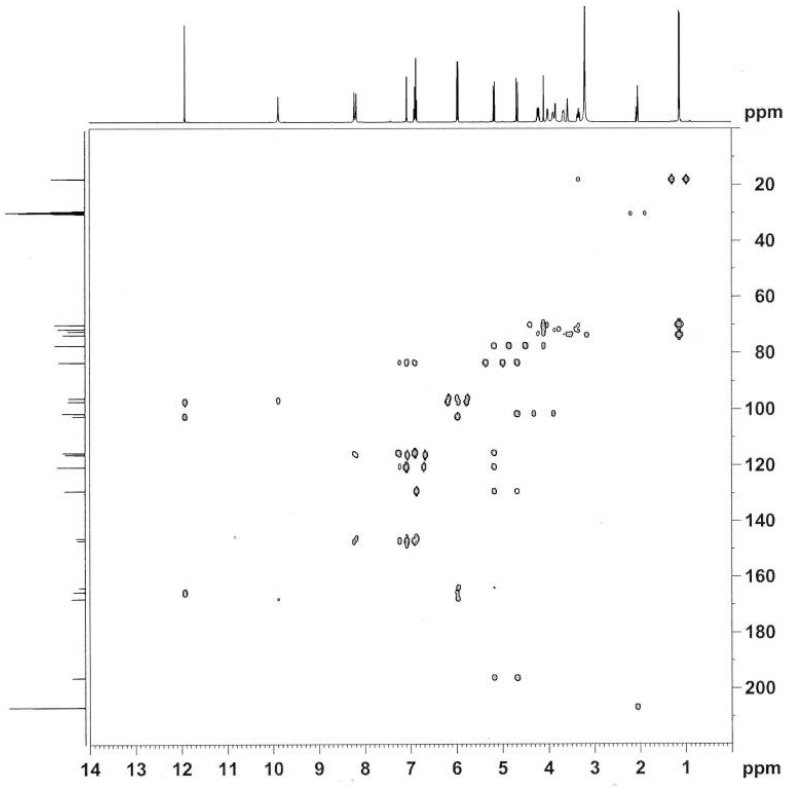

Figure A49 HMBC NMR spectrum (acetone-d_6) of astilbin (**8**)

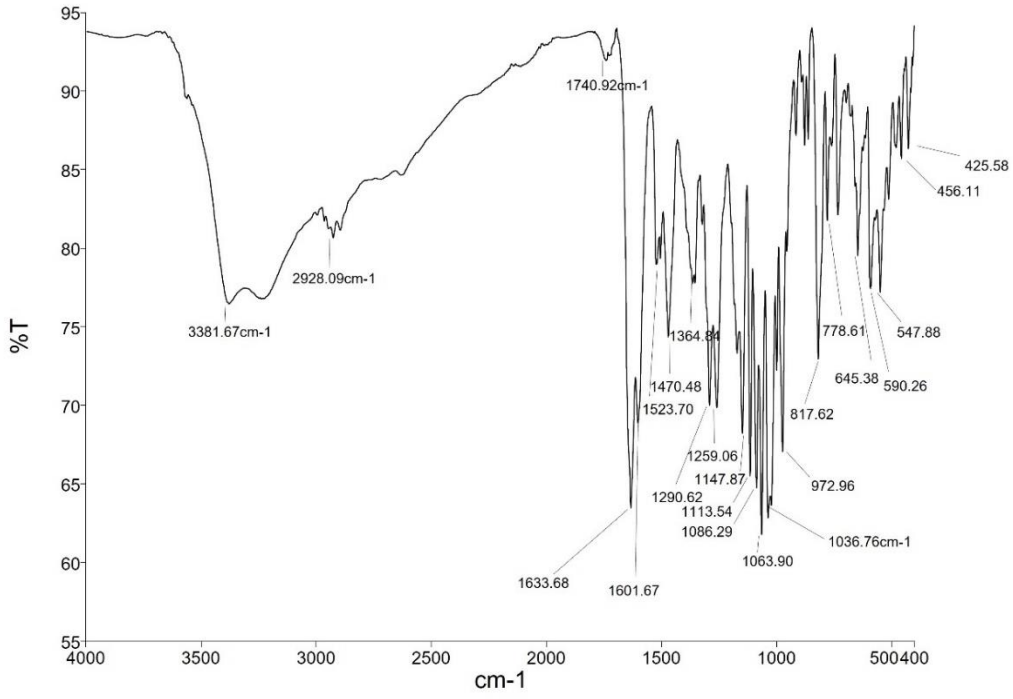

Figure A50 IR (ATR) spectrum of astilbin (**8**)

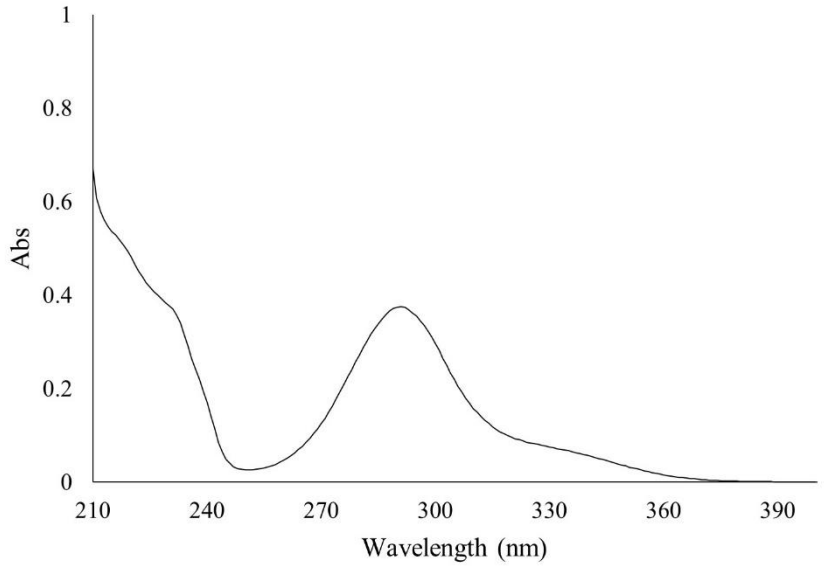

Figure A51 UV spectrum of astilbin (**8**) in MeOH

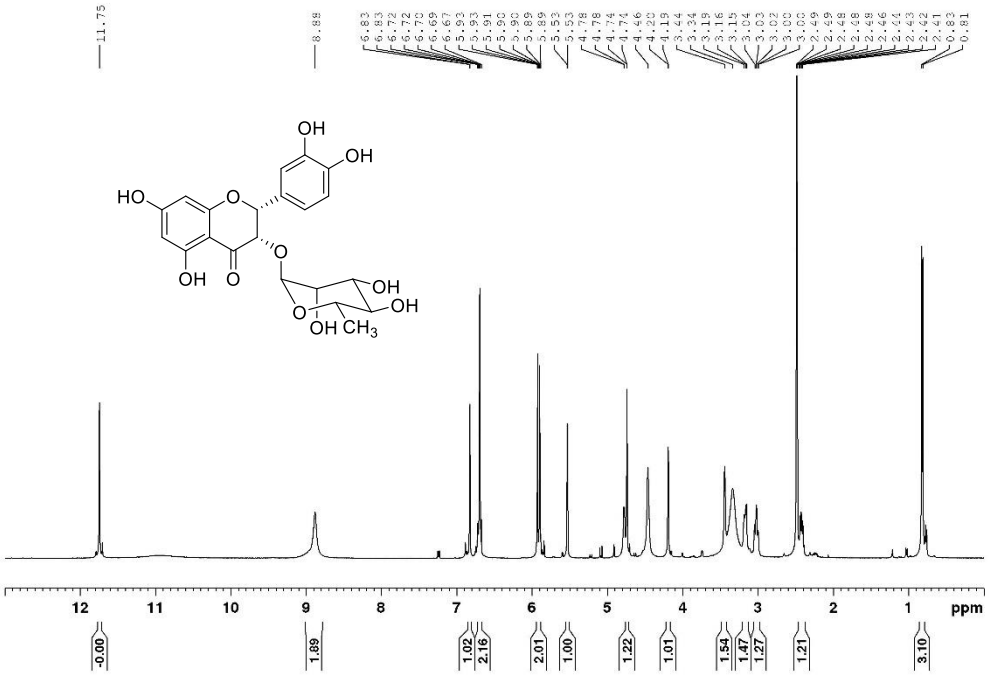

Figure A52 ^{1}H NMR spectrum (DMSO-d_6, 400 MHz) of isoastilbin (**9**)

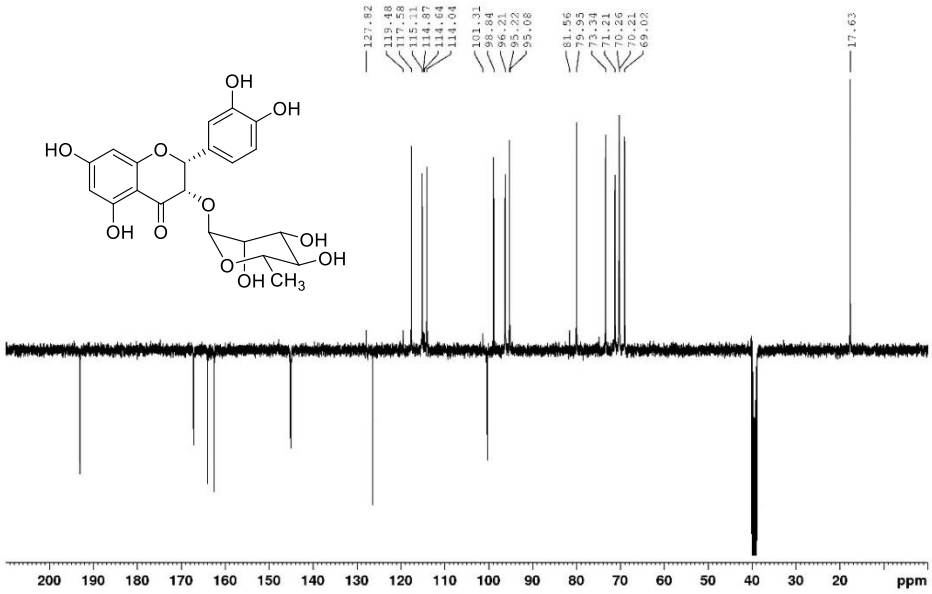

Figure A53 DEPTQ NMR spectrum (DMSO-d_6, 100 MHz) of isoastilbin (**9**)

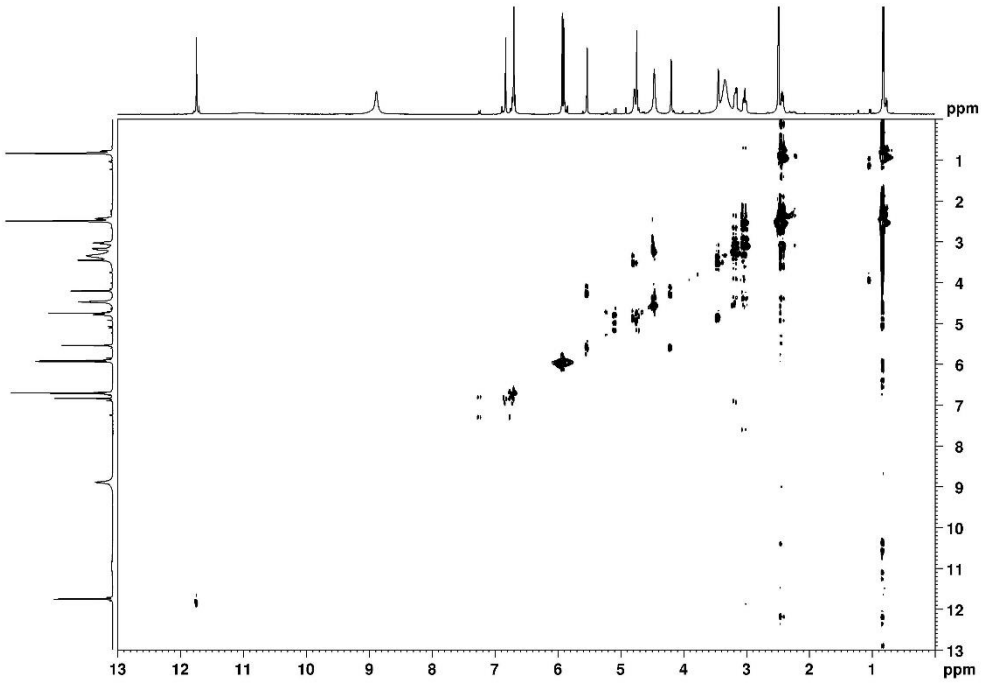

Figure A54 COSY NMR spectrum (DMSO-d_6) of isoastilbin (**9**)

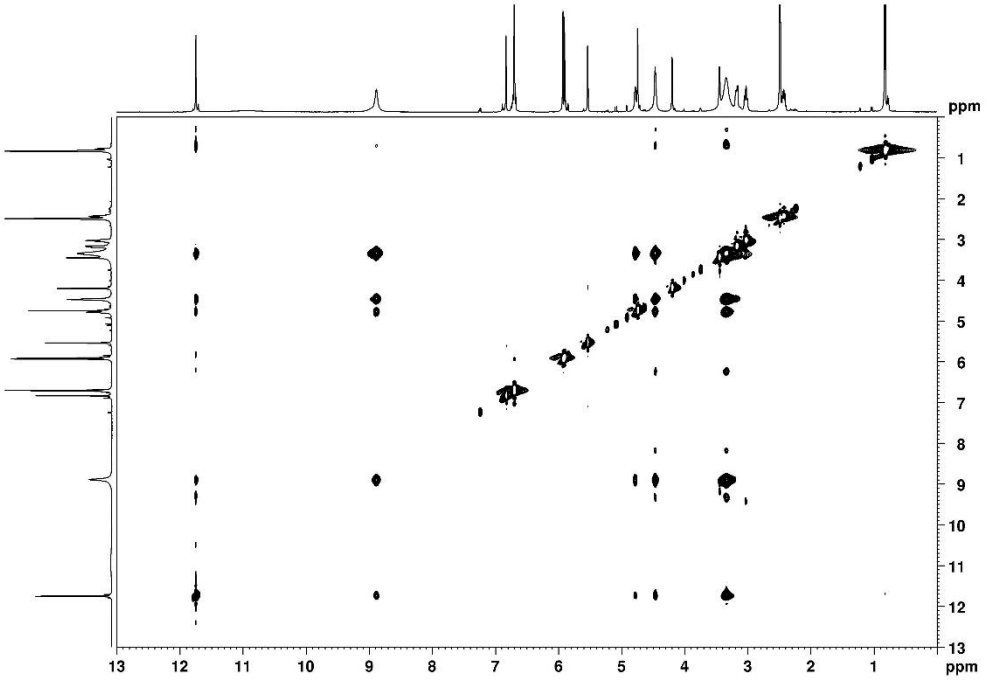

Figure A55 NOESY NMR spectrum (DMSO-d_6) of isoastilbin (**9**)

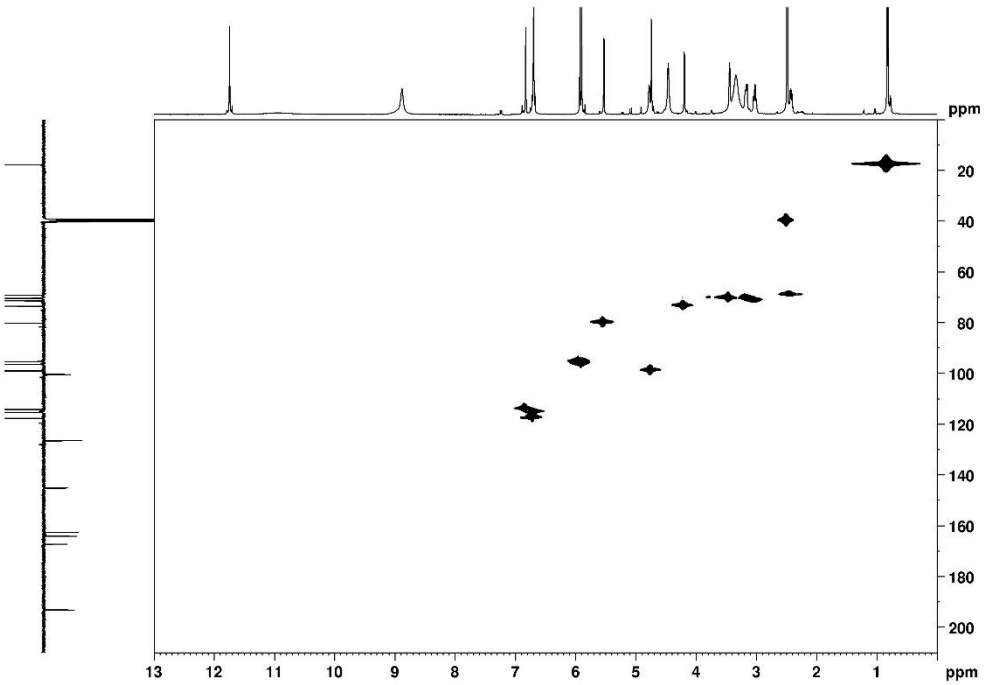

Figure A56 HMQC NMR spectrum (DMSO-d_6) of isoastilbin (**9**)

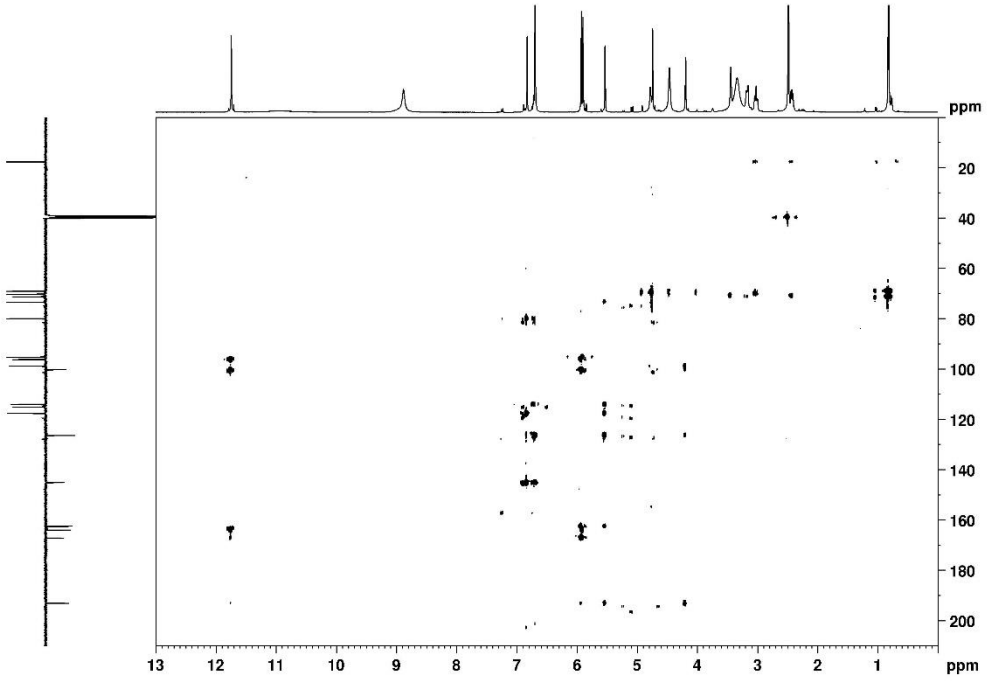

Figure A57 HMBC NMR spectrum (DMSO-d_6, 100 MHz) of isoastilbin (**9**)

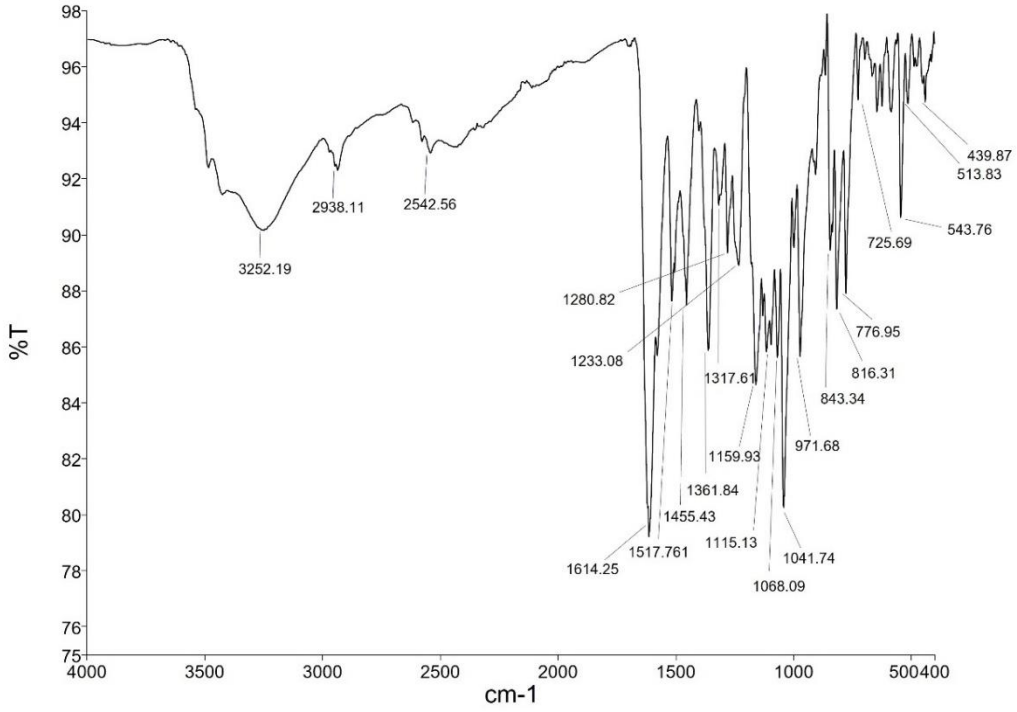

Figure A58 IR (ATR) spectrum of isoastilbin (**9**)

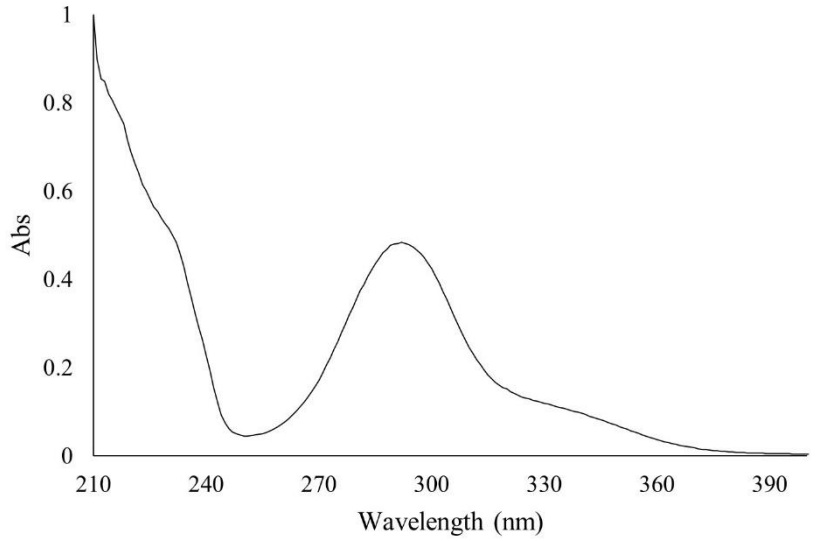

Figure A59 UV (MeOH) spectrum of isoastilbin (**9**)

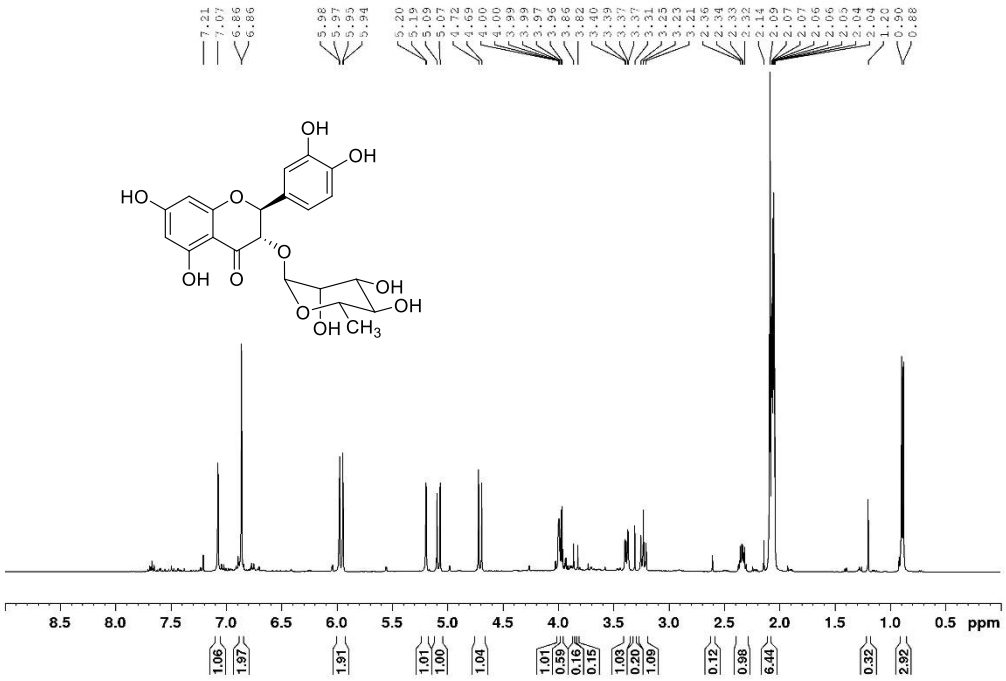

Figure A60 ^{1}H NMR spectrum (acetone-d_6, 400 MHz) of neoastilbin (**10**)

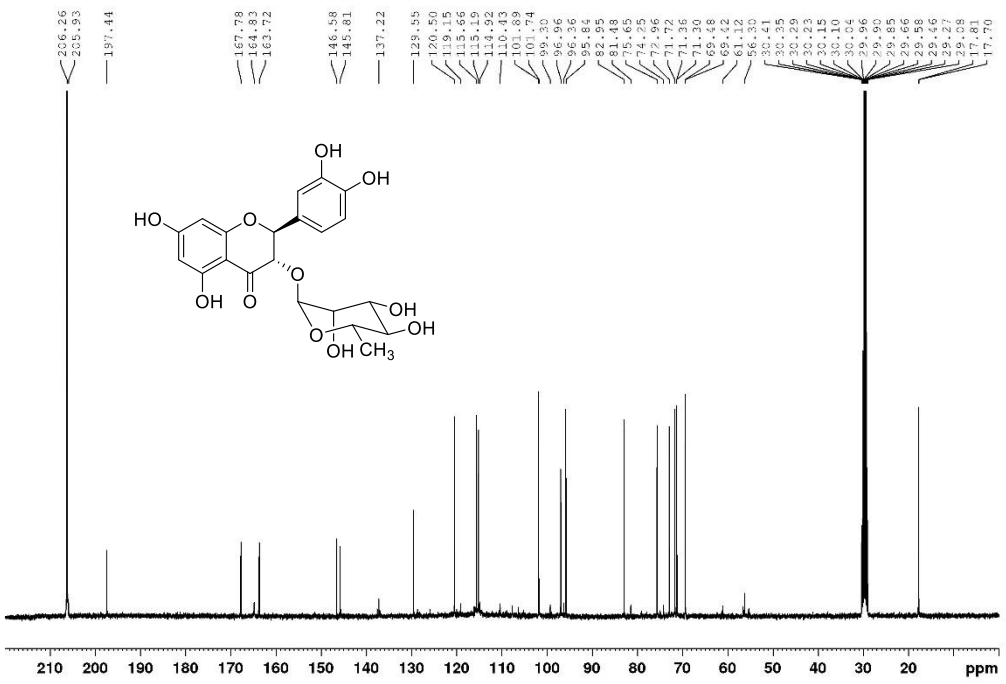

Figure A61 ^{13}C NMR spectrum (acetone-d_6, 100 MHz) of neoastilbin (**10**)

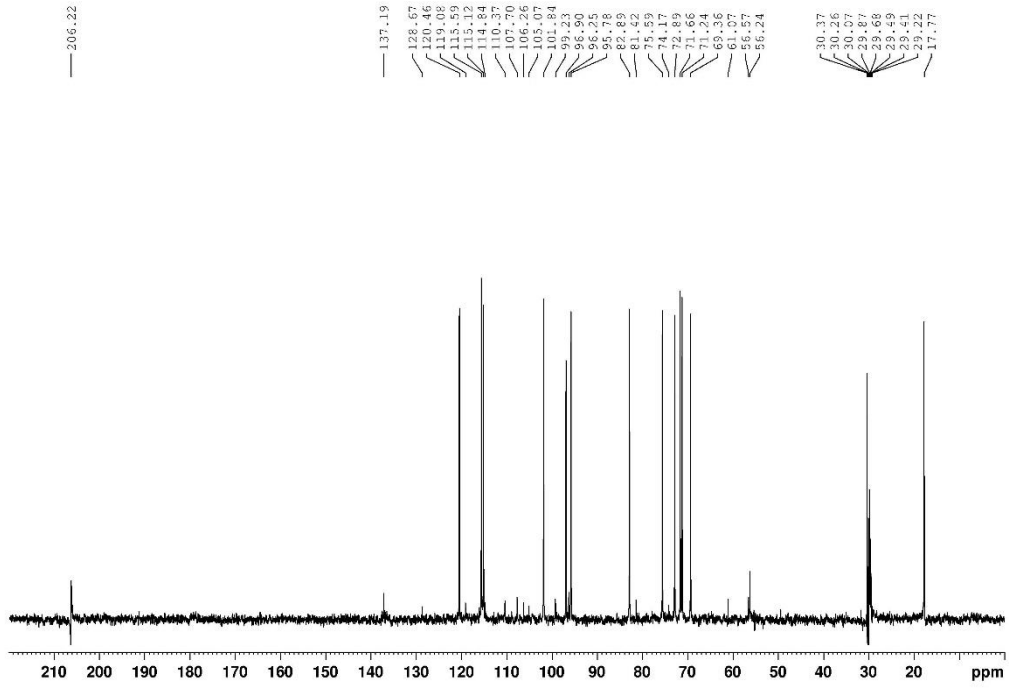

Figure A62 DEPT135 NMR spectrum (acetone-d_6, 100 MHz) of neoastilbin (**10**)

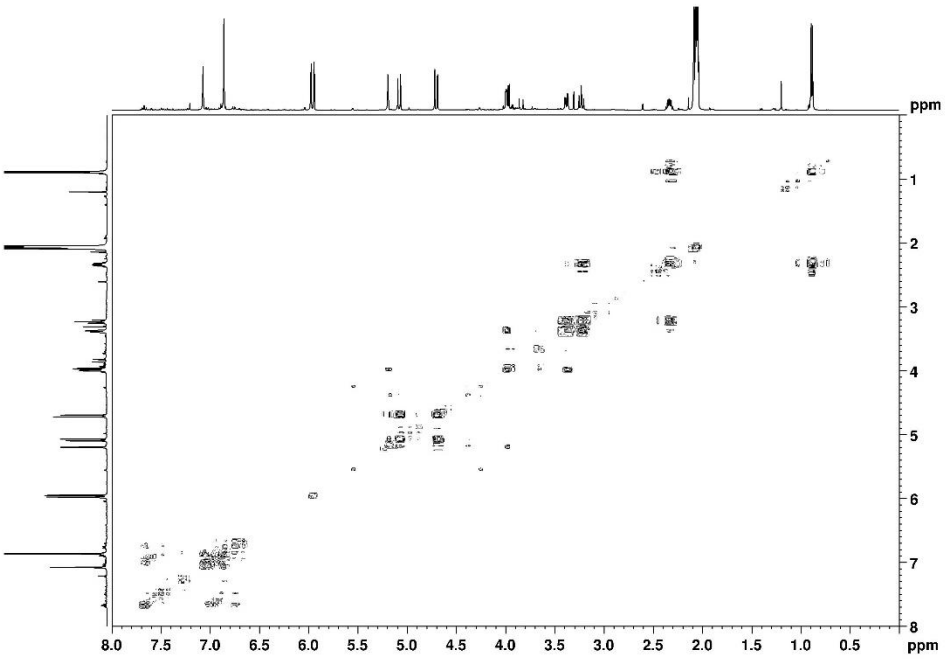

Figure A63 COSY NMR spectrum (acetone-d_6) of neoastilbin (**10**)

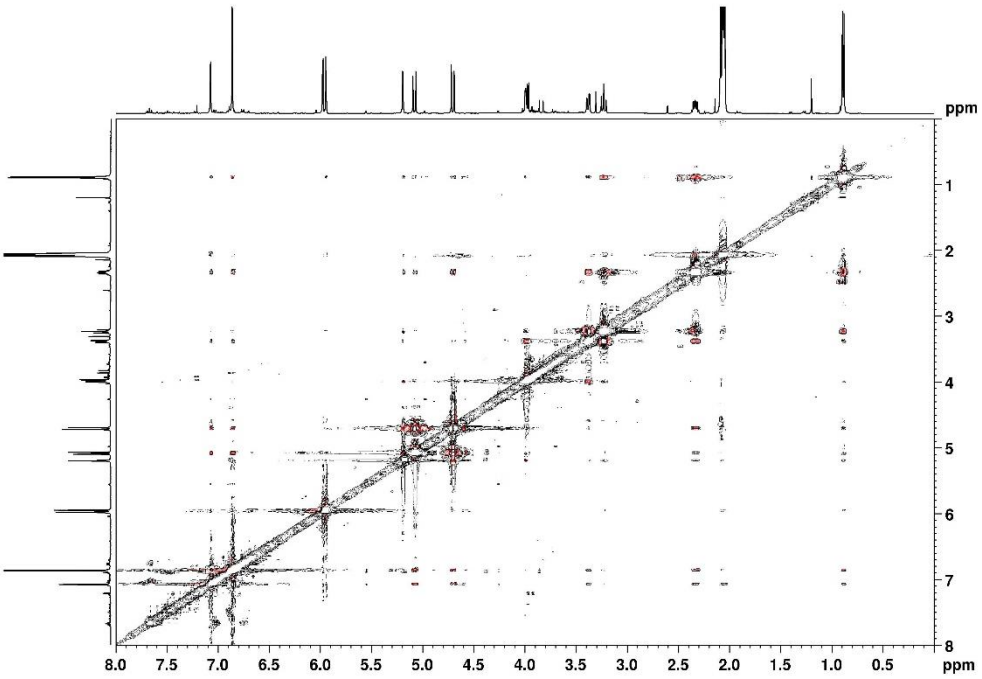

Figure A64 NOESY NMR spectrum (acetone-d_6) of neoastilbin (**10**)

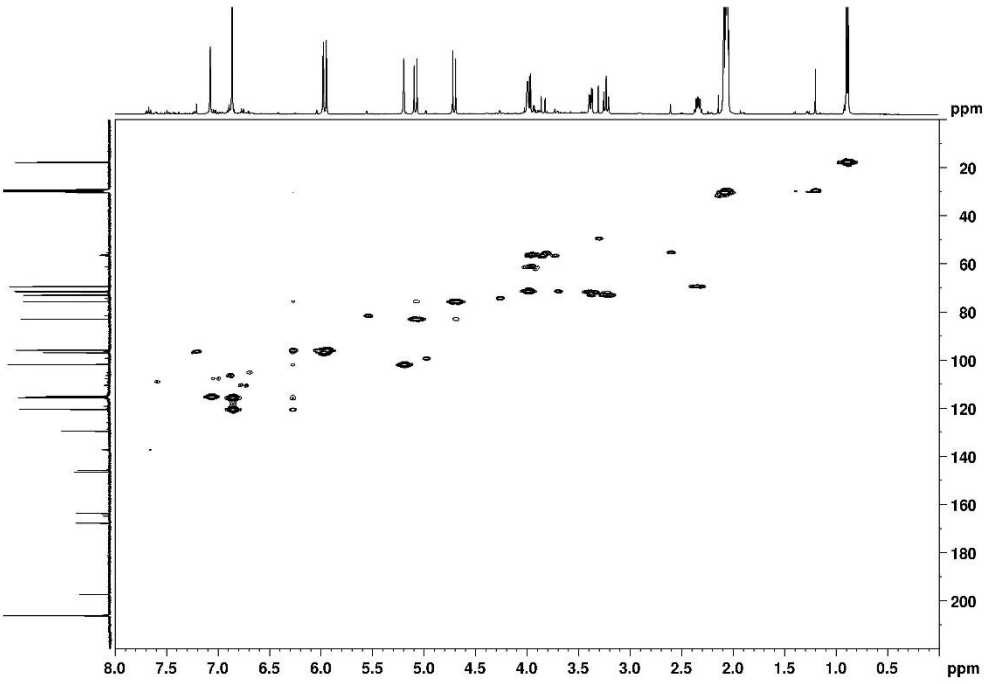

Figure A65 HMQC NMR spectrum (acetone-d_6) of neoastilbin (**10**)

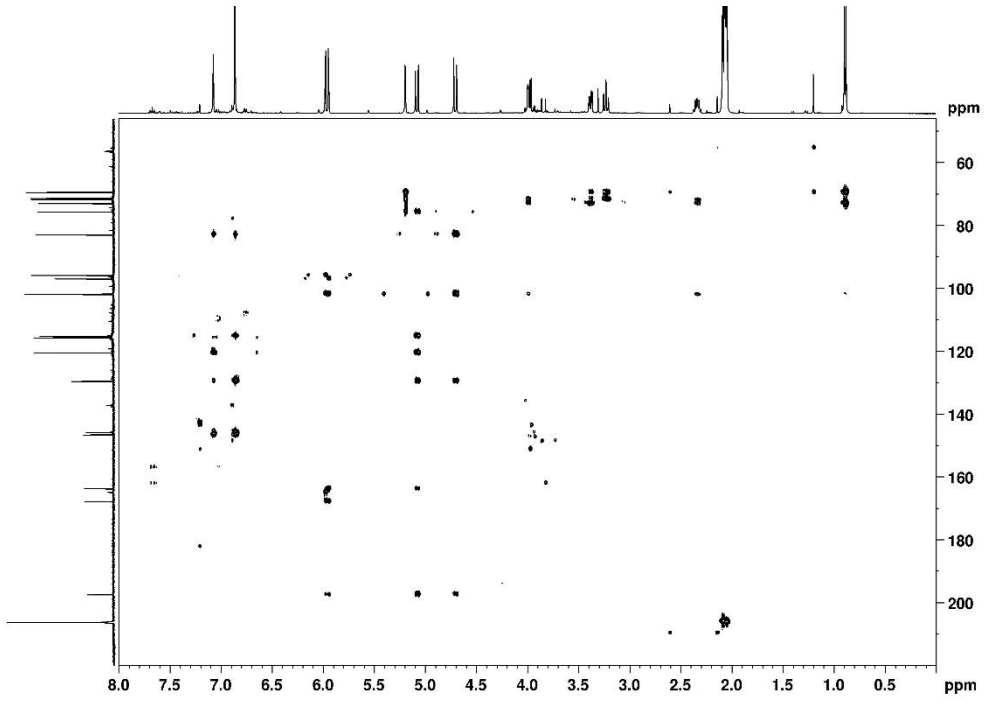

Figure A66 HMBC NMR spectrum (acetone-d_6) of neoastilbin (**10**)

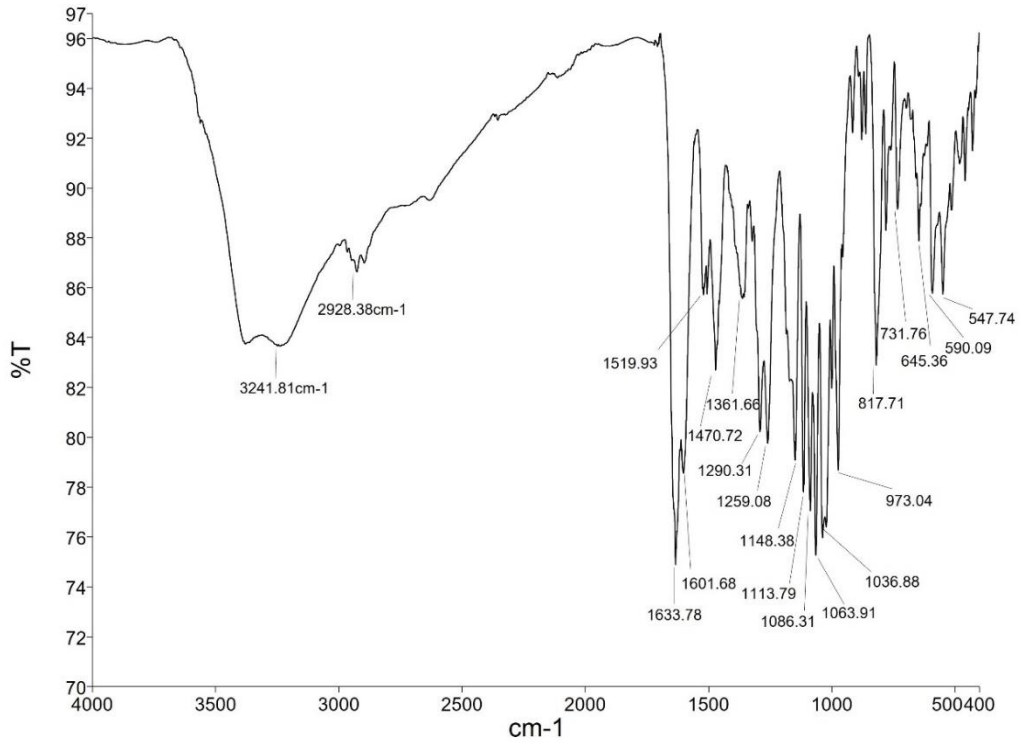

Figure A67 IR (ATR) spectrum of neoastilbin (**10**)

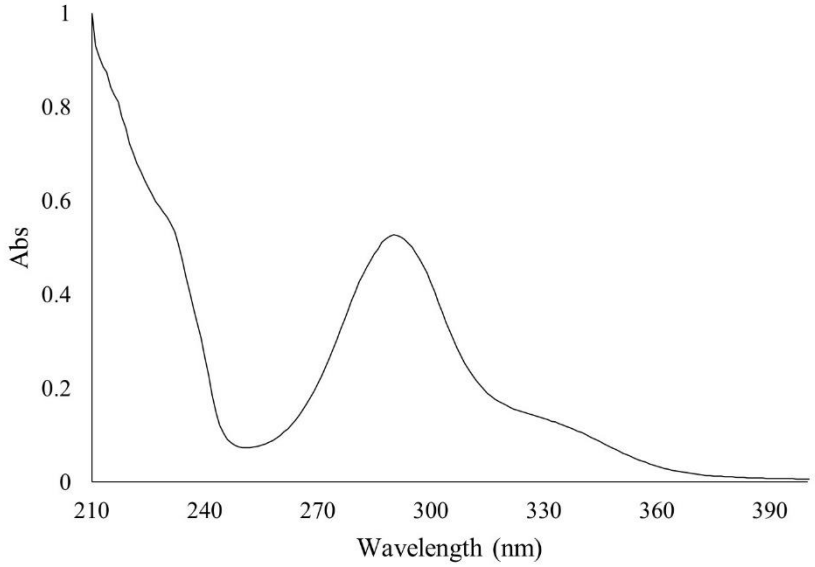

Figure A68 UV (MeOH) spectrum of neoastilbin (**10**)

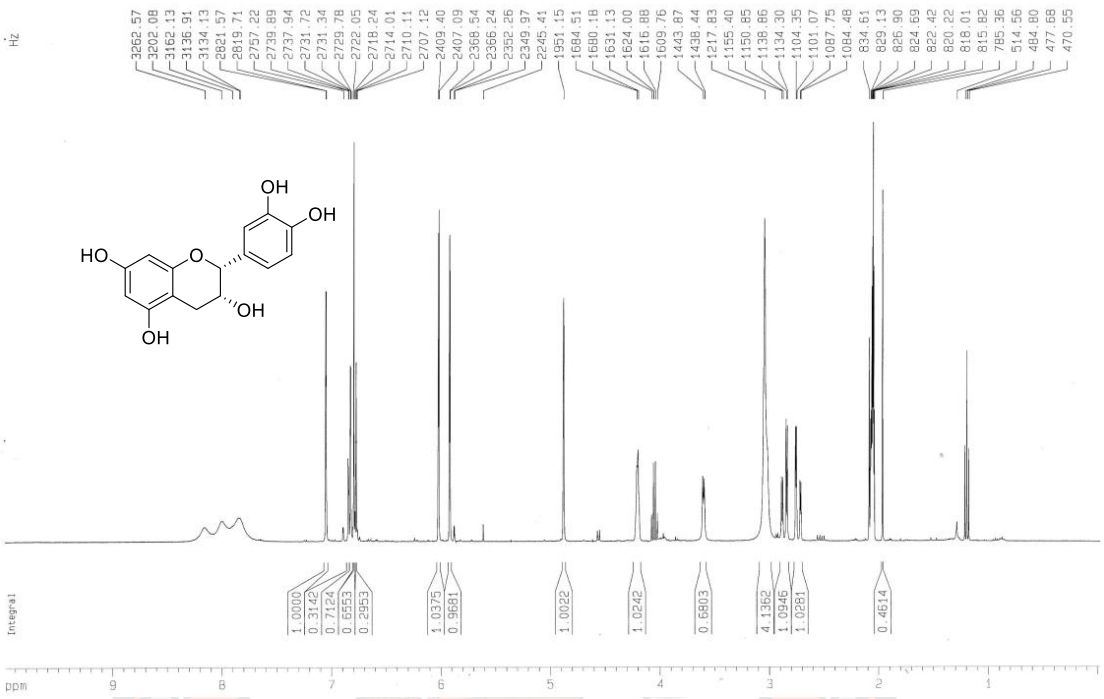

Figure A69 ^{1}H NMR spectrum (acetone-d_6, 400 MHz) of epicatechin (**11**)

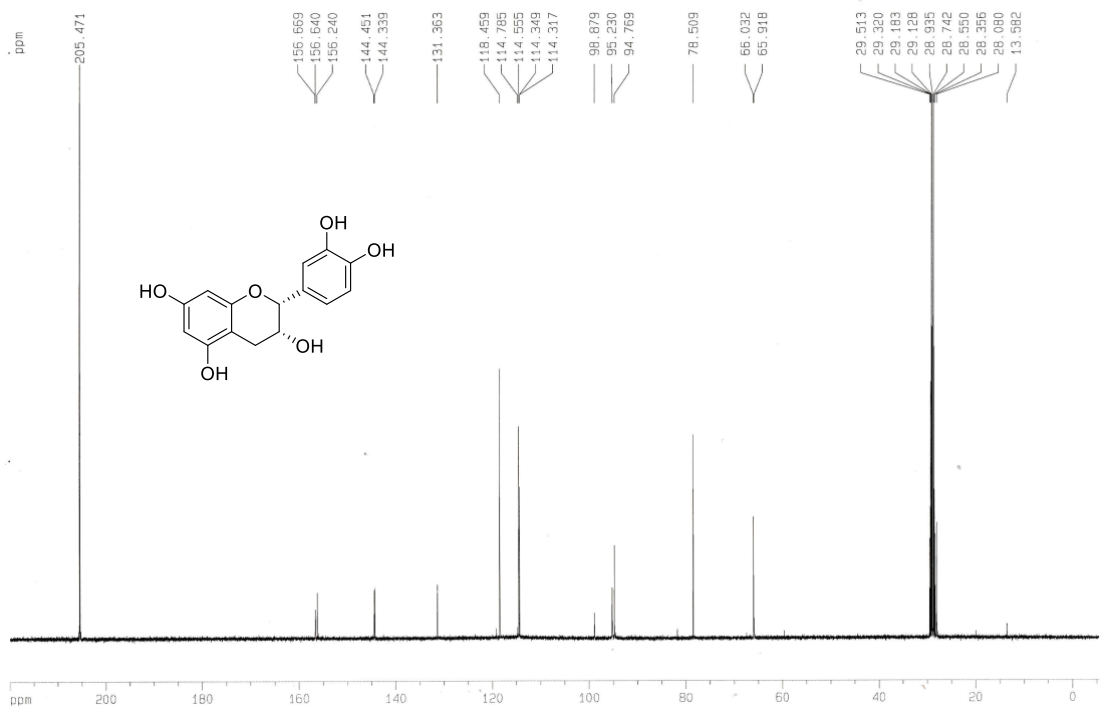

Figure A70 ^{13}C NMR spectrum (acetone-d_6, 100 MHz) of epicatechin (**11**)

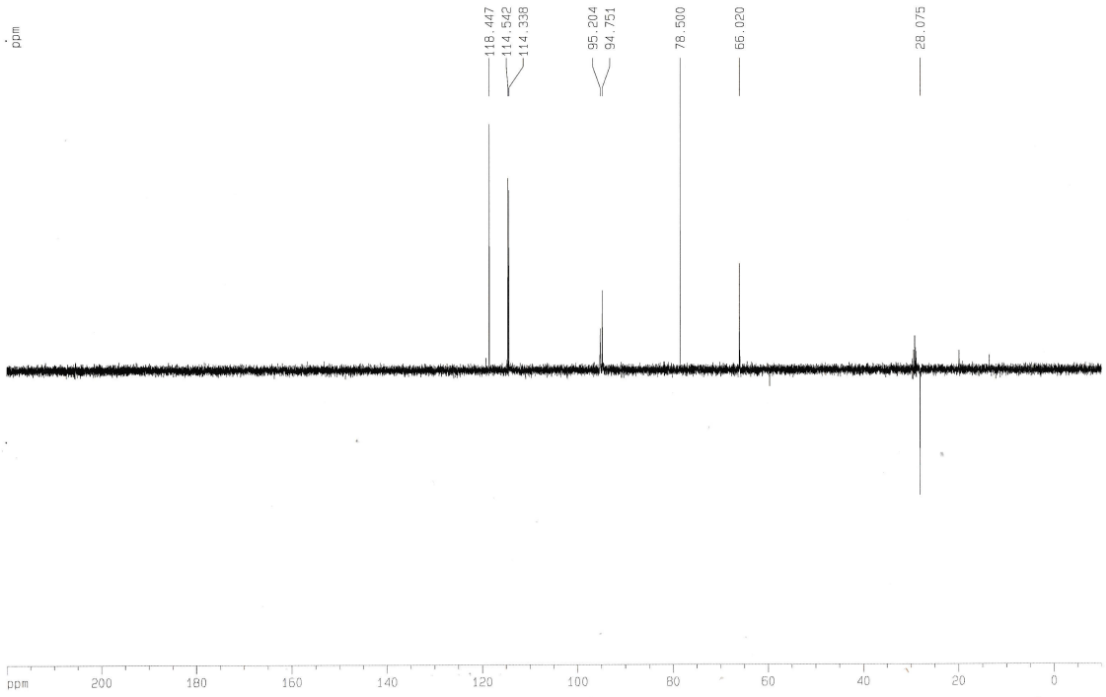

Figure A71 DEPT135 NMR spectrum (acetone-d_6, 100 MHz) of epicatechin (**11**)

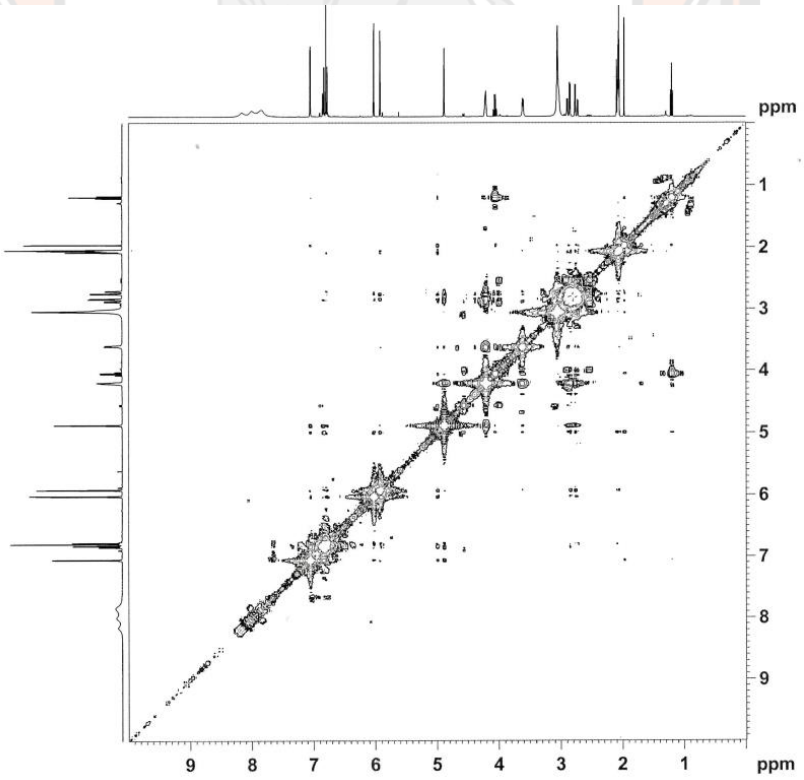

Figure A72 COSY NMR spectrum (acetone-d_6) of epicatechin (**11**)

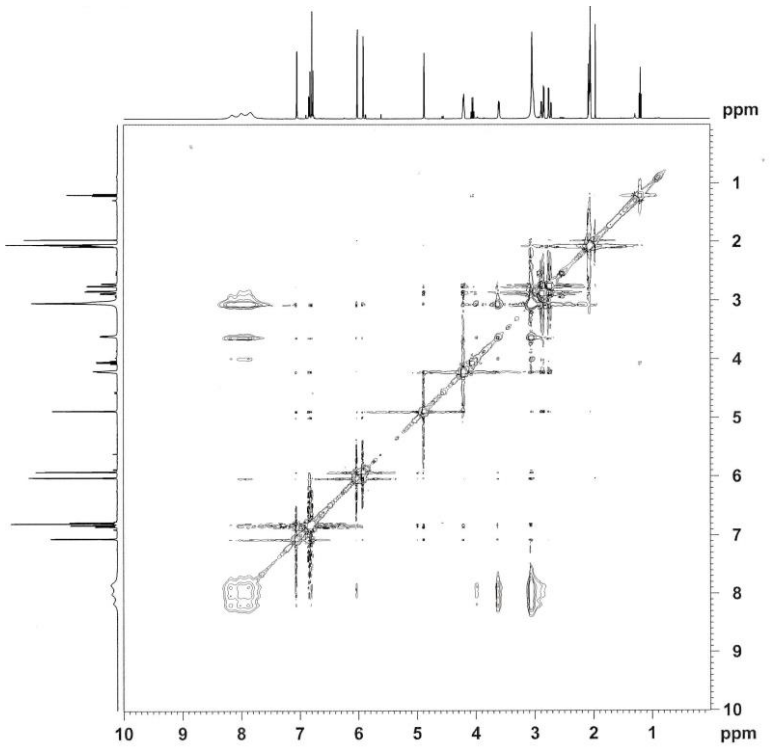

Figure A73 NOESY NMR spectrum (acetone-d_6) of epicatechin (**11**)

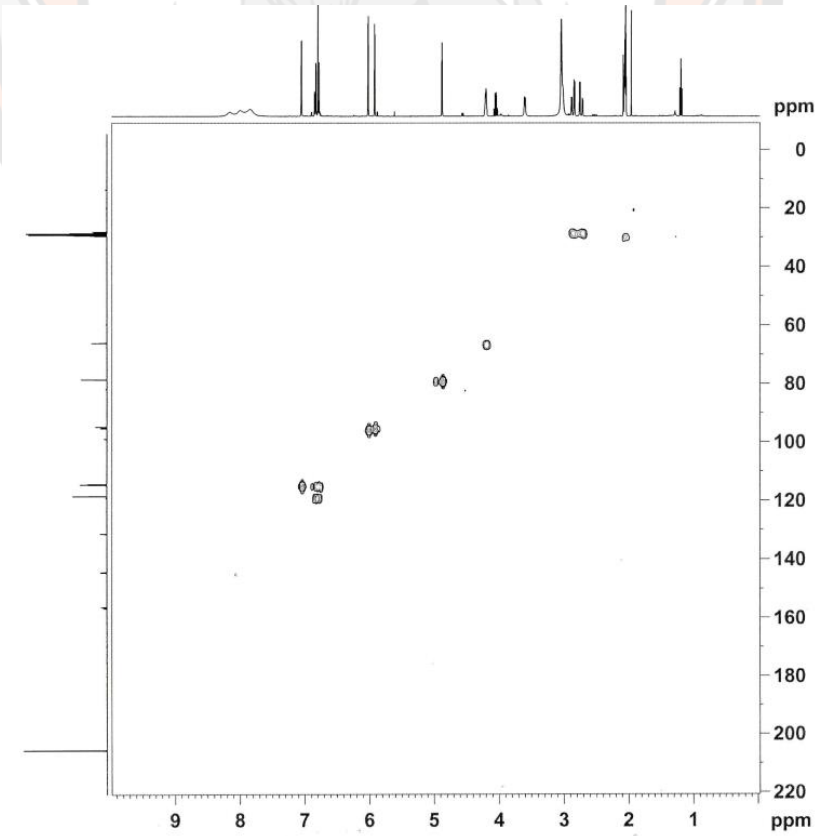

Figure A74 HMQC NMR spectrum (acetone-d_6) of epicatechin (**11**)

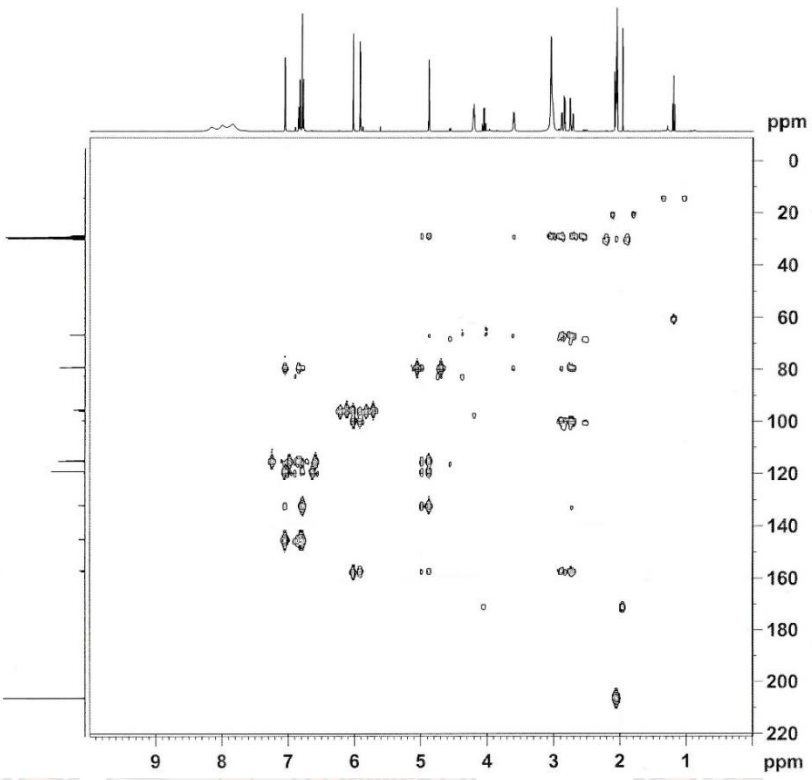

Figure A75 HMBC spectrum (acetone-d_6) of epicatechin (**11**)

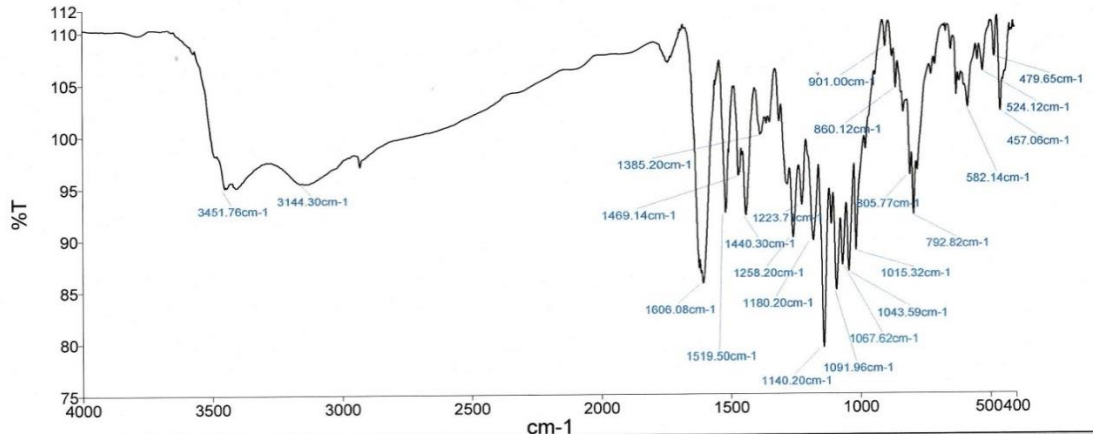

Figure A76 IR (ATR) spectrum of epicatechin (**11**)

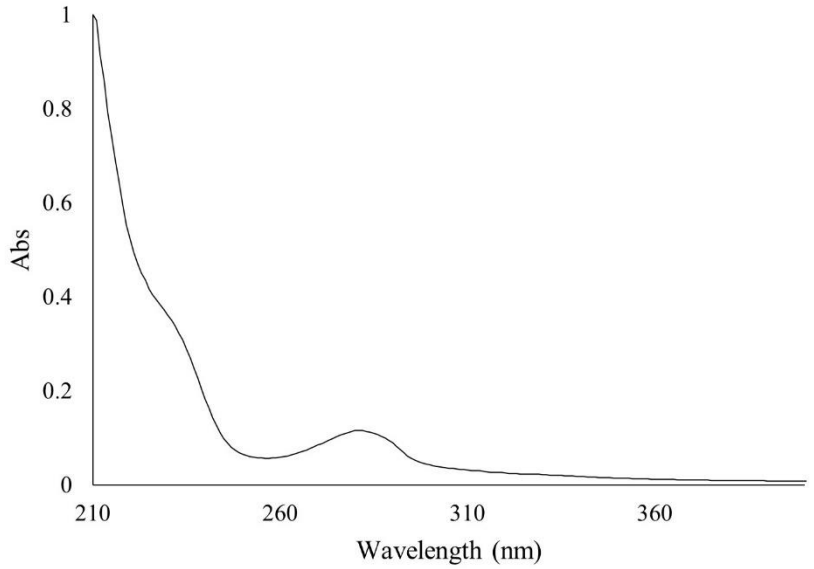

Figure A77 UV (MeOH) spectrum of epicatechin (**11**)

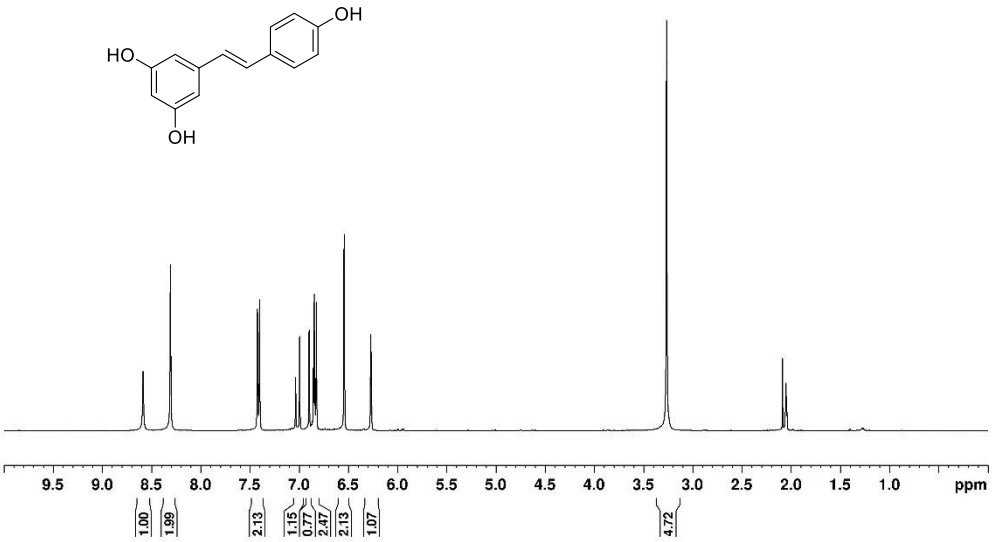

Figure A78 ^{1}H NMR spectrum (acetone-d_6, 400 MHz) of resveratrol (**12**)

Figure A79 DEPTQ NMR spectrum (acetone-d_6, 100 MHz) of resveratrol (**12**)

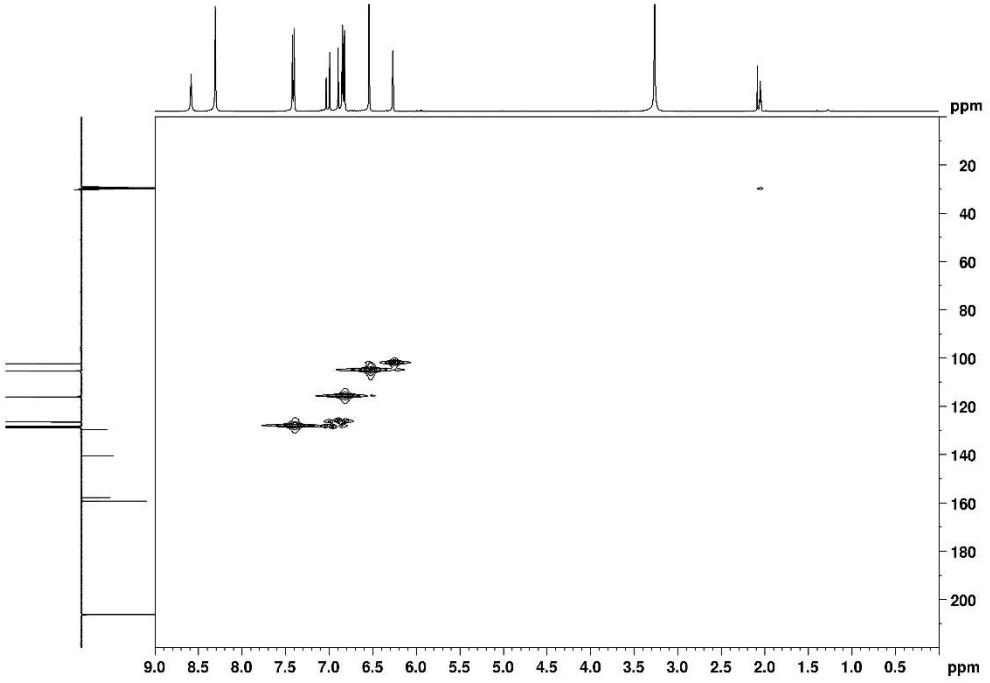

Figure A80 HMQC NMR spectrum (acetone-d_6) of resveratrol (**12**)

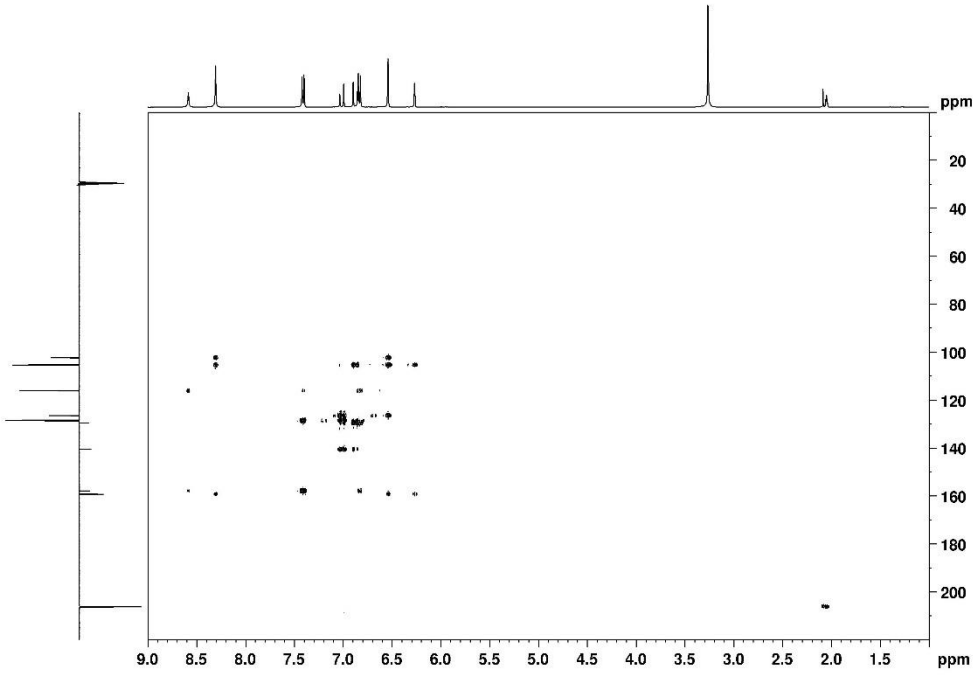

Figure A81 HMBC NMR spectrum (acetone-d_6) of resveratrol (**12**)

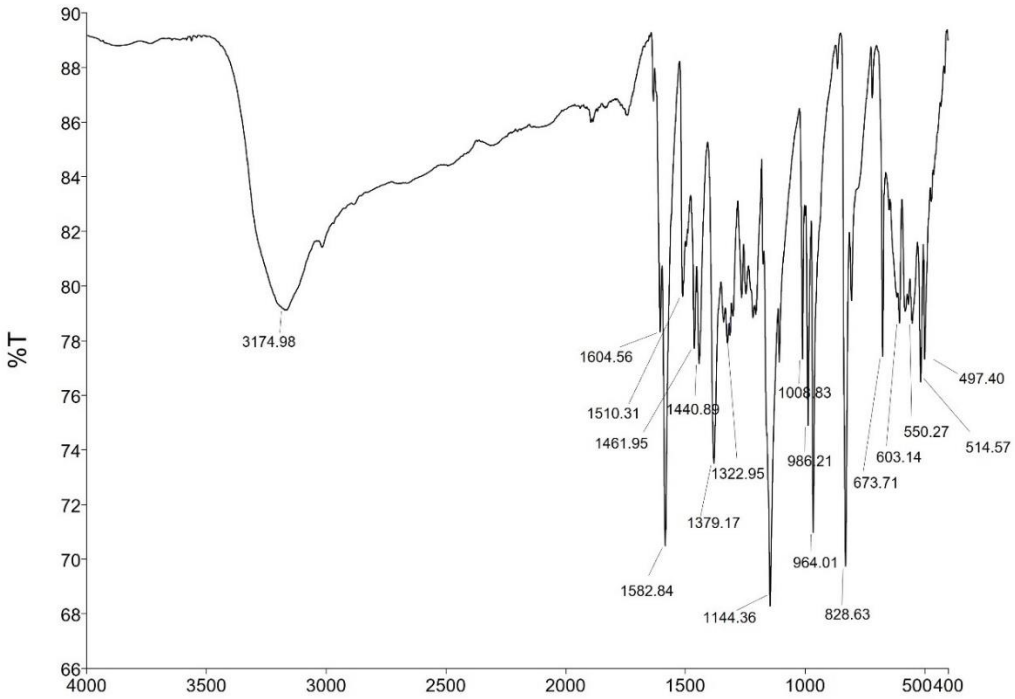

Figure A82 IR (ATR) spectrum of resveratrol (**12**)

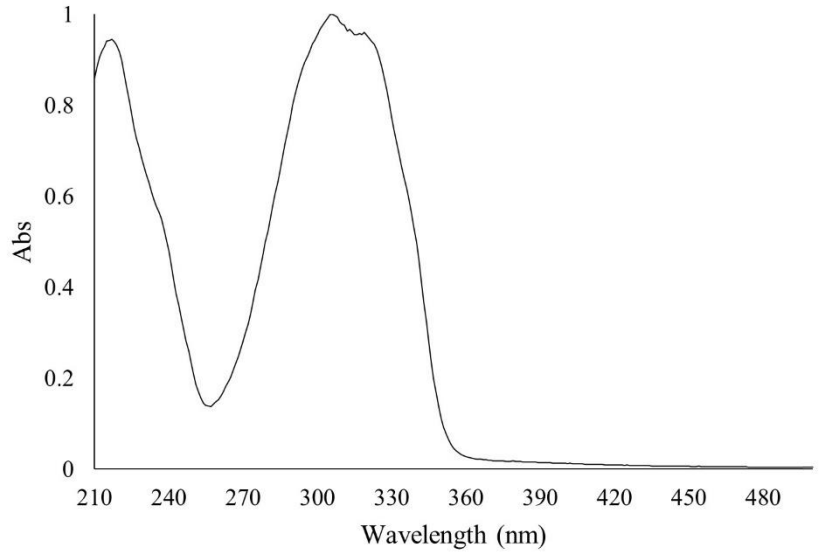

Figure A83 UV (MeOH) spectrum of resveratrol (**12**)

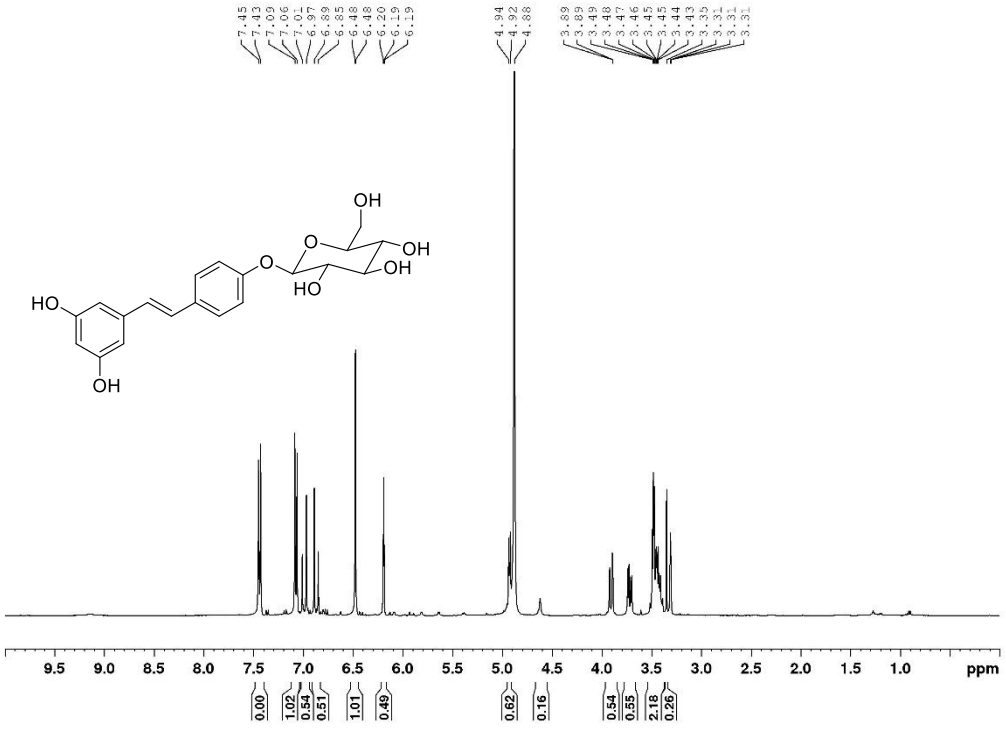

Figure A84 ^{1}H NMR spectrum (acetone-d_6, 400 MHz) of resveratrol 4'-*O*-*β*-D-glucoside (**13**)

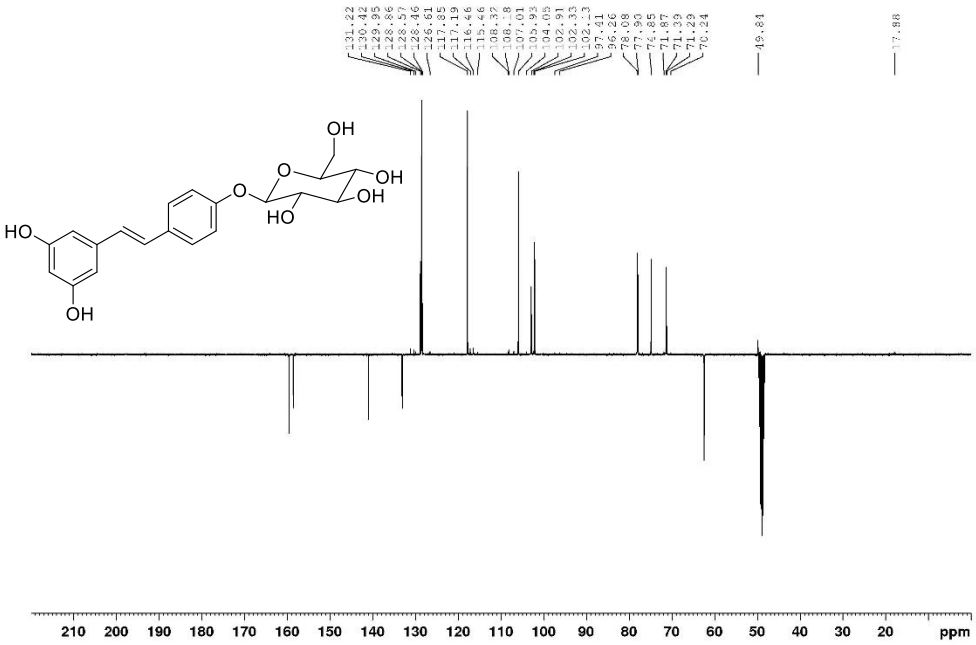

Figure A85 DEPTQ NMR spectrum (acetone-d_6, 100 MHz) of resveratrol 4'-*O*-β-D-glucoside (**13**)

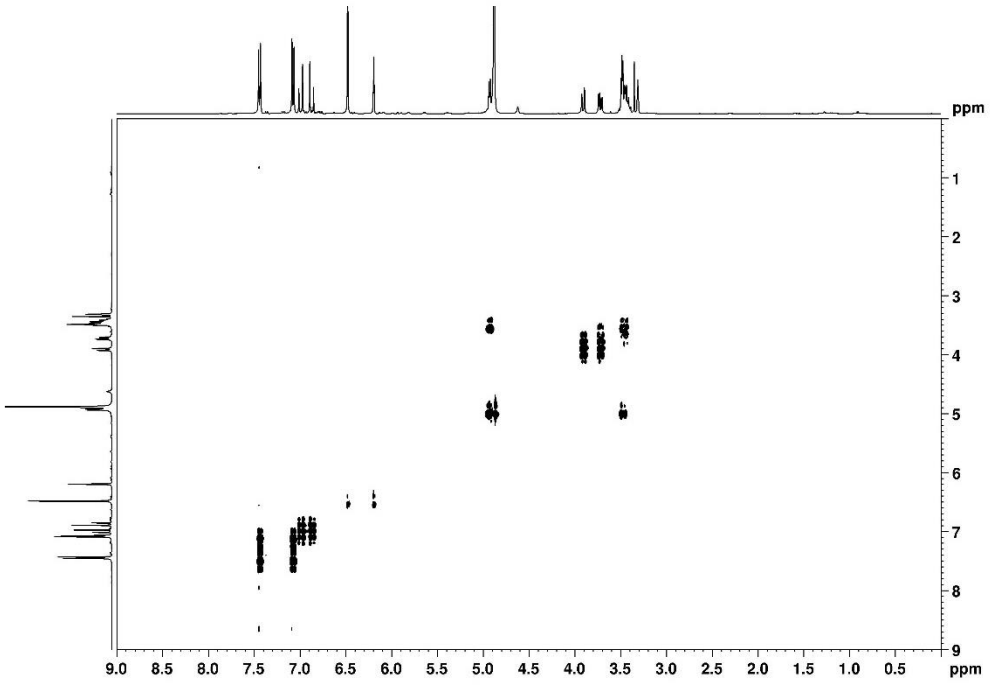

Figure A86 COSY NMR spectrum (acetone-d_6) of resveratrol 4'-*O*-β-D-glucoside (**13**)

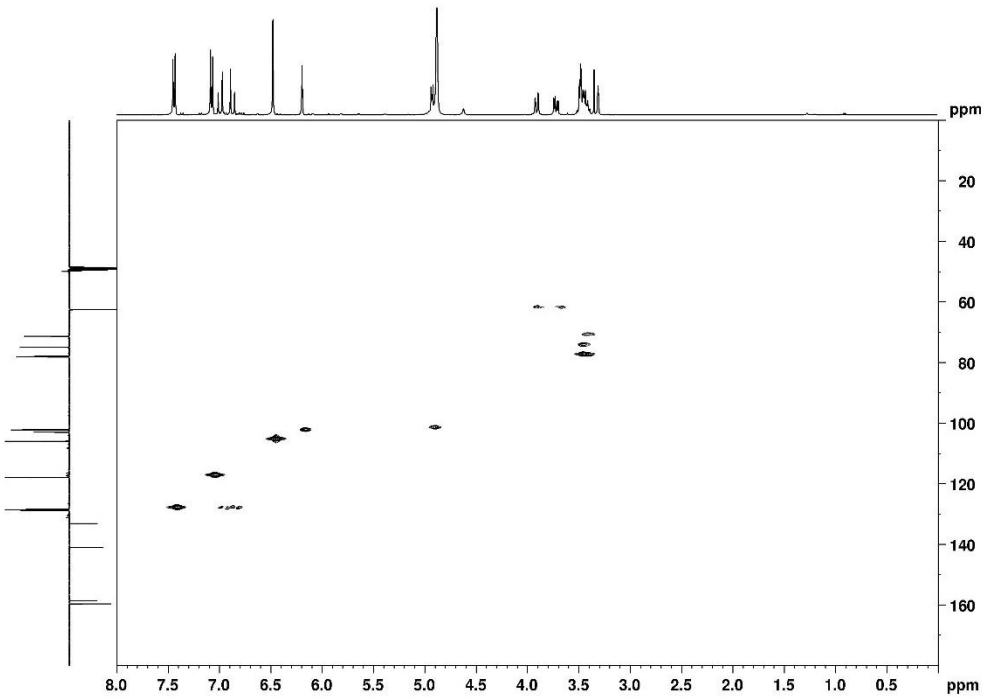

Figure A87 HMQC NMR spectrum (acetone-d_6) of resveratrol 4'-*O*-β-D-glucoside (**13**)

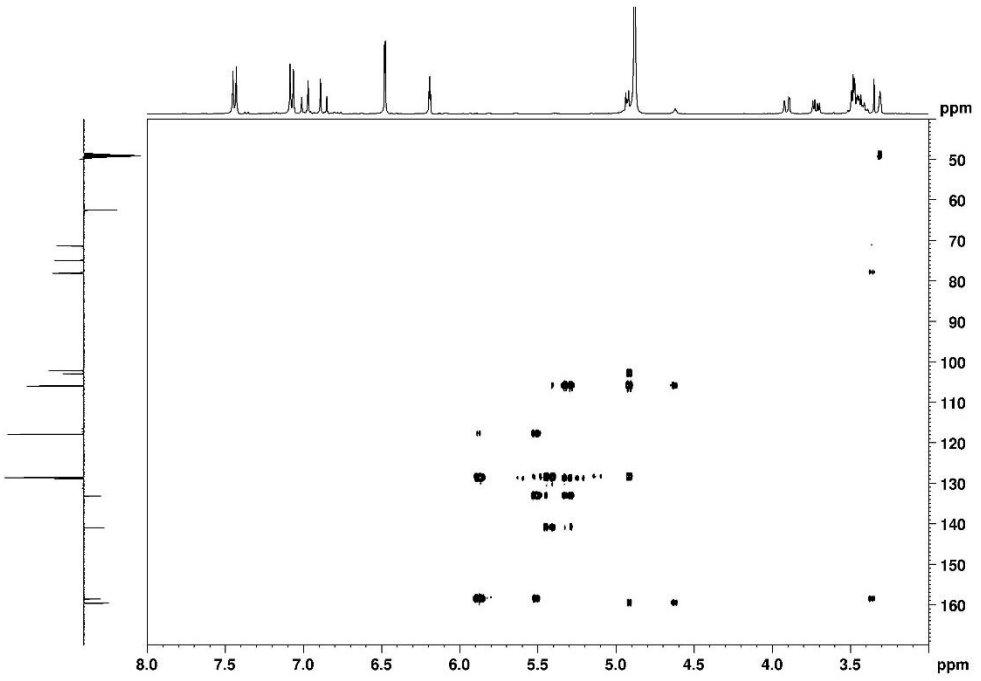

Figure A88 HMBC NMR spectrum (acetone-d_6) of resveratrol 4'-*O*-β-D-glucoside (**13**)

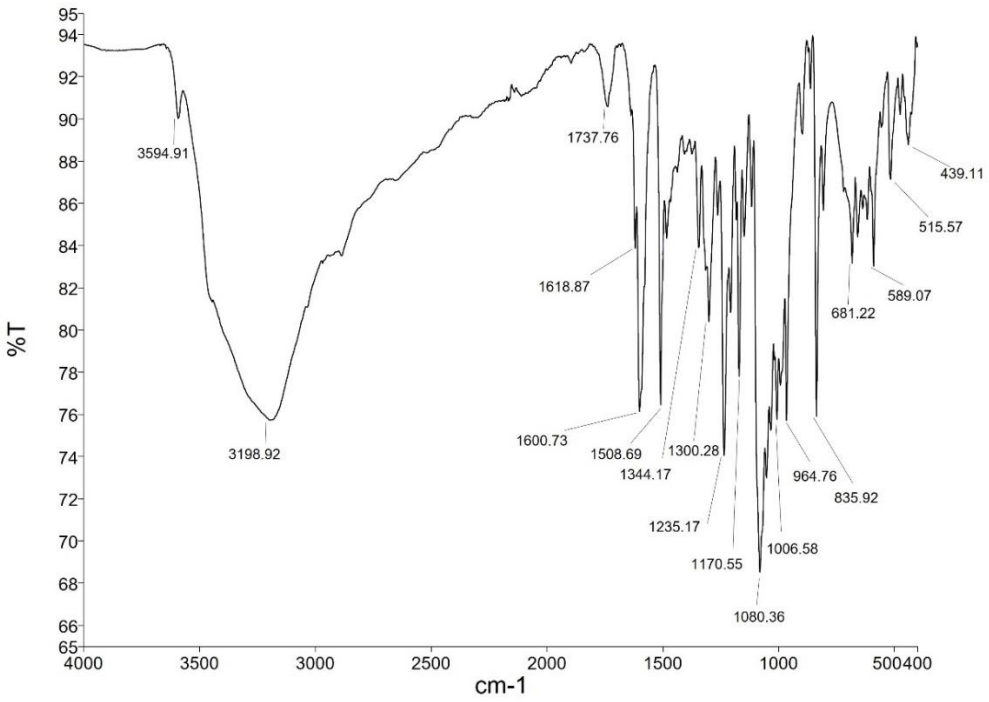

Figure A89 IR (ATR) spectrum of resveratrol 4'-*O*-*β*-D-glucoside (**13**)

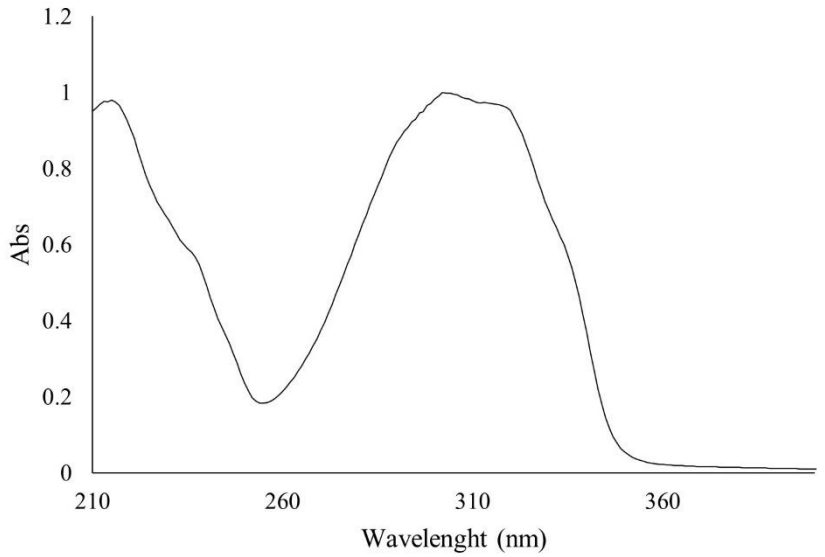

Figure A90 UV (MeOH) spectrum of resveratrol 4'-*O*-*β*-D-glucoside (**13**)

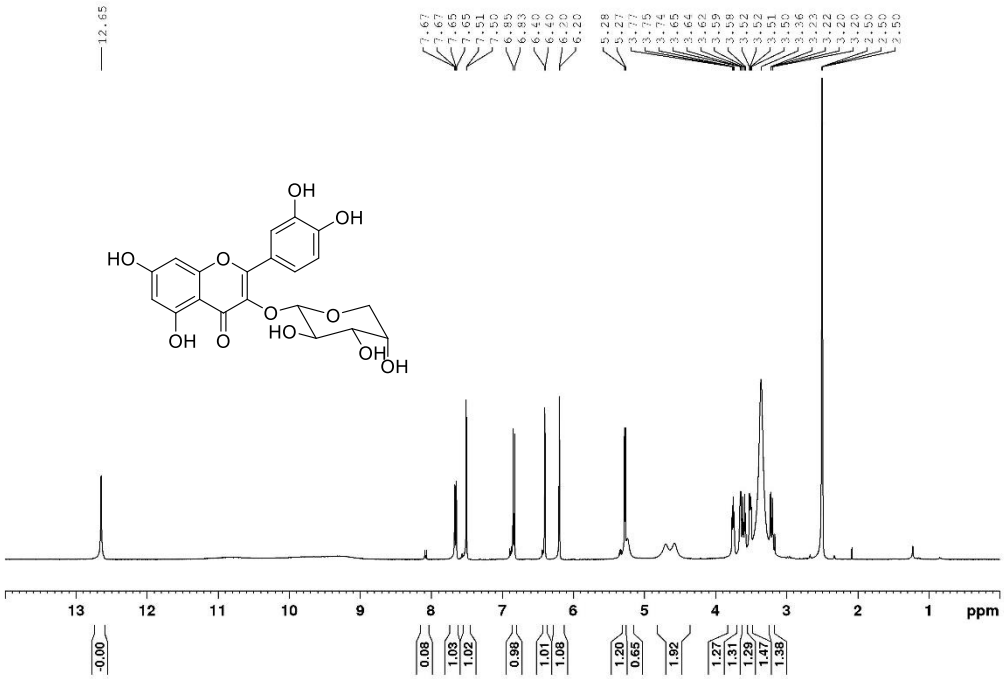

Figure A91 ^{1}H NMR spectrum (DMSO-d_6, 400 MHz) of quercetin 3-*O*-β-D-arabinoside (**14**)

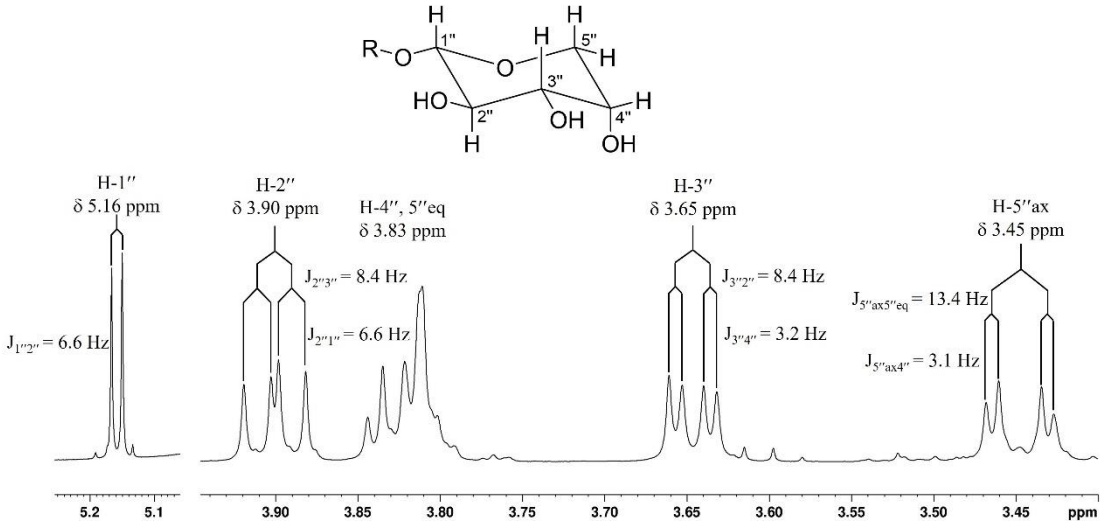

Figure A92 ^{1}H NMR spectrum (acetone-d_6, 400 MHz) of arabinoside from quercetin 3-*O*-β-D-arabinoside (**14**)

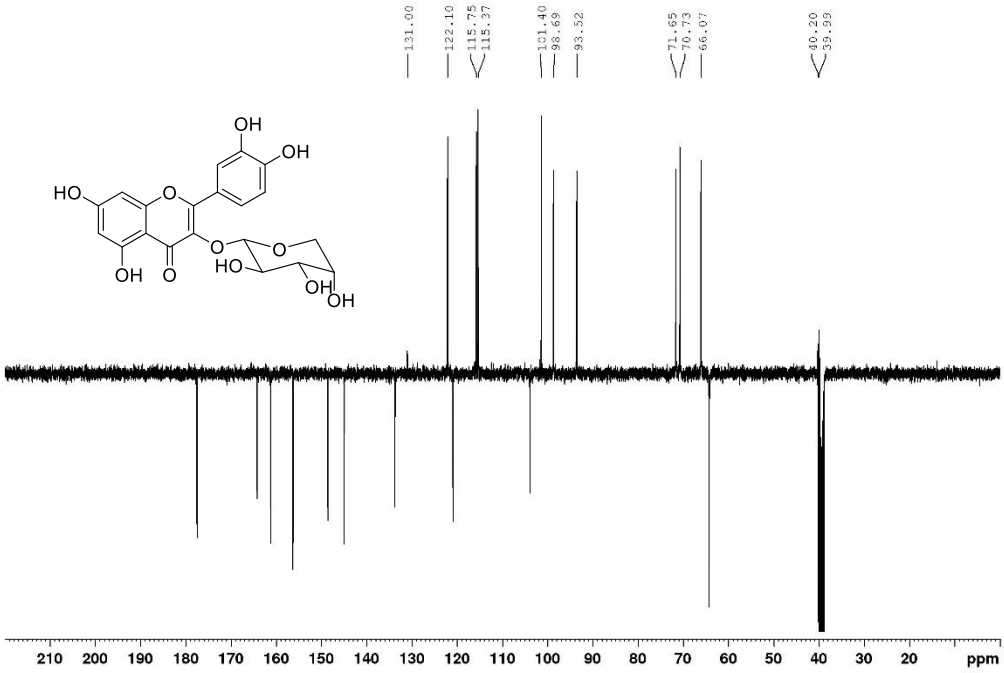

Figure A93 DEPTQ NMR spectrum (DMSO-d_6, 100 MHz) of quercetin 3-*O*-β-D-xyloside (**14**)

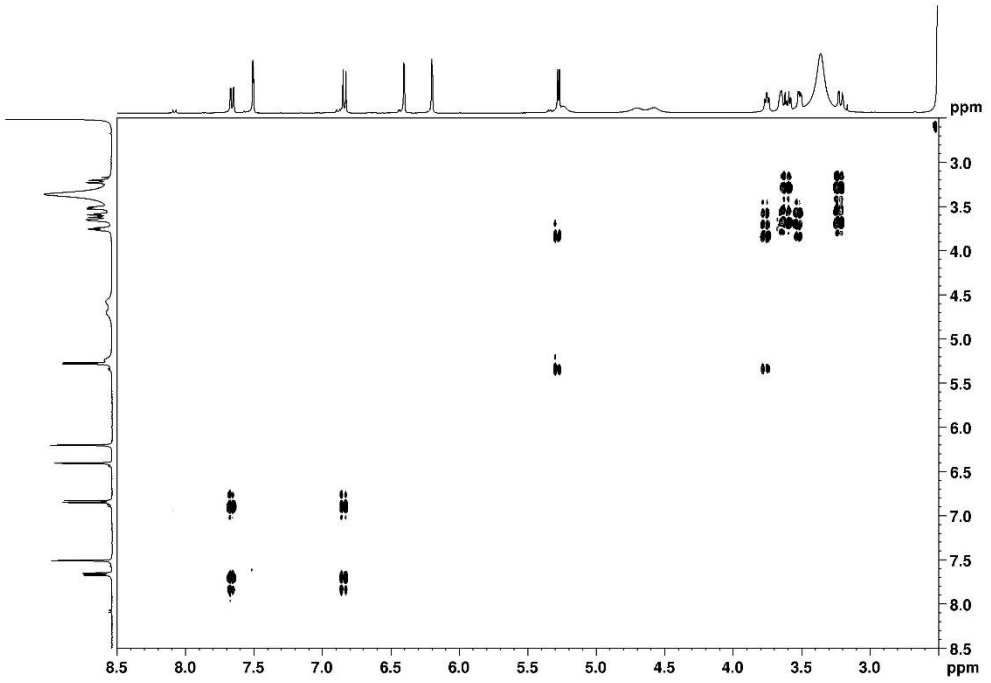

Figure A94 COSY NMR spectrum (DMSO-d_6) of quercetin 3-*O*-β-D-xyloside (**14**)

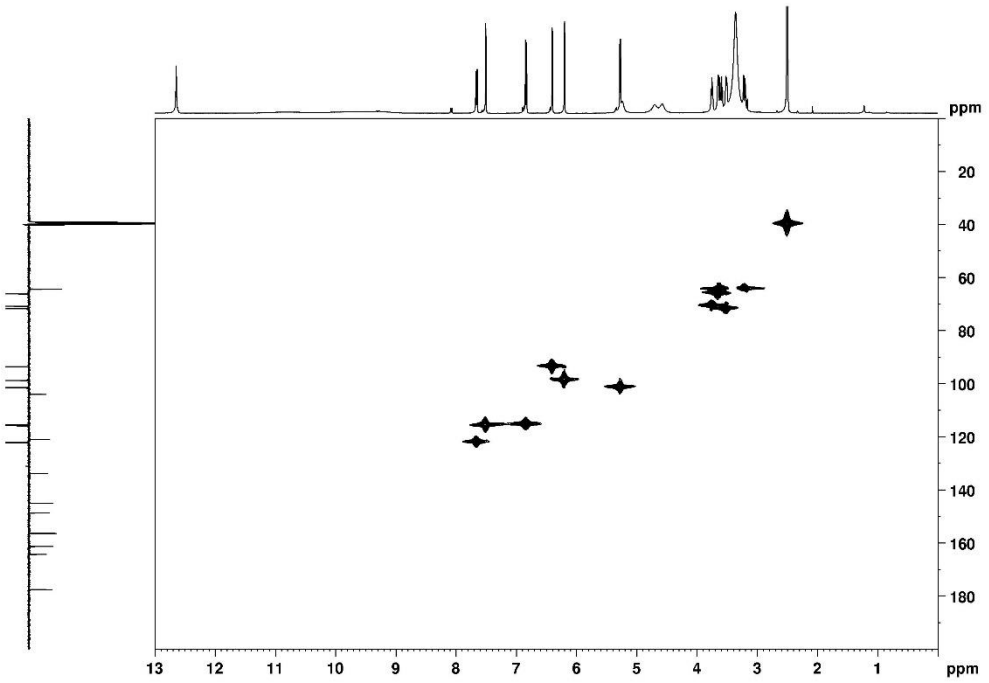

Figure A95 HMQC NMR spectrum (DMSO-d_6) of quercetin 3-*O*-β-D-xyloside (**14**)

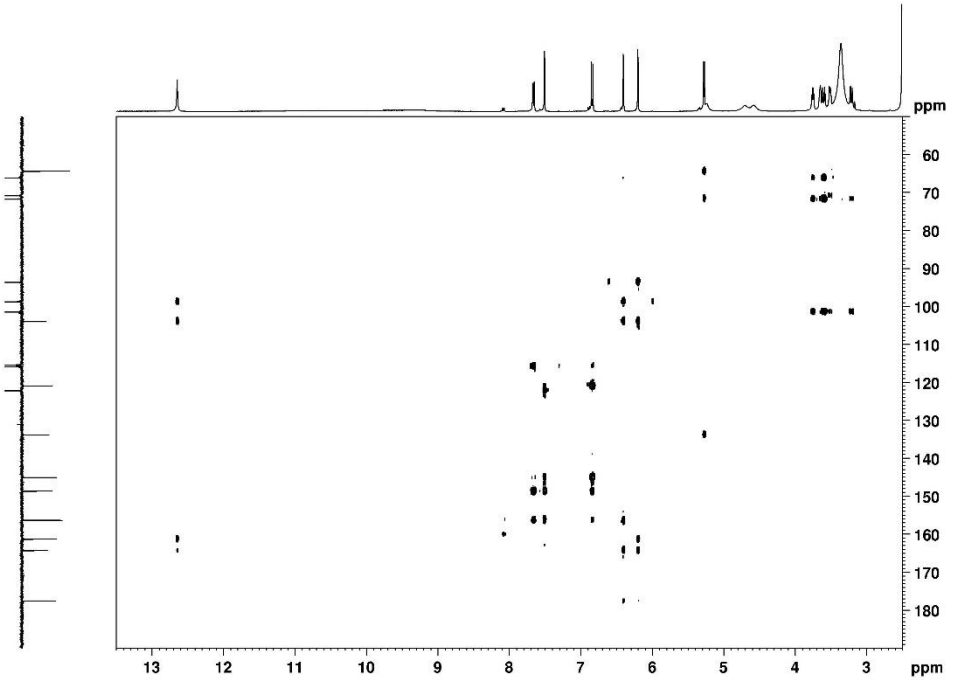

Figure A96 HMBC NMR spectrum (DMSO-d_6) of quercetin 3-*O*-β-D-xyloside (**14**)

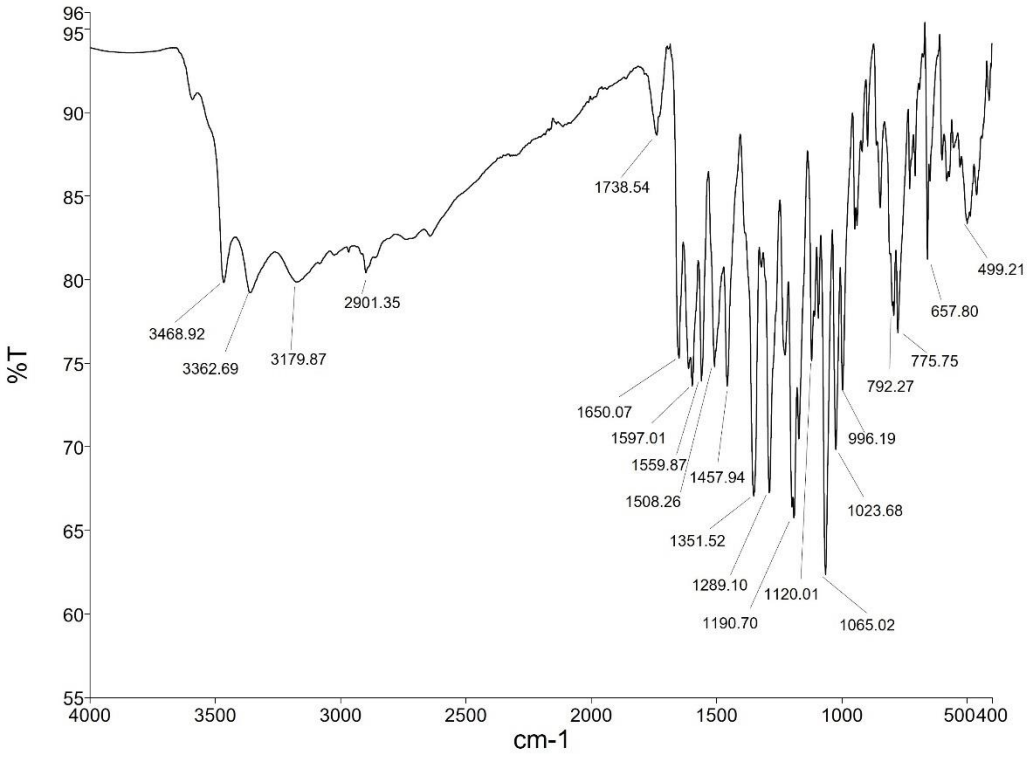

Figure A97 IR (ATR) spectrum of quercetin quercetin 3-*O*-*β*-D-xyloside (**14**)

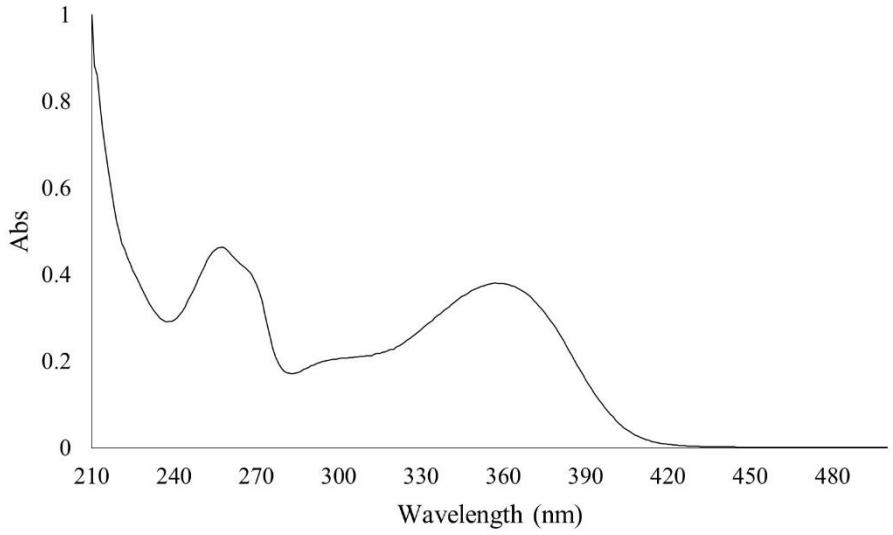

Figure A98 UV (MeOH) spectrum of quercetin 3-*O*-*β*-D-xyloside (**14**)

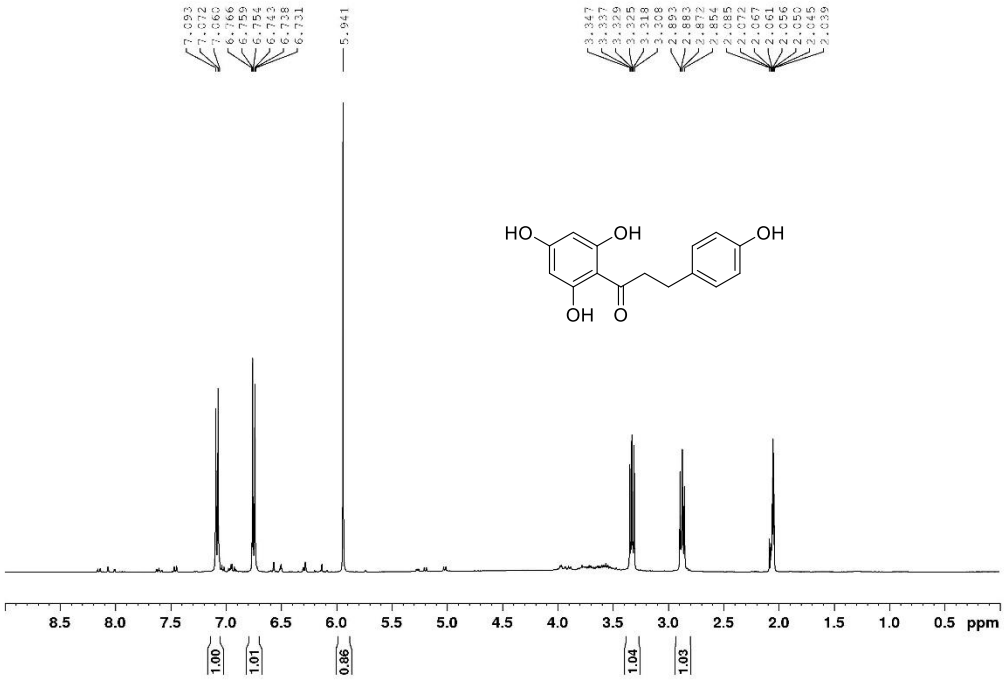

Figure A99 ^{1}H NMR spectrum (acetone-d_6, 400 MHz) of phloretin (**15**)

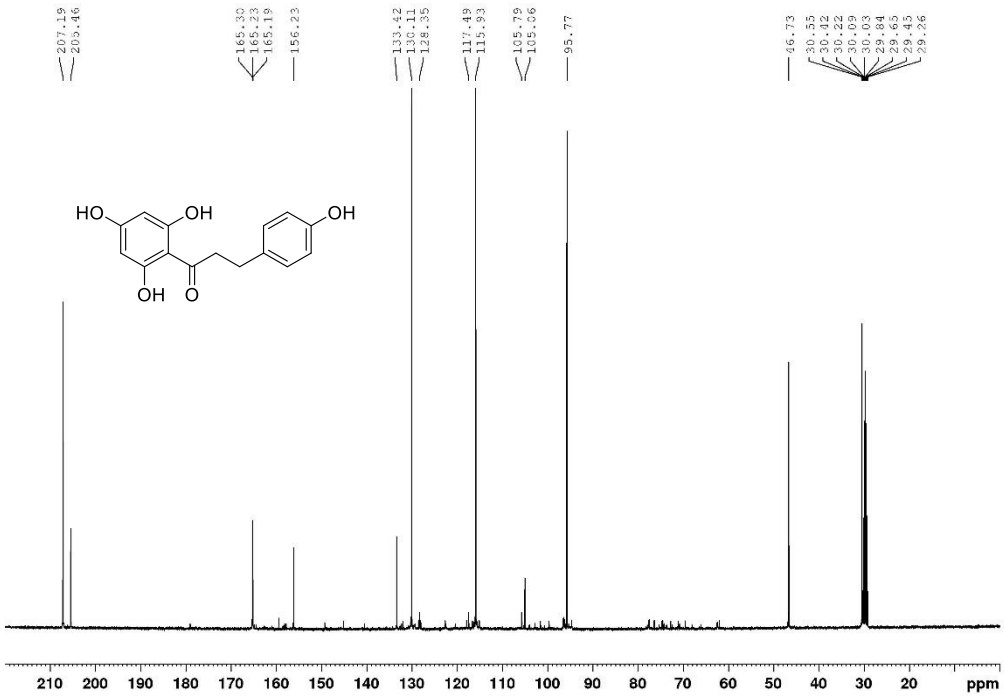

Figure A100 ^{13}C NMR spectrum (acetone-d_6, 100 MHz) of phloretin (**15**)

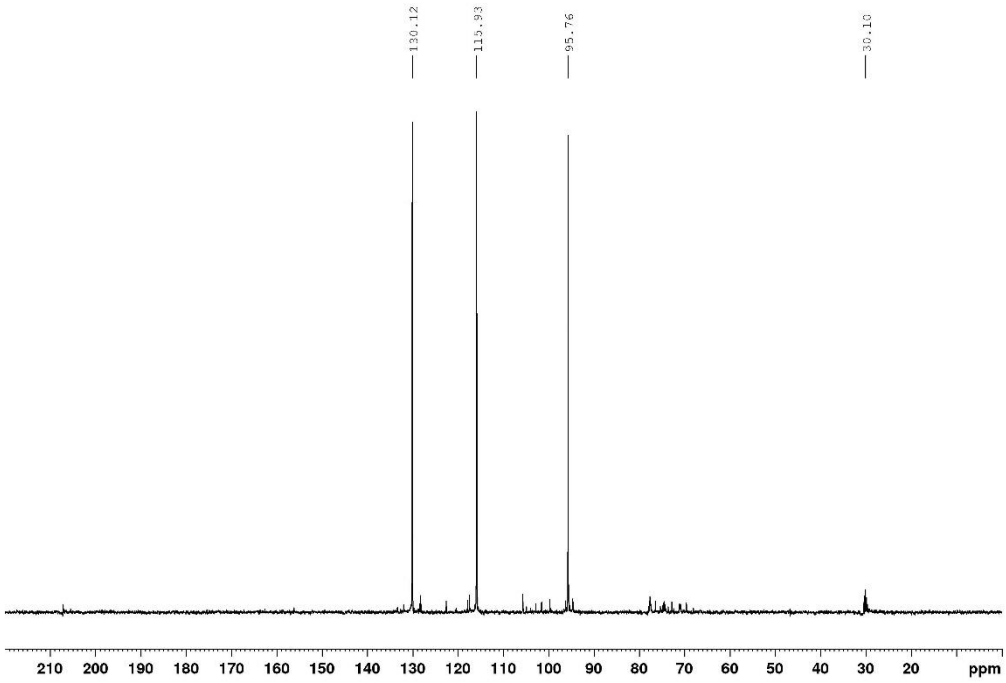

Figure A101 DEPT135 NMR spectrum (acetone-d_6, 100 MHz) of phloretin (**15**)

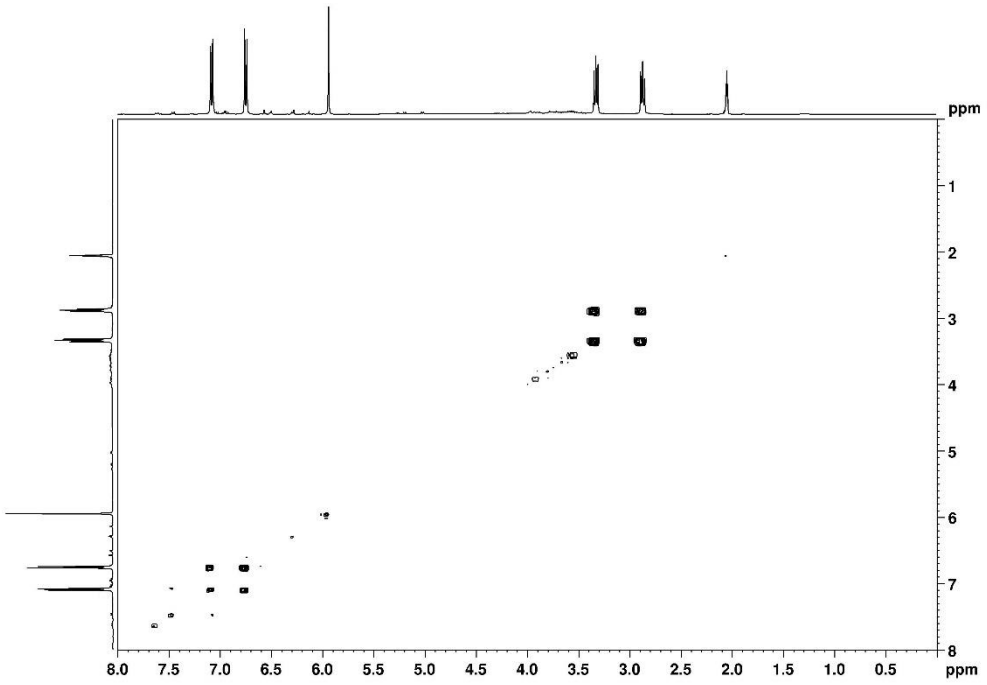

Figure A102 COSY NMR spectrum (acetone-d_6) of phloretin (**15**)

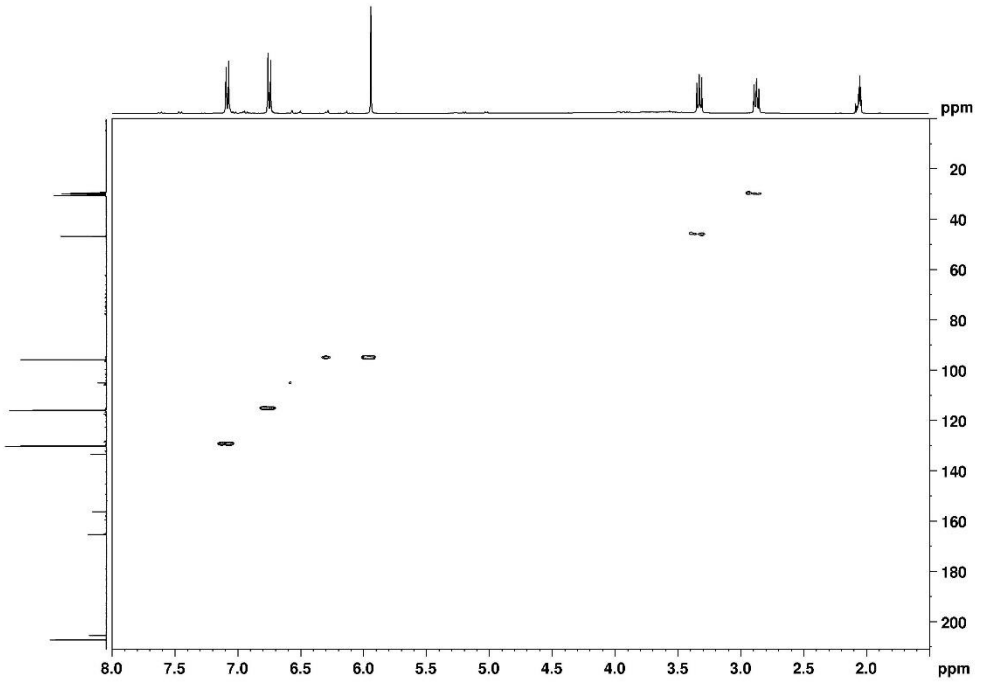

Figure A103 HMQC NMR spectrum (acetone-d_6) of phloretin (**15**)

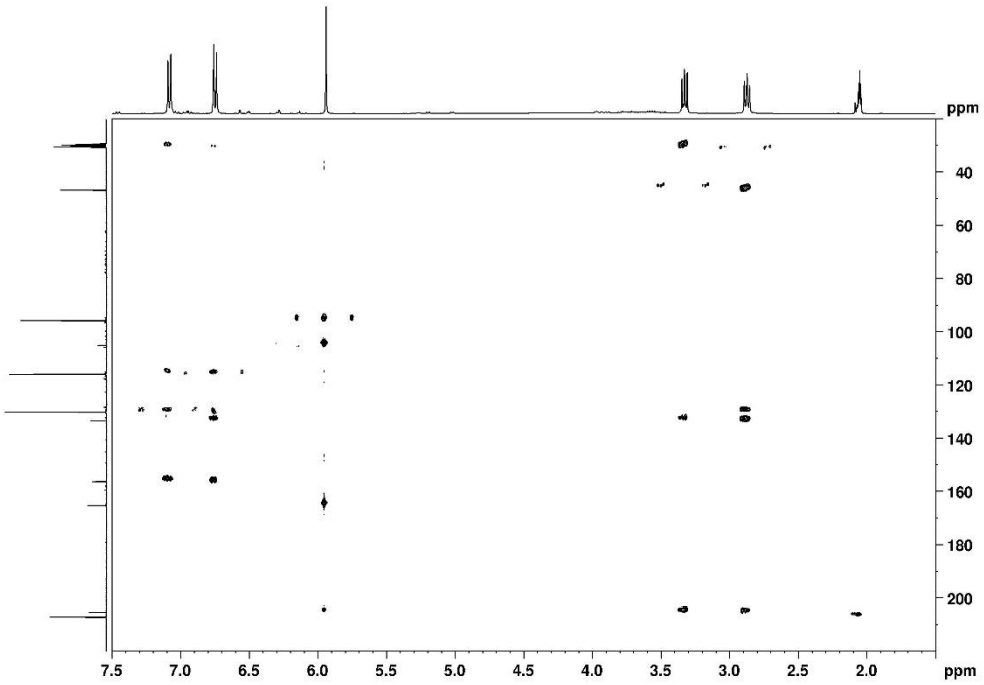

Figure A104 HMBC NMR spectrum (acetone-d_6) of phloretin (**15**)

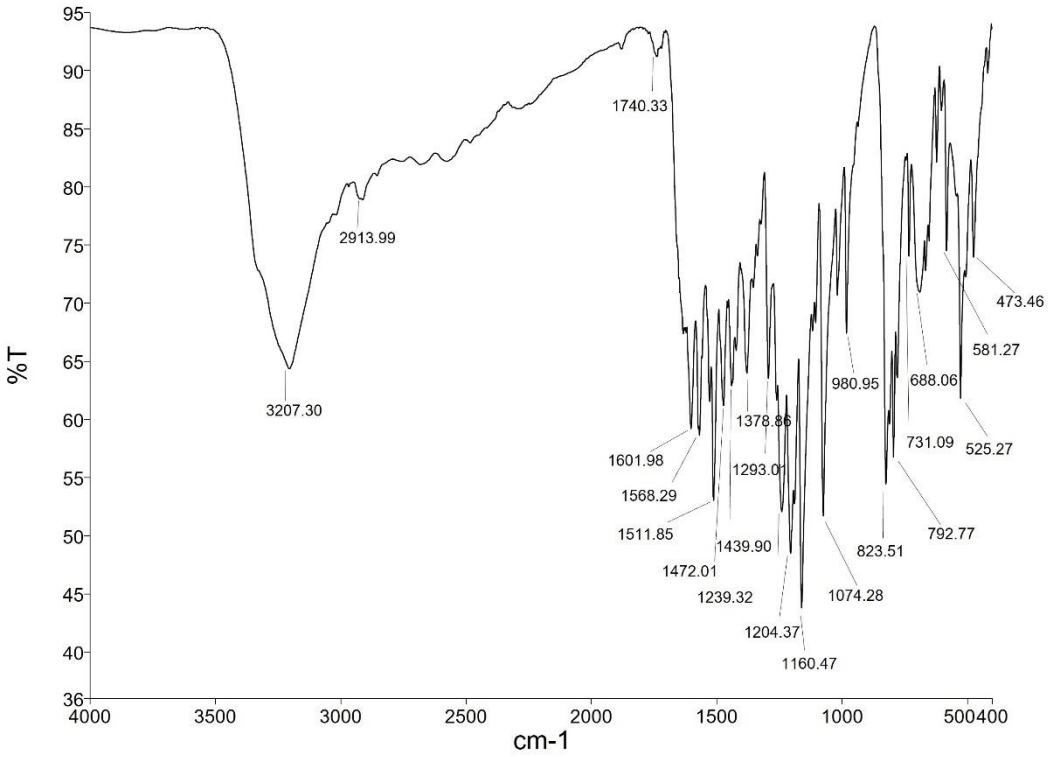

Figure A105 IR (ATR) spectrum of phloretin (**15**)

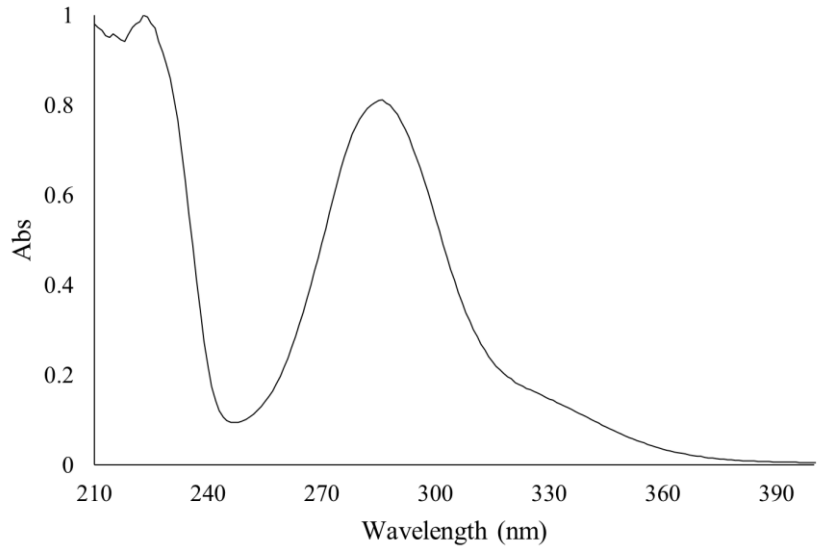

Figure A106 UV (MeOH) spectrum of phloretin (**15**)

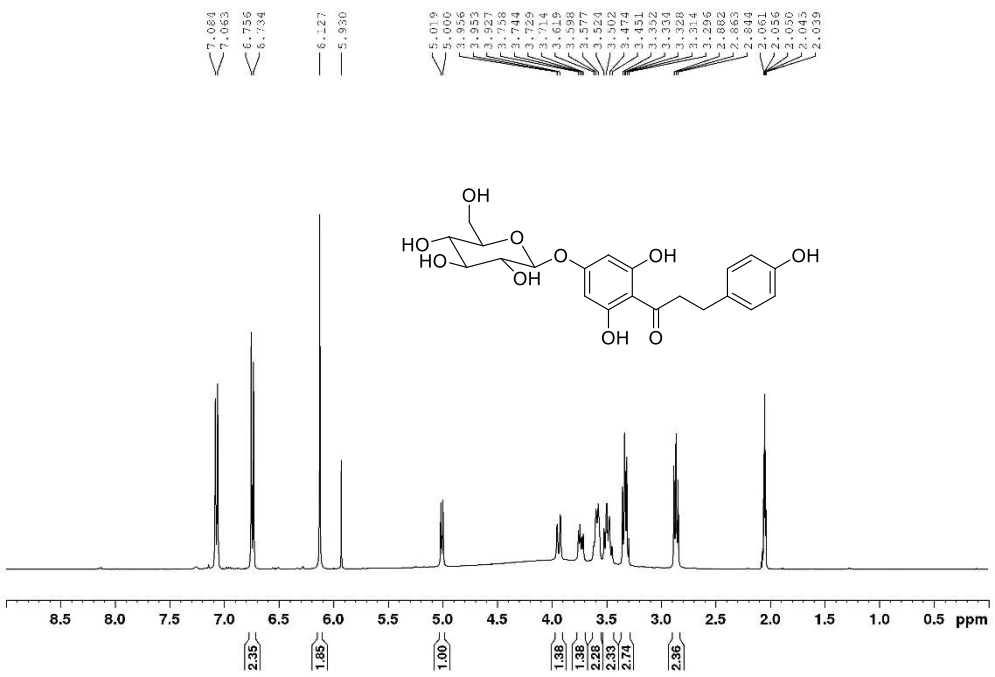

Figure A107 ^{1}H NMR spectrum (acetone-d_6, 400 MHz) of phloretin 4'-*O*-β-D-glucoside (**16**)

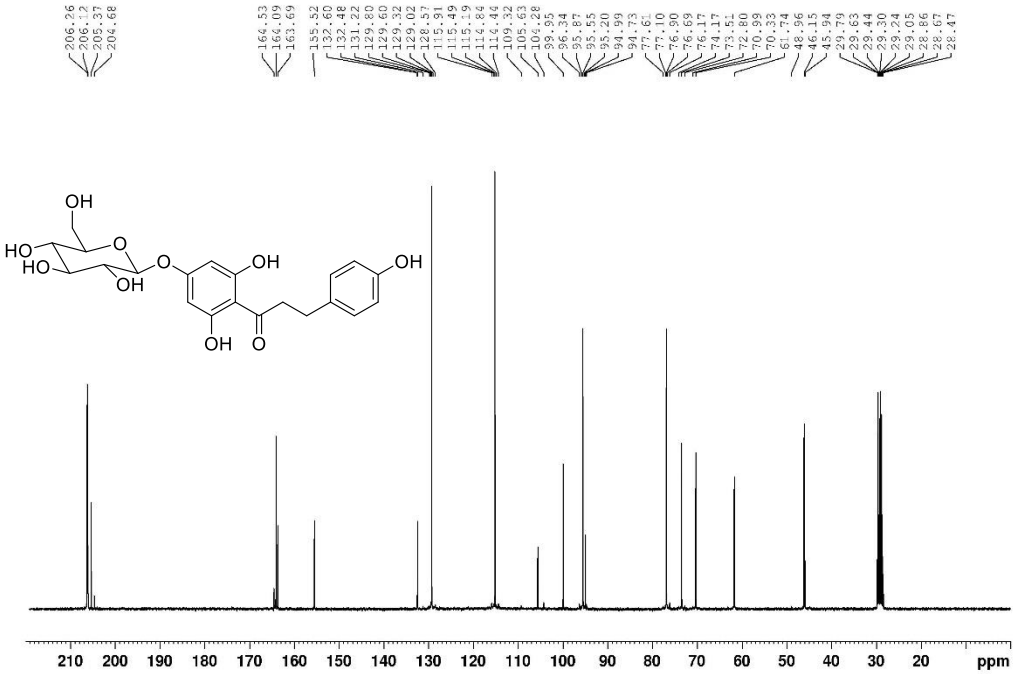

Figure A108 ^{13}C NMR spectrum (acetone-d_6, 100 MHz) of phloretin 4'-*O*-β-D-glucoside (**16**)

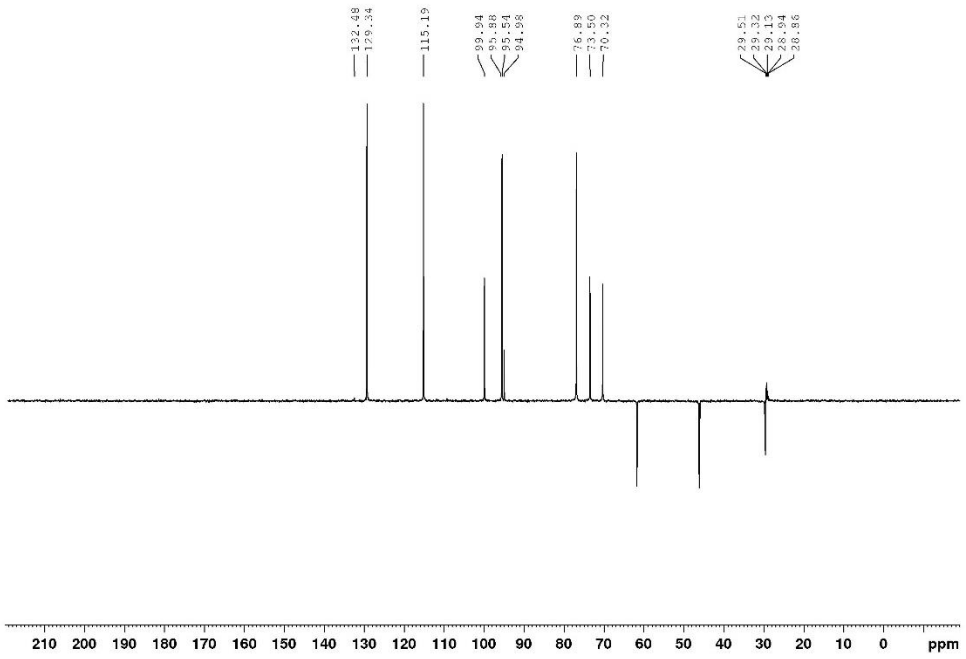

Figure A109 DEPT135 NMR spectrum (acetone-d_6, 100 MHz) of phloretin 4'-*O*-β-D-glucoside (**16**)

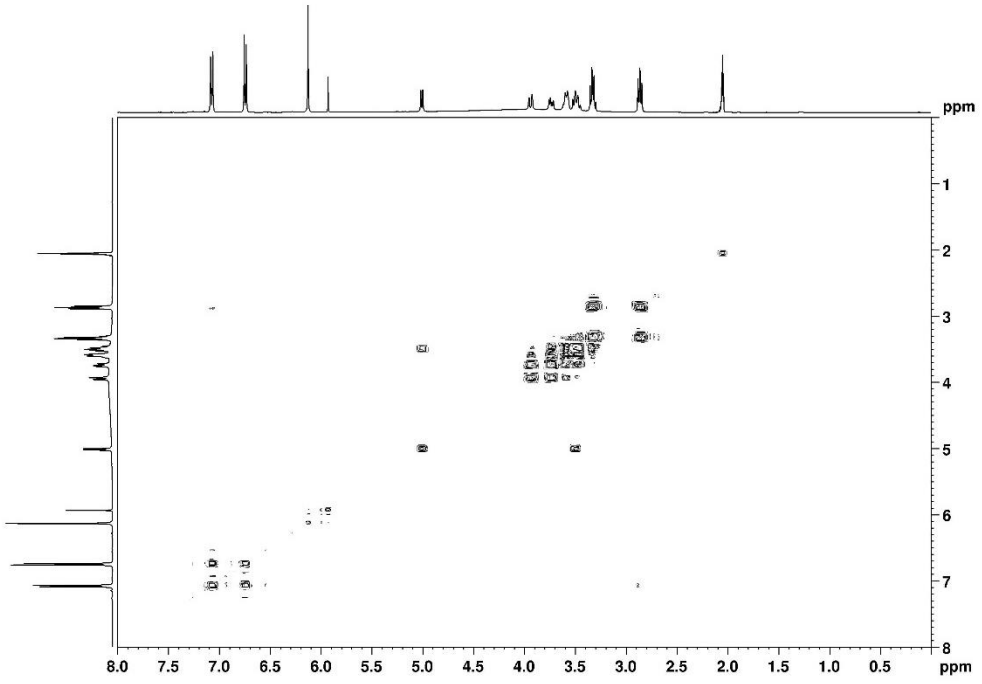

Figure A110 COSY NMR spectrum (acetone-d_6) of phloretin 4'-*O*-β-D-glucoside (**16**)

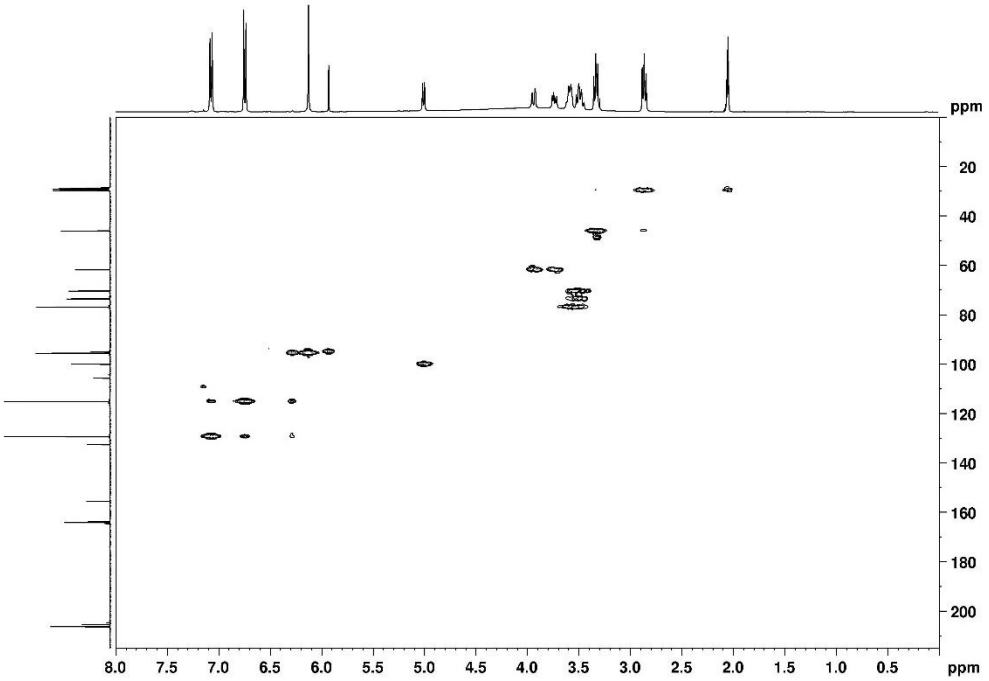

Figure A111 HMQC NMR spectrum (acetone-d_6) of phloretin 4'-*O*-β-D-glucoside (**16**)

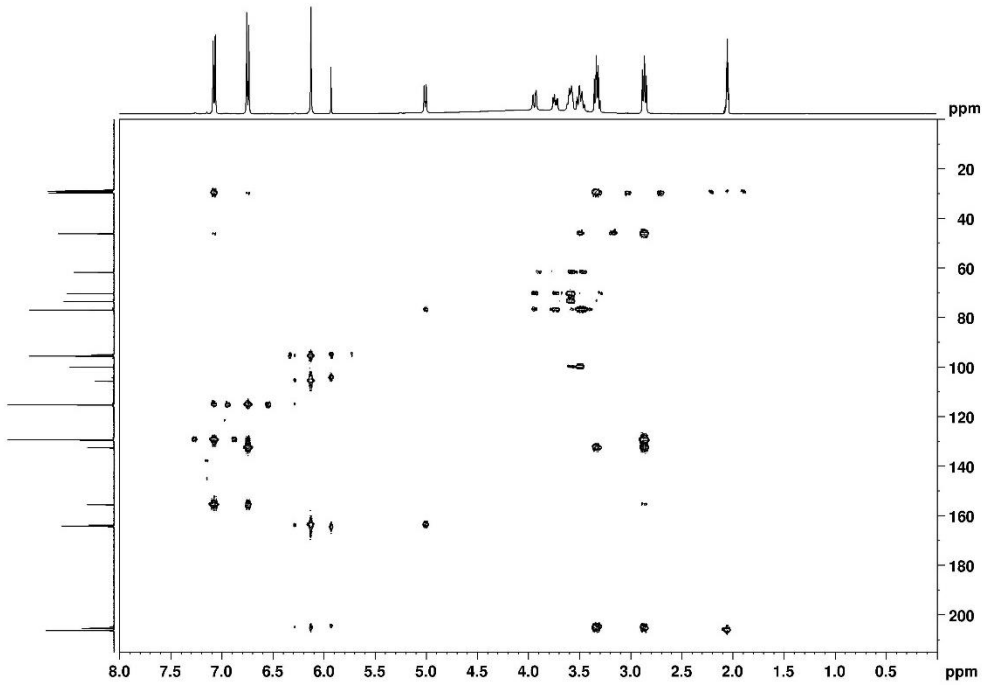

Figure A112 HMBC NMR spectrum (acetone-d_6) of phloretin 4'-*O*-β-D-glucoside (**16**)

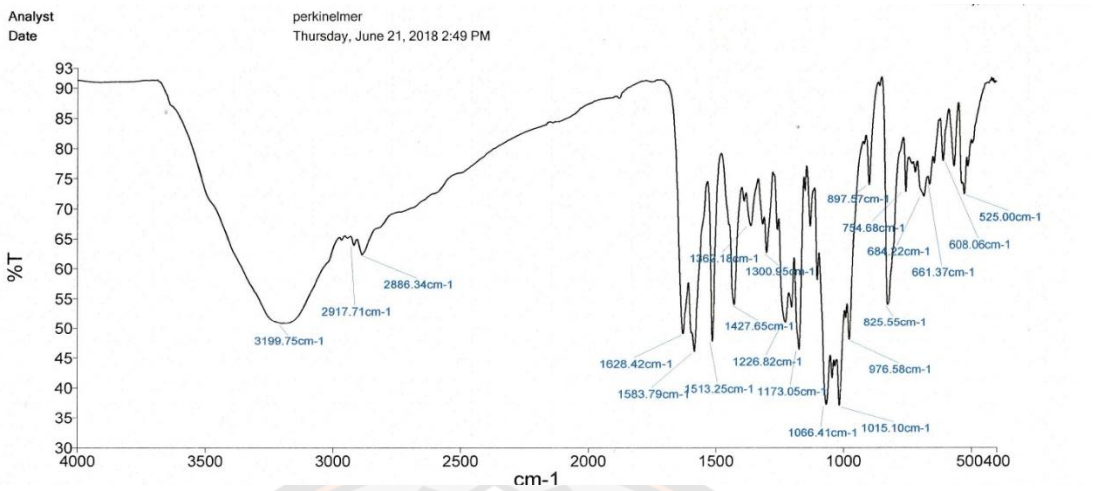

Figure A113 IR (ATR) spectrum of phloretin 4'-*O*-*β*-D-glucoside (**16**)

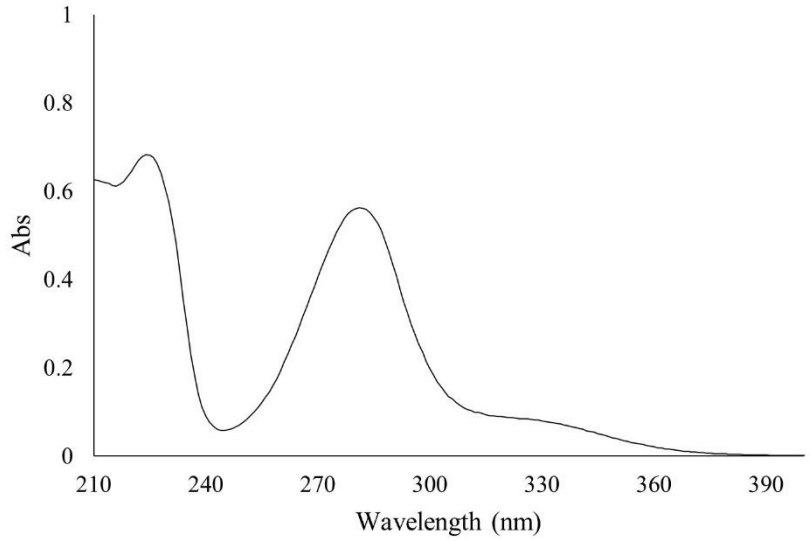

Figure A114 UV (MeOH) spectrum of phloretin 4'-*O*-*β*-D-glucoside (**16**)

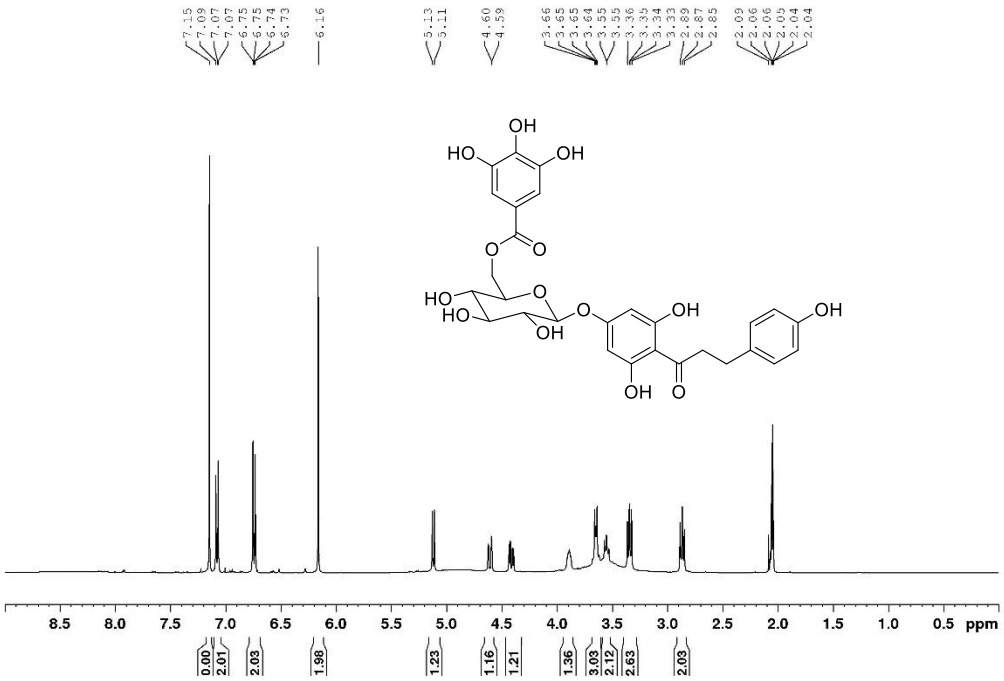

Figure A115 ^{1}H NMR spectrum (acetone-d_6, 400 MHz) of phloretin 4'-*O*-(6''-*O*-galloyl)-*β*-D-glucoside (**17**)

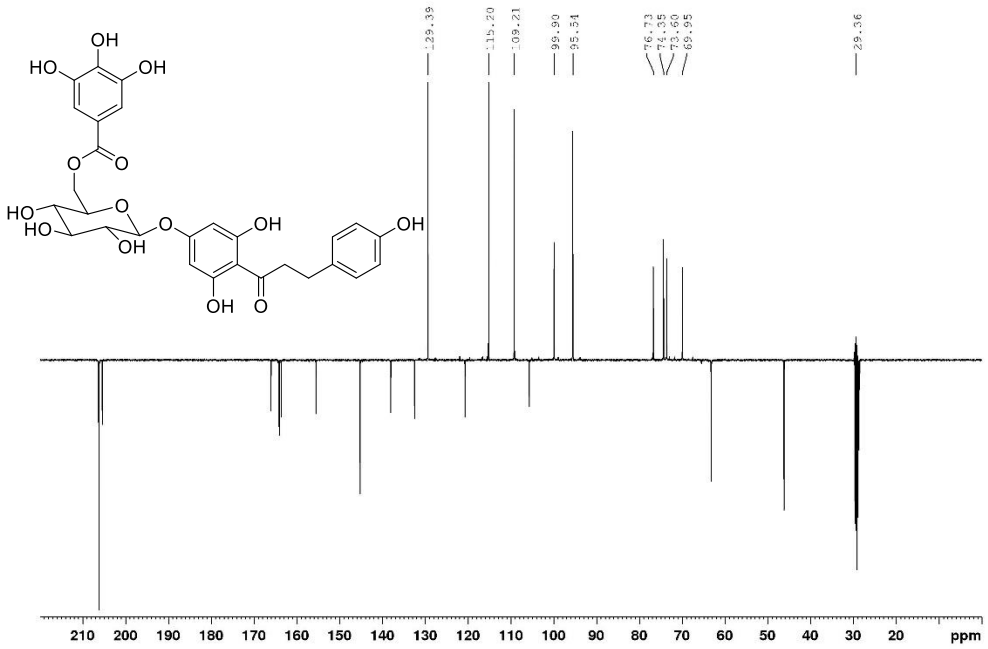

Figure A116 DEPTQ NMR spectrum (acetone-d_6, 100 MHz) of phloretin 4'-*O*-(6''-*O*-galloyl)-*β*-D-glucoside (**17**)

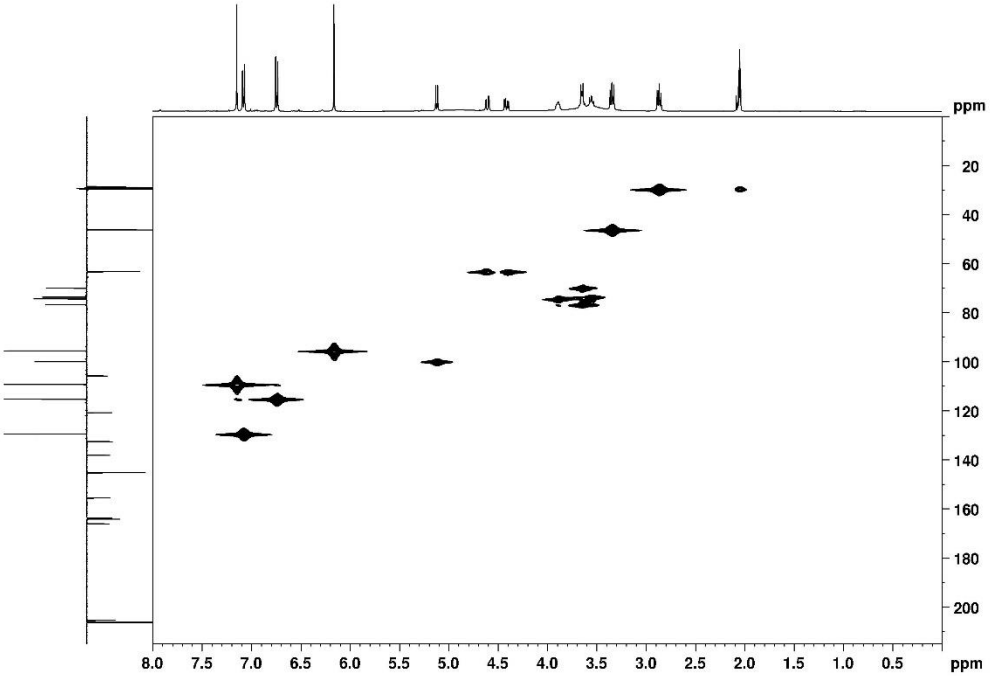

Figure A117 HMQC NMR spectrum (acetone-d_6) of phloretin 4'-*O*-(6''-*O*-galloyl)-β-D-glucoside (**17**)

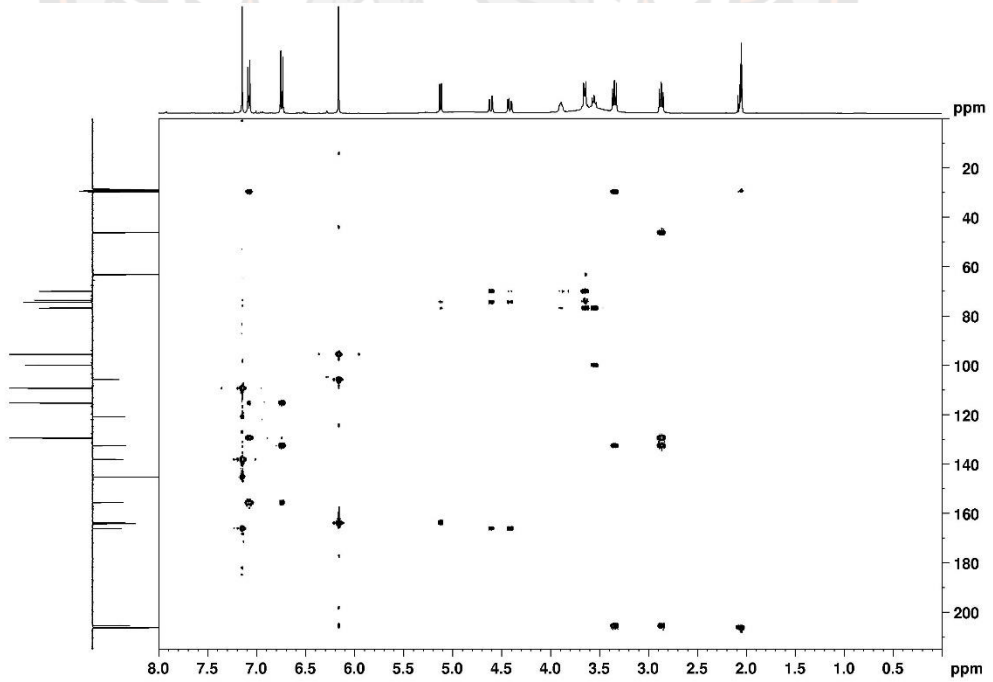

Figure A118 HMBC NMR spectrum (acetone-d_6) of phloretin 4'-*O*-(6''-*O*-galloyl)-β-D-glucoside (**17**)

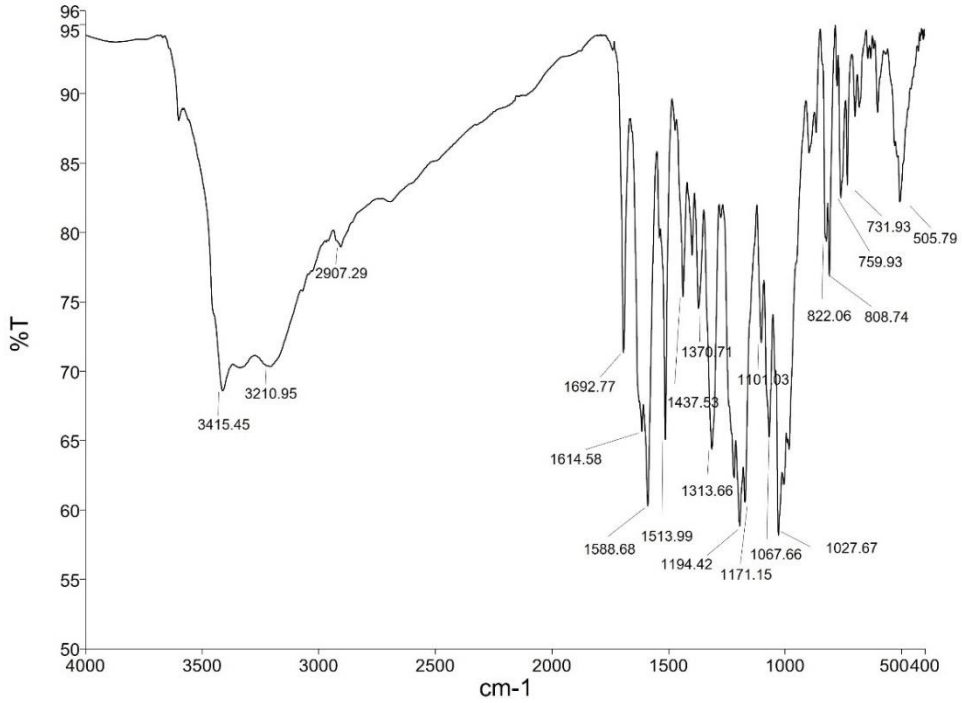

Figure A119 IR (ATR) spectrum of phloretin 4'-*O*-(6"-*O*-galloyl)-*β*-D-glucoside (**17**)

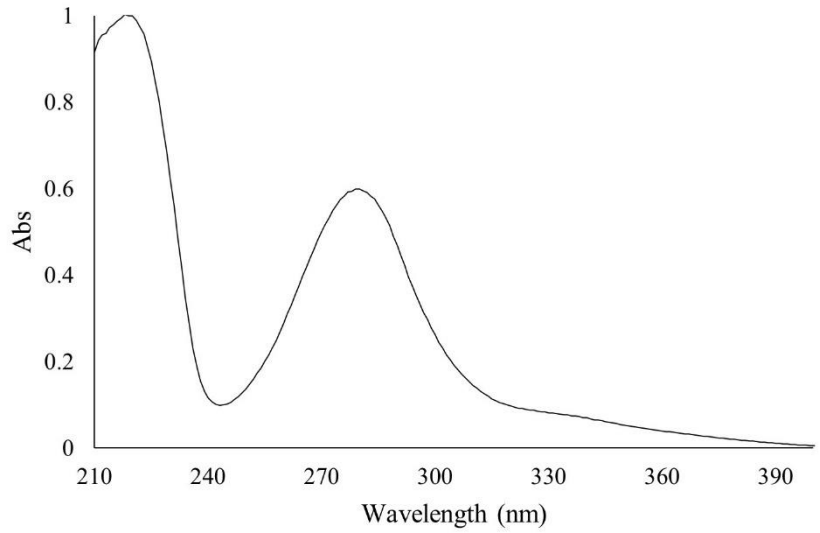

Figure A120 UV (MeOH) spectrum of phloretin 4'-*O*-(6"-*O*-galloyl)-*β*-D-glucoside (**17**)

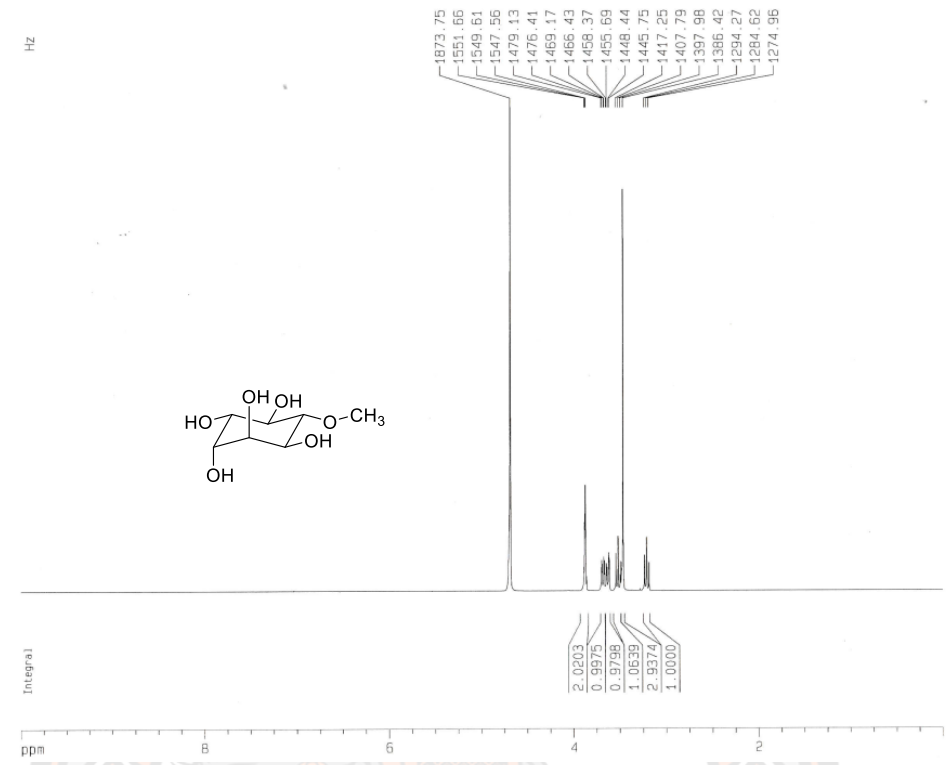

Figure A121 ^{1}H NMR spectrum (D_2O, 400 MHz) of pinitol (**18**)

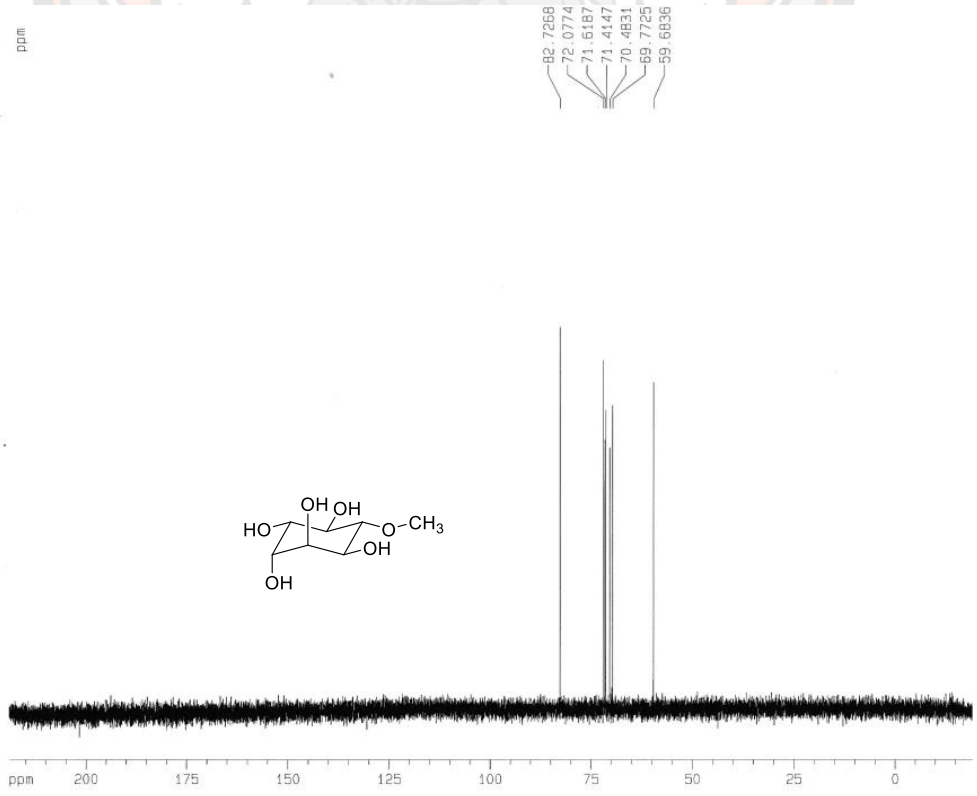

Figure A122 ^{13}C NMR spectrum (D_2O, 100 MHz) of pinitol (**18**)

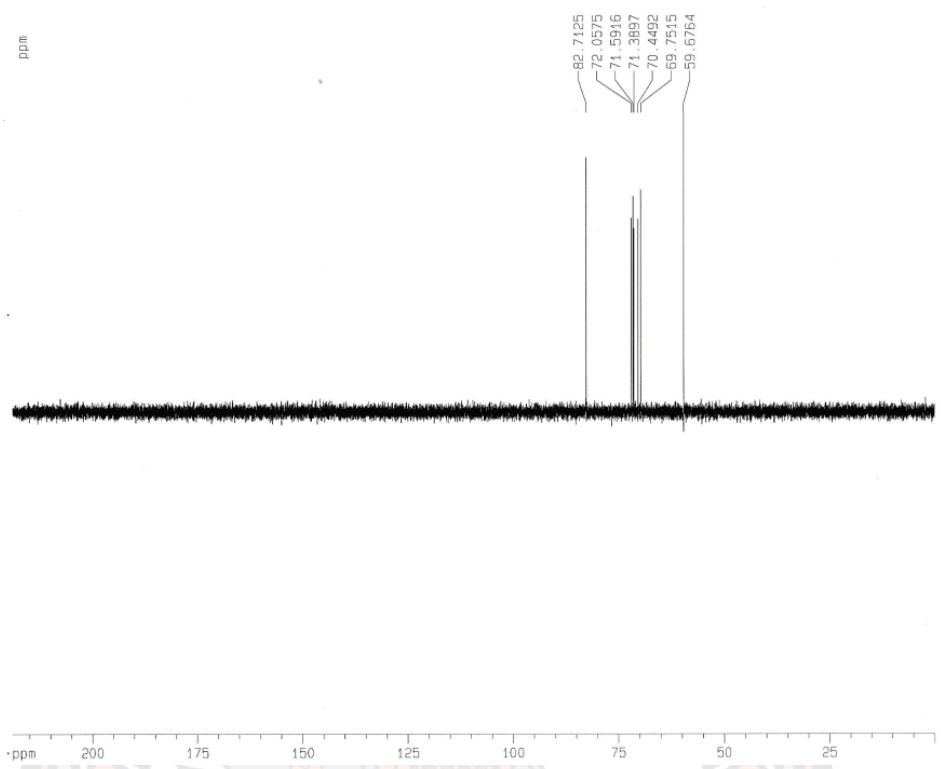

Figure A123 DEPT135 NMR spectrum (D_2O, 100 MHz) of pinitol (**18**)

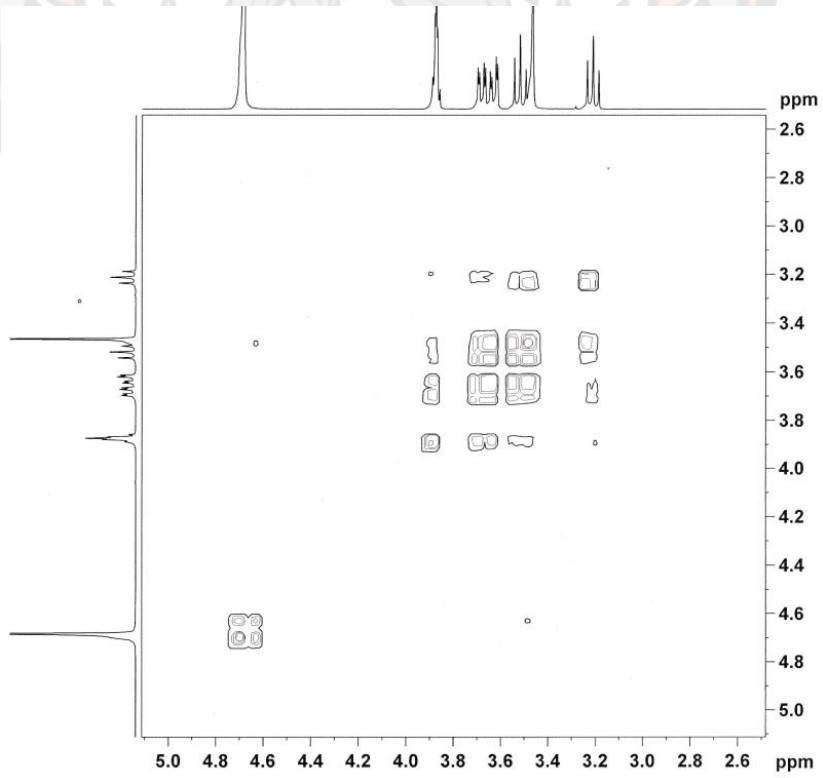

Figure A124 COSY NMR spectrum (D_2O) of pinitol (**18**)

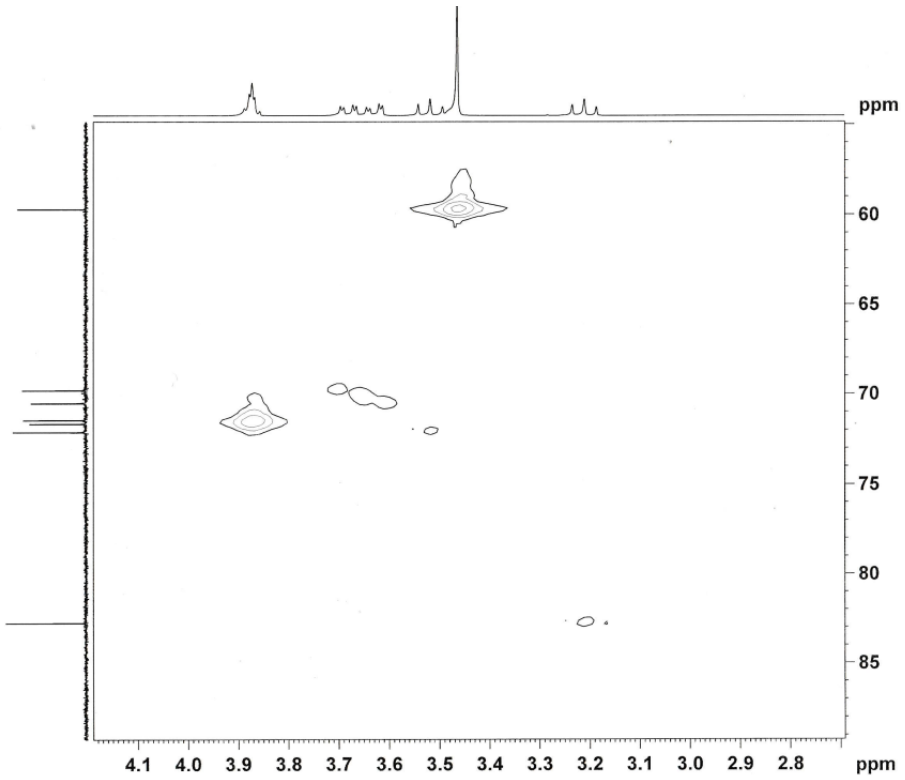

Figure A125 HMQC NMR spectrum (D_2O) of pinitol (**18**)

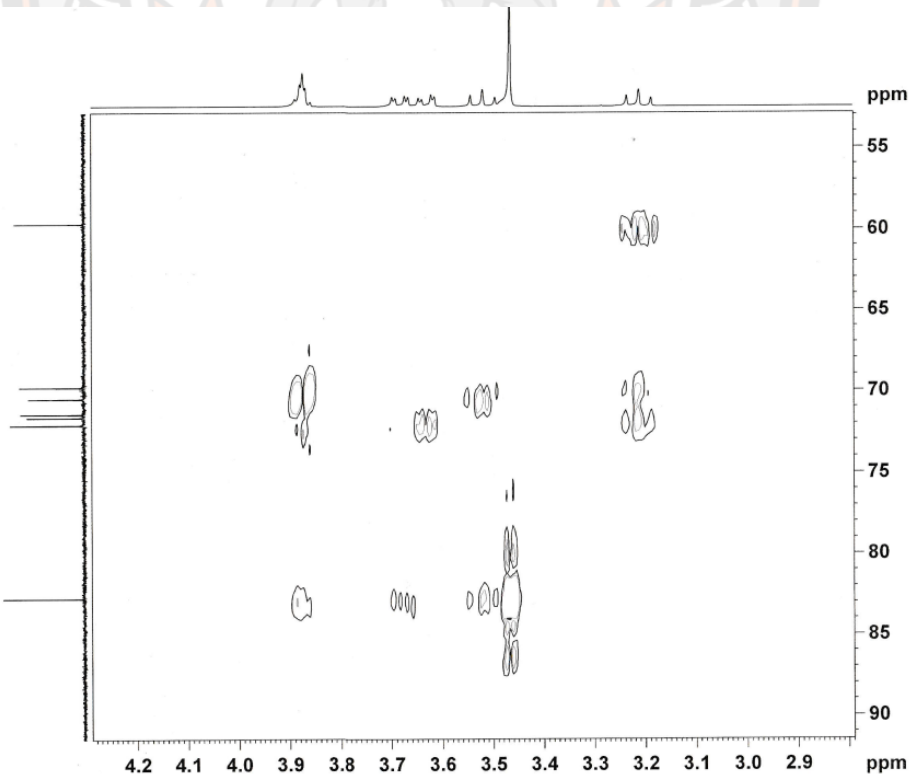

Figure A126 HMBC NMR spectrum (D_2O) of pinitol (**18**)

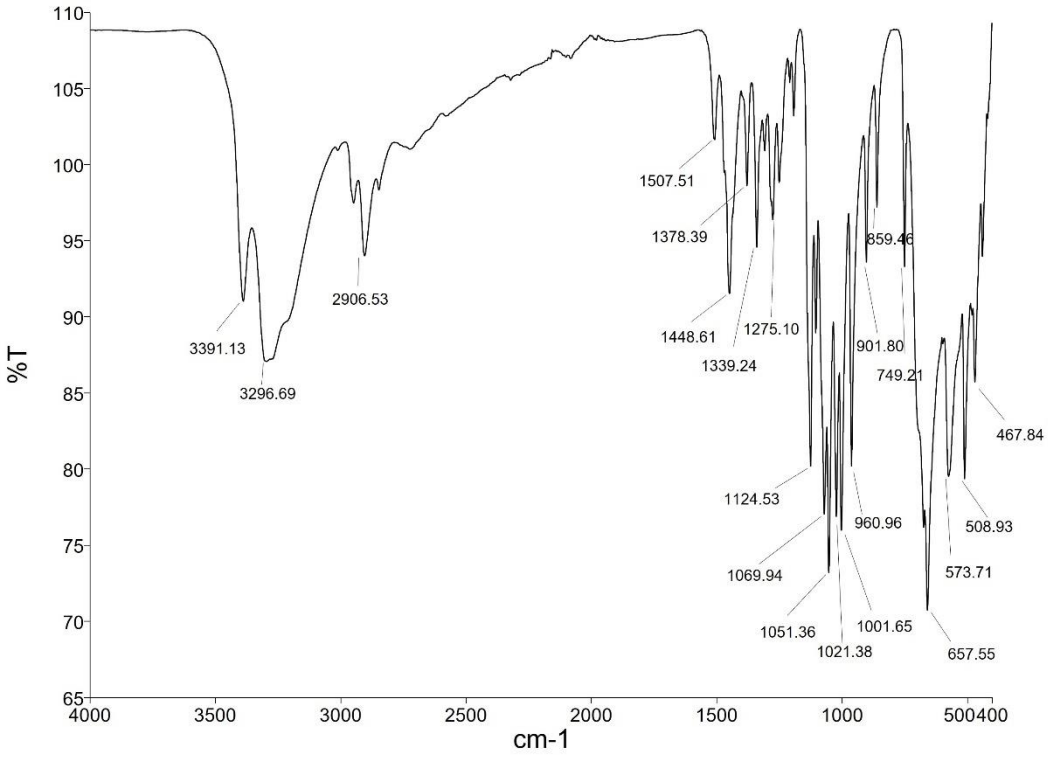

Figure A127 IR (ATR) spectrum of pinitol (**18**)

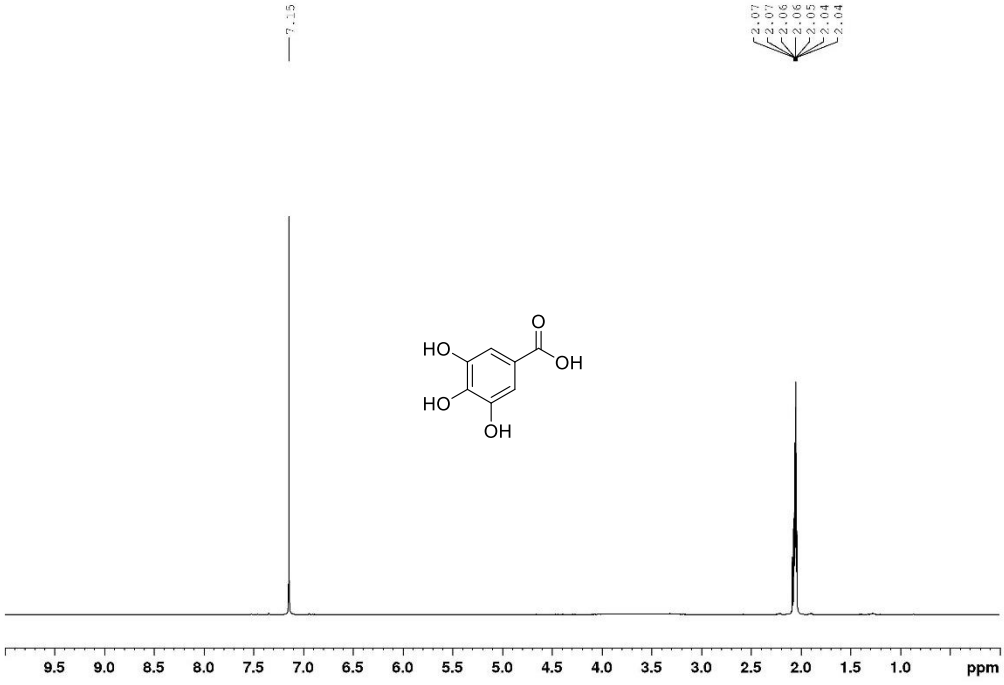

Figure A128 ^{1}H NMR spectrum (acetone-d_6, 400 MHz) of gallic acid (**19**)

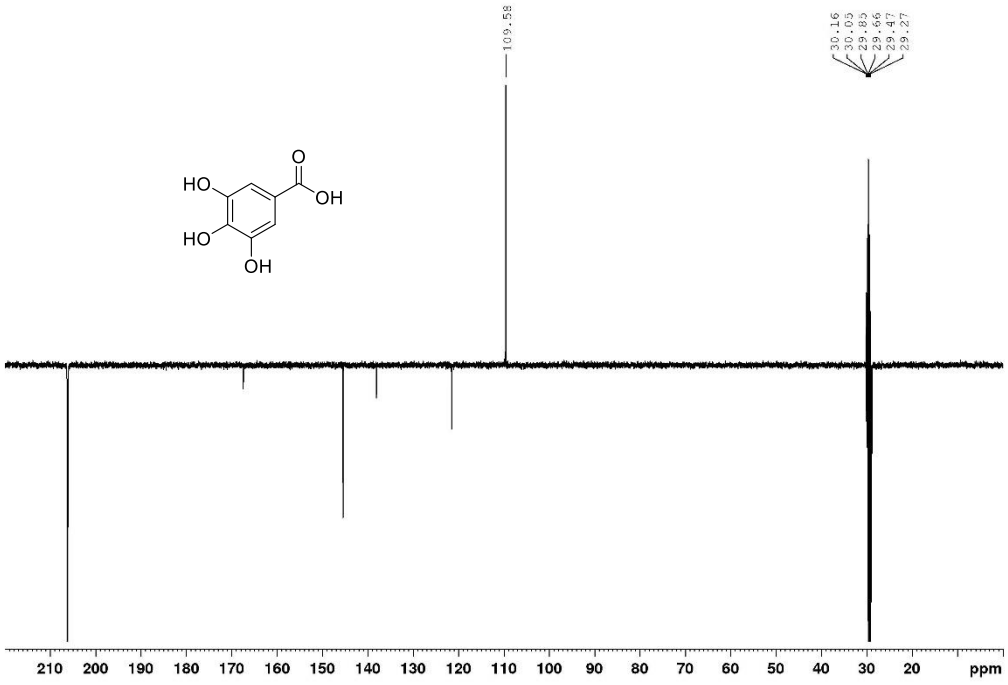

Figure A129 DEPTQ NMR spectrum (acetone-d_6, 100 MHz) of gallic acid (**19**)

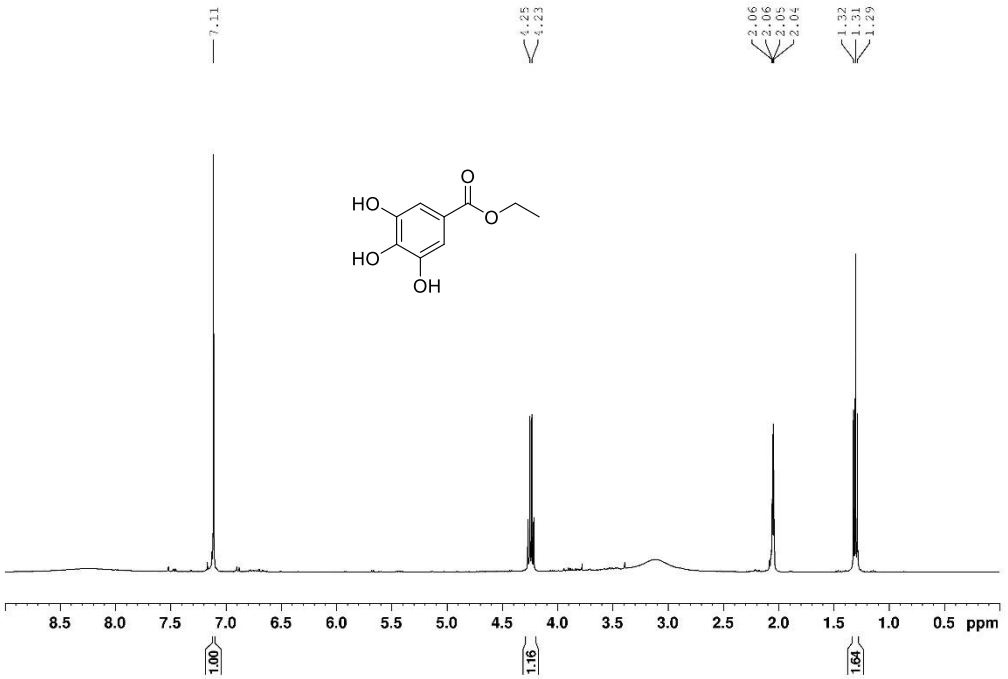

Figure A130 ^{1}H NMR spectrum (acetone-d_6, 400 MHz) of gallic acid ethyl ester (**20**)

Figure A131 DEPTQ NMR spectrum (acetone-d_6, 100 MHz) of gallic acid ethyl ester (**20**)

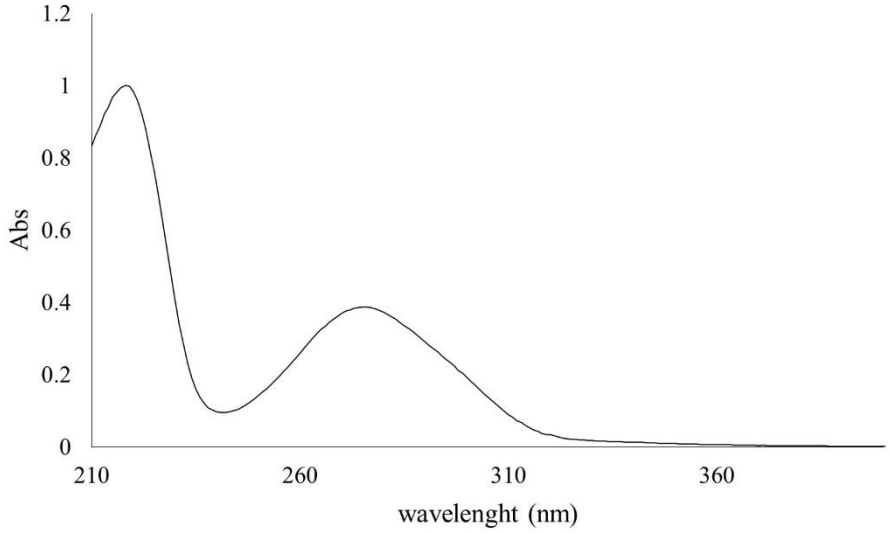

Figure A132 UV (MeOH) spectrum of gallic acid ethyl ester (**20**)

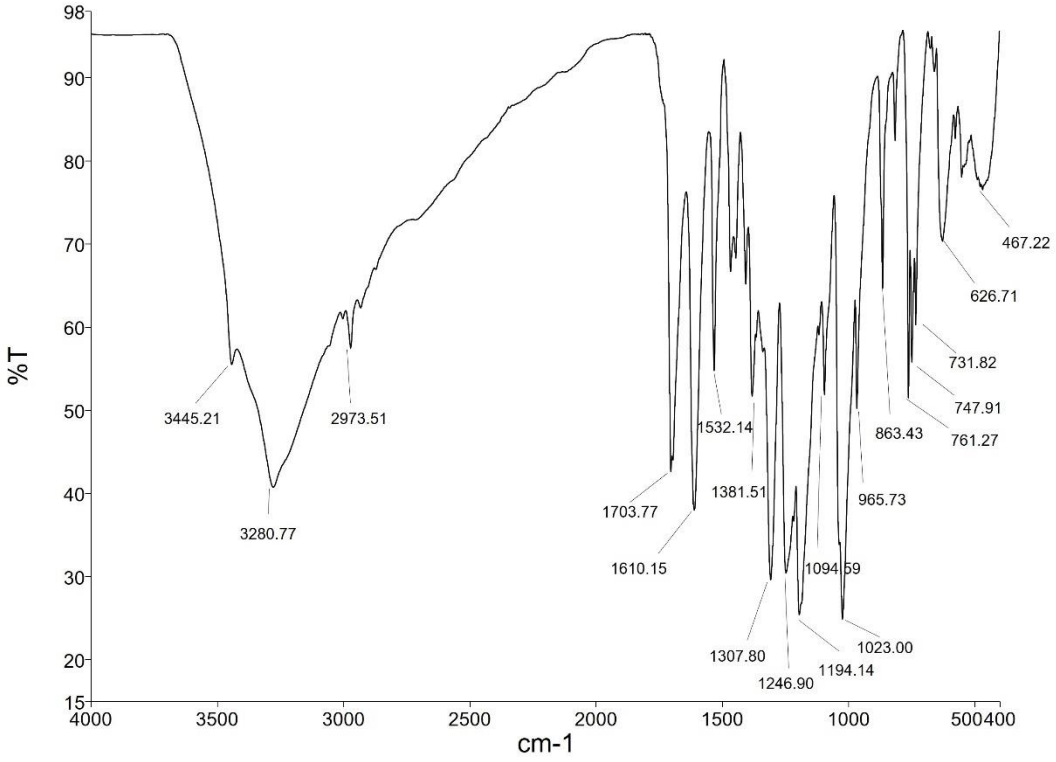

Figure A133 IR (ATR) spectrum of gallic acid ethyl ester (**20**)

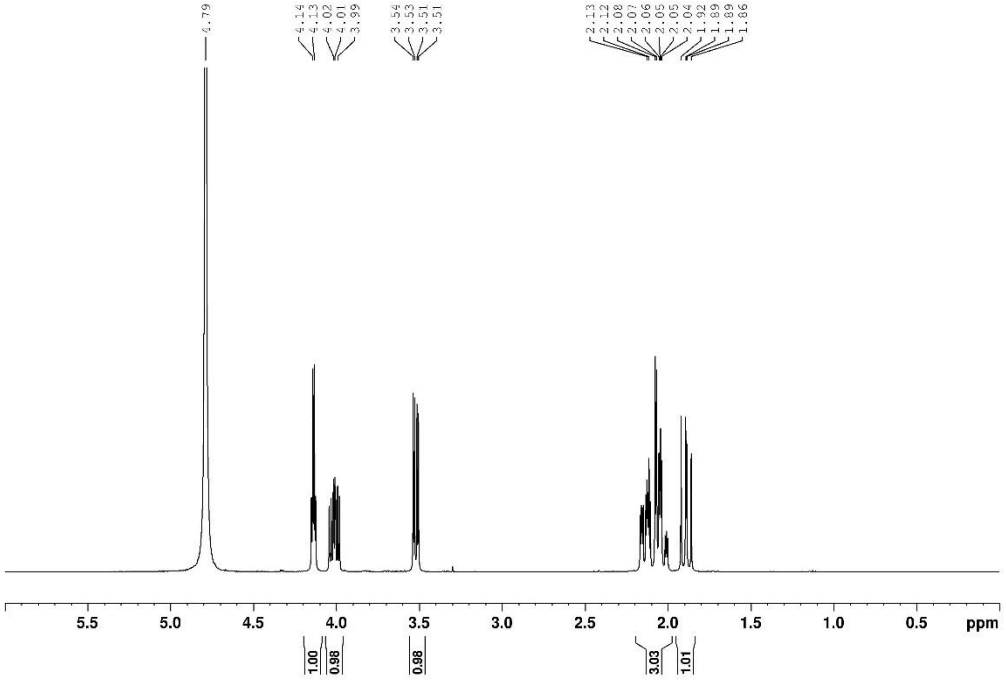

Figure A134 ^{1}H NMR spectrum (D_2O, 400 MHz) of quinic acid (**21**)

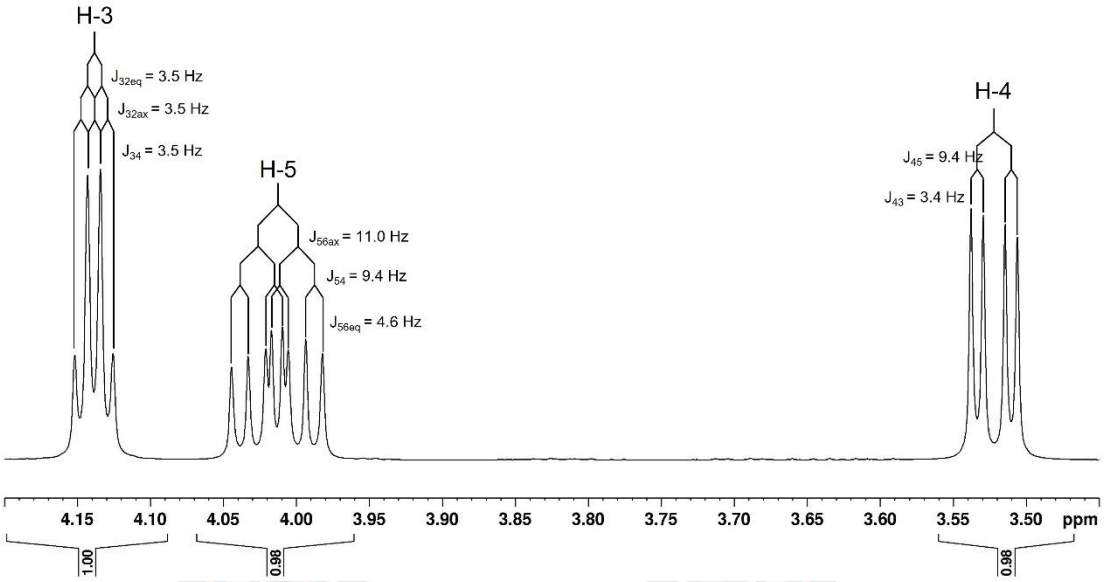

Figure A135 ^{1}H NMR spectrum (D_2O, 400 MHz) of quinic acid (**21**) in range 3 – 4.2 ppm

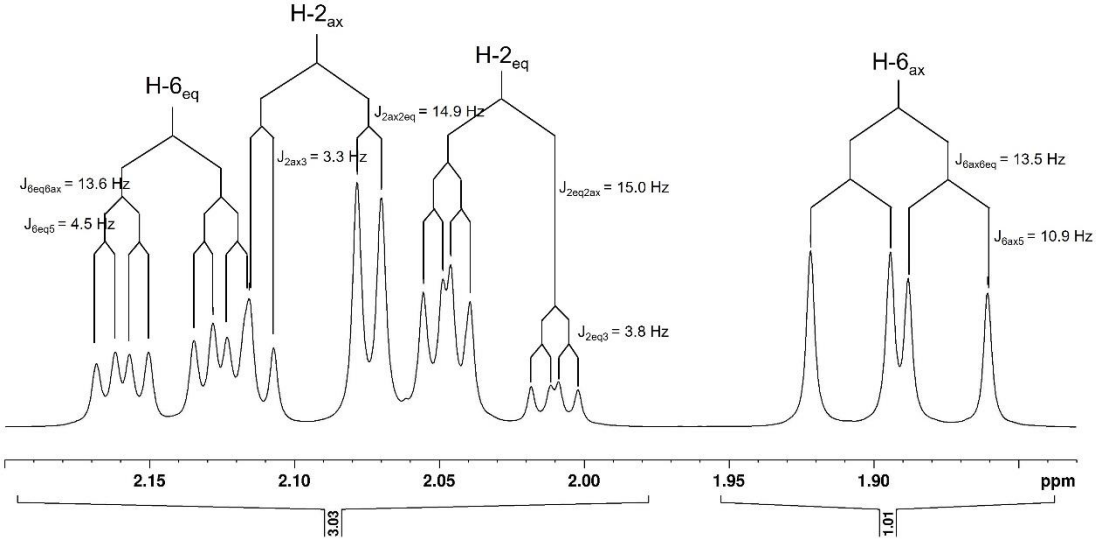

Figure A136 ^{1}H NMR spectrum (D_2O, 400 MHz) of quinic acid (**21**) in range 2 – 2.2 ppm

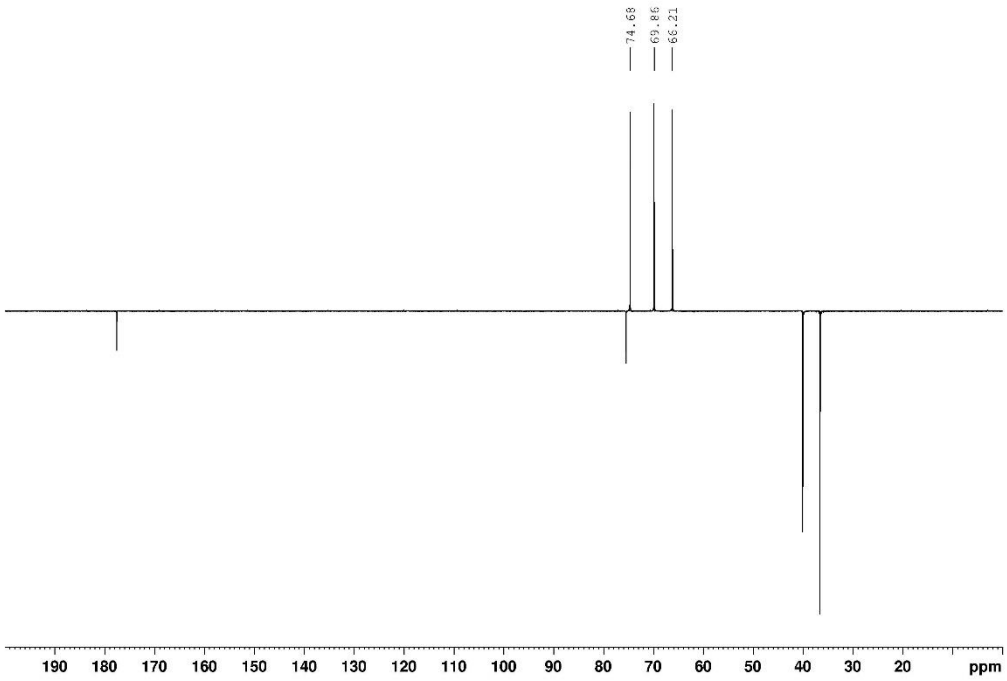

Figure A137 DEPTQ NMR spectrum (D_2O, 100 MHz) of quinic acid (**21**)

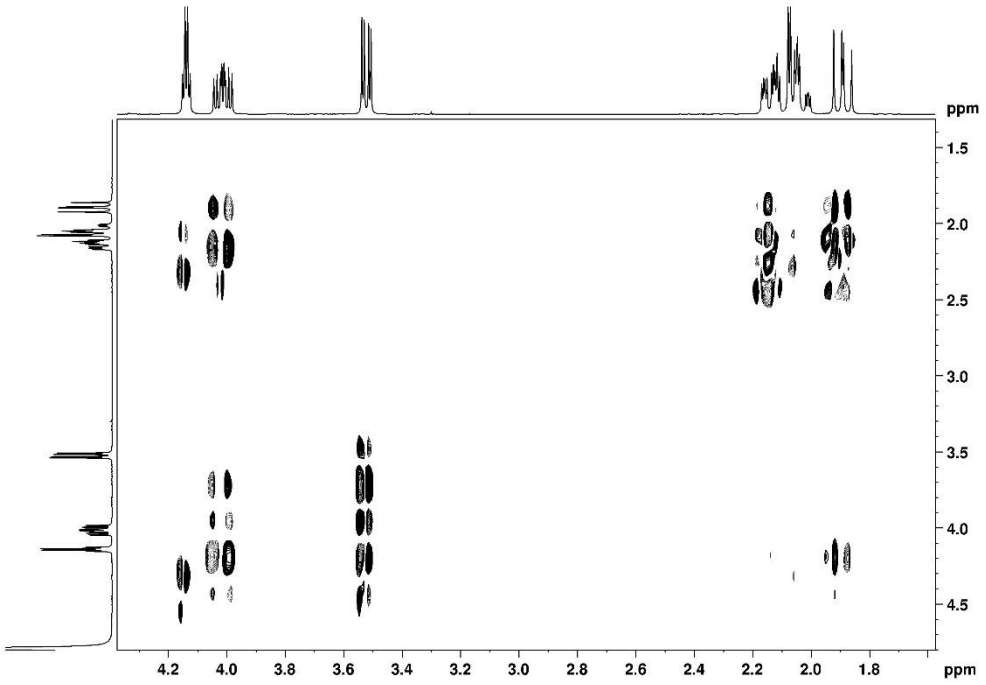

Figure A138 HMQC spectrum (D_2O, 100 MHz) of quinic acid (**21**)

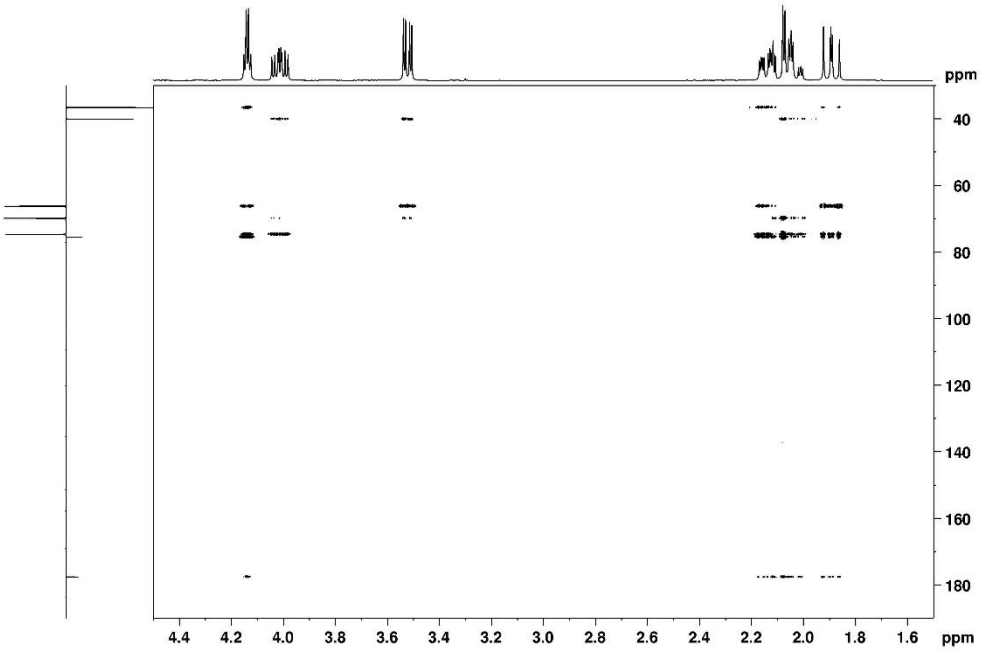

Figure A139 HMBC spectrum (D_2O, 100 MHz) of quinic acid (**21**)

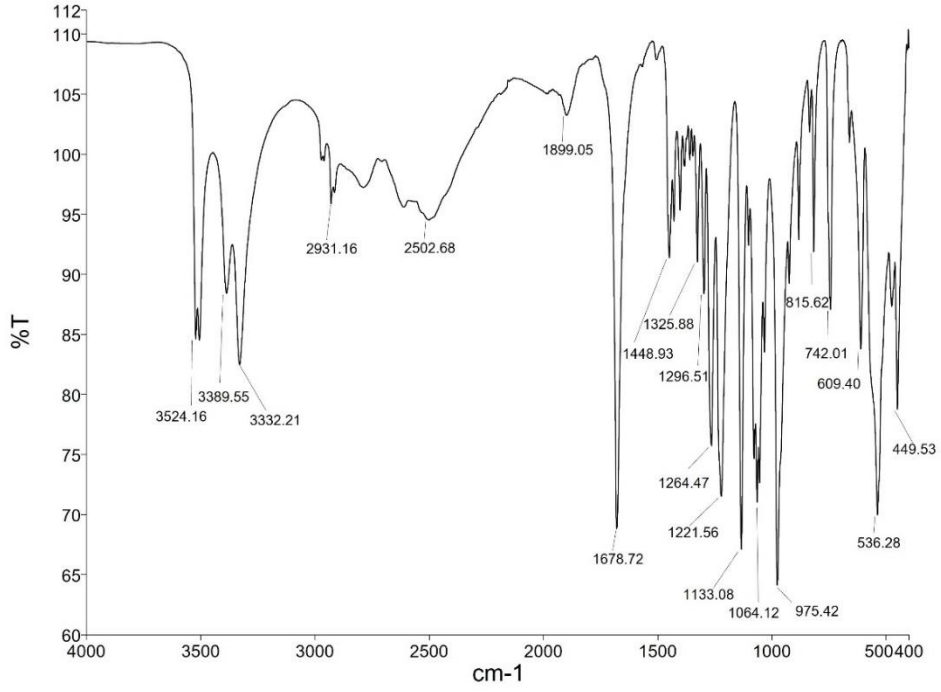

Figure A140 IR (ATR) spectrum of quinic acid (**21**)

REFERENCES

1. Cos P, Vlietinck AJ, Berghe DV, Maes L. Anti-infective potential of natural products: How to develop a stronger in vitro 'proof-of-concept'. Journal of Ethnopharmacology. 2006;106(3):290-302.
2. Duraipandiyan V, Ayyanar M, Ignacimuthu S. Antimicrobial activity of some ethnomedicinal plants used by Paliyar tribe from Tamil Nadu, India. BMC Complementary and Alternative Medicine. 2006;6(1):1-7.
3. Karimi A, Majlesi M, Rafieian-Kopaei M. Herbal versus synthetic drugs; beliefs and facts. Journal of nephropharmacology. 2015;4(1):27.
4. Monaco nature encyclopedia discover the biodiversity: Alpinia mutica [Internet]. 2000.
5. Sirat HM, Rahman AA, Itokawa H, Morita H. Constituents of the rhizomes of two Alpinia species of Malaysia. Planta Medica. 1996;62(02):188-9.
6. Jantan I, Pisar M, Sirat HM, Basar N, Jamil S, Ali RM, et al. Inhibitory effects of compounds from Zingiberaceae species on platelet activating factor receptor binding. Phytotherapy Research. 2004;18(12):1005-7.
7. Sirat HM, Jani NA. Chemical constituents of the leaf of Alpinia mutica Roxb. Nat Prod Res. 2013;27(16):1468-70.
8. Yuenyongsawad S, Bunluepuech K, Wattanapiromsakul C, Tewtrakul S. Anti-cancer activity of compounds from Bauhinia strychnifolia stem. Journal of Ethnopharmacology. 2013;150(2):765-9.
9. Bunluepuech K, Wattanapiromsakul C, Madaka F, Tewtrakul S. Anti-HIV-1 integrase and anti-allergic activities of Bauhinia strychnifolia. Songklanakarin Journal of Science & Technology. 2013;35(6).
10. Kongkiatpaiboon S, Duangdee N, Tayana N, Schinnerl J, Bacher M, Chewchinda S. Yanangdaengin, a dihydrochalcone glucoside galloyl ester as active antioxidative agent from leaves of Lysiphyllum strychnifolium (syn. Bauhinia strychnifolia). Chinese Herbal Medicines. 2020;12(4):452-5.
11. Chutoam P, Klongthalay S, Somsak V. Effect of crude leaf extract of Bauhinia strychnifolia in BALB/c mice infected with plasmodium berghei. Malar Cont Elimination. 2015;4:S1-002.
12. Itharat A, Sayompark S, Hansakul P, Dechayont B. In vitro antioxidant activities of extracts of Bauhinia strychnifolia stems and leaves: comparison with activities in green tea extracts. Med Aromat Plants. 2016;5(243):2167-0412.100024.
13. Sato VH, Chewchinda S, Nuamnaichati N, Mangmool S, Sungthong B, Lertsatitthanakorn P, et al. Pharmacological mechanisms of the water leaves extract of Lysiphyllum strychnifolium for its anti-inflammatory and anti-hyperuricemic actions for gout treatment. Pharmacognosy Magazine. 2019;15(60):98.
14. Somsak V, Noilod J, Chachiyo S, Kraithep S. Antimalarial activity of ethanolic leaf extract of Bauhinia strychnifolia in mice infected with Plasmodium berghei. Malar Cont Elimination. 2015;4:131.
15. Sukprasert S, Deenonpoe R, Yimsoo T, Yingmema W, Prasopdee S, Krajang A, et al. Antidote activity and protective effects of Lysiphyllum strychnifolium (Craib) A. Schmitz extract against organophosphate pesticide in omethoate-treated rats. Journal of traditional and complementary medicine. 2021;11(3):189.
16. Kidruangphokin M. Chemical constituents of *Bauhinia strychnifolia* leaf [Thesis

M. Sc. in Chemistry]. Naresuan University: Naresuan University; 2018.
17. Nanditha A, Ma RC, Ramachandran A, Snehalatha C, Chan JC, Chia KS, et al. Diabetes in Asia and the Pacific: implications for the global epidemic. Diabetes Care. 2016;39(3):472-85.
18. Guariguata L, Whiting DR, Hambleton I, Beagley J, Linnenkamp U, Shaw JE. Global estimates of diabetes prevalence for 2013 and projections for 2035. Diabetes Res Clin Pract. 2014;103(2):137-49.
19. Rask-Madsen C, King GL. Vascular complications of diabetes: mechanisms of injury and protective factors. Cell metabolism. 2013;17(1):20-33.
20. Poznyak A, Grechko AV, Poggio P, Myasoedova VA, Alfieri V, Orekhov AN. The diabetes mellitus–atherosclerosis connection: The role of lipid and glucose metabolism and chronic inflammation. International Journal of Molecular Sciences. 2020;21(5):1835.
21. Lardinois CK, Greenfield MS, Schwartz HC, Vreman HJ, Reaven GM. Acarbose treatment of non-insulin-dependent diabetes mellitus. Archives of internal medicine. 1984;144(2):345-7.
22. Yabe-Nishimura C. Aldose reductase in glucose toxicity: a potential target for the prevention of diabetic complications. Pharmacological reviews. 1998;50(1):21-34.
23. Bischoff H. The mechanism of alpha-glucosidase inhibition in the management of diabetes. Clinical and investigative medicine Medecine clinique et experimentale. 1995;18(4):303-11.
24. Malek SNA, Phang CW, Ibrahim H, Wahab NA, Sim KS. Phytochemical and cytotoxic investigations of Alpinia mutica rhizomes. Molecules. 2011;16(1):583-9.
25. Ibrahim H, Sivasothy Y, Syamsir DR, Nagoor NH, Jamil N, Awang K. Essential oil composition and antimicrobial activities of two closely related species, Alpinia mutica Roxb. and Alpinia latilabris Ridl., from Peninsular Malaysia. The Scientific World Journal. 2014;2014.
26. Salim M, Rajendran R, Ajikumaran Nair S, Dan M, Baby S. Chemical composition and biological activities of rhizome and fruit rind oils of Alpinia mutica from south India. Journal of EssEntial oil rEsEarch. 2016;28(5):428-35.
27. Sirat HM, Rahman AA. Essential Oil Constituents of Alpinia mutica Roxb. Journal of Essential Oil Research. 1998;10(1):83-4.
28. Huong LT, Dai DN, Thang TD, Bach TT, Ogunwande IA. The essential oils of the leaf, pseudostem root and fruit of Alpinia mutica roxb. Journal of Essential Oil Bearing Plants. 2016;19(8):2049-55.
29. Sirat HM, Khalid NFM, Jani NA, Basar N. Chemical composition of the fruits oil of Alpinia mutica Roxb.(Zingiberaceae). Journal of Essential Oil Research. 2009;21(5):457-8.
30. Mustahil NA, Sukari MA, Abdul AB, Ali NA, Ee Cheng Lian G. Evaluation of biological activities of Alpinia mutica Roxb. and its chemical constituents. Pak J Pharm Sci. 2013;26(2).
31. Jantan I, Raweh S, Sirat H, Jamil S, Yasin YM, Jalil J, et al. Inhibitory effect of compounds from Zingiberaceae species on human platelet aggregation. Phytomedicine. 2008;15(4):306-9.
32. Jantan Ib, Ahmad Fb, Ahmad AS. Constituents of the rhizome and seed oils of Greater Galangal Alpinia galangal (L.) Willd. from Malaysia. Journal of Essential Oil Research. 2004;16(3):174-6.

33. Sirat HM, Nordin AB. Chemical Composition of the Rhizome Oil of Alpinia conchigera Griff from Malaysia. Journal of Essential Oil Research. 1995;7(2):195-7.
34. Organization TBG. *Lysiphyllum strychnifolium* (W. G. Craib) A. Schmitz 2015 [cited 2022 28 September 2022]. Available from: http://www.qsbg.org/Database/plantdb/herbarium/herbarium-specimen.asp?QSBGNO=108507.
35. Kidruangphokin M, Chuenpratoom T, Sriwattanawarunyoo C, Boonphong S, editors. Pinitol from *Bauhinia strychnifolia* leaves. The 10th National Science Research Conference "Science Leading for Thailand Innovation 40; 2018 24-25 May; Mahasarakham, Thailand2018.
36. Sampaopan Y, Kitprapiumpon N, Kongkiatpaiboon S, Duangdee N, Wongyai S. Isolation and HPLC analysis of astilbin in Lysiphyllum strychnifolium (syn. Bauhinia strychnifolia) Stems. Science & Technology Asia. 2021:208-15.
37. Bunluepuech K, Tewtrakul S. Anti-HIV-1 integrase activity of Thai Medicinal Plants. Songklanakarin Journal of Science & Technology. 2009;31(3).
38. Sukprasert S, Pansuksan K, Sriyakul K. Lysiphyllum strychnifolium (Craib) A. Schmitz extract, a novel neuraminidase inhibitor of avian influenza virus subtype H5N1. Journal of Herbal Medicine. 2020;20:100330.
39. Kaewpiboon C, Lirdprapamongkol K, Srisomsap C, Winayanuwattikun P, Yongvanich T, Puwaprisirisan P, et al. Studies of the in vitro cytotoxic, antioxidant, lipase inhibitory and antimicrobial activities of selected Thai medicinal plants. BMC Complementary and Alternative Medicine. 2012;12(1):1-8.
40. Kraithep S, Matrakool B, Thunyaharn S, Yingsiwaphat V, Pojpanichapong S, Danthaiwattana S, et al. Antioxidant and Antimicrobial Activity of Bauhinia strychnifolia Craib Stem Extract Against Oral Pathogens. Royal Thai Army Medical Journal. 2017;70(2):73-9.
41. Thiraworawong T, Sukpan N, Charounlertdajkul N, Ariyavechakul P, Anantasiristaporn T, Lertsatitthanakorn P, editors. Antibacterial activity against *Propionibacterium acnes* of *Lysiphyllum strychnifolium* (Craib) A. Schmitz leaves extract products. The International Conference of Pharmaceutical Sciences and Medicines 2018 (ICPAM 2018); 2018; Chonburi, Thailand.
42. Alrefai H, Allababidi H, Levy S, Levy J. The endocrine system in diabetes mellitus. Endocrine. 2002;18(2):105-19.
43. Masharani U, German M. Pancreatic hormones and diabetes mellitus. Greenspan's basic & clinical endocrinology. 2011;8.
44. Atkinson MA, Eisenbarth GS, Michels AW. Type 1 diabetes. The Lancet. 2014;383(9911):69-82.
45. Simmons KM, Michels AW. Type 1 diabetes: A predictable disease. World journal of diabetes. 2015;6(3):380.
46. Fan W. Epidemiology in diabetes mellitus and cardiovascular disease. Cardiovascular endocrinology. 2017;6(1):8.
47. Watada H, Tamura Y. Impaired insulin clearance as a cause rather than a consequence of insulin resistance. Journal of diabetes investigation. 2017;8(6):723.
48. Chang AM, Smith MJ, Bloem CJ, Galecki AT, Halter JB. Effect of lowering postprandial hyperglycemia on insulin secretion in older people with impaired glucose tolerance. American Journal of Physiology-Endocrinology and Metabolism. 2004;287(5):E906-E11.

49. Hasheminasabgorji E, Jha JC. Dyslipidemia, diabetes and atherosclerosis: role of inflammation and ROS-redox-sensitive factors. Biomedicines. 2021;9(11):1602.
50. Kitabchi AE, Umpierrez GE, Miles JM, Fisher JN. Hyperglycemic crises in adult patients with diabetes. Diabetes Care. 2009;32(7):1335-43.
51. Saedi E, Gheini MR, Faiz F, Arami MA. Diabetes mellitus and cognitive impairments. World journal of diabetes. 2016;7(17):412.
52. Gray GM. Carbohydrate digestion and absorption: Role of the small intestine. New England Journal of Medicine. 1975;292(23):1225-30.
53. Krentz AJ, Bailey CJ. Oral antidiabetic agents. Drugs. 2005;65(3):385-411.
54. Bruni C, Sica V, Auricchio F, Covelli I. Further kinetic and structural characterization of the lysosomal α-D-glucoside glucohydrolase from cattle liver. Biochimica et Biophysica Acta (BBA)-Enzymology. 1970;212(3):470-7.
55. Suzuki Y, Uchida K. Three forms of α-glucosidase from welsh onion (Allium fistulosum L.). Agricultural and biological chemistry. 1984;48(5):1343-5.
56. Hedrington MS, Davis SN. Considerations when using alpha-glucosidase inhibitors in the treatment of type 2 diabetes. Expert opinion on pharmacotherapy. 2019;20(18):2229-35.
57. Dong H-Q, Li M, Zhu F, Liu F-L, Huang J-B. Inhibitory potential of trilobatin from Lithocarpus polystachyus Rehd against α-glucosidase and α-amylase linked to type 2 diabetes. Food Chemistry. 2012;130(2):261-6.
58. Pérez-Torres I, Castrejón-Téllez V, Soto ME, Rubio-Ruiz ME, Manzano-Pech L, Guarner-Lans V. Oxidative stress, plant natural antioxidants, and obesity. International Journal of Molecular Sciences. 2021;22(4):1786.
59. Halliwell B, Gutteridge J. The definition and measurement of antioxidants in biological systems. Free radical biology & medicine. 1995;18(1):125-6.
60. Halliwell B. How to characterize a biological antioxidant. Free radical research communications. 1990;9(1):1-32.
61. López-Alarcón C, Denicola A. Evaluating the antioxidant capacity of natural products: A review on chemical and cellular-based assays. Analytica Chimica Acta. 2013;763:1-10.
62. Carocho M, Ferreira IC. A review on antioxidants, prooxidants and related controversy: Natural and synthetic compounds, screening and analysis methodologies and future perspectives. Food and chemical toxicology. 2013;51:15-25.
63. Landis GN, Tower J. Superoxide dismutase evolution and life span regulation. Mechanisms of ageing and development. 2005;126(3):365-79.
64. Rahman K. Studies on free radicals, antioxidants, and co-factors. Clinical interventions in aging. 2007;2(2):219.
65. Bouayed J, Bohn T. Exogenous antioxidants—double-edged swords in cellular redox state: health beneficial effects at physiologic doses versus deleterious effects at high doses. Oxidative Medicine and Cellular Longevity. 2010;3(4):228-37.
66. Moon J-K, Shibamoto T. Antioxidant assays for plant and food components. Journal of Agricultural and Food Chemistry. 2009;57(5):1655-66.
67. Škrovánková S, Mišurcová L, Machů L. Antioxidant activity and protecting health effects of common medicinal plants. Adv Food Nutr Res. 2012;67:75-139.
68. Piljac-Žegarac J, Šamec D, Piljac A. Herbal Teas: A Focus on Antioxidant Properties. Tea in Health and Disease Prevention. 2013:129-40.
69. Zhao J, Deng J, Chen Y, Li S. Advanced phytochemical analysis of herbal tea in

China. Journal of Chromatography A. 2013;1313:2-23.
70. Poswal FS, Russell G, Mackonochie M, MacLennan E, Adukwu EC, Rolfe V. Herbal teas and their health benefits: a scoping review. Plant Foods for Human Nutrition. 2019;74(3):266-76.
71. agency Em. Glossary on herbal tea 2010 [cited 2022 28 September 2022]. Available from: https://www.ema.europa.eu/en/documents/regulatory-procedural-guideline/glossary-herbal-teas_en.pdf.
72. Pastoriza S, Pérez-Burillo S, Rufián-Henares JÁ. How brewing parameters affect the healthy profile of tea. Current Opinion in Food Science. 2017;14:7-12.
73. Ramalho SA, Nigam N, Oliveira GB, de Oliveira PA, Silva TOM, dos Santos AGP, et al. Effect of infusion time on phenolic compounds and caffeine content in black tea. Food Research International. 2013;51(1):155-61.
74. Langley-Evans SC. Antioxidant potential of green and black tea determined using the ferric reducing power (FRAP) assay. International journal of food sciences and nutrition. 2000;51(3):181-8.
75. Braud L, Peyre L, De Sousa G, Armand M, Rahmani R, Maixent J-M. Effect of Brewing Duration on the Antioxidant and Hepatoprotective Abilities of Tea Phenolic and Alkaloid Compounds in at-BHP Oxidative Stress-Induced Rat Hepatocyte Model. Molecules. 2015;20(8):14985-5002.
76. Komes D, Horžić D, Belščak A, Ganić KK, Vulić I. Green tea preparation and its influence on the content of bioactive compounds. Food Research International. 2010;43(1):167-76.
77. Lin SD, Yang JH, Hsieh YJ, Liu EH, Mau JL. Effect of different brewing methods on quality of green tea. Journal of Food Processing and Preservation. 2014;38(3):1234-43.
78. Saklar S, Ertas E, Ozdemir IS, Karadeniz B. Effects of different brewing conditions on catechin content and sensory acceptance in Turkish green tea infusions. Journal of food science and technology. 2015;52(10):6639-46.
79. Sharpe E, Hua F, Schuckers S, Andreescu S, Bradley R. Effects of brewing conditions on the antioxidant capacity of twenty-four commercial green tea varieties. Food Chemistry. 2016;192:380-7.
80. Suphrom N, Insumrong K, Sriboon P, Sonyot W, Ingkaninan K, Boonphong S. Chromatographic fingerprint and free radical scavenging activity of Boesenbergia xiphostachya (Gagnep.) Loes rhizome extract. International Journal of Science. 2018;15(1):1-8.
81. Van Den Dool H, Kratz PD. A generalization of the retention index system including linear temperature programmed gas-liquid partition chromatography. 1963.
82. Kafkas E, Cabaroglu T, Selli S, Bozdoğan A, Kürkçüoğlu M, Paydaş S, et al. Identification of volatile aroma compounds of strawberry wine using solid-phase microextraction techniques coupled with gas chromatography–mass spectrometry. Flavour and Fragrance Journal. 2006;21(1):68-71.
83. Matsui T, Yoshimoto C, Osajima K, Oki T, Osajima Y. In vitro survey of α-glucosidase inhibitory food components. Biosci Biotechnol Biochem. 1996;60(12):2019-22.
84. Piangpraichom S, Suphrom N, Boonphong S, Prasanphan S, editors. The study of phytochemistry fingerprnts and antioxidant activity from *Memecylon scutellatum* Naudin leaf. Proceedings of the Congress on Conservation Biological Diversity in

Thailand; 2014 May 23-25, 2014; Thailand.
85. Wesołowska A, Jadczak P, Kulpa D, Przewodowski W. Gas chromatography-mass spectrometry (GC-MS) analysis of essential oils from AgNPs and AuNPs elicited Lavandula angustifolia in vitro cultures. Molecules. 2019;24(3):606.
86. Shapi M, Hesso A. Thermal decomposition of polystyrene: volatile compounds from large-scale pyrolysis. Journal of analytical and applied pyrolysis. 1990;18(2):143-61.
87. Hao C-Y, Fan R, Qin X-W, Hu L-S, Tan L-H, Xu F, et al. Characterization of volatile compounds in ten Piper species cultivated in Hainan Island, South China. International Journal of Food Properties. 2018;21(1):633-44.
88. Tananaki C, Liolios V, Kanelis D, Rodopoulou MA. Investigation of Volatile Compounds in Combination with Multivariate Analysis for the Characterization of Monofloral Honeys. Applied Sciences. 2021;12(1):264.
89. Milos M, Radonic A. Gas chromatography mass spectral analysis of free and glycosidically bound volatile compounds from Juniperus oxycedrus L. growing wild in Croatia. Food Chemistry. 2000;68(3):333-8.
90. Yáñez X, Pinzón ML, Solano F, Sánchez LR. Chemical composition of the essential oil of Psidium caudatum McVaugh. Molecules. 2002;7(9):712-6.
91. Zhang H, Li Y, Mi J, Zhang M, Wang Y, Jiang Z, et al. GC-MS profiling of volatile components in different fermentation products of Cordyceps sinensis mycelia. Molecules. 2017;22(10):1800.
92. Stojanovic G, Palic R, Alagic S, Zeković Z. Chemical composition and antimicrobial activity of the essential oil and CO2 extracts of semi-oriental tobacco, Otlja. Flavour and Fragrance Journal. 2000;15(5):335-8.
93. Chen C-KJ, Shokhireva TK, Berry RE, Zhang H, Walker F. The effect of mutation of F87 on the properties of CYP102A1-CYP4C7 chimeras: altered regiospecificity and substrate selectivity. JBIC Journal of Biological Inorganic Chemistry. 2008;13(5):813-24.
94. Olsen HT, Stafford GI, Van Staden J, Christensen SB, Jäger AK. Isolation of the MAO-inhibitor naringenin from Mentha aquatica L. Journal of Ethnopharmacology. 2008;117(3):500-2.
95. Tang SW, Sukari MA, Ee GCL. Characterization of flavonoid derivatives from Boesenbergia rotunda (L.). Malaysian Journal of Analytical Sciences. 2007;11(1):154-9.
96. Potipiranun T, Adisakwattana S, Worawalai W, Ramadhan R, Phuwapraisirisan P. Identification of pinocembrin as an anti-glycation agent and α-glucosidase inhibitor from fingerroot (Boesenbergia rotunda): The tentative structure–activity relationship towards MG-trapping activity. Molecules. 2018;23(12):3365.
97. Priscilla DH, Roy D, Suresh A, Kumar V, Thirumurugan K. Naringenin inhibits α-glucosidase activity: A promising strategy for the regulation of postprandial hyperglycemia in high fat diet fed streptozotocin induced diabetic rats. Chemico-Biological Interactions. 2014;210:77-85.
98. Proença C, Freitas M, Ribeiro D, Oliveira EF, Sousa JL, Tome SM, et al. α-Glucosidase inhibition by flavonoids: an in vitro and in silico structure–activity relationship study. Journal of enzyme inhibition and medicinal chemistry. 2017;32(1):1216-28.
99. Zhao X, Chen R, Shi Y, Zhang X, Tian C, Xia D. Antioxidant and anti-inflammatory activities of six flavonoids from Smilax glabra Roxb. Molecules.

2020;25(22):5295.
100. Park J, Boo YC. Isolation of resveratrol from vitis viniferae caulis and its potent inhibition of human tyrosinase. Evidence-Based Complementary and Alternative Medicine. 2013;2013.
101. Pandey RP, Parajuli P, Shin JY, Lee J, Lee S, Hong Y-S, et al. Enzymatic biosynthesis of novel resveratrol glucoside and glycoside derivatives. Applied and Environmental Microbiology. 2014;80(23):7235-43.
102. Rodrigues CFB, Gaeta HH, Belchor MN, Ferreira MJP, Pinho MVT, de Oliveira Toyama D, et al. Evaluation of potential thrombin inhibitors from the white mangrove (Laguncularia racemosa (L.) CF Gaertn.). Marine Drugs. 2015;13(7):4505-19.
103. Qin X, Xing YF, Zhou Z, Yao Y. Dihydrochalcone compounds isolated from crabapple leaves showed anticancer effects on human cancer cell lines. Molecules. 2015;20(12):21193-203.
104. Raya-Gonzalez D, Pamatz-Bolanos T, Rosa E, Martinez-Munoz RE, Ron-Echeverria O, Martinez-Pacheco MM. D-(+)-pinitol, a component of the heartwood of Enterolobium cyclocarpum (Jacq.) Griseb. Zeitschrift für Naturforschung C. 2008;63(11-12):922-4.
105. Han L, Fang C, Zhu R, Peng Q, Li D, Wang M. Inhibitory effect of phloretin on α-glucosidase: Kinetics, interaction mechanism and molecular docking. International Journal of Biological Macromolecules. 2017;95:520-7.
106. Zhang AJ, Rimando AM, Mizuno CS, Mathews ST. α-Glucosidase inhibitory effect of resveratrol and piceatannol. The Journal of Nutritional Biochemistry. 2017;47:86-93.
107. Bandeira SdM, Da Fonseca LJS, Guedes GdS, Rabelo LA, Goulart MO, Vasconcelos SML. Oxidative stress as an underlying contributor in the development of chronic complications in diabetes mellitus. International Journal of Molecular Sciences. 2013;14(2):3265-84.
108. Sroka Z, Cisowski W. Hydrogen peroxide scavenging, antioxidant and anti-radical activity of some phenolic acids. Food and Chemical Toxicology. 2003;41(6):753-8.
109. Bates SH, Jones RB, Bailey CJ. Insulin-like effect of pinitol. Br J Pharmacol. 2000;130(8):1944-8.
110. Davis A, Christiansen M, Horowitz JF, Klein S, Hellerstein MK, Ostlund Jr RE. Effect of pinitol treatment on insulin action in subjects with insulin resistance. Diabetes Care. 2000;23(7):1000-5.
111. Hernández-Mijares A, Bañuls C, Peris JE, Monzó N, Jover A, Bellod L, et al. A single acute dose of pinitol from a naturally-occurring food ingredient decreases hyperglycaemia and circulating insulin levels in healthy subjects. Food Chemistry. 2013;141(2):1267-72.
112. Kang M-J, Kim J-I, Yoon S-Y, Kim JC, Cha I-J. Pinitol from soybeans reduces postprandial blood glucose in patients with type 2 diabetes mellitus. J Med Food. 2006;9(2):182-6.
113. Kim MJ, Yoo KH, Kim JH, Seo YT, Ha BW, Kho JH, et al. Effect of pinitol on glucose metabolism and adipocytokines in uncontrolled type 2 diabetes. Diabetes Res Clin Pract. 2007;77(3):S247-S51.
114. Stull A, Wood K, Thyfault J, Campbell W. Effects of acute pinitol supplementation on plasma pinitol concentration, whole body glucose tolerance, and

activation of the skeletal muscle insulin receptor in older humans. Hormone and metabolic research. 2009;41(05):381-6.
115. Nikniaz Z, Mahdavi R, Ghaemmaghami SJ, Yagin NL, Nikniaz L. Effect of different brewing times on antioxidant activity and polyphenol content of loosely packed and bagged black teas (Camellia sinensis L.). Avicenna journal of phytomedicine. 2016;6(3):313.
116. Astill C, Birch MR, Dacombe C, Humphrey PG, Martin PT. Factors affecting the caffeine and polyphenol contents of black and green tea infusions. Journal of Agricultural and Food Chemistry. 2001;49(11):5340-7.
117. Farakte, Singh GN, editors. Effect of brewing temperature , tea types and particle size on infusion of tea components.
118. Murthy PS, Naidu MM. Recovery of phenolic antioxidants and functional compounds from coffee industry by-products. Food and Bioprocess Technology. 2012;5(3):897-903.
119. Vuong QV, Tan SP, Stathopoulos CE, Roach PD. Improved extraction of green tea components from teabags using the microwave oven. Journal of Food Composition and Analysis. 2012;27(1):95-101.
120. Nguyen QV, Chuyen HV. Processing of herbal tea from roselle (Hibiscus sabdariffa L.): Effects of drying temperature and brewing conditions on total soluble solid, phenolic content, antioxidant capacity and sensory quality. Beverages. 2020;6(1):2.
121. Yang D-J, Hwang LS, Lin J-T. Effects of different steeping methods and storage on caffeine, catechins and gallic acid in bag tea infusions. Journal of Chromatography A. 2007;1156(1-2):312-20.
122. Ailiesei GL, Ciobanu M, Balan M, Stavarache C, Barbes L, Nicolescu A, et al. NMR detected metabolites in complex natural fluids. Quinic acid in apple juice. Ovidius Univ Ann Chem. 2015;26:51-6.
123. López-Sánchez J, Moreno DA, García-Viguer C. D-pinitol, a highly valuable product from carob pods: Health-promoting effects and metabolic pathways of this natural super-food ingredient and its derivatives. AIMS agriculture and food. 2018;3(1):41-63.
124. Gao Y, Zhang M, Wu T, Xu M, Cai H, Zhang Z. Effects of d-Pinitol on Insulin Resistance through the PI3K/Akt Signaling Pathway in Type 2 Diabetes Mellitus Rats. Journal of Agricultural and Food Chemistry. 2015;63(26):6019-26.
125. Rengarajan T, Nandakumar N, Balasubramanian MP. d-Pinitol a low-molecular cyclitol prevents 7, 12-Dimethylbenz [a] anthracene induced experimental breast cancer through regulating anti-apoptotic protein Bcl-2, mitochondrial and carbohydrate key metabolizing enzymes. Biomedicine & Preventive Nutrition. 2012;2(1):25-30.
126. Zheng K, Zhao Z, Lin N, Wu Y, Xu Y, Zhang W. Protective effect of pinitol against inflammatory mediators of rheumatoid arthritis via inhibition of protein tyrosine phosphatase non-receptor type 22 (PTPN22). Medical science monitor: international medical journal of experimental and clinical research. 2017;23:1923.
127. Lin T-H, Tan T-W, Tsai T-H, Chen C-C, Hsieh T-F, Lee S-S, et al. D-pinitol inhibits prostate cancer metastasis through inhibition of αVβ3 integrin by modulating FAK, c-Src and NF-κB pathways. International Journal of Molecular Sciences. 2013;14(5):9790-802.
128. Gutierrez BL, Zhong G-Y, Brown SK. Genetic diversity of dihydrochalcone

content in Malus germplasm. Genetic Resources and Crop Evolution. 2018;65(5):1485-502.
129. WILLIAMS AH. Chemical evidence from the flavonoids relevant to the classification of Malus species. Botanical Journal of the Linnean Society. 1982;84(1):31-9.
130. Sun Y, Li W, Liu Z. Preparative isolation, quantification and antioxidant activity of dihydrochalcones from Sweet Tea (Lithocarpus polystachyus Rehd.). Journal of Chromatography B. 2015;1002:372-8.
131. Tanaka T, Tanaka O, Kohda H, Chou W-H, Chen F-H. Isolation of trilobatin, a sweet dihydrochalcone-glucoside from leaves of Vitis piasezkii Maxim. and V. saccharifera Makino. Agricultural and biological chemistry. 1983;47(10):2403-4.
132. Wang Y, Yauk Y-K, Zhao Q, Hamiaux C, Xiao Z, Gunaseelan K, et al. Biosynthesis of the dihydrochalcone sweetener trilobatin requires phloretin glycosyltransferase2. Plant physiology. 2020;184(2):738-52.